

Quantification and characterization of
nanoparticles in environmental matrices:
release from surface coatings and distributions
in natural waters

Agil Azimzada

Doctor of Philosophy

Department of Chemical Engineering
McGill University
Montreal, Quebec, Canada

August 2021

A thesis submitted to McGill University in partial fulfilment of the
requirements of the degree of Doctor of Philosophy

Copyright © 2021 Agil Azimzada

Abstract

Nanoparticle (NP) emissions to the environment are increasing as a result of anthropogenic activities, prompting concerns with respect to the ecosystem and human health. In order to evaluate the risk of NPs, it is necessary to know their concentrations in various environmental compartments, on regional and global scales; however, these data have remained elusive, mainly due to the analytical difficulties of measuring NPs in complex natural matrices. The fundamental aim of this work was thus to develop an improved analytical strategy for the high-throughput detection, quantification, and characterization of NPs in complex natural waters. To this end, inductively coupled plasma mass spectrometry (ICP-MS) was optimized for single particle analysis. Enhanced sensitivities that enable the determinations of smallest NPs and multi-element analysis that can provide potential insight into NP origins on a particle-by-particle basis were an important focal point of the project. Using state-of-the-art techniques, the methods of single particle analysis were applied for the monitoring of NPs in two important environmental contexts: (i) understanding the emission patterns of engineered TiO₂ NPs from a prevalently used nano-enabled product, *i.e.* surface coatings, under natural weathering scenarios, and (ii) examining the presence and distribution of three major NPs (Ag-, Ce- and Ti-NPs), including engineered ones, in global natural waters.

Measurements were performed with respect to particle sizes (distributions), mass/number concentrations and compositions/purities. Surface-leaching experiments were designed to elicit the role of seasonal changes, weathering variables, surface exposure scenarios, and coating matrix (paint or stain) properties in NP release patterns. The data clearly showed the strong impact of weathering on NP release trends, with wet and freeze-thaw (*i.e.* rainfall and slushy snow) conditions notably favouring NP leaching. Under the harshest conditions, up to 10^{11} TiO₂-NP m⁻²-coating were released, corresponding to the mass release of <200 µg-Ti m⁻²-coating, with most of the released NPs found in the 20-60 nm range. Multi-element measurements on the Ti-NPs indicated that they were often associated with a secondary metal in both the liquid paint (Al was detected in ~20% of the Ti-NPs; Zr in ~1% of the Ti-NPs) and the liquid stain (Fe was detected in ~7%, Si in ~8% and Al in ~3 % of the Ti-NPs). In contrast, for the vast majority of Ti-NPs being leached out of the painted/stained surfaces, only Ti was detected. Metal interactions in the paint were explained by binding of the TiO₂ within a complex paint matrix; while in the stain, TiO₂ NPs were hypothesized to be found in heteroagglomerates, potentially with aluminosilicates (Fe, Si and Al). In rain and snow

(Montreal), Ti was the only element detected in about half of the Ti-NPs; in the other half, Ti often co-occurred with Fe, Si and Al. The results indicate that single element, likely anthropogenic, Ti-NPs are already prevalent in the natural precipitation and that NP release from surface coatings will further increase their presence in the environment. Although NP release is a primary determinant in environmental risk, subsequent NP behavior leading to losses or re-suspension can be equally critical.

Natural waters were monitored globally, which entailed a sampling campaign from 46 sites in 13 countries and was aimed to link NP occurrences and distributions to particle type, size, origin, and sampling location. The results demonstrated the ubiquitous presence of NPs in the environment, including the remotest landscapes, such as Northern Canada and within Iceland glaciers. Globally, total Ti- and Ce-NP concentrations (regardless of origin) were often found to be within $10^4 - 10^7$ NP mL⁻¹, whereas Ag NPs exhibited sporadic occurrences with low concentrations generally up to 10^5 NP mL⁻¹. This generally corresponded to mass concentrations of <1 ng L⁻¹ for Ag-NPs, <100 ng L⁻¹ for Ce-NPs and <10 µg L⁻¹ for Ti-NPs, given that measured sizes were often below 15 nm for Ce- and Ag-NPs and above 30 nm for Ti-NPs. In view of current toxicological data, observed NP levels do not yet appear to exceed toxicity thresholds for the environment or human health; however, NPs of likely anthropogenic origins appear to be already substantial in certain areas, such as urban centers. The original multiplexed data presented in this body of research is much needed for reliable parametrization and validation of NP exposure models and for NP risk monitoring. The work also lays a foundation for broader systematic analysis of NP release and distribution patterns in the ecosystem.

Résumé

Les émissions de nanoparticules (NPs) dans l'environnement augmentent en raison des activités anthropiques, présentant des risques pour l'environnement et la santé humaine. Afin d'évaluer le risque des NPs, il est nécessaire de connaître leurs concentrations dans divers milieux environnementaux, à l'échelle régionale et mondiale. Cependant, ces données sont souvent manquantes à cause, notamment, des difficultés analytiques liées à la mesure des NPs dans des matrices naturelles. L'objectif fondamental de ce travail était donc de développer une stratégie analytique améliorée pour la détection, la quantification et la caractérisation des NPs dans les eaux naturelles complexes. Pour se faire, la technique de « couplage plasma induit par haute fréquence – spectrométrie de masse » (ICP-MS) a été optimisée pour l'analyse de particules individuelles. D'une part, les sensibilités instrumentales ont été améliorées afin de permettre la détermination des plus petites NPs et, d'autre part, une analyse multi-élémentaire (à l'aide d'un spectromètre de masse à temps de vol, ICP-TOF-MS) de chaque nanoparticule a été effectuée dans le but d'avoir de l'information sur l'origine naturelle ou anthropique des NPs. En utilisant ces techniques de pointe, les méthodes d'analyse ont été appliquées pour la surveillance des NPs dans deux contextes environnementaux importants afin de: (i) mieux comprendre l'émission de NPs de TiO₂ à partir d'un produit nano-activé couramment utilisé (c.-à-d. revêtements de surfaces) soumis à divers scénarios météorologiques réels, et (ii) déterminer la présence et la distribution de trois NPs majeures (Ag-, Ce- et Ti-NP) dans les eaux naturelles mondiales.

Des mesures conduisant à la détermination de la taille des particules (distributions), de leur concentration en masse/nombre et leur composition/pureté ont été effectuées. Des expériences de lixiviation en surface ont été conçues pour déterminer le rôle des changements saisonniers, des variables d'altération naturelle, des scénarios d'exposition de surface et de la composition de la matrice de revêtement (peinture ou teinture) dans le processus de relargage des NPs. Les résultats ont clairement montré le fort impact de la météo, notamment les conditions humides et gel-dégel, sur les tendances de relargage de NPs. Dans les conditions les plus sévères, jusqu'à 10¹¹ TiO₂-NPs m⁻²-revêtement ont été relarguées, ce qui correspondait à <200 µg-Ti m⁻²-revêtement. La plupart des NPs relarguées se trouvaient dans la gamme des 20 à 60 nm. Les mesures multi-élémentaires des Ti-NPs ont indiqué qu'elles étaient souvent associées à un métal secondaire dans la peinture (Al a été détecté dans ~20 % des Ti-NPs; Zr dans ~1 % des Ti-NPs) et la teinture liquide (Fe a été détecté dans 7 %, Si dans ~ 8 % et Al

dans ~ 3 % des Ti-NPs). En revanche, pour la grande majorité des Ti-NPs extraites des surfaces peintes, seul le Ti a été détecté. Les interactions métalliques dans la peinture peuvent être expliquées par les liaisons intermoléculaires de TiO_2 avec les différents composés de la matrice complexe de la peinture ; tandis que dans la teinture, les NPs de TiO_2 sont supposées se trouver dans des hétéro-agglomérats, potentiellement avec des aluminosilicates (Fe, Si et Al). Dans la pluie et la neige (Montréal), le Ti était le seul élément détecté dans environ la moitié des Ti-NPs. Dans l'autre moitié, Ti coexistait souvent avec Fe, Si et Al. Les résultats indiquent que les Ti-NP monométalliques, vraisemblablement anthropiques, sont déjà répandues dans les précipitations naturelles et que la libération de NPs par les revêtements de surface augmentera encore leur présence dans l'environnement. Bien que le relargage de NPs soit un facteur de risque environnemental principal, le comportement ultérieur des NPs conduisant à des pertes ou à une remise en suspension peut être tout aussi critique.

L'évaluation des eaux naturelles à l'échelle mondiale, qui a nécessité une campagne d'échantillonnage sur 46 sites dans 13 pays, visait à relier la présence et la distribution des NPs à leur type, leur taille, leur origine et leur lieu d'échantillonnage. Dans l'ensemble, les données ont montré l'omniprésence de NPs dans l'environnement, y compris dans des endroits les plus reculés de la planète, comme le nord du Canada et les glaciers d'Islande. Globalement, les concentrations totales de Ti- et Ce-NPs (quelle que soit leur origine) se situaient souvent entre 10^4 et 10^7 NP mL^{-1} , tandis que la présence des Ag-NPs était sporadique et à de faibles concentrations, généralement jusqu'à 10^5 NP mL^{-1} . Cela correspondait, généralement, à des concentrations massiques <1 ng L^{-1} pour les Ag-NPs, <100 ng L^{-1} pour les Ce-NPs et <10 μg L^{-1} pour les Ti-NPs, étant donné que les tailles estimées étaient souvent inférieures à 15 nm pour les Ce-NPs et Ag-NPs et au-dessus de 30 nm pour les Ti-NPs. Au vu des données toxicologiques actuelles, les concentrations de NPs observées ne semblent pas encore dépasser les seuils de toxicité pour l'environnement ou la santé humaine. Cependant, les concentrations de NPs qui sont vraisemblablement d'origine anthropique paraissent déjà importantes dans certaines zones, comme les centres urbains. Les données multiplexées originales présentées dans ce travail de recherche sont indispensables pour une paramétrisation et une validation fiable des modèles d'exposition aux NPs, ainsi que pour la surveillance de leurs risques. Ce travail peut également servir de base pour une analyse systématique plus large des modèles de rejet et de distribution de NPs dans l'écosystème.

Acknowledgements

First and foremost, I would like to express my deep gratitude to my supervisors, Prof. Kevin J. Wilkinson and Prof. Phillip Servio, for their academic and moral support, continued guidance, and unwavering encouragement throughout my PhD. I am particularly thankful to them for providing me with the opportunity to work on an exciting project, for guiding me towards the right path, and for helping me grow into my potential. I am also extremely grateful to Jeffrey M. Farner, Madjid Hadioui, and Ibrahim Jreije for sharing their expertise and ideas; for their contributions with experimental design, method development, and analytical measurements; as well as for their friendship, support, and encouragement.

I am very thankful to Dr. Phil Shaw at Nu Instruments for giving me the opportunity to intern at their company and to work on a state-of-the-art, prototype instrument, as well as for his relentless support and invaluable advice for data processing. This was a great learning experience that will undoubtedly benefit my future. I also appreciate the help and support of Ariane Donard throughout the internship. I am thankful to Carolyn Liu-Lang for her assistance with sample preparation and measurements, and Laurie Fréchette-Viens for her initial introduction to the data processing software. I am extremely grateful to numerous collaborators across the world who contributed to the success of the ambitious global sampling campaign. This work would indeed not be possible without their trust in the project and generous support. I also thank all technicians and administrative staff for their help throughout this journey.

I owe a deep debt of gratitude to Roya Jamarani and Thomas Vlastic for their unwavering moral support and encouragement, as well as their administrative guidance. I am equally grateful to all my friends and colleagues, notably Anya Filina, Shawn Chahal, Elise Morel, and Juliana Galhardi, for moral support, coffee breaks, and all kinds of interesting discussions. I can never be thankful enough to my family and numerous friends, for their love, support, kindness, and patience.

My research was supported by the Natural Sciences and Engineering Research Council of Canada (NSERC), the NSERC PURE CREATE network, and the Fonds de Recherche du Quebec - Nature and Technologies. I am honoured to be the recipient for a McGill Engineering Doctoral award (MEDA) and an EcotoQ Excellence Scholarship.

Contributions to Original Knowledge

- Development of state-of-the-art analytical methodologies (based on ICP-MS technology) for high-throughput element-specific detection, quantification, and characterization of smallest NPs *i.e.* with size detection limits as low as 12 nm for TiO₂ NPs and 3 nm for Ag and CeO₂ NPs in natural waters;
- Quantification and characterization of anthropogenic NP release from a nano-enabled product, *i.e.* surface coatings, under natural (outdoor) weathering conditions against the background of naturally occurring NPs and colloids;
- Determinations of the roles of different weathering factors, such as temperature, precipitation, and freezing/freeze-thaw, on NP emission patterns from outdoor surface coatings;
- Measurements of distributions, sizes, and mass/number concentrations of NPs in global samples collected from 46 sites across 13 countries;
- Experimental insight into NP origins based on purity/impurity and composition analysis of NPs performed on a particle-by-particle basis;
- Comprehensive original (quantitative) data that will be useful for reliable parametrization and validation of NP exposure models and NP risk assessments.

Preface and Contributions of Authors

In accordance with the “McGill Guidelines for Thesis Preparation”, this thesis is prepared in a manuscript-based format. Chapter 1 presents a broad introduction to the subject-matter of this thesis, including a comprehensive literature review; sets the research objectives; and provides an overview of the following chapters. Chapter 2-4 are comprised of three original research manuscripts. Chapter 5 presents the overall conclusions and implications of this body of research, as well as proposes research priorities and recommendations. The specific contributions of the authors are as following:

- Agil Azimzada: experimental design and planning; preparation of experimental setup; sampling and sample preparation; method development; analytical measurements; SP-ICP-(TOF)MS data processing; data organization and statistical analysis; data interpretation; making of graphics and figures; literature review; the writeup of the whole thesis, including the introduction, three original research manuscripts and conclusions (all chapters);
- Kevin J. Wilkinson: experimental design and planning; project supervision; sampling; data interpretation; manuscript/thesis review and feedback (all chapters);
- Madjid Hadioui: method development; troubleshooting; analytical measurements; data processing; data interpretation; manuscript feedback (Chapters 2, 3 and 4);
- Jeffrey M. Farner: experimental design and planning; preparation of experimental setup; sampling and sample preparation; data interpretation; manuscript feedback (Chapters 2, 3 and 4);
- Ibrahim Jreije: sampling and sample preparation; method development; analytical measurements; data processing; data interpretation; manuscript feedback (Chapters 2, 3 and 4);
- Phil Shaw: development of data processing software; troubleshooting; analytical measurements (Chapters 3 and 4);
- Nathalie Tufenkji: experimental design and planning (Chapters 2 and 3);
- Carolyn Liu-Kang: sampling and sample preparation; analytical measurements (Chapters 2 and 3).

Table of Contents

Abstract	I
Résumé	III
Acknowledgements	V
Contributions to Original Knowledge	VI
Preface and Contributions of Authors	VII
Table of Contents.....	VIII
List of Figures	XII
List of Tables.....	XVII
Chapter 1 Introduction	1
1.1 Emissions, transport, and transformations of engineered nanoparticles	2
1.1.1 Motivation	2
1.1.2 Routes of entry of ENPs into the environment.....	3
1.1.3 Transport pathways of ENPs in the environment.....	4
Atmosphere	5
Soil	6
Aquatic media	6
1.1.4 Physicochemical transformations of ENPs.....	7
Agglomeration.....	7
Agglomeration: role of pH and ionic strength	8
Agglomeration: role of organic matter.....	8
Surface bio-modification.....	9
Chemical transformations	10
Bio-mediated reactions.....	10
Atmospheric transformations	11
1.2 Determinations of ENPs in environmental matrices.....	11
1.2.1 Limitations of exposure models	11
1.2.2 Analytical measurements of ENPs: challenges and opportunities	13
1.2.3 ICP-MS: history and background.....	15
1.2.4 ICP-MS: technical description and types of instrumentation.....	16
Working principle	16
Quadrupole.....	16
Sector-field.....	17
Time-of-flight.....	17
1.2.5 Single particle ICP-MS: operating principle and theory	18
Operating principle.....	18

Theory	18
1.2.6 Single particle ICP-MS: background interferences and SDLs	20
Interferences	20
SDLs in the literature	22
1.3 Discrimination of ENPs from naturally occurring colloids.....	24
Microscopy and X-ray techniques.....	24
ICP-MS: bulk elemental ratios	25
ICP-MS: NP-by-NP approach.....	26
1.4 Scope and Experimental Approach.....	27
Sequential analysis	27
Simultaneous whole spectrum analysis.....	27
Experimental scope	28
1.5 Research Objectives	29
1.6 Thesis Organization	30
1.7 References	31
Chapter 2 Release of TiO₂ nanoparticles from painted surfaces in cold climates: characterization using a high sensitivity single-particle ICP-MS	41
2.1 Introduction	42
2.2 Materials and Methods	43
Preparation of exposure panels	43
Outdoor weathering setup	43
Indoor (controlled) weathering setup	44
Sample preparation for SP-ICP-MS.....	44
SP-ICP-MS analysis and data acquisition.....	44
SP-ICP-MS data processing	45
Total metal analysis.....	45
2.3 Results and Discussion	45
Optimization of SP-ICP-MS for TiO ₂ NPs	45
Detection of Ti NPs in natural precipitation	47
TiO ₂ NPs in paint	48
TiO ₂ NP release due to weathering	48
How did weathering conditions affect TiO ₂ NP release?.....	51
Are the sizes of weathered TiO ₂ NPs similar to those that were originally in the paint?	54
Environmental considerations and implications	55
Acknowledgements	55
2.4 References	55
2.5 Supplementary Information.....	59
Chapter 3 Single- and multi-element quantification and characterization of TiO₂ nanoparticles released from outdoor stains and paints	67

3.1	Introduction	68
3.2	Materials and Methods	69
	Weathering panels	69
	Natural weathering setups	70
	Indoor weathering	71
	Sample preparation for SP-ICP-MS/SP-ICP-TOF-MS	71
	SP-ICP-MS analysis and data acquisition	72
	SP-ICP-TOF-MS analysis and data acquisition	72
	SP-ICP-MS/SP-ICP-TOF-MS data processing	73
	Ti analysis by quantitative ICP-MS	73
3.3	Results and Discussion	74
	Technical considerations in the SP-ICP-MS and SP-ICP-TOF-MS measurements ...	74
	Characterization of TiO ₂ NPs in the paint and stain	75
	Release of NPs from painted and stained surfaces	75
	Role of exposure mode (vertical or slanted), season (fall or winter) and coating type (paint or stain)	77
	Distinguishing the engineered NPs from background NPs in the precipitation using SP-ICP-TOF-MS	80
	Environmental implications	85
	Acknowledgements	86
	Author Contributions	86
3.4	References	86
3.5	Supplementary Information	91

Chapter 4 Quantification and characterization of Ti-, Ce- and Ag-nanoparticles in global surface waters and precipitation 99

4.1	Introduction	100
4.2	Materials and Methods	101
	Global sampling campaign	101
	Sample preparation for analysis	102
	SP-ICP-MS measurements	102
	SP-ICP-TOF-MS measurements	103
	Data processing for SP-ICP-MS/SP-ICP-TOF-MS	103
4.3	Results and Discussion	104
	NP occurrence and concentrations across the globe	104
	NP composition and origins	107
	NP sizes and origins	109
	Global environmental implications	111
	Acknowledgements	113
	Author Contributions	113
	Competing interests	113
4.4	References	113
4.5	Supplementary Information	118

Chapter 5 Conclusions and Future Outlook.....	127
5.1 Conclusions and environmental implications.....	128
5.2 Future research directions and recommendations.....	131

List of Figures

- Figure 1-1** Processes governing the formation, transformation, distribution, and fate of nanoparticles in different environmental compartments.
- Figure 2-1** (A) Particle size distribution of Ti-containing NPs found in snow melt water, as measured with high-sensitivity magnetic-sector ICP-MS using a dwell time of 50 μ s. (B) Raw signal intensity (cps) near the particle size detection limit.
- Figure 2-2** (A) Time-resolved SP-ICP-MS signal and the corresponding (B) particle size distribution obtained for Ti-containing NPs in snow melt (10x diluted).
- Figure 2-3** Quantification of Ti in the natural precipitation as well as the precipitation following its contact with painted panels: (A) total Ti measured by ICP-MS, (B) Ti NP measured by SP ICP-MS, and (C) the net release of total and nanoparticulate Ti during the winter and summer seasons.
- Figure 2-4** Time-resolved SP-ICP-MS signal (*i.e.* raw data) for Ti-containing NPs in (A) snow meltwater and (B) snow after 2 weeks of contact with a painted panel. Particle size distributions were obtained for (C) Ti-containing NPs in the natural precipitation background and (D) for NP released from the painted surfaces, over several weeks during the winter season.
- Figure 2-5** NP mass release under different exposure conditions, quantified by SP-ICP-MS and normalized by the exposure area of painted panels.
- Figure 2-6** (A) NP mass release normalized by the exposure area of painted panels, for samples that were exposed to Milli-Q water (no NP background) under (wet) conditions of room temperature (RT) and freeze-thaw (FT) and (B) the corresponding mean NP sizes.
- Figure 2-7** Particle size distributions for TiO₂ NPs following their release from painted surfaces that were exposed to several weeks of FT cycles in Milli-Q water (no NP background).
- Figure 2-S1** A photo of the outdoor weathering setup on the 4th floor roof of Wong building (McGill University, Montreal, QC).
- Figure 2-S2** (A) Particle size distribution of TiO₂ NPs (148,100 NP/mL) after spiking engineered TiO₂ NPs (nominal size of 25 nm) into the rainwater medium, (B) Cumulative particle size distributions of TiO₂ in the rainwater (54,640

NP/mL) and for the TiO₂ NPs suspended in Milli-Q water (106,500 NP/mL) before mixing.

- Figure 2-S3** Time-resolved SP-ICP-MS signals (*i.e.* raw data) obtained for ²³⁸U, ¹⁰⁷Ag, ¹⁹⁷Au, ¹⁴⁶Nd, ¹³⁹La, ¹⁴⁰Ce, ⁵⁷Fe, ⁴⁹Ti and ¹¹⁵In in a filtered (0.45 µm) rainwater sample (collected in Montreal, QC).
- Figure 2-S4** Time-resolved SP-ICP-MS signal obtained following the analysis of (A) fresh Milli-Q water and (B) Milli-Q water exposed to outdoor air for 2 days, as well as (C, D) their corresponding particle size distributions.
- Figure 2-S5** Time-resolved SP-ICP-MS signal obtained following the analysis of (A) fresh Milli-Q water and (B) Milli-Q water exposed to indoor air for 3 weeks, as well as (C, D) their corresponding particle size distributions.
- Figure 2-S6** Particle size distributions obtained for TiO₂ NPs in a liquid paint sample diluted 2×10^7 x w/w with (A) Milli-Q water and (B) 5 mg L⁻¹ of fulvic acid (Suwannee River standard fulvic acid, SRFA II) following 30 min of ultrasonication.
- Figure 2-S7** Daily temperatures (maxima, minima and mean T) as well as precipitation (rain, snow, total precipitation) in the winter and summer of 2018, as collected from Montreal International Airport weather station (45°28'14.000" N, 73°44'27.000" W) and retrieved from the Environment and Climate Change Canada database.
- Figure 2-S8** Particle size distribution of TiO₂ NPs released following a 4-day soaking of a painted panel in Milli-Q water (no NP background).
- Figure 3-1** Experimental setups for two weathering scenarios: (A) vertical exposure – consisting of a painted/stained panel vertically positioned in a polypropylene container, (B) slanted exposure – made up of two containers stacked on top of each other and separated by a polypropylene mesh, where the top container contains a painted/stained panel fixed in a slanted position.
- Figure 3-2** Quantification of Ti-containing NPs in the precipitation (*i.e.* background) and in the precipitation following its contact with (A-B) painted and (C-D) stained panels (*i.e.* sample). Sample weathering experiments were conducted using two exposure designs (Fig. 1), (A, C) vertical and (B, D) slanted, for painted and stained panels.

- Figure 3-3** Cumulative concentrations of sub-0.45- μm Ti determined by (A) ICP-MS on acidified samples and (B) SP-ICP-MS, obtained by integration of the NP peaks. Ti was measured following its release from the **paint** surfaces in vertical and slanted exposure modes (N=4 for each condition).
- Figure 3-4** Cumulative concentrations of sub-0.45- μm Ti determined by (A) ICP-MS on acidified samples and (B) SP-ICP-MS, obtained by integration of the NP peaks. Ti was measured following its release from the **stained** surfaces in vertical and slanted exposure modes (N=4 for each condition).
- Figure 3-5** Examples of SP-ICP-TOF-MS raw peak data corresponding to Ti-containing NPs detected in the different matrices. Association of Ti with (A) Al or with (B) Al and Zr in the liquid paint. Association of Ti with (C) Si or with (D) Fe and Al in the liquid stain. Association of Ti with (E) Fe and (F) Si and Al in Montreal rain.
- Figure 3-6** Elemental fractions of Ti in Ti-containing NPs for (A) liquid paint (diluted in Milli-Q water), (B) paint leachate, (C) liquid stain (diluted in Milli-Q water), (D) stain leachate, and (E) Montreal rainwater. Measurements were performed using a SP-ICP-TOF-MS.
- Figure 3-7** Elemental mass ratios measured on individual particles for major associations of the Ti in (A-B) liquid paint, (C-D) liquid stain and (E-F) Montreal rain samples. Measurements were performed using a SP-ICP-TOF-MS.
- Figure 3-S1** (A) Particle size distribution of Ti-containing NPs in a melted snow as measured by a magnetic-sector SP-ICP-MS coupled to a desolvator and using a dwell time of 50 μs . (B) an example of the raw ICP-MS signal data for the smallest detected NP with a size of 15 nm.
- Figure 3-S2** Particle size distributions measured using SP-ICP-TOF-MS for Ti-containing NPs in (A) diluted paint, (C) diluted stain and (E) rainwater, as well as the raw peak data for NPs that were near the instrumental size detection limits.
- Figure 3-S3** Particle size distribution of TiO_2 NPs in (A) liquid paint and (B) liquid stain, as measured by a high-resolution SP-ICP-MS. The samples were analyzed immediately following a $2 \times 10^7 \times$ dilution of the liquid paint and $2 \times 10^5 \times$ times dilution of the stain in Milli-Q water.
- Figure 3-S4** (A) Daily temperatures (maxima, minima and mean T), (B) total precipitation (total liquid equivalent of rain and snow), (C) rain precipitation and (D) snow

on ground data for the fall of 2018 and winter of 2019, as collected from the Montreal International Airport weather station (45°28'14.000" N, 73°44'27.000" W) and retrieved from the Environment and Climate Change Canada database.

Figure 3-S5 Examples of particle size distributions of Ti-containing NPs (**A**) in a rainwater as well as in the leachates of (**B**) paint and (**C**) stain. NP frequencies in the leachate samples were calculated following the subtraction of the background NPs (*i.e.* pre-existing NPs in the rainwater).

Figure 3-S6 Time-resolved ICP-TOF-MS signal simultaneously measured for (**A**) Ce, (**B**) Zr, (**C**) Fe, (**D**) Ti, (**E**) Si and (**F**) Al in liquid paint that was diluted 2×10^7 x with Milli-Q water.

Figure 3-S7 Time-resolved ICP-TOF-MS signal simultaneously measured for (**A**) Ce, (**B**) Zr, (**C**) Fe, (**D**) Ti, (**E**) Si and (**F**) Al in the liquid stain that was diluted with Milli-Q water. While Ce, Zr, Ti, Si and Al were measured in 2×10^4 x diluted samples, Fe was measured in 2×10^5 x diluted samples due to its relatively higher concentration.

Figure 3-S8 Time-resolved ICP-TOF-MS signal measured for ^{27}Al in diluted liquid paint (2×10^7 x) and in the leachate following the weathering of a painted surface in Milli-Q water.

Figure 4-1 Nanoparticle concentrations in global surface waters and precipitation. Particle number concentrations for Ti-, Ce- and Ag-containing NPs (denoted by blue, orange and violet bars, respectively) collected at 46 sampling sites across 13 countries and measured in surface waters (**a**) and precipitation (**b**).

Figure 4-2 Particle compositions and their link to particle masses (or sizes). **a**, Ti fractions in Ti-containing particles as determined in TiO_2 nanoparticle standard (NIST 1898) and in natural precipitation samples collected at six locations: Sao Paulo (BRA), Montreal (CAN), Munich (DEU), Durham (USA), Vancouver (CAN) and Sólheimajökull (ISL). **b-g**, In selected samples of Sao Paulo, Montreal and Sólheimajökull, each Ti-particle is identified as containing 'only Ti' or 'Ti with additional metals/metalloids' and the corresponding number fraction (%) (**b-d**) of these particle categories as a function of total metallic particle mass (*i.e.* distributions, **e-f**) are reported.

- Figure 4-3** **Metallic associations of nanoparticles on a single particle level.** **a**, Ratios of the number of Ti-containing NPs to the number of Al-, Si- or Fe-containing NPs. **b**, Ratios of Ti mass to mass of Al, Si or Fe in the NP. **c**, Ratios of the number of Ti-containing NPs to the number of those both Ti-Al, Ti-Si or Ti-Fe. **d**, Ratios of the total mass of Ti in Ti-containing NPs to that of the Al, Si or Fe. Blue, red, and green bars denote Ti/Al, Ti/Si and Ti/Fe (mass or number) ratios, respectively.
- Figure 4-4** **Nanoparticle size distributions and mean sizes by water type.** **a**. Particle size distributions as determined for Ti-, Ce- and Ag-containing NPs in London (The Long Water Lake), Göttingen (Leine River), Toronto (Lake Ontario) and Yukon (Kluane Lake) surface waters. Measured (mean) sizes for Ti- (**b**) and Ce-containing (**c**) NPs detected in 46 samples. Samples were categorized by water type.
- Figure 4-S1** **Particle stability.** Time-resolved particle number concentrations and sizes as measured for TiO₂ NPs in a melted snow sample collected in Montreal, Quebec.
- Figure 4-S2** **Concentrations of La nanoparticles in global precipitation and surface waters.** **a,b**, Particle number concentrations for La-containing NPs as measured in surface waters (**a**) and precipitation (**b**) collected at 46 sampling sites across 13 countries.
- Figure 4-S3** **Time-resolved measurements of nanoparticles in surface waters.** **a,b**, Particle number concentrations measured for Ti- (**a**) and Ce-containing (**b**) NPs in surface water samples collected from two sampling points at Saint Lawrence River (SLR) and a recreational pond in Parc La Fontaine (PLF) in Montreal (Quebec, Canada). Each timepoint (TP) refer to the date when the samplings were performed. **c,d**, Natural precipitation (**c**) and temperature (**d**) data are collected from the Montreal International Airport weather station (45°28'14.000" N, 73°44'27.000" W) and retrieved from the Environment and Climate Change Canada database.
- Figure 4-S4** **Modelled size distributions taking into account multi-element nature of particles.** Modelled size distributions of NPs detected in snow from the Sólheimajökull glacier (ISL), assuming a range of particle densities (2-8 g cm⁻³). Given that the experimental determinations were limited to metals and

metalloids only (*i.e.* excluded oxygen, halogens, etc.), particle sizes were predicted based upon the total masses of (almost) all metals/metalloids (*i.e.* 23-238 amu) detected in single particles (*i.e.* metal only). Total masses were assigned additional mass uncertainties of 20% (column 2) or 50% (column 3), due to the presence of the undetected elements.

Figure 4-S5 Detection limits of the multi-element analysis. Upper limits of the potential missing contributions of 14 metals in Ti-containing NPs, for cases in which Ti was detected as the only metallic component. % values are calculated based on the mass detection limit of each metal in relationship to the Ti content detected in individual Ti-containing NPs.

List of Tables

- Table 1-1** Spectral interferences observed in ICP-MS for isotopes of select metals. The table is adapted from May and Wiedmeyer (1998)¹¹⁸.
- Table 1-2** Size detection limits observed for TiO₂, CeO₂, Ag and ZnO NPs as measured by SP-ICP-MS systems in various matrices.
- Table 2-1** Quantification of the release of particulate TiO₂ NPs (<450 nm) from painted panel surfaces, following their natural weathering for several weeks in Winter 2018 and Summer 2018.
- Table 2-S1** Recoveries (%) of ionic Ti (based on Ti-49 isotope) as well as those of TiO₂ NPs spiked in a rainwater matrix.
- Table 4-S1** Sampling information for global surface water samples.
- Table 4-S2** Sampling information for global natural precipitation samples
- Table 4-S3 Nanoparticle measurements on surface water samples.** Measurements were performed by a high-sensitivity sector-field single-particle ICP-MS.
- Table 4-S4 Nanoparticle measurements on natural precipitation samples.** Measurements were performed by a high-sensitivity sector-field single-particle ICP-MS.

Chapter 1 Introduction

1.1 Emissions, transport, and transformations of engineered nanoparticles

1.1.1 Motivation

Rapid advances in nanotechnology have led to the extensive use of nano-enabled products and increased production volumes of engineered nanoparticles (ENPs).¹ ENPs are defined as man-made entities with three dimensions in the size range of 1-100 nm. ENP particle sizes are the primary determinant for their nano-specific physicochemical properties, which distinguish them from bulk materials of similar compositions. This is because ENPs, due to their very small sizes, are comprised of a relatively higher ratio of surface atoms as compared to interior ones, which yield enhanced surface energies and chemical reactivities.² In addition, making use of quantum confinement effects³, which arise as a function of particle size (in nanoscale range), ENPs are often tailored to achieve novel properties (*e.g.* optical, electrical) that are desirable for specific uses. ENP types can include a variety of compositions, shapes, coatings and structures – variations that make them suitable for targeted applications in a wide range of market sectors, ranging from consumer goods to medical industries.

ENPs are reportedly included in thousands of nano-enabled products, with silicon dioxide (SiO₂), titanium dioxide (TiO₂), and zinc oxide (ZnO) leading the list of the most produced (on a mass basis), while Ag and CeO₂ nanoparticles (NPs) are among the commonly used ENPs, according to Nanotechnology Consumer Products Inventory (CPI).⁴ Notable commercial applications include personal care products, surface coatings, pharmaceuticals, medical devices, fuels, electronics, and clothing.⁵ Despite the difficulties in determining the global production volumes of ENPs with high certainty, SiO₂ and TiO₂ ENP production quantities are often estimated to be >100,000 and >10,000 tons per year, respectively; while for Ag and CeO₂ ENPs, these numbers are thought to be an order or two orders of magnitude lesser (*i.e.* thousands of tons per year).⁶⁻⁸ Given the current pace of industrialization and increasing global market demand for ENPs, orders of magnitude of increases in their production volumes can be projected over the next decades. This trend will drive the inevitable emission of ENPs into the environment at increasingly higher rates. Upon their release, ENPs could, unfortunately, pose environmental risks,⁹ in large part owing to the same physicochemical properties that rendered them novel and highly reactive. This has thus prompted intensive research efforts on the environmental and health implications of ENPs, and better understanding of their fate, bioavailability, and toxicity.

1.1.2 Routes of entry of ENPs into the environment

Based on modelling data⁶, a vast majority of ENPs finish up in landfills (63-91%) and soils (8-28%), with a smaller fraction ending up in surface waters (up to 7%) and air (up to 2%). The global annual flux of ENPs into landfills, atmosphere, soil, and water is predicted to exceed 300,000 tons/year³ with only a fraction being directly discharged into the environment, often during the production or usage phases of the ENPs. For example, this may include inadvertent release of ENPs from a nanomaterial production plant (*e.g.* into air or surface waters)¹⁰, uses of nano-enabled sunscreen products (often contains TiO₂ and ZnO ENPs) at beaches or swimming pools¹¹, or the combustion of nano-enabled fuels¹² (*e.g.* often contains CeO₂ ENPs). The majority of ENPs are thought to enter the environment via urban sewer systems where they pass through municipal or industrial waste management facilities, prior to being released into the nature.^{13, 14} Domestic waste is an important input of ENPs into wastewater streams, due to growing uses of nano-enabled personal care products, health supplements, and food packaging, while indirect releases of ENPs owing to urban or industrial pollution, including run-offs from building façades and construction materials, also represent a major emission scenario.⁸

ENPs likely undergo a series of physicochemical changes, prior to and upon their entry into wastewater streams, where the type and extent of transformations often depends upon the ENP type and its intrinsic properties, its route of transport and relevant environmental conditions, and waste management or treatment practices (*e.g.* aerobic/anaerobic treatment, ozone treatment, flocculation).¹⁵ Reliable tracking of ENPs in the environment, particularly in a complex medium such as wastewater, is a challenging task, as their transport dynamics will also be dictated by their spatiotemporal transformations. Previous research, based upon experimental data and modelling, has established that a majority of ENPs (up to 90% or more) entering wastewaters will likely end up in sewage sludge (*i.e.* biosolids), with a smaller but still significant fraction (up to 10%) finding their way into wastewater effluents.^{6, 13, 14} Depending on the country and its waste management regulations, sewage sludge may be subject to further processing or transport, but often it ends up in landfills and/or waste incineration plants or it may be applied to soil as an agricultural fertilizer. High temperature incineration processes (>900 °C) result in the vast majority of ENPs being partitioned into the bottom ashes, which are subsequently disposed of in landfills.¹⁶ Although the emission of ENPs via exhaust gas is likely to be low due to the high efficiency of modern flue gas cleaning systems with respect to the removal of sub-micron particles, some ENP escape into air may still occur.¹⁷ Consequently, all possible waste disposal/recycling scenarios, including effluent discharge, sludge handling

and waste incineration, inevitably lead to the contamination of air, soil, and surface waters with ENPs.

1.1.3 Transport pathways of ENPs in the environment

Upon their entry into the environment, whether via direct or indirect routes, all ENPs are continually subject to diffusive and convective forces that will drive their mass transport. These forces coupled with the gravitational force and intermolecular forces, such as Van der Waals, electrical double layer, and steric forces, will determine the transport rate and trajectory of the ENPs, or will immobilize them via sedimentation or attachment to various surfaces.^{18, 19} The transport behaviour of ENPs in turn governs their transfer, within an environmental compartment or from one compartment to another (*e.g.* air to soil), resulting in their ubiquitous presence and incorporation into natural biogeochemical cycles, along with naturally occurring (nanoscale) colloids (**Fig. 1-1**). The transport of particles, including ENPs, may occur over short-range (*e.g.* microscopic to local)²⁰ or long-range (*e.g.* regional to global) distances^{21, 22}. For example, the long-range atmospheric transport of particulates is a common phenomenon, with air currents estimated to move millions of tons of particles between the continents every year. While most of these particles originate from natural sources, such as soil erosion and deserts or volcanic emissions (*e.g.* estimated 200 Tg of volcanic fine ash per year, of which ~20 Tg in nanoparticulate forms), a smaller but still a consequential portion (*i.e.* an order of magnitude less) results from anthropogenic processes, although the exact contributions of ENPs are yet unknown.²² On a local or regional level, transport of contaminants mostly driven by urban and industrial pollution is becoming increasingly common.²³

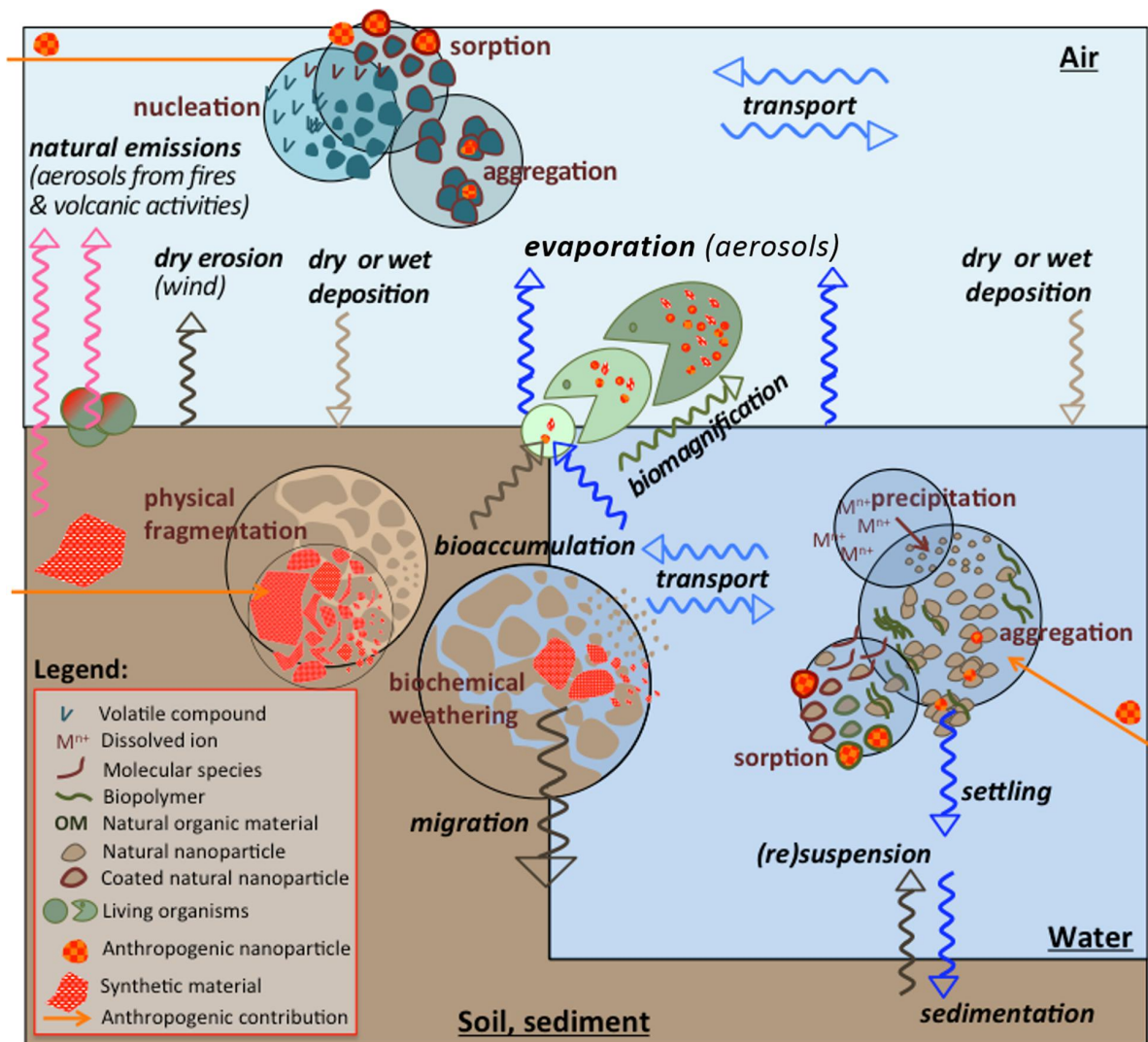


Figure 1-1. Processes governing the formation, transformation, distribution, and fate of nanoparticles in different environmental compartments. The figure is reproduced from Lespes *et al*²⁴ under the terms of the Creative Commons Attribution Licence.

Atmosphere. Atmospheric aerosols may subsequently transfer to other compartments, such as soil or water, via dry and wet deposition (**Fig. 1-1**). Dry deposition involves the removal of atmospheric constituents primarily through gravitational settling, whereby particles of sizes above $0.8 \mu\text{m}$ are typically impacted. Particles that are $<0.08 \mu\text{m}$ (*i.e.* 80 nm), on the other hand, tend to follow the movement of air masses and may travel long distances before being washed out by natural precipitation (rain, snow, mist) – a process that is called wet deposition. Particles of intermediate size range (*i.e.* 80-800 nm) exhibit behaviours that are influenced by a combination of these two deposition processes.^{25, 26} As a result, nano-scale particles are expected to dominate in natural precipitation samples, although the meteorological conditions, geographical location and natural terrain may likely affect the distribution of aerosols and their deposition pathways.²⁷

Soil. Urban and industrial pollution scenarios, including atmospheric deposition, as well as waste management practices (*e.g.* landfills, soil fertilization) and direct environmental discharge, render soil a vulnerable compartment to ENP contamination.^{3, 8} The transport of ENPs in soils is governed by the same physicochemical laws that dictate the behaviour of colloidal particles in saturated porous media and is affected by the physicochemical state of the particles.²⁰ As ENPs migrate through tortuous paths in soil, a portion of them might undergo (natural) physicochemical filtration as they interact with various surfaces.²⁸ Nonetheless, because ENPs are intentionally designed to be stable (via surface functionalization), some might successfully seep through granular soil structures and end up in groundwater systems, posing the risk of contaminating drinking water supplies. While tracking of these ENPs in soil and into groundwater systems is experimentally complex, some NPs are in fact known for their (direct) intentional use for groundwater remediation. For example, ENPs of zero-valent-iron (nZVI) are often employed²⁹ in large amounts (up to several tons per contamination site) for the *in situ* remediation of sub-surface environments contaminated with chlorinated organic solvents – despite the fact that environmental implications of these ENPs are largely unknown.

Aquatic media. Surface waters represent an important medium for the transport and transformation for ENPs, with rivers, ocean currents, and glaciers being the key global movers of (nano)particulates.²² As with soils and air, the exact contribution of ENPs in global waters is unclear, although they are estimated to constitute less than 1 % of total nanoparticulates, which primarily includes naturally occurring colloids (*e.g.* colloids released from deep-sea hydrothermal vents) and incidentally generated anthropogenic NPs.^{3, 30} ENPs are continually subject to physicochemical transformations, which affect their transport pathways in surface waters (**Fig. 1-1**). For example, ENPs that agglomerate will be subject to gravitational settling and will be partitioned into the sediment, whereas those that have high affinity to various biotic or abiotic surfaces may be lost by sorption.³¹ Indeed, due to their high surface energies, ENPs are naturally prone to interact with surfaces, which may also increase their probability to interact with biological species. When the conditions are conducive to their bioaccumulation, ENPs can be internalized by aquatic organisms and may eventually be excreted back in a new bio-transformed state.^{32, 33} ENPs that persist in their nano-forms may travel longer distances and may eventually migrate to soils or sediments. Sediments are considered³⁴ an important sink for the retention of NPs, which might be released back into water under appropriate conditions, *e.g.* water turbulence, changes in water chemistry. Furthermore, sea spray aerosols, primarily generated due to bursting waves and wind, may lead to transport of ENPs back to atmosphere and their subsequent cycling throughout the ecosystem.^{22, 35}

The transport pathways for the ENPs (**Fig. 1-1**) illustrate their presumed ubiquity and the inevitability of their interactions with biological species, including humans. With the growing industrialization, the importance of ENPs in global cycling will only rise, potentially leading to their enhanced bioaccessibility. In that context, data on the environmental concentrations of ENPs and their characterization by size, composition and origin are critical in order to perform reliable risk assessments.

1.1.4 Physicochemical transformations of ENPs

In the environment, ENPs may undergo transformations via physical, chemical, or biological processes that will affect their fate and behaviour. These processes are governed by the intrinsic properties of ENPs, including their size, composition, crystallinity, shape, coating, and surface charge, as well as the environmental conditions, including pH, ionic strength, temperature, redox conditions and presence of organic matter.³⁶ For example, owing to the biochemical complexity of natural aquatic environments – which often contain a multitude of inorganic or organic colloidal particles, dissolved organic matter, and ionic species – the interplay between ENPs and environmental constituents are complex, with an endless array of possible outcomes. While some ENPs may completely lose their nano-properties through dissolution into dissolved ionic species or agglomeration into larger particles, other modifications may be more subtle, such as changes to the surface coatings or transformations into different chemical species (*e.g.* via sulfidation).¹⁵ The fact that these processes may occur simultaneously, are often irreversible, and may vary in a space- and time-dependent manner, further highlights their importance in understanding ENP fate and hazard.

Agglomeration. Agglomeration (or aggregation) refers to formation of particle clusters and is one of the key processes dominating the ultimate fate of ENPs. While aggregation and agglomeration terms are often used interchangeably, this chapter will conveniently use the term agglomeration, which describes the formation of (loosely bound) particle clumps via weak physical forces (whereas aggregation results in more strongly bound particle assemblages).³⁷ Once in the environment, ENPs may undergo either homoagglomeration (*i.e.* agglomeration between ENPs) or heteroagglomeration (*i.e.* agglomeration between ENPs and other entities), although the latter is more common³⁸ due to the abundance of natural colloids and surfaces, such as clay minerals, Fe and Mn hydrous oxides, sediments, organic matter and extracellular polymeric substances (EPS).^{15,34} Agglomeration is fundamentally controlled by the number of collisions between two entities and the probability that these collisions will result in an attachment. As exhaustively laid out by Praetorius *et al.*³⁹, possible agglomeration

(aggregation) pathways even in a simple system (*e.g.* two particle populations) are numerous: the process fundamentally initiates with a dimer formation (*e.g.* an ENP and a colloid) and may continue with the formation of more complex multimeric species, with each species exhibiting a different transport behaviour or reactivity. Nonetheless, it is generally accepted that the fate and behaviour of ENPs is primarily dictated by that of the larger particulate matter that they attach to. For example, using experimental input values (for Rhine River), model simulations concluded that TiO₂ ENPs heteroagglomerating with large suspended particulates, are orders of magnitude more likely to partition into the sediments than remain in the overlying water.⁴⁰ This could imply reduced bioaccessibility of water-borne ENPs in the short-term; however, sediments may still later act as a reservoir for ENP release back into flowing water or a source for benthic organisms.⁴¹

Agglomeration: role of pH and ionic strength. Agglomeration is strongly influenced by environmental factors, such as pH, ionic strength, natural organic matter (NOM) and biological (living) systems.³⁶ For example, since TiO₂ ENPs are typically manufactured with a negative surface charge, a decrease in pH is shown to enhance their agglomeration (*i.e.* as they approach their point of zero charge (PZC)).⁴² Nonetheless, the effects of pH on ENPs may evolve, as particles develop new surface coatings over time with PZCs that are different from the original coating.¹⁷ Ionic strength is another key parameter regulating ENP stability, and its impact depends on electrolyte type and concentration. As predicted by the DLVO theory, increase in ionic strength promotes the agglomeration behaviour of ENPs, by driving the compression of electrical double layers and thus, favouring the attractive forces (*e.g.* Van der Waals) to overcome the (reduced) repulsive energy barrier. This phenomenon has been observed with many ENPs, including CuO/Cu⁴³, TiO₂^{44,45}, Ag^{46,47}, ZnO^{48,49}, and Au⁵⁰, in both aquatic systems and saturated porous media. Due to their high ionic strength, marine waters are indeed known to be conducive to the agglomeration of particles and their subsequent sedimentation.³¹ Agglomeration is particularly enhanced in the presence of divalent electrolytes (*e.g.* Ca²⁺, Mg²⁺) as compared to monovalent one (*e.g.* Na⁺, K⁺). This is because multi-valent cations are more effective in neutralizing (negative) surface charge and may also act as a bridge between particles.

Agglomeration: role of organic matter. In aqueous environments, be they surface waters or saturated porous media, ENPs are likely to interact with a variety of organic species, such as NOM and biological exudates. These macromolecules may modify the surface functionalization of the ENPs, thereby affecting their subsequent stability and transport behaviour. Sorption of NOM compounds⁵¹, such as fulvic acid and humic acid, is generally

known to confer stability to ENPs via electrostatic or steric stabilization. This is particularly relevant for NOMs of high-molecular weight, which preferentially sorb to ENPs, driven by their greater number (and variety) of active sites (*e.g.* functional groups) or hydrophobic interactive units (for hydrophobic interactions).⁵² Nonetheless, the co-presence of ENPs and NOM may not always lead to ENP stabilization, owing to other environmental factors. For example, NOM sorption on (negatively charged) ENPs is a pH-dependent process, with high pH environments shown to hinder this interaction by deprotonating the functional groups and increasing the magnitude of ζ -potential. Even following a successful sorption step, ENP-NOM units may still undergo particle agglomeration in high ionic strength media, through shrinking of electrical double layers around the units and/or formation of ion-NOM bridges. Furthermore, NOMs are sometimes shown to promote particle agglomeration under conditions where they can exert strong hydrophobic interactions.³¹

Surface bio-modification. In natural environments, ENPs are destined to interact with various biological systems, including unicellular and multicellular organisms, and subcellular components, as well as biological exudates, also known as extracellular polymeric substances (EPS). At a molecular level, these interactions occur with biomolecules, such as proteins, lipids, saccharides, and nucleic acids, driving the formation of “biomolecular corona” on ENP surfaces.⁵³ Corona formation is a continuously evolving process whereby biomolecules competitively adhere to ENP surfaces, resulting in two layers: primary “hard corona” (*i.e.* tightly bound, low dissociation) and secondary “soft corona” (*i.e.* loosely bound, in exchange with surrounding).⁵⁴ This process often starts with the adherence of the most abundant species, which are later substituted by species of higher affinity (if available). The overall composition of the corona in turn governs the agglomeration and transport behaviour of the ENPs, determining their biological or environmental fate. For example, in a biological fluid, protein corona composed of human serum albumin or immunoglobulin G was found⁵⁵ to enhance the stability of Ag and Au ENPs, whereas corona formed with fibrinogen protein caused rapid and irreversible aggregation of the ENPs. In a marine environment, periodic algal blooms, which are associated with the release of high concentrations of EPS, were shown⁵⁶ to stabilize Au ENPs for several days and hinder their rapid agglomeration, despite the high ionic strength of the medium. Likewise, Ellis *et al.*⁵⁷ attributed the stability and transformation dynamics of Ag ENPs, to seasonal variabilities observed in water chemistry and the biological activity of a surface water. In summary, the agglomeration of ENPs is strongly impacted by their interactions with organic constituents, whether they are degradation by-products (*i.e.* NOM) or biological molecules from living systems.

Chemical transformations. Transformation of ENPs via chemical processes is another important scenario that may govern their fate and ecotoxicity. These processes may include dissolution, oxidation, reduction, sulfidation and other photochemically or biologically mediated reactions, which are often initiated on the surface of ENPs and advance as dictated by the reaction kinetics and transport (*i.e.* diffusion) rate of the reactants.^{17, 58} Dissolution, sometimes involving oxidation (*e.g.* Ag⁰ to Ag⁺), may completely transform ENPs.⁵⁹ While some ENPs, such as Ag, ZnO and Cu/CuO, are inherently prone to dissolution at environmentally relevant conditions, others (*e.g.* TiO₂, SiO₂) are not easily soluble. Low ENP concentrations (*i.e.* ng L⁻¹), smaller particle sizes and lack of surface coating (*i.e.* bare) are often associated with enhanced dissolution.⁵⁸ Aerobic (*i.e.* dissolved O₂) and low pH conditions render dissolution thermodynamically favourable, particularly in biochemically rich matrices, where ligand-assisted dissolution is relevant.⁵⁹ For example, Ag ENP dissolution is shown to increase in the presence of environmental ligands, such as thiol-containing compounds (*e.g.* cysteine, glutathione)⁶⁰, chlorides⁴⁶, NOM (*e.g.* fulvic acid)⁶¹, EPS (*e.g.* algal exudates)⁵⁹ and bacterial biofilms³⁴. This is because surface-released ions (Ag⁺) can form complexes with ligands (*e.g.* Ag-cysteine, AgCl₄⁻³) that will drive the desorption of surface bound Ag⁺, thus favouring further particle dissolution (and oxidation) to restore the equilibrium. Soluble ENPs, and particularly ENPs made up of chalcophile elements, may also easily undergo sulfidation reaction to form metal sulfides.¹⁷ This has been demonstrated^{62, 63} with Ag, ZnO and CuO ENPs in wastewater systems, which tend to contain elevated sulfur concentrations.

Bio-mediated reactions. Biologically mediated reactions of ENPs in natural environments are also common.^{17, 34} For example, Au ENPs, while thermodynamically stable in simple media, have been shown⁶⁴ to completely biodissolve, following their interactions with a freshwater macrophyte and its associated microbiome. ENP-released dissolved species may sometimes undergo further transformations that can lead to emergence of new NP species. For example, Azodi *et al.*⁶⁵ revealed the formation of secondary (smaller) Ag NPs following the dissolution of Ag ENPs in a wastewater and the subsequent precipitation (via reduction) of the dissolved species. Similarly, secondary precipitation of dissolved Zn into ZnS NPs was observed in biofilms.³⁴ While TiO₂ ENPs are strongly resistant to redox, dissolution and sulfidation reactions and generally remain as aggregates, they may still undergo occasional alterations. For example, incineration processes are often associated with the transformation of TiO₂ ENPs into CaTiO₃ nanoparticles – likely owing to the original matrix of TiO₂ ENPs in nano-products, *e.g.* paint residues abundant with Ca.⁶⁶ TiO₂ ENPs are also known⁶⁷ to

participate in (unintentional) photochemical reactions that affect the environment (*i.e.* generates free radicals) without necessarily modifying the particle composition.

Atmospheric transformations. ENP transformation processes, such as coagulation, condensation, dissolution, and photo-induced reactions, are also ubiquitous in the atmosphere, ultimately affecting ENP deposition.⁶⁸ For example, coagulation is driven by the high diffusive (*i.e.* Brownian motion) potential of ENPs, with hetero-coagulation being more dominant over homo-coagulation (as in water). Condensation is a mechanism by which various inorganic or organic chemical species condense on particle surfaces and lead to particle growth (via either reaction or accumulation). Traditionally, sulfuric acid is thought to be the predominant constituent in condensation induced growth, with estimated growth rates between 1-10 nm h⁻¹; however, Wang *et al.*⁶⁹ recently discovered that nitric acid and ammonia induced particle growth rates that can well exceed 100 nm h⁻¹. This finding implies that small ENPs – despite their high diffusive potential and tendency to coagulate – can potentially undergo rapid growth, without necessarily being scavenged by other atmospheric aerosols (via coagulation). On the other hand, it is also known⁷⁰ that the airborne NPs are often subject to scavenging by rainfall, and this process depends on a combination of factors, including aerosol size, cloud-aerosol interactions, chemical reactions, mixing processes, and rainfall intensity and frequency. All of these atmospheric processes are indeed complex, involving physicochemical transformations that will alter the ultimate fate and toxicity of ENPs.

1.2 Determinations of ENPs in environmental matrices

1.2.1 Limitations of exposure models

Exposure models are considered an essential tool in predicting environmental concentrations of ENPs, which are critical to the regulatory risk assessment process. Although these models suffer a number of limitations, their importance is underscored when considering that experimental data on ENPs in real environmental media is very scarce, owing mainly to the analytical difficulties of their detection and quantification in complex matrices within a background of natural colloids. Existing exposure models can be divided into two categories: material flow analysis (MFA) and environmental fate models (EFM).⁷¹ While MFA models track material flows throughout the life-cycle of ENPs (*i.e.* production, manufacturing, use, disposal) and predict the release quantities into the environment, EFM models (often) use MFA predictions as an input to model subsequent transformations of ENPs and their distributions within various environmental compartments. Application of an exposure model to a system –

whether it is limited by boundaries of a country, a compartment, or the whole ecosystem – requires the specification of the basic modelling structure, including the mathematical approach (*e.g.* probabilistic or deterministic), time dynamics (*i.e.* static or dynamic) and parametrization.⁷² Parameterization represents a particularly decisive process, determining the overall reliability of the modelling results.

Main MFA parameters include ENP production volumes, allocation of ENP mass to product categories, product-release rates, and transfer factors to various technical compartments.¹⁷ Correct parametrization can potentially yield reliable modelling results; however, this is often complicated by the lack of lab/field generated experimental data or certified reports. For example, ENP production volumes are the primary determinant for ENP release, representing the maximum potential discharge; nonetheless, data on production volumes and their distribution in nano-products is near absent, with any available data often not making a distinction between nano and conventional forms of the corresponding chemicals. Determination of product-release rates, particularly under real weathering conditions, is critical since product release rates are extremely variable (*i.e.* up to several orders of magnitude) depending on the product matrix. For example, release rates of Ag ENPs from nano-enabled socks (*i.e.* near complete discharge after a few washes)⁷³ are estimated to be substantially greater than those of TiO₂ ENPs from surface coatings^{74, 75} – although only few experimental data are available on the latter. Once ENPs are released into environmental compartments, their subsequent transfer and persistence rates are also mostly unknown. Similarly, EFM models often utilize input parameters that are based on assumptions of transformation (*e.g.* agglomeration, dissolution) or transfer coefficients determined from oversimplified systems.^{71, 76} Consequently, model parametrization is often performed using simplified assumptions, extrapolations, expert opinions, uncertified reports, or best guesses, which cumulatively increase the overall uncertainty of the modelling results.

Recent emergence of time-sensitive models that attempt to capture “delayed” ENP release patterns due to product storage⁷² or size-specific probabilistic (dynamic) models⁷⁷, represent significant progress towards reliable modelling. Nonetheless, models are still inherently vulnerable to generalization, since they are likely to overlook (i) the complexity of transformation or transport patterns; (ii) the time-sensitivity of input parameters, (iii) the role of geo-specific factors, *e.g.* scale, terrain, weathering; and (iv) the occurrences of episodic events or localization of emission impact (*e.g.* via natural barriers, on macroscopic or microscopic scale). Reliable risk assessments will therefore require temporally and spatially resolved analytical data on the concentrations, compositions and origins (*i.e.* anthropogenic or

natural) of NPs in the environment. These experimental data can then be used to (i) reliably determine modelling (input) parameters, (ii) validate modelling results, or (iii) directly assess the environmental risk of ENPs on local, regional or global scales.

1.2.2 Analytical measurements of ENPs: challenges and opportunities

The detection, quantification, and characterization of ENPs in complex environmental matrices is critical to their reliable risk assessment. While an array of powerful analytical tools is available for NP characterization, ENP determinations in natural media are still a challenging task.⁷⁸ This is primarily because ENPs are very small objects (*i.e.* <100 nm) that generally occur at very low concentrations (*i.e.* ng L⁻¹), against a complex background of inorganic/organic colloids and particulates, dissolved ions and molecules, natural organic matter, biological exudates, and living species.⁷⁹ Accurate measurements of ENPs thus often require their particle-by-particle discrimination from naturally occurring colloids, which often have similar compositions and sizes. For example, environmental matrices are typically abundant with naturally occurring Ti-containing minerals, such as ilmenite, brookite, rutile and anatase, at concentrations that far exceed those of the TiO₂ ENPs. In this case, successful analysis of the ENPs cannot be made solely on the basis of size, but requires information on their chemical compositions, which can be used to fingerprint particles of different origins.

Most analytical techniques, unfortunately, are prone to a number of limitations, which will either render ENP analysis impossible or severely degrade the quality and accuracy of the measurements. These limitations will vary depending on the operating principle of the analytical technique. For example, although rapid and non-invasive analysis can be performed using light scattering techniques, such as dynamic light scattering (DLS) or nanoparticle tracking analysis (NTA), these techniques are not suitable for complex natural matrices, where colloids are often highly polydisperse.⁸⁰ This is because these techniques that derive size distributions based on light scattering often scatter light with an intensity that is proportional to their hydrodynamic diameter to the sixth power (d_H^6) – the presence of large colloids or aggregates will mask the signal of smaller particles (*e.g.* ENPs).⁸¹ The lack of chemical specificity limits the application of these techniques to simple systems with known constituents only. Furthermore, while the microscopic techniques such as transmission electron microscopy (TEM), scanning electron microscopy (SEM) and atomic force microscopy (AFM), can offer a wealth of information on ENPs, including size, crystallinity, morphology, shape and coating, with spatial resolutions down to 1 nm, these analyses are generally labor-intensive, often requiring complex sample preparation processes (*e.g.* drying, coating) and measurement

conditions (*i.e.* vacuum for TEM).⁸⁰ This in turn renders the monitoring process low-throughput and likely introduces artefacts (*e.g.* via agglomeration during sample drying) that will adversely impact the accuracy and representivity of the measurements – particularly, in natural samples, where ENP occurrences are already low (*i.e.* low concentrations or spatially localized). TEM and SEM are often equipped with energy-dispersive x-ray spectroscopy (EDX), which allow them to probe the elemental compositions of materials.⁸⁰ Nonetheless, the capabilities of even advanced microscopy are generally still insufficient for high-throughput element-specific quantification of ENPs, while quantitatively discriminating them from natural colloids.

Chromatographic approaches, such as hydrodynamic chromatography⁸² or field-flow fractionation (FFF)⁸³, can also be applied to the separation of NPs by their (hydrodynamic) size, prior to their chemical or size identification with an on-line or off-line detector system. FFF is by far the most widely used fractionation approach, with the method of asymmetric flow-FFF (A-F4) being particularly common. While this technique is applicable to colloids of a wide spectrum of sizes (nano to micro), the optimization process is time-consuming, requiring fine-tuning of several parameters, including carrier flow, carrier composition, and membrane chemistry.⁸⁴ These parameters are also dependent on the type of ENPs and their surface properties as well as their matrix of origin, further compounding the optimization process. Consequently, use of A-F4 is often complex for the routine analysis of ENPs in natural media. Furthermore, as FFF systems are pre-fractionation techniques only, their utility is still, to a large extent, determined by the detector system⁷⁹ – be it a particle counter, imaging tool or chemical analyzer – and its capability to resolve ENPs among other colloids is presently limited.

An ideal technique for environmental monitoring of ENPs will exhibit high speed, (chemical) specificity, and sensitivity, while enabling high-throughput measurements and requiring no or simple sample pre-treatment. To this end, inductively coupled plasma mass spectrometry (ICP-MS) is a promising technique, due to its powerful capabilities in rapid chemical/isotopic analysis and metal quantification, with sensitivities that enable ultra-trace (*i.e.* down to pg L^{-1}) determinations.⁸⁵ Notably, operation of ICP-MS in a single-particle mode (SP-ICP-MS) offers opportunities that are well-suited to the characterization of NPs, enabling their discrimination from dissolved metals and providing data on particle size distributions and particle mass/number concentrations.⁸⁶ In particular, recent innovations with time-of-flight SP-ICP-MS that offer simultaneous multi-element analysis capabilities, have revolutionized nanoanalytics, making it possible to estimate the origin of the NPs on a particle-by-particle

basis.⁸⁷ While SP-ICP-MS systems still suffer from limitations, such as matrix interferences in complex waters, it is nonetheless emerging as a technique of choice for (environmental) nanogeochemical analysis.

1.2.3 ICP-MS: history and background

The first use of an ICP source combined with a mass spectrometer (MS) dates back to 1980 by R.S. Houk⁸⁸, whose work led to the first paper on ICP-MS. In 1983, the first commercial ICP-MS was introduced by Sciex Ltd, with other companies following suit shortly afterwards.⁸⁹ ICP-MS quickly became the primary tool for trace metal determinations in complex matrices, owing to its appealing features, which included robustness, high specificity (*i.e.* isotopic discrimination), wide linear dynamic range, high sensitivity, rapid analysis, and high sample throughput. Early ICP-MS instruments were only based on quadrupole mass analyzers and have low mass resolutions and poor limits of detection as compared to sector-field ICP-MS, which were introduced in 1989.⁸⁵ Nowadays, ICP-MS is routinely being used – by government institutions and private industries – in testing of food, pharmaceuticals, consumer products, raw materials, environmental and biological samples for design, manufacturing, diagnostic or quality control purposes.

The possibilities of hyphenating ICP-MS with other techniques, in an on-line or off-line regime, further enhances its capabilities. Until the 2000s, this strategy was particularly advantageous for the characterization of colloids, because it enabled size fractionation of the particles using filtration, ultracentrifugation or chromatographic approaches, prior to their chemical analysis with ICP-MS.⁹⁰ While the hyphenation approach was able to provide element-specific quantification for different size ranges, it suffered several shortcomings, including low reliability of size cut-offs, low size resolution (*i.e.* actual size ranges are large), lack of particle number information, and introduction of artifacts. The development of SP-ICP-MS was a breakthrough in addressing these shortcomings, since it enabled particle determinations by size and quantity (*i.e.* mass or number), without requiring coupling to a secondary system. Although the basic principles of SP-ICP-MS were first established⁹¹ by Degueldre and Favarger in 2003, early instrumentation suffered from technical limitations, such as poor sampling rates and lack of continuous signal acquisition, which greatly complicated the reliable analysis of the smallest colloids (*i.e.* nano-range). In the following years, nanoanalytics with SP-ICP-MS experienced an accelerated growth, driven by increasing awareness of expanding uses of ENPs and the associated need for their analytical detection. In

the 2010s, single particle analysis notably benefited from instrumental innovations, such as triple quadrupole ICP-MS systems⁹², which are better equipped to cope with matrix interferences; high sensitivity/resolution sector-field systems with continuous ultra-fast sampling rates (every 10 μ s)⁹³; and purpose-built ICP-TOF-MS systems for multi-element analysis of particles⁹⁴.

1.2.4 ICP-MS: technical description and types of instrumentation (analyzer)

Working principle. ICP-MS consists of a sample introduction system, ion excitation source (*i.e.* ICP plasma), plasma-vacuum interface, mass analyzer (*e.g.* quadrupole) and ion detector, with the precise technical components depending on the nature of the instrument (*e.g.* quadrupole vs sector-field vs time-of-flight).⁹⁵ Typically, a liquid sample is introduced via a peristaltic pump. It then passes through a nebulizer, which generates a fine mist of aerosol (using an argon stream) into a spray chamber, which removes the largest droplets and can help dampen possible flow rate variations caused by the pump.⁹⁶ Fine aerosols are then transported into a high-energy plasma, which is generated and maintained with an oscillating radiofrequency (RF) magnetic field and a continuous argon stream. Plasma temperatures may reach 10,000 K with conditions that are conducive to the instantaneous (*i.e.* few milliseconds) desolvation, dissociation, atomization and ionization of aerosols.⁹⁷ Ionized species then pass through an interface region, which often consists of two cones (sampler and skimmer). The goal is to cleanly extract ions from the plasma (*i.e.* atmospheric pressure) into a vacuum compartment (*i.e.* mass analyzer). The design of the interface system facilitates the preferential sampling of the analyte-rich central portion of the plasma, while excluding most of the Ar atoms. The pressure differential across the cones drives the transmission of the ions into the mass spectrometer, passing through an ion lens optics, which focuses the ion beam while removing undesired neutral or negatively charged species.⁹⁵

Quadrupole. Three types of mass analyzers are currently employed for commercial ICP-MS systems: quadrupole, sector-field, and time-of-flight. The quadrupole mass analyzer, which is by far the most widely used one, features four parallel cylindrical rods that exert an electrostatic field (induced by RF and DC voltages) and control the separation of ions based on their mass-to-charge (m/z) ratios.⁹⁸ That is, with a given combination of voltages, only species with a specific m/z can reach the detector, while the rest are ejected due to their unstable trajectories. Nonetheless, due to their low mass resolving powers ($m/\Delta m \sim 300$), quadrupole instruments are often vulnerable to interferences resulting from species that exhibit m/z values

that are same as the target analyte (*e.g.* $m/z = 48$ (Ti) for $^{48}\text{Ti}^+$, $^{48}\text{Ca}^+$ and $^{32}\text{S}^{16}\text{O}^+$).⁹⁹ Hence, these instruments are typically equipped with a collision/reaction cell technology (between ion optics and MS), which enable the partial or complete removal of the interfering ions (and often the analyte ion of interest). For example, in a collision cell, polyatomic interferences are preferentially removed by collision with He (single element analyte ions collide less frequently). Another popular approach is employing ion-molecule reaction schemes (reaction cell) to shift the m/z of the analyte ion such that it can be detected without interferences (or the interfering ion so that it no longer interferes).¹⁰⁰ Nonetheless, these interventions are often difficult to perform during NP analysis, as they may compromise sensitivity (*i.e.* lesser ion transmission), effectively raising detection limits.

Sector-field. Sector-field instruments utilize magnetic fields to separate and focus a beam of ions of a given m/z (through a slit) to the detector. These instruments typically offer higher (~ 10 - $20\times$) ionic sensitivities, when run at low resolution. They also exhibit high mass resolving powers ($m/\Delta m$ up to 13,000), which allows them to resolve even isobaric interferences (*e.g.* ^{48}Ti from ^{48}Ca).⁹³ Nonetheless, the high mass resolution is obtained at the expense of reducing the ion beam transmission (*i.e.* via reducing entrance slit width), which causes a decrease in sensitivity. Therefore, in some cases, measurements can be performed at a low-resolution/high-sensitivity mode, using low-abundant isotopes with lesser interferences (*e.g.* ^{49}Ti as opposed to ^{48}Ti), that would otherwise be immeasurable with other ICP-MS systems.¹⁰¹ Overall, these features offer flexible solutions for the analysis of ENPs in a wide variety of natural matrices.

Time-of-flight. Time-of-flight (TOF) provides the capability for (quasi) simultaneous analysis of the whole elemental mass spectrum (7-250 amu), which provides some advantages for SP-ICP-MS and laser ablation ICP-MS.¹⁰² Its operation relies on acceleration of ions with uniform kinetic energies in a flight tube, where lighter ions (*i.e.* lower m/z) travel at faster velocities, and therefore, arrive the detector earlier than the heavier isotopes do. Isotopes are then identified on the basis that each m/z corresponds to a unique time of flight. It would take less than 50 μs for the heaviest ions to travel through a flight tube of 1 m. This translates to a capacity of about 33,000 mass spectra per second⁸⁷ (*i.e.* 33 kHz or 30 μs per acquisition) in the commercial instruments, although the number of extractions can be increased by restricting the mass range of analysis. At these sampling rates, however, traditional TOF instruments are unable to cope with the continuous stream of data and are forced to sum up many spectra prior to processing isotope counts. This effectively yields data reporting on the order of milliseconds

(*i.e.* minimum of 1-3 ms), while the duration of a single NP event should last much less, only ~200-500 μs .¹⁰³ As a result, NP measurements made with TOF ICP-MS may suffer from poor particle size detection limits and inaccurate size determinations. Recent developments in TOF instrumentation have addressed these shortcomings, enabling uninterrupted data streaming at sub-100 μs acquisition rates.

1.2.5 Single particle ICP-MS: operating principle and theory

Operating principle. SP-ICP-MS is emerging as an essential tool for direct determinations of ENPs in the environment, providing data on their particle mass/size distributions, particle number concentrations and dissolution. Its growing appeal is underpinned by the fact that it can utilize already available ICP-MS instrumentation without hardware modifications.⁸⁵ Nonetheless, the quality of the NP measurements, notably size detection limits, will vary depending on the technical parameters of the system.

SP-ICP-MS discriminates NP species from an ionic background, based upon their spatiotemporal distributions in the plasma, following the vaporization, atomization, and ionization of the aerosols.¹⁰⁴ In this process, NPs generate dense packets of ions that are discrete in space and time. The ion packets register as short bursts of signal spikes (upon hitting the detector), which can be distinguished from the continuous background signal that results from dissolved species or interferences. While the temporal duration of a NP-induced spike event is often between 200-500 μs ,¹⁰⁵ state-of-the-art SP-ICP-MS systems have ultrafast acquisition times (dwell times), as short as 10 μs ⁹³ for a single acquisition. These high acquisition rates enable a high-resolution temporal profiling of the NP spikes and the quantification of (integrated) ion counts corresponding to each spike. In simultaneous multi-isotope analysis (*i.e.* ICP-TOF-MS), NPs of multi-element compositions generate multiple spikes that overlap on the time trace (*e.g.* overlapping spikes of ¹³⁷Ba and ⁴⁸Ti arise from BaTiO₃ NPs).⁹⁴ Spike intensity (*i.e.* ion count per NP) can then be linked to NP mass and hence its size (assuming particle shape and density), while the frequency of the spikes is used to determine particle number concentrations.¹⁰⁶ Accurate sizing and quantification of NPs requires a calibration approach that can determine both particle transport efficiency (TE) and ionic sensitivity of the instrument.

Theory. Ionic sensitivity indicates the number of ion counts generated as a signal from a certain concentration/mass of the analyte. Thus, when measured signal intensities (cps) are

plotted against the respective concentrations of the ionic standards (ng L^{-1}), the slope would represent the sensitivity, S (cps L ng^{-1}). TE (%) is defined as the fraction of an aspirated sample that successfully reaches the detector and is measured to account for a series of losses that occur at the nebulization, ionization, ion extraction and ion transfer stages.¹⁰⁷ The most notable losses occur at the nebulization stage, whereby only a small fraction of the sample (*e.g.* often 3-6 %) passes on to the plasma. A popular approach to determine TE is by measuring a stable NP suspension with known particle number concentrations (*i.e.* particle frequency method) or by using expected particle sizes (*i.e.* size method).¹⁰⁶ For example, the TE can be measured using a stable Au NP suspension with a known particle number concentration of C_{NP} (μL^{-1}) at an aspiration rate of Q ($\mu\text{L s}^{-1}$). Given that during an acquisition time of t (s), the number of detected NP events is N_{det} , TE can be calculated as:

$$TE = \frac{N_{det}}{C_{NP} \times Q \times t} \quad (1)$$

Then, sensitivity can be normalized with respect to mass (*i.e.* S_m , counts fg^{-1}) as following:

$$S_m = \frac{S}{TE \times Q} \quad (2)$$

Integration of counts for a NP, followed by its background subtraction will yield a net NP intensity of I_{NP} (counts), which can be used to calculate the NP mass (m_{NP} , fg) assuming an analyte (mass) fraction of f_m .

$$m_{NP} = \frac{I_{NP}}{S_m \times f_m} \quad (3)$$

Given a particle density of ρ_{NP} (g cm^{-3}), NP volume (V_{NP} , nm^3) will correspond to

$$V_{NP} = \frac{10^6 \times I_{NP}}{\rho_{NP} \times S_m \times f_m} \quad (4)$$

Under the assumption of a spherical shape, particle diameter (D_{NP} , nm) can be calculated for the NP:

$$D_{NP} = \left(\frac{6 \times 10^6 \times I_{NP}}{\pi \times \rho_{NP} \times S_m \times f_m} \right)^{\frac{1}{3}} \quad (5)$$

Likewise, Equation (5) can be modified to determine the size detection limit, SDL (D_{SDL} , nm), by substituting I_{NP} with I_{TL} (counts), which stands for detection threshold limit.

$$D_{SDL} = \left(\frac{6 \times 10^6 \times I_{TL}}{\pi \times \rho_{NP} \times S_m \times f_m} \right)^{\frac{1}{3}} \quad (6)$$

In SP-ICP-MS, any signal intensity that exceeds this defined threshold, I_{TL} , indicates a particle event; the signal below this threshold is attributed to dissolved analyte, interferences and/or smaller (undetected) NPs.¹⁰⁸ Definition of the detection threshold, I_{TL} , may rely on various statistical approaches, such as (iterative) mean and standard deviation analysis¹⁰⁹, compound Poisson statistics¹⁰⁸, and k-means clustering¹¹⁰. Furthermore, advanced peak recognition algorithms are recently developed⁹³ that can detect NP peaks based on their inflection points and assign I_{TL} values that vary as a function of local (NP) background. In all cases, I_{TL} is directly proportional to the concentration of background interferences (I_{BG}) (*i.e.* $I_{TL} = f(I_{BG})$). In view of Equation (6), it then becomes clear that SDLs can be improved (*i.e.* reduced) either via technical improvements to the sensitivity of the instrument (*i.e.* increase S_m) or by reducing background interferences (*i.e.* decrease I_{BG}). Understanding interferences that are relevant to the target analyte is thus critical to an accurate quantification and sizing of NPs.

1.2.6 Single particle ICP-MS: background interferences and SDLs

Interferences. Accurate detection and quantification of NPs requires reliable discrimination of the NP signal from that of the background. While this discrimination is generally straightforward for large NPs, it becomes increasingly complex for smaller NPs, owing to lower signal-to-background ratios. When dissolved analyte is abundant – a case that is particularly relevant for easily soluble NPs (*e.g.* ZnO, CuO, Ag) – experimental approaches, such as sample dilution, NP separation^{82, 83} or ion-exchange purification^{111, 112}, can be employed to reduce this dissolved content. Resolving or removing interferences is even more complex, because each isotope, interference type and concentration varies with respect to the matrix type and plasma conditions.¹¹³ While matrix-induced signal alterations, also known as non-spectral interferences, do not directly increase the background noise, they still impact the accuracy of NP detection by suppressing or enhancing the measured signal.¹¹⁴ For example, the presence of a complex matrix of high ionic strength, such as found in seawater, is likely to suppress the signal intensities, due to the abundance of other highly ionizable metals which reduce the analyte ionization, as well as space-charge effects.¹¹³ In many cases, sample dilution is sufficient for overcoming these interferences; however, if dilution is deemed impractical, matrix-matched calibration¹¹⁵, isotope dilution¹¹⁶, the use of internal standards¹¹⁷, or the

simultaneous introduction of the analyte and calibrant (*e.g.* with ICP-TOF-MS)¹¹⁴ may offer potential solutions.

Spectral interferences arise when various atomic or polyatomic species exhibit the same *m/z* as the analyte of interest.¹¹³ Polyatomic interferences (**Table 1-1**) can be catalogued as argon-based (*e.g.* $^{40}\text{Ar}^{16}\text{O}^+$ interferes with $^{56}\text{Fe}^+$) or matrix-based (*e.g.* $^{12}\text{C}^{16}\text{O}^+$ interferes with $^{28}\text{Si}^+$), while isobaric (atomic) interferences may occur in singly charged or, less commonly, doubly charged forms (*e.g.* $^{48}\text{Ca}^+$ and $^{96}\text{Zr}^{2+}$ interferes with $^{48}\text{Ti}^+$). Spectral interferences are particularly detrimental to NP analysis, often being a dominant contributor to the background noise for natural samples. To reduce this noise, several strategies can be adopted, with the most common being the use of collision or reaction cells, which enable the preferential removal of the interfering species over the analyte via kinetic energy discrimination or targeted reaction schemes (*e.g.* with single/triple quadrupole ICP-MS).¹⁰⁰ Another approach is the physical resolution of interferences using a sector-field ICP-MS. While both chemical and physical resolution approaches are effective in reducing spectral interferences, they are often achieved at the expense of a significant loss in sensitivity. This consequently does not lead to substantial improvements of the SDLs, especially given that the NP mass is related to its diameter via a cubic relationship, *i.e.* a 2x improvement to an SDL would require 8x gain in mass sensitivity. Sample dilution, while often useful, does not necessarily guarantee an adequate drop in background noise; furthermore, too much dilution may require a proportionate increase in data acquisition time, which is often impractical.

Table 1-1 Spectral interferences observed in ICP-MS for isotopes of select metals. The table is adapted from May and Wiedmeyer (1998)⁹⁹.

Isotope	Abundance (%)	Potential interference
^{28}Si	92.21	$^{14}\text{N}_2^+$, $^{12}\text{C}^{16}\text{O}^+$
^{29}Si	4.7	$^{14}\text{N}^{15}\text{N}^+$, $^{14}\text{N}_2^1\text{H}^+$, $^{13}\text{C}^{16}\text{O}^+$, $^{12}\text{C}^{17}\text{O}^+$, $^{12}\text{C}^{16}\text{O}^1\text{H}^+$
^{46}Ti	7.99	$^{32}\text{S}^{14}\text{N}^+$, $^{14}\text{N}^{16}\text{O}_2^+$, $^{15}\text{N}_2^{16}\text{O}^+$
^{47}Ti	7.32	$^{32}\text{S}^{14}\text{N}^1\text{H}^+$, $^{30}\text{Si}^{16}\text{O}^1\text{H}^+$, $^{32}\text{S}^{15}\text{N}^+$, $^{33}\text{N}^{14}\text{N}^+$, $^{33}\text{S}^{14}\text{N}^+$, $^{15}\text{N}^{16}\text{O}_2^+$, $^{14}\text{N}^{16}\text{O}_2^1\text{H}^+$, $^{12}\text{C}^{35}\text{Cl}^+$, $^{31}\text{P}^{16}\text{O}^+$
^{48}Ti	73.98	$^{32}\text{S}^{16}\text{O}^+$, $^{34}\text{S}^{14}\text{N}^+$, $^{33}\text{S}^{15}\text{N}^+$, $^{14}\text{N}^{16}\text{O}^{18}\text{O}^+$, $^{14}\text{N}^{17}\text{N}_2^+$, $^{12}\text{C}_4^+$, $^{36}\text{Ar}^{12}\text{C}^+$
^{49}Ti	5.46	$^{32}\text{S}^{17}\text{O}^+$, $^{32}\text{S}^{16}\text{O}^1\text{H}^+$, $^{35}\text{Cl}^{14}\text{N}^+$, $^{34}\text{S}^{15}\text{N}^+$, $^{33}\text{S}^{16}\text{O}^+$, $^{14}\text{N}^{17}\text{O}_2^1\text{H}^+$, $^{14}\text{N}^{35}\text{Cl}^+$, $^{36}\text{Ar}^{13}\text{C}^+$, $^{36}\text{Ar}^{12}\text{C}^1\text{H}^+$, $^{12}\text{C}^{37}\text{Cl}^+$, $^{31}\text{P}^{18}\text{O}^+$
^{50}Ti	5.25	$^{32}\text{S}^{18}\text{O}^+$, $^{32}\text{S}^{17}\text{O}^1\text{H}^+$, $^{36}\text{Ar}^{14}\text{N}^+$, $^{35}\text{Cl}^{15}\text{N}^+$, $^{36}\text{S}^{14}\text{N}^+$, $^{33}\text{S}^{17}\text{O}^+$, $^{34}\text{S}^{16}\text{O}^+$, $^1\text{H}^{14}\text{N}^{35}\text{Cl}^+$, $^{34}\text{S}^{15}\text{O}^1\text{H}^+$
^{56}Fe	91.66	$^{40}\text{Ar}^{16}\text{O}^+$, $^{40}\text{Ca}^{16}\text{O}^+$, $^{40}\text{Ar}^{15}\text{N}^1\text{H}^+$, $^{38}\text{Ar}^{18}\text{O}^+$, $^{38}\text{Ar}^{17}\text{O}^1\text{H}^+$, $^{37}\text{Cl}^{18}\text{O}^1\text{H}^+$
^{57}Fe	2.19	$^{40}\text{Ar}^{16}\text{O}^1\text{H}^+$, $^{40}\text{Ca}^{16}\text{O}^1\text{H}^+$, $^{40}\text{Ar}^{17}\text{O}^+$, $^{38}\text{Ar}^{18}\text{O}^1\text{H}^+$, $^{38}\text{Ar}^{19}\text{F}^+$
^{58}Fe	0.33	$^{40}\text{Ar}^{18}\text{O}^+$, $^{40}\text{Ar}^{17}\text{O}^1\text{H}^+$
^{107}Ag	51.8	$^{91}\text{Zr}^{16}\text{O}^+$

¹⁰⁹ Ag	48.2	⁹² Zr ¹⁶ O ¹ H ⁺
¹⁹⁷ Au	100	¹⁸¹ Ta ¹⁶ O ⁺
¹⁵¹ Eu	47.82	¹³⁵ Ba ¹⁶ O ⁺
¹⁵³ Eu	52.2	¹³⁷ Ba ¹⁶ O ⁺

SDLs in the literature. SDLs will vary substantially for different NPs, depending on the analyzed isotope and its natural abundance, matrix-specific interferences, and technical parameters of the instrumentation. **Table 1-2** displays typical SDLs observed for a few major NPs in various water matrices as measured by different ICP-MS systems. For example, using single quadrupole ICP-MS, SDLs reported for TiO₂ NPs were often above 60-100 nm, whereas SDLs for Ag, Au and CeO₂ NPs typically ranged between 15-40 nm. Despite the capabilities of ICP-TOF-MS in multi-element analysis, these instruments often exhibited even poorer SDLs, owing to their lower sampling/acquisition rates (per isotope), which results in loss of quality for NP peaks (*i.e.* less resolved). In natural matrices, Ca, S, N and O (*i.e.* S-N, S-O, C-O polyatomic interferences) are often abundant, rendering the analysis of NPs, such as TiO₂ and SiO₂, particularly complex.¹¹⁸ In addition, SDLs are further elevated when multi-element nature of particles are considered (*e.g.* SDL is higher for FeTiO₃ than TiO₂). In this context, the incentive for improving SDLs is extremely high, as it would allow for determinations of increasingly smaller NPs, which are likely to be of greatest environmental risk.

Table 1-2 Size detection limits observed for TiO₂, CeO₂, Ag and ZnO NPs as measured by SP-ICP-MS systems in various matrices. Q, SF and TOF, respectively, refer to quadrupole, sector-field and time-of-flight ICP-MS, while IEC indicate coupling to an ion-exchange column for removal of dissolved ions (*e.g.* Ag⁺, Zn²⁺).

NP	Year	Water matrix	Mass filter	Isotope	Dwell time (μs)	SDL (nm)	Reference
TiO ₂	2014	River	Q	⁴⁷ Ti ⁺	10,000	130	Gondikas <i>et al.</i> ¹¹
	2016	River	Q	⁴⁷ Ti ⁺	100	70	Donovan <i>et al.</i> ¹¹⁹
	2017	Creek	Q	⁴⁹ Ti ⁺	3,000	79	Reed <i>et al.</i> ¹²⁰
	2017	Creek	SF	⁴⁸ Ti ⁺	3,000	42	Reed <i>et al.</i> ¹²⁰
	2017	River	Q	⁴⁷ Ti ⁺	100	64	Londono <i>et al.</i> ¹²¹
	2018	River / lake	Q	⁴⁷ Ti ⁺	100	70	Donovan <i>et al.</i> ¹²²
	2018	River	TQ	⁶³ TiNH ⁺	4,000	81	Gondikas <i>et al.</i> ¹²³
	2018	River	Q	⁴⁸ Ti ⁺	3,000	100	Peters <i>et al.</i> ¹²⁴
	2018	River / pool	Q	⁴⁹ Ti ⁺	10,000	148-173	Venkatesan <i>et al.</i> ¹²⁵
	2019	Sewage	TOF	⁴⁸ Ti ⁺	-	>100	Loosli <i>et al.</i> ¹²⁶
	2019	Pool / rain	SF	⁴⁹ Ti ⁺	50	12	Hadioui <i>et al.</i> ¹⁰¹
	2020	River	SF	⁴⁷ Ti ⁺	1,000	>80	Phalyvong <i>et al.</i> ¹²⁷
	2020	River	Q	⁴⁹ Ti ⁺	100	48	Rand <i>et al.</i> ¹²⁸

	2021	River	SF	$^{47}\text{Ti}^+$	1,000	>60	Phalyvong <i>et al.</i> ¹²⁹
	2021	Wastewater	Q	$^{47}\text{Ti}^+$	50	71	Nabi <i>et al.</i> ¹³⁰
	2021	Wastewater	TOF	$^{47}\text{Ti}^+$	2,020	105-110	Mehrabi <i>et al.</i> ¹³¹
CeO₂	2016	River	Q	$^{140}\text{Ce}^+$	100	18-20	Donovan <i>et al.</i> ¹³²
	2017	Soil extract	TOF	$^{140}\text{Ce}^+$	-	15-18	Praetorius <i>et al.</i> ⁸⁷
	2018	River / lake	Q	$^{140}\text{Ce}^+$	100	23	Donovan <i>et al.</i> ¹²²
	2018	River	Q	$^{140}\text{Ce}^+$	100	10	Peters <i>et al.</i> ¹²⁴
	2020	River / rain	Q	$^{140}\text{Ce}^+$	500	16.8	Jreije <i>et al.</i> ¹³³
	2020	River / rain	SF	$^{140}\text{Ce}^+$	50	2.3	Jreije <i>et al.</i> ¹³³
	2020	River / rain	TOF	$^{140}\text{Ce}^+$	76.5	15	Jreije <i>et al.</i> ¹³³
	2020	Algal medium	SF	$^{140}\text{Ce}^+$	50	<8	Morel <i>et al.</i> ¹³⁴
	2020	River	SF	$^{140}\text{Ce}^+$	1,000	24	Phalyvong <i>et al.</i> ¹²⁷
	2021	River	SF	$^{140}\text{Ce}^+$	1,000	5	Phalyvong <i>et al.</i> ¹²⁹
	2021	Wastewater	TOF	$^{140}\text{Ce}^+$	2,020	25-30	Mehrabi <i>et al.</i> ¹³¹
Ag	2013	Milli-Q	IEC-Q	$^{107}\text{Ag}^+$	3,000	>20	Hadioui <i>et al.</i> ¹³⁵
	2014	Lake	Q	$^{107}\text{Ag}^+$	10,000	30	Furtado <i>et al.</i> ¹³⁶
	2014	Tap / surface water	Q	$^{107}\text{Ag}^+$	10,000	30	Mitrano <i>et al.</i> ¹³⁷
	2014	Milli-Q	IEC-Q	$^{107}\text{Ag}^+$	1,000	15	Hadioui <i>et al.</i> ¹¹¹
	2014	Wastewater / river	Q	$^{107}\text{Ag}^+$, $^{109}\text{Ag}^+$	5,000	40	Telgmann <i>et al.</i> ¹³⁸
	2016	Lake	Q	$^{107}\text{Ag}^+$, $^{109}\text{Ag}^+$	5,000	24	Jimenez-Lamana <i>et al.</i> ¹³⁹
	2016	Wastewater / river	Q	$^{107}\text{Ag}^+$	100	24	Proulx <i>et al.</i> ⁸²
	2016	Milli-Q	Q	$^{107}\text{Ag}^+$	5,000	40	Telgmann <i>et al.</i> ¹⁴⁰
	2017	Wastewater	Q	$^{107}\text{Ag}^+$	500	17	Azimzada <i>et al.</i> ⁵⁹
	2017	Milli-Q / lake	Q	$^{107}\text{Ag}^+$	5,000	40	Martin <i>et al.</i> ¹⁴¹
	2017	WWTP mesocosm	SF	-	100	5.4-40	Tuoriniemi <i>et al.</i> ¹⁴²
	2018	River / lake	Q	-	100	25	Donovan <i>et al.</i> ¹²²
	2018	Lake	SF	$^{107}\text{Ag}^+$	50	12	Martin <i>et al.</i> ¹⁴³
	2018	Tap / river / wastewater	Q	$^{107}\text{Ag}^+$	3,000	20	Luo <i>et al.</i> ¹⁴⁴
	2018	River	Q	$^{107}\text{Ag}^+$	3,000	14	Peters <i>et al.</i> ¹²⁴
	2019	Pool / rain	SF	$^{107}\text{Ag}^+$	50	3.5	Hadioui <i>et al.</i> ¹⁰¹
	2020	River	Q	-	50	18	Loosli <i>et al.</i> ¹⁴⁵
	2021	Wastewater	Q	$^{107}\text{Ag}^+$	50	21	Nabi <i>et al.</i> ¹³⁰
	2021	Wastewater	TOF	$^{107}\text{Ag}^+$	2,020	20	Mehrabi <i>et al.</i> ¹³¹
	ZnO	2015	River	IEC-Q	$^{66}\text{Zn}^+$	500	70
2016		River	Q	$^{67}\text{Zn}^+$	100	35-40	Donovan <i>et al.</i> ¹³²
2017		River	Q	$^{66}\text{Zn}^+$	100	43	Londono <i>et al.</i> ¹²¹
2019		River / rain	IEC-SF	$^{66}\text{Zn}^+$	50	14.3-17.7	Frechette-Viens <i>et al.</i> ¹¹²
2021		Wastewater	TOF	$^{66}\text{Zn}^+$	2,020	100	Mehrabi <i>et al.</i> ¹³¹

The use of ultra-small dwell times (10-50 μs) is a strategy that can drive down the SDLs by improving signal-to-noise ratios; however, this also requires a substantial increase in instrumental sensitivities. Recently, Hadioui *et al.*¹⁰¹ combined a high-sensitivity sector-field ICP-MS with a dry aerosol generation system (*i.e.* analyte desolvated before entering the plasma) and performed uninterrupted measurements at 30-50 μs dwell times. This high-sensitivity system (*i.e.* 150-200x enhanced ionic sensitivity as compared to quadrupole systems) enabled the analysis of low-abundant ^{49}Ti isotope, which has much lesser interferences than the primary ^{48}Ti (**Table 1-1**), leading to SDLs for TiO_2 as small as 8 nm in

Milli-Q water and < 15 nm in natural systems. Similar setups led to SDLs below 5 nm for Ag and Au NPs. These advances thus offer immense opportunities for the previously impossible analysis of the smallest ENPs in environmental systems. That being said, another major challenge in nanoanalytics is to distinguish smallest ENPs from naturally occurring colloids. Discrimination of particles by their origin can ultimately allow for targeted quantification of ENPs, paving the way for their reliable risk assessments.

1.3 Discrimination of ENPs from naturally occurring colloids

Discrimination of the ENPs from their geogenic natural background is a pre-requisite to their quantitative monitoring, which will ultimately enable their reliable risk assessment. However, given the predicted low concentrations of ENPs in the environment, their discrimination with respect to the ubiquitously present natural nano-scale materials is a challenging task.⁸⁷ In any case, any attempt to determine source of environmental colloidal particles will depend on establishing qualitative or quantitative criteria based upon inherent differences between anthropogenic and natural NPs. Most often, differences are thought to arise because anthropogenic NPs are often designed to exhibit a uniform set of physicochemical properties (*e.g.* shape, size, coating). During their production, they typically undergo a series of synthetic (purification) processes that provide them with a unique chemical identity (*e.g.* purity, shift in isotopic distribution).^{123, 146, 147} In contrast, naturally occurring NPs commonly originate^{126, 148} from mineral formation, byproducts of mineral weathering, biogeochemical products of microbial activities or nucleation in supersaturated fluids – processes that often induce physicochemical heterogeneities in the particles. Consequently, discrimination criteria may vary depending on particle type and the environmental context, but generally are predicated on physicochemical parameters, such as structural homogeneity, crystallinity, surface morphology, particle shape, surface coating, redox state, compositional homogeneity (*i.e.* purity/impurity), elemental associations with tracers, isotopic distribution patterns, deviations from natural abundance ratios and deliberate isotopic labelling.^{79, 149}

Microscopy and X-ray techniques. Advanced microscopy (*e.g.* TEM, SEM) along with X-ray based techniques are often used to provide insight into the possible origins of (nano)particles. For example, del Real *et al.*¹⁵⁰ demonstrated that most TiO₂ NPs detected in sewage sludge – the compartment that reportedly^{6, 13} receives the highest fraction of ENPs – exhibited smooth surfaces and faceted regular shapes, likely indicating an anthropogenic origin. This contrasted these NPs with NPs of irregular shapes and rough morphologies that

were observed in regular soil samples. In addition, surface coatings are sometimes used to track ENPs released from consumer products, as they may often retain the surface modifications that are characteristic of the original matrix. Kaegi *et al.*¹⁵¹ and Al-Kattan *et al.*⁷⁵ attributed distinctive (Ca-containing) coatings observed on paint-released TiO₂ ENPs to the organic binder of the paint. Similar results were observed for Ag ENPs emitted from outdoor painted surfaces.⁷⁴ Crystal phase is another potential distinguishing feature as, depending on the (manufacturing) source of ENPs, a certain phase of particles might be more dominant than others (*e.g.* anatase-to-rutile ratios are higher for TiO₂ ENPs as compared to natural TiO₂ NPs). CeO₂ ENPs (*i.e.* tetravalent) are synthesized via oxidation and subsequent precipitation of naturally occurring trivalent Ce-minerals (*e.g.* monazite, bastnaesite). Relying on this signature difference in oxidation states, Gogos *et al.*¹⁵² concluded that the fractions of anthropogenic Ce (*i.e.* tetravalent) in sewage sludge samples (*i.e.* 50-100%) were substantially higher than those in soils (*i.e.* up to 30%). Put together, it is clear that microscopic and X-ray based techniques can provide a wealth of qualitative and semi-quantitative information pertaining to the origin of NPs. Nonetheless, these determinations are often laborious and low throughput, often involving sample preparation processes (*e.g.* pre-concentration, drying) that are susceptible to contamination or artifacts (*e.g.* agglomeration). These methods fall short of providing quantitative measures of anthropogenic contributions.

ICP-MS: bulk elemental ratios. Owing to its robustness, chemical specificity and high throughput quantification capabilities, ICP-MS offers promising opportunities in quantitative source discrimination of NPs. Several papers previously attempted to quantify fluxes of anthropogenic NPs based on bulk elemental ratios. For example, Gondikas *et al.*¹²³ monitored Ti/Al ratios in old Danube Lake throughout, pre- and post-bathing season and attributed the elevated ratios (with respect to reference baseline) to Ti emissions from sunscreens, which are indeed known to be a major source of TiO₂ ENPs. Sediment core analysis indicated that the steady increase in Ti/Al ratios as of late 1990s coincided with the increasing market penetration of TiO₂-containing sunscreens. Reed *et al.*¹²⁰ and Rand *et al.*¹²⁸ conducted similar studies, except that instead of only relying on natural background variations, they additionally correlated the increase in the concentrations of Ti to that of a tracer organic chemical, oxybenzone, which is also emitted from sunscreens. In a different work¹⁰, the abundance of Ti with respect to other naturally occurring elements (*e.g.* Al, Fe, V) was shown to increase at a river downstream of a confluence with an industrial drainage canal, which presumably led to the influx of anthropogenic TiO₂ from a nearby ENP production facility. This conclusion was reached based on the examination of both sediments and suspended

particulate matter, suggesting that while some ENPs likely remained in the water column, the rest were sedimented onto the riverbed. A series of other works^{126, 127, 129, 130, 153, 154} utilized different natural tracers, such as Nb, Y, and V, to estimate fluxes of anthropogenic (nano)particles into surface waters (*e.g.* lake, river), wastewaters and stormwaters. The common aspect of all these works is that they predicted the fluxes relying on pre-defined (anticipated) emission scenarios (*e.g.* sunscreen use, sewage spills, urban run-off with rain), which would presumably increase the elemental ratio of the target element with respect to the naturally occurring tracer (*e.g.* elemental ratios before, during and after the emission). This approach, while insightful, may easily be prone to artifacts, since it assumes that the variations in elemental ratios can only be attributed to anthropogenic emissions of NPs, whereas in reality numerous factors (*e.g.* perturbation of sediment) could contribute to these ratios. Even if the estimates are technically accurate, this approach still cannot provide insight into the total quantity/proportion of ENPs in a given sample (at a given time).

ICP-MS: NP-by-NP approach. Particle specific multi-element determinations, with SP-ICP-TOF-MS, can potentially enable particle-by-particle probing of NPs by their origins in any given sample, ideally with no reliance on external information. In this case, discrimination is performed through the fingerprinting of particles with respect to their chemical purity, composition or isotopic distribution, which are expected to differ between ENPs and particles of geogenic origin. For example, CeO₂ ENPs are intentionally designed to be pure (single-metal) entities, while their precursors, Ce-minerals, occur naturally as multi-element particles often containing other rare-earth elements, notably La with typical Ce:La ratios of 2:1. Indeed, Praetorius *et al.*⁸⁷ used this ratio as a discrimination criterion in order to distinguish soil-based natural Ce-NPs and (spiked) CeO₂ ENPs with high levels of certainty. A similar strategy can be applied for the discrimination of other ENPs, such as TiO₂, given that natural Ti-minerals are known to contain important quantities of other metals (*e.g.* Al, Fe, Mn).^{123, 150} Notably, ~90% of naturally occurring Ti exists as ilmenite (FeTiO₃). Although a few papers have attempted to use such information to discriminate TiO₂ ENPs from naturally occurring Ti-particles, their ICP-TOF-MS systems had TiO₂ detection limits above 100 nm (**Table 1-2**), thus hampering the detection of the particles of actual interest (*i.e.* 1-100 nm). Measurement of variations of the isotopic composition can offer some unique insight into NP origins, given that industrial synthetic processes are expected to induce isotopic fractionation in the ENPs.^{146, 147} Although this approach is already often used for source attribution of trace metals in the environment, its applicability on an individual NP basis is still hindered by the poor detection limits and low duty cycles of currently available ICP-TOF-MS instrumentation. Yang *et al.*¹⁴⁷

recently applied a dual isotopic fingerprinting strategy (*i.e.* based on Si-O isotope combinations) in an attempt to categorize SiO₂ NPs by their natural origins and different manufacturer sources. While the data showed that source tracing of Si is indeed possible, these measurements were performed on bulk samples following the digestion of SiO₂ NPs. Therefore, they fell short of providing NP-specific origin information. Despite these challenges, future technical improvements to the sensitivity of multi-element analysis techniques – aided by isotopic fingerprinting using machine learning – hold great promise for a particle-by-particle quantitative profiling of NPs. These strategies can ultimately enable independent monitoring of NPs in natural samples with respect to their sizes, number/mass concentrations and origins, thus contributing to better regulation of nano-enabled products.

1.4 Scope and Experimental Approach

Sequential analysis. Lack of field-generated analytical data represents a missing link for reliable exposure modelling/monitoring of ENPs in the environment. To that end, SP-ICP-MS provides numerous opportunities that are well-suited to the rapid and high-throughput sizing and quantification of NPs in natural matrices. Nonetheless, as **Table 1-2** demonstrated, previously reported SDLs were often too high (*e.g.* >60-100 nm for TiO₂ ENPs). Therefore, an important aspect of this work was to develop methodologies that substantially improve the SDLs of the technique for several major NPs. This was achieved by setting up a state-of-the-art measurement system: a desolvation system was coupled to a high-sensitivity sector-field ICP-MS with capabilities of measuring every 10 μs (*i.e.* dwell time), in an uninterrupted manner. In this manner, lower backgrounds and higher rates of NP transport and ion transmission efficiencies were achieved, thus increasing the instrumental sensitivity (up to 150-200x compared to traditional quadrupole instruments), *i.e.* ion counts generated per mass (of an isotope). Large sets of time-resolved data (*i.e.* millions of datapoints within <1 min for a single replicate analysis) were then analyzed using a robust software that was able to resolve smallest NPs by studying characteristics of (NP-induced) peaks and their local backgrounds. These improvements effectively enabled the analysis of Ag and CeO₂ ENPs as small as 3-4 nm and TiO₂ ENPs <15 nm in natural waters.

Simultaneous whole spectrum analysis. Cutting-edge advances in simultaneous multi-element analysis were applied with the goal of probing of the compositions/purities of individual NPs. These experiments were performed using a prototype high-speed ICP-TOF-MS that allowed for the simultaneous analysis of the full spectrum of metals/metalloids (*i.e.* 7-

256 amu) every $<30 \mu\text{s}$, while featuring a continuous, uninterrupted data acquisition. This is a substantial advancement with respect to traditional TOF ICP-MS systems, which – owing to data transfer limitations – were able to report data only on the order of milliseconds, thus compromising mass detection limits and accuracies. As a result, the prototype TOF ICP-MS system, with its novel data acquisition method and re-designed ion optics and interference removal cell, attained significantly (i) lower SDLs (*e.g.* $>30 \text{ nm}$ for TiO_2 as opposed to $>80\text{--}100 \text{ nm}$ with the traditional TOF systems), and (ii) improved accuracies of mass detection (*i.e.* highly resolved peak profiles). The generated multi-dimensional (*i.e.* >200 isotopes), time-resolved data (*i.e.* ever $\sim 25 \mu\text{s}$) was state-of-the-art, providing potential insights into NP origins in the environment.

Experimental scope. These original methodologies of single particle analysis were applied to the monitoring of ENPs in two important environmental contexts: (i) release of TiO_2 ENPs from outdoor surface coatings (Chapter 2 and 3) and (ii) presence and distribution of Ti-, Ce- and Ag-ENPs in global natural waters with respect to naturally occurring NPs (Chapter 4). Indeed, given the growing uses of TiO_2 ENPs in surface coatings, surface-leaching of ENPs represents an important pathway of their emissions into the environment. While a few papers^{75, 155-157} have previously examined NP leaching from paints, they were often limited to lab studies (rather than field measurements) that employed analytical methods that were not able to quantitatively distinguish between NP and dissolved forms of the released metals. In this work, a comprehensive set of experiments was carefully designed to characterize the emissions of ENPs from surface coatings, with respect to their release rates, mass/number concentrations and size distributions. This work included measurements performed under outdoor weathering conditions, as a function of: (i) seasonal weather, (ii) surface exposure scenario (immersion or dripping) and (iii) coating matrix (paint or stain). Outdoor release experiments were coupled with lab-controlled weathering studies in order to elucidate the roles of critical weathering variables – temperature, freeze-thaw cycles and humidity – in ENP release and (subsequent) persistence. SP-ICP-TOF-MS data revealed compositional differences between coating-released TiO_2 ENPs and Ti-NPs naturally occurring in the natural precipitation. Consequently, the generated data is highly sought after for reliable parametrization of exposure models, which currently are lacking the input of environmentally relevant ENP-specific emission data.

Direct determinations of NPs in environmental matrices, with their source discrimination (anthropogenic or natural), can provide critical data for validating exposure models or directly informing ENP risk assessments. To date, these data have remained elusive, mainly due to the analytical difficulties of measuring NPs in complex matrices. Using state-of-

the-art methods, this work provides the first large-scale measurements of NPs in global natural waters. This entailed an ambitious sampling campaign that covered 46 sampling sites across 13 countries, including a wide range of samples, including lakes, rivers, canals, ponds, creeks, and natural precipitation. The focus of analysis was three major NPs – TiO₂, CeO₂ and Ag – that are suspected to have significant anthropogenic contributions. The experiments were designed to not only generate data on worldwide NP concentrations, but also to root out connections, if any, between (i) NP occurrence/distributions; (ii) NP types, concentrations, and purities; and (iii) natural/urban setting of sampling sites. The work thereby lays the foundation for high-throughput quantitative profiling of NPs, which will be essential for future monitoring of ENPs in different environmental systems.

1.5 Research Objectives

The fundamental aim of this work was to develop analytical strategies for the detection, quantification, and characterization of NPs in complex natural waters, with SDLs that enable the analysis of smallest NPs. Experiments were designed to provide data on (i) ENP release patterns for a prevalently used nano-enabled product (surface coatings), and (ii) presence and distribution of NPs, including ENPs, in global natural waters. Both types of data are critically needed for reliable parametrization and validation of ENP exposure models and for ENP risk monitoring. Hence, the specific objectives of this thesis were laid out as following:

1. To quantify and characterize TiO₂ ENPs emitted from outdoor surface coatings with respect to their particle sizes (distributions) and mass/number concentrations;
2. To elicit the role of seasonal changes, weathering variables, surface exposure scenarios, and coating matrix properties in ENP release patterns and the subsequent persistence of the ENPs in the environment;
3. To quantify and examine the distributions of three prevalent NPs – TiO₂, CeO₂ and Ag – with expected anthropogenic contributions, in a wide variety of natural waters on a global scale;
4. To assess the origin of NPs (anthropogenic or natural) based on the distribution patterns of NPs, their chemical compositions (*i.e.* purity) on a single particle basis, and the environmental settings of sampling sites.

1.6 Thesis Organization

This thesis is comprised of three original research manuscripts that are published/accepted:

Chapter 2. Azimzada, A., Farner, J. M., Hadioui, M., Liu-Kang, C., Jreije, I., Tufenkji, N., Wilkinson, K. J., Release of TiO₂ nanoparticles from painted surfaces in cold climates: characterization using a high sensitivity single-particle ICP-MS. *Environmental Science: Nano* **2020**, 7(1), 139-148.

In this chapter, we examine the release of TiO₂ ENPs from outdoor painted surfaces under natural weathering conditions. The outdoor experiments along with indoor control studies were designed to quantify/characterize the paint leached TiO₂ ENPs and identify the weathering factors that contribute to enhanced ENP release.

Chapter 3. Azimzada, A.; Farner, J. M.; Jreije, I.; Hadioui, M.; Liu-Kang, C.; Tufenkji, N.; Shaw, P.; Wilkinson, K. J., Single-and multi-element quantification and characterization of TiO₂ nanoparticles released from outdoor stains and paints. *Frontiers in Environmental Science* **2020**, 8, 91.

In this chapter, we present the results of an outdoor weathering study that lasted for over 20 weeks throughout fall, winter and spring. The work sought to identify the role of seasonal weathering, modes of surface exposure and coating chemistry in ENP emissions from surface coatings. The data also demonstrates the chemical differences between coating released TiO₂ ENPs and Ti-NPs pre-existing in the natural precipitation.

Chapter 4. Azimzada, A.; Jreije, I.; Hadioui, M.; Shaw, P.; Farner, J. M.; Wilkinson, K. J., Quantification and characterization of Ti-, Ce- and Ag-nanoparticles in global surface waters and precipitation. *Environmental Science & Technology* **2021**, 55, 14, 9836-9844.

In this chapter, we present analytical data on concentrations and sizes of Ti-, Ce- and Ag-NPs in a wide array of natural water samples collected at 46 sites across the world. The results link NP occurrences and distributions to particle type, origin, and sampling location. The work represents the first large-scale measurements of NPs and lays the foundation towards high-throughput reliable monitoring of ENPs in environmental matrices.

Chapter 5. This chapter states the overarching conclusions of the studies and future implications of ENPs for the environment and human health. The research recommendations and future outlook are also included.

1.7 References

1. Gottschalk, F.; Nowack, B., The release of engineered nanomaterials to the environment. *Journal of Environmental Monitoring* **2011**, *13* (5), 1145-1155.
2. Auffan, M.; Rose, J.; Bottero, J.-Y.; Lowry, G. V.; Jolivet, J.-P.; Wiesner, M. R., Towards a definition of inorganic nanoparticles from an environmental, health and safety perspective. *Nature Nanotechnology* **2009**, *4* (10), 634.
3. Hochella, M. F.; Mogk, D. W.; Ranville, J.; Allen, I. C.; Luther, G. W.; Marr, L. C.; McGrail, B. P.; Murayama, M.; Qafoku, N. P.; Rosso, K. M., Natural, incidental, and engineered nanomaterials and their impacts on the Earth system. *Science* **2019**, *363* (6434), eaau8299.
4. Vance, M. E.; Kuiken, T.; Vejerano, E. P.; McGinnis, S. P.; Hochella Jr, M. F.; Rejeski, D.; Hull, M. S., Nanotechnology in the real world: Redeveloping the nanomaterial consumer products inventory. *Beilstein Journal of Nanotechnology* **2015**, *6* (1), 1769-1780.
5. Gottschalk, F.; Sonderer, T.; Scholz, R. W.; Nowack, B., Possibilities and limitations of modeling environmental exposure to engineered nanomaterials by probabilistic material flow analysis. *Environmental Toxicology and Chemistry* **2010**, *29* (5), 1036-1048.
6. Keller, A. A.; McFerran, S.; Lazareva, A.; Suh, S., Global life cycle releases of engineered nanomaterials. *Journal of Nanoparticle Research* **2013**, *15* (6), 1692.
7. Giese, B.; Klaessig, F.; Park, B.; Kaegi, R.; Steinfeldt, M.; Wigger, H.; von Gleich, A.; Gottschalk, F., Risks, release and concentrations of engineered nanomaterial in the environment. *Scientific Reports* **2018**, *8* (1), 1-18.
8. Piccinno, F.; Gottschalk, F.; Seeger, S.; Nowack, B., Industrial production quantities and uses of ten engineered nanomaterials in Europe and the world. *Journal of Nanoparticle Research* **2012**, *14* (9), 1-11.
9. Bundschuh, M.; Filser, J.; Lüderwald, S.; McKee, M. S.; Metreveli, G.; Schaumann, G. E.; Schulz, R.; Wagner, S., Nanoparticles in the environment: where do we come from, where do we go to? *Environmental Sciences Europe* **2018**, *30* (1), 1-17.
10. Slomberg, D. L.; Auffan, M.; Guéniche, N.; Angeletti, B.; Campos, A.; Borschneck, D.; Aguerre-Chariol, O.; Rose, J., Anthropogenic release and distribution of titanium dioxide particles in a river downstream of a nanomaterial manufacturer industrial site. *Frontiers in Environmental Science* **2020**, *8* (76).
11. Gondikas, A. P.; Kammer, F. v. d.; Reed, R. B.; Wagner, S.; Ranville, J. F.; Hofmann, T., Release of TiO₂ nanoparticles from sunscreens into surface waters: a one-year survey at the old Danube recreational Lake. *Environmental Science & Technology* **2014**, *48* (10), 5415-5422.
12. Dale, J. G.; Cox, S. S.; Vance, M. E.; Marr, L. C.; Hochella Jr, M. F., Transformation of cerium oxide nanoparticles from a diesel fuel additive during combustion in a diesel engine. *Environmental Science & Technology* **2017**, *51* (4), 1973-1980.
13. Kiser, M.; Westerhoff, P.; Benn, T.; Wang, Y.; Perez-Rivera, J.; Hristovski, K., Titanium nanomaterial removal and release from wastewater treatment plants. *Environmental Science & Technology* **2009**, *43* (17), 6757-6763.
14. Westerhoff, P.; Song, G.; Hristovski, K.; Kiser, M. A., Occurrence and removal of titanium at full scale wastewater treatment plants: implications for TiO₂ nanomaterials. *Journal of Environmental Monitoring* **2011**, *13* (5), 1195-1203.
15. Abbas, Q.; Yousaf, B.; Ali, M. U.; Munir, M. A. M.; El-Naggar, A.; Rinklebe, J.; Naushad, M., Transformation pathways and fate of engineered nanoparticles (ENPs) in distinct interactive environmental compartments: A review. *Environment International* **2020**, *138*, 105646.

16. Vejerano, E. P.; Leon, E. C.; Holder, A. L.; Marr, L. C., Characterization of particle emissions and fate of nanomaterials during incineration. *Environmental Science: Nano* **2014**, *1* (2), 133-143.
17. Wigger, H.; Kägi, R.; Wiesner, M.; Nowack, B., Exposure and Possible Risks of Engineered Nanomaterials in the Environment—Current Knowledge and Directions for the Future. *Reviews of Geophysics* **2020**, *58* (4), e2020RG000710.
18. Wilkinson, K. J.; Lead, J. R., *Environmental colloids and particles: behaviour, separation and characterisation*. John Wiley & Sons: 2007; Vol. 10.
19. Elimelech, M.; Gregory, J.; Jia, X., *Particle deposition and aggregation: measurement, modelling and simulation*. Butterworth-Heinemann: 2013.
20. Petosa, A. R.; Jaisi, D. P.; Quevedo, I. R.; Elimelech, M.; Tufenkji, N., Aggregation and deposition of engineered nanomaterials in aquatic environments: role of physicochemical interactions. *Environmental Science & Technology* **2010**, *44* (17), 6532-6549.
21. Prospero, J.; Glaccum, R.; Nees, R., Atmospheric transport of soil dust from Africa to South America. *Nature* **1981**, *289* (5798), 570-572.
22. Hochella, M. F.; Aruguete, D. M.; Kim, B.; Madden, A. S., Naturally occurring inorganic nano particles: General assessment and a global budget for one of earth's last unexplored major geochemical components. In *Nature's Nanostructures*, Pan Stanford Publishing Pte. Ltd.: 2012; pp 1-42.
23. Rahim, M. F.; Pal, D.; Ariya, P. A., Physicochemical studies of aerosols at Montreal Trudeau Airport: The importance of airborne nanoparticles containing metal contaminants. *Environmental Pollution* **2019**, *246*, 734-744.
24. Lespes, G.; Faucher, S.; Slaveykova, V. I., Natural Nanoparticles, Anthropogenic Nanoparticles, Where Is the Frontier? *Frontiers in Environmental Science* **2020**, *8*, 71.
25. Emerson, E. W.; Hodshire, A. L.; DeBolt, H. M.; Bilsback, K. R.; Pierce, J. R.; McMeeking, G. R.; Farmer, D. K., Revisiting particle dry deposition and its role in radiative effect estimates. *Proceedings of the National Academy of Sciences* **2020**, *117* (42), 26076-26082.
26. Ruijrok, W.; Davidson, C. I.; W. Nicholson, K., Dry deposition of particles. *Tellus B* **1995**, *47* (5), 587-601.
27. Le Roux, G.; Hansson, S. V.; Claustres, A., Inorganic Chemistry in the Mountain Critical Zone: Are the mountain water towers of contemporary society under threat by trace contaminants? In *Developments in Earth Surface Processes*, Elsevier: 2016; Vol. 21, pp 131-154.
28. Tufenkji, N.; Elimelech, M., Correlation equation for predicting single-collector efficiency in physicochemical filtration in saturated porous media. *Environmental Science & Technology* **2004**, *38* (2), 529-536.
29. Zhang, T.; Lowry, G. V.; Capiro, N. L.; Chen, J.; Chen, W.; Chen, Y.; Dionysiou, D. D.; Elliott, D. W.; Ghoshal, S.; Hofmann, T., In situ remediation of subsurface contamination: opportunities and challenges for nanotechnology and advanced materials. *Environmental Science: Nano* **2019**, *6* (5), 1283-1302.
30. Hochella, M. F.; Lower, S. K.; Maurice, P. A.; Penn, R. L.; Sahai, N.; Sparks, D. L.; Twining, B. S., Nanominerals, mineral nanoparticles, and earth systems. *Science* **2008**, *319* (5870), 1631-1635.
31. Corsi, I.; Bergami, E.; Grassi, G., Behavior and bio-interactions of anthropogenic particles in marine environment for a more realistic ecological risk assessment. *Frontiers in Environmental Science* **2020**, *8*, 60.
32. Wang, S.; Lv, J.; Ma, J.; Zhang, S., Cellular internalization and intracellular biotransformation of silver nanoparticles in *Chlamydomonas reinhardtii*. *Nanotoxicology* **2016**, *10* (8), 1129-1135.

33. Montes, M. O.; Hanna, S. K.; Lenihan, H. S.; Keller, A. A., Uptake, accumulation, and biotransformation of metal oxide nanoparticles by a marine suspension-feeder. *Journal of Hazardous Materials* **2012**, *225*, 139-145.
34. Desmau, M.; Carboni, A.; Le Bars, M.; Doelsch, E.; Benedetti, M. F.; Auffan, M.; Levard, C.; Gelibert, A., How microbial biofilms control the environmental fate of engineered nanoparticles? *Frontiers in Environmental Science* **2020**, *8*, 82.
35. Clarke, A. D.; Owens, S. R.; Zhou, J., An ultrafine sea-salt flux from breaking waves: Implications for cloud condensation nuclei in the remote marine atmosphere. *Journal of Geophysical Research: Atmospheres* **2006**, *111* (D6).
36. Lowry, G. V.; Gregory, K. B.; Apte, S. C.; Lead, J. R., Transformations of nanomaterials in the environment. *Environmental Science & Technology* **2012**, *46* (13), 6893-6899.
37. Nichols, G.; Byard, S.; Bloxham, M. J.; Botterill, J.; Dawson, N. J.; Dennis, A.; Diart, V.; North, N. C.; Sherwood, J. D., A review of the terms agglomerate and aggregate with a recommendation for nomenclature used in powder and particle characterization. *Journal of Pharmaceutical Sciences* **2002**, *91* (10), 2103-2109.
38. Labille, J.; Harns, C.; Bottero, J.-Y.; Brant, J., Heteroaggregation of titanium dioxide nanoparticles with natural clay colloids. *Environmental Science & Technology* **2015**, *49* (11), 6608-6616.
39. Praetorius, A.; Badetti, E.; Brunelli, A.; Clavier, A.; Gallego-Urrea, J. A.; Gondikas, A.; Hassellöv, M.; Hofmann, T.; Mackevica, A.; Marcomini, A., Strategies for determining heteroaggregation attachment efficiencies of engineered nanoparticles in aquatic environments. *Environmental Science: Nano* **2020**, *7* (2), 351-367.
40. Praetorius, A.; Scheringer, M.; Hungerbühler, K., Development of Environmental Fate Models for Engineered Nanoparticles: A Case Study of TiO₂ Nanoparticles in the Rhine River. *Environmental Science & Technology* **2012**, *46* (12), 6705-6713.
41. Lammel, T.; Thit, A.; Mouneyrac, C.; Baun, A.; Sturve, J.; Selck, H., Trophic transfer of CuO NPs and dissolved Cu from sediment to worms to fish—a proof-of-concept study. *Environmental Science: Nano* **2019**, *6* (4), 1140-1155.
42. Shi, W.; Han, Y.; Guo, C.; Su, W.; Zhao, X.; Zha, S.; Wang, Y.; Liu, G., Ocean acidification increases the accumulation of titanium dioxide nanoparticles (nTiO₂) in edible bivalve mollusks and poses a potential threat to seafood safety. *Scientific Reports* **2019**, *9* (1), 1-10.
43. Conway, J. R.; Adeleye, A. S.; Gardea-Torresdey, J.; Keller, A. A., Aggregation, dissolution, and transformation of copper nanoparticles in natural waters. *Environmental Science & Technology* **2015**, *49* (5), 2749-2756.
44. Han, P.; Wang, X.; Cai, L.; Tong, M.; Kim, H., Transport and retention behaviors of titanium dioxide nanoparticles in iron oxide-coated quartz sand: Effects of pH, ionic strength, and humic acid. *Colloids and Surfaces A: Physicochemical and Engineering Aspects* **2014**, *454*, 119-127.
45. Farner, J. M.; De Tommaso, J.; Mantel, H.; Cheong, R. S.; Tufenkji, N., Effect of freeze/thaw on aggregation and transport of nano-TiO₂ in saturated porous media. *Environmental Science: Nano* **2020**, *7* (6), 1781-1793.
46. Chambers, B. A.; Afroz, A. N.; Bae, S.; Aich, N.; Katz, L.; Saleh, N. B.; Kirisits, M. J., Effects of chloride and ionic strength on physical morphology, dissolution, and bacterial toxicity of silver nanoparticles. *Environmental Science & Technology* **2014**, *48* (1), 761-769.
47. Baalousha, M.; Nur, Y.; Römer, I.; Tejamaya, M.; Lead, J., Effect of monovalent and divalent cations, anions and fulvic acid on aggregation of citrate-coated silver nanoparticles. *Science of the Total Environment* **2013**, *454*, 119-131.

48. Han, Y.; Kim, D.; Hwang, G.; Lee, B.; Eom, I.; Kim, P. J.; Tong, M.; Kim, H., Aggregation and dissolution of ZnO nanoparticles synthesized by different methods: Influence of ionic strength and humic acid. *Colloids and Surfaces A: Physicochemical and Engineering Aspects* **2014**, *451*, 7-15.
49. Bian, S.-W.; Mudunkotuwa, I. A.; Rupasinghe, T.; Grassian, V. H., Aggregation and dissolution of 4 nm ZnO nanoparticles in aqueous environments: influence of pH, ionic strength, size, and adsorption of humic acid. *Langmuir* **2011**, *27* (10), 6059-6068.
50. Barreto, A.; Luis, L. G.; Girão, A. V.; Trindade, T.; Soares, A. M.; Oliveira, M., Behavior of colloidal gold nanoparticles in different ionic strength media. *Journal of Nanoparticle Research* **2015**, *17* (12), 493.
51. Buffle, J.; Wilkinson, K. J.; Stoll, S.; Filella, M.; Zhang, J., A generalized description of aquatic colloidal interactions: the three-colloidal component approach. *Environmental Science & Technology* **1998**, *32* (19), 2887-2899.
52. Mwaanga, P.; Carraway, E. R.; Schlautman, M. A., Preferential sorption of some natural organic matter fractions to titanium dioxide nanoparticles: influence of pH and ionic strength. *Environmental Monitoring and Assessment* **2014**, *186* (12), 8833-8844.
53. Monopoli, M. P.; Åberg, C.; Salvati, A.; Dawson, K. A., Biomolecular coronas provide the biological identity of nanosized materials. *Nature Nanotechnology* **2012**, *7* (12), 779-786.
54. Del Pino, P.; Pelaz, B.; Zhang, Q.; Maffre, P.; Nienhaus, G. U.; Parak, W. J., Protein corona formation around nanoparticles—from the past to the future. *Materials Horizons* **2014**, *1* (3), 301-313.
55. Sasidharan, A.; Riviere, J. E.; Monteiro-Riviere, N. A., Gold and silver nanoparticle interactions with human proteins: impact and implications in biocorona formation. *Journal of Materials Chemistry B* **2015**, *3* (10), 2075-2082.
56. Gondikas, A.; Gallego-Urrea, J.; Halbach, M.; Derrien, N.; Hassellöv, M., Nanomaterial fate in seawater: A rapid sink or intermittent stabilization? *Frontiers in Environmental Science* **2020**, *8*, 151.
57. Ellis, L.-J. A.; Baalousha, M.; Valsami-Jones, E.; Lead, J. R., Seasonal variability of natural water chemistry affects the fate and behaviour of silver nanoparticles. *Chemosphere* **2018**, *191*, 616-625.
58. Levard, C.; Hotze, E. M.; Lowry, G. V.; Brown Jr, G. E., Environmental transformations of silver nanoparticles: impact on stability and toxicity. *Environmental Science & Technology* **2012**, *46* (13), 6900-6914.
59. Azimzada, A.; Tufenkji, N.; Wilkinson, K. J., Transformations of silver nanoparticles in wastewater effluents: links to Ag bioavailability. *Environmental Science: Nano* **2017**, *4* (6), 1339-1349.
60. Sigg, L.; Lindauer, U., Silver nanoparticle dissolution in the presence of ligands and of hydrogen peroxide. *Environmental Pollution* **2015**, *206*, 582-587.
61. Collin, B.; Tsyusko, O. V.; Starnes, D. L.; Unrine, J. M., Effect of natural organic matter on dissolution and toxicity of sulfidized silver nanoparticles to *Caenorhabditis elegans*. *Environmental Science: Nano* **2016**, *3* (4), 728-736.
62. Brunetti, G.; Donner, E.; Laera, G.; Sekine, R.; Scheckel, K. G.; Khaksar, M.; Vasilev, K.; De Mastro, G.; Lombi, E., Fate of zinc and silver engineered nanoparticles in sewerage networks. *Water Research* **2015**, *77*, 72-84.
63. Ma, R.; Stegemeier, J.; Levard, C.; Dale, J. G.; Noack, C. W.; Yang, T.; Brown, G. E.; Lowry, G. V., Sulfidation of copper oxide nanoparticles and properties of resulting copper sulfide. *Environmental Science: Nano* **2014**, *1* (4), 347-357.
64. Avellan, A.; Simonin, M.; McGivney, E.; Bossa, N.; Spielman-Sun, E.; Rocca, J. D.; Bernhardt, E. S.; Geitner, N. K.; Unrine, J. M.; Wiesner, M. R., Gold nanoparticle

biodissolution by a freshwater macrophyte and its associated microbiome. *Nature Nanotechnology* **2018**, *13* (11), 1072-1077.

65. Azodi, M.; Sultan, Y.; Ghoshal, S., Dissolution behavior of silver nanoparticles and formation of secondary silver nanoparticles in municipal wastewater by single-particle ICP-MS. *Environmental Science & Technology* **2016**, *50* (24), 13318-13327.

66. Massari, A.; Beggio, M.; Hreglich, S.; Marin, R.; Zuin, S., Behavior of TiO₂ nanoparticles during incineration of solid paint waste: A lab-scale test. *Waste Management* **2014**, *34* (10), 1897-1907.

67. Turolla, A.; Piazzoli, A.; Budarz, J. F.; Wiesner, M. R.; Antonelli, M., Experimental measurement and modelling of reactive species generation in TiO₂ nanoparticle photocatalysis. *Chemical Engineering Journal* **2015**, *271*, 260-268.

68. John, A. C.; Küpper, M.; Manders-Groot, A. M.; Debray, B.; Lacome, J.-M.; Kuhlbusch, T. A., Emissions and possible environmental implication of engineered nanomaterials (ENMs) in the atmosphere. *Atmosphere* **2017**, *8* (5), 84.

69. Wang, M.; Kong, W.; Marten, R.; He, X.-C.; Chen, D.; Pfeifer, J.; Heitto, A.; Kontkanen, J.; Dada, L.; Kürten, A., Rapid growth of new atmospheric particles by nitric acid and ammonia condensation. *Nature* **2020**, *581* (7807), 184-189.

70. Andronache, C.; Grönholm, T.; Laakso, L.; Phillips, V.; Venäläinen, A., Scavenging of ultrafine particles by rainfall at a boreal site: observations and model estimations. *Atmospheric Chemistry and Physics* **2006**, *6* (12), 4739-4754.

71. Nowack, B., Evaluation of environmental exposure models for engineered nanomaterials in a regulatory context. *NanoImpact* **2017**, *8*, 38-47.

72. Sun, T. Y.; Bornhöft, N. A.; Hungerbühler, K.; Nowack, B., Dynamic probabilistic modeling of environmental emissions of engineered nanomaterials. *Environmental Science & Technology* **2016**, *50* (9), 4701-4711.

73. Benn, T. M.; Westerhoff, P., Nanoparticle silver released into water from commercially available sock fabrics. *Environmental Science & Technology* **2008**, *42* (11), 4133-4139.

74. Kaegi, R.; Sinnet, B.; Zuleeg, S.; Hagendorfer, H.; Mueller, E.; Vonbank, R.; Boller, M.; Burkhardt, M., Release of silver nanoparticles from outdoor facades. *Environmental Pollution* **2010**, *158* (9), 2900-2905.

75. Al-Kattan, A.; Wichser, A.; Vonbank, R.; Brunner, S.; Ulrich, A.; Zuin, S.; Nowack, B., Release of TiO₂ from paints containing pigment-TiO₂ or nano-TiO₂ by weathering. *Environmental Science: Processes & Impacts* **2013**, *15* (12), 2186-2193.

76. Nowack, B.; Baalousha, M.; Bornhöft, N.; Chaudhry, Q.; Cornelis, G.; Cotterill, J.; Gondikas, A.; Hassellöv, M.; Lead, J.; Mitrano, D. M., Progress towards the validation of modeled environmental concentrations of engineered nanomaterials by analytical measurements. *Environmental Science: Nano* **2015**, *2* (5), 421-428.

77. Zheng, Y.; Nowack, B., Size-Specific, Dynamic, Probabilistic Material Flow Analysis of Titanium Dioxide Releases into the Environment. *Environmental Science & Technology* **2021**, *55* (4), 2392-2402.

78. Mourdikoudis, S.; Pallares, R. M.; Thanh, N. T., Characterization techniques for nanoparticles: comparison and complementarity upon studying nanoparticle properties. *Nanoscale* **2018**, *10* (27), 12871-12934.

79. Von der Kammer, F.; Ferguson, P. L.; Holden, P. A.; Masion, A.; Rogers, K. R.; Klaine, S. J.; Koelmans, A. A.; Horne, N.; Unrine, J. M., Analysis of engineered nanomaterials in complex matrices (environment and biota): general considerations and conceptual case studies. *Environmental Toxicology and Chemistry* **2012**, *31* (1), 32-49.

80. Laborda, F.; Bolea, E.; Cepriá, G.; Gómez, M. T.; Jiménez, M. S.; Pérez-Arantegui, J.; Castillo, J. R., Detection, characterization and quantification of inorganic engineered

nanomaterials: A review of techniques and methodological approaches for the analysis of complex samples. *Analytica Chimica Acta* **2016**, *904*, 10-32.

81. Boyd, R. D.; Pichaimuthu, S. K.; Cuenat, A., New approach to inter-technique comparisons for nanoparticle size measurements; using atomic force microscopy, nanoparticle tracking analysis and dynamic light scattering. *Colloids and Surfaces A: Physicochemical and Engineering Aspects* **2011**, *387* (1-3), 35-42.

82. Proulx, K.; Hadioui, M.; Wilkinson, K. J., Separation, detection and characterization of nanomaterials in municipal wastewaters using hydrodynamic chromatography coupled to ICPMS and single particle ICPMS. *Analytical and Bioanalytical Chemistry* **2016**, *408* (19), 5147-5155.

83. Mitrano, D. M.; Barber, A.; Bednar, A.; Westerhoff, P.; Higgins, C. P.; Ranville, J. F., Silver nanoparticle characterization using single particle ICP-MS (SP-ICP-MS) and asymmetrical flow field flow fractionation ICP-MS (AF4-ICP-MS). *Journal of Analytical Atomic Spectrometry* **2012**, *27* (7), 1131-1142.

84. Gigault, J.; Pettibone, J. M.; Schmitt, C.; Hackley, V. A., Rational strategy for characterization of nanoscale particles by asymmetric-flow field flow fractionation: a tutorial. *Analytica Chimica Acta* **2014**, *809*, 9-24.

85. Meermann, B.; Nischwitz, V., ICP-MS for the analysis at the nanoscale—a tutorial review. *Journal of Analytical Atomic Spectrometry* **2018**, *33* (9), 1432-1468.

86. Mozhayeva, D.; Engelhard, C., A critical review of single particle inductively coupled plasma mass spectrometry—A step towards an ideal method for nanomaterial characterization. *Journal of Analytical Atomic Spectrometry* **2020**, *35*, 1740-1783.

87. Praetorius, A.; Gundlach-Graham, A.; Goldberg, E.; Fabienke, W.; Navratilova, J.; Gondikas, A.; Kaegi, R.; Günther, D.; Hofmann, T.; von der Kammer, F., Single-particle multi-element fingerprinting (spMEF) using inductively-coupled plasma time-of-flight mass spectrometry (ICP-TOFMS) to identify engineered nanoparticles against the elevated natural background in soils. *Environmental Science: Nano* **2017**, *4* (2), 307-314.

88. Houk, R. S.; Fassel, V. A.; Flesch, G. D.; Svec, H. J.; Gray, A. L.; Taylor, C. E., Inductively coupled argon plasma as an ion source for mass spectrometric determination of trace elements. *Analytical Chemistry* **1980**, *52* (14), 2283-2289.

89. Gray, A. L., The ICP as an ion source—origins, achievements and prospects. *Spectrochimica Acta Part B: Atomic Spectroscopy* **1985**, *40* (10-12), 1525-1537.

90. Von der Kammer, F.; Legros, S.; Hofmann, T.; Larsen, E. H.; Loeschner, K., Separation and characterization of nanoparticles in complex food and environmental samples by field-flow fractionation. *TrAC Trends in Analytical Chemistry* **2011**, *30* (3), 425-436.

91. Degueldre, C.; Favarger, P.-Y.; Bitea, C., Zirconia colloid analysis by single particle inductively coupled plasma–mass spectrometry. *Analytica Chimica Acta* **2004**, *518* (1-2), 137-142.

92. Balcaen, L.; Bolea-Fernandez, E.; Resano, M.; Vanhaecke, F., Inductively coupled plasma–Tandem mass spectrometry (ICP-MS/MS): A powerful and universal tool for the interference-free determination of (ultra) trace elements—A tutorial review. *Analytica Chimica Acta* **2015**, *894*, 7-19.

93. Shaw, P.; Donard, A., Nano-particle analysis using dwell times between 10 μ s and 70 μ s with an upper counting limit of greater than 3×10^7 cps and a gold nanoparticle detection limit of less than 10 nm diameter. *Journal of Analytical Atomic Spectrometry* **2016**, *31* (6), 1234-1242.

94. Borovinskaya, O.; Hattendorf, B.; Tanner, M.; Gschwind, S.; Günther, D., A prototype of a new inductively coupled plasma time-of-flight mass spectrometer providing temporally resolved, multi-element detection of short signals generated by single particles and droplets. *Journal of Analytical Atomic Spectrometry* **2013**, *28* (2), 226-233.

95. Wilschefski, S. C.; Baxter, M. R., Inductively coupled plasma mass spectrometry: introduction to analytical aspects. *The Clinical Biochemist Reviews* **2019**, *40* (3), 115.
96. Sharp, B. L., Pneumatic nebulisers and spray chambers for inductively coupled plasma spectrometry. A review. Part 2. Spray chambers. *Journal of Analytical Atomic Spectrometry* **1988**, *3* (7), 939-963.
97. Thompson, M., *Handbook of inductively coupled plasma spectrometry*. Springer Science & Business Media: 2012.
98. Miller, P. E.; Denton, M. B., The quadrupole mass filter: basic operating concepts. *Journal of Chemical Education* **1986**, *63* (7), 617.
99. May, T. W.; Wiedmeyer, R. H., A table of polyatomic interferences in ICP-MS. *Atomic Spectroscopy* **1998**, *19*, 150-155.
100. Rua-Ibarz, A.; Bolea-Fernandez, E.; Pozo, G.; Dominguez-Benetton, X.; Vanhaecke, F.; Tirez, K., Characterization of iron oxide nanoparticles by means of single-particle ICP-mass spectrometry (SP-ICP-MS)—chemical versus physical resolution to overcome spectral overlap. *Journal of Analytical Atomic Spectrometry* **2020**, *35* (9), 2023-2032.
101. Hadioui, M.; Geneviève, K.; Azimzada, A.; Jreije, I.; Frechette-Viens, L.; Wilkinson, K. J., Lowering the size detection limits of Ag and TiO₂ nanoparticles by Single Particle ICP-MS. *Analytical Chemistry* **2019**, *91* (20).
102. Hendriks, L.; Gundlach-Graham, A.; Günther, D., Analysis of inorganic nanoparticles by single-particle inductively coupled plasma time-of-flight mass spectrometry. *CHIMIA International Journal for Chemistry* **2018**, *72* (4), 221-226.
103. Bevers, S.; Montaña, M. D.; Rybicki, L.; Hofmann, T.; von der Kammer, F.; Ranville, J. F., Quantification and characterization of nanoparticulate zinc in an urban watershed. *Frontiers in Environmental Science* **2020**, *8*, 84.
104. Laborda, F.; Bolea, E.; Jiménez-Lamana, J., Single particle inductively coupled plasma mass spectrometry: a powerful tool for nanoanalysis. *Analytical Chemistry* **2014**, *86* (5), 2270-2278.
105. Gundlach-Graham, A.; Mehrabi, K., Monodisperse microdroplets: a tool that advances single-particle ICP-MS measurements. *Journal of Analytical Atomic Spectrometry* **2020**, *35* (9), 1727-1739.
106. Pace, H. E.; Rogers, N. J.; Jarolimek, C.; Coleman, V. A.; Higgins, C. P.; Ranville, J. F., Determining transport efficiency for the purpose of counting and sizing nanoparticles via single particle inductively coupled plasma mass spectrometry. *Analytical Chemistry* **2011**, *83* (24), 9361-9369.
107. Tharaud, M.; Louvat, P.; Benedetti, M. F., Detection of nanoparticles by single-particle ICP-MS with complete transport efficiency through direct nebulization at few-microlitres-per-minute uptake rates. *Analytical and Bioanalytical Chemistry* **2021**, *413* (3), 923-933.
108. Hendriks, L.; Gundlach-Graham, A.; Günther, D., Performance of sp-ICP-TOFMS with signal distributions fitted to a compound Poisson model. *Journal of Analytical Atomic Spectrometry* **2019**, *34* (9), 1900-1909.
109. Hadioui, M.; Merdzan, V.; Wilkinson, K. J., Detection and characterization of ZnO nanoparticles in surface and waste waters using single particle ICPMS. *Environmental Science & Technology* **2015**, *49* (10), 6141-6148.
110. Bi, X.; Lee, S.; Ranville, J. F.; Sattigeri, P.; Spanias, A.; Herckes, P.; Westerhoff, P., Quantitative resolution of nanoparticle sizes using single particle inductively coupled plasma mass spectrometry with the K-means clustering algorithm. *Journal of Analytical Atomic Spectrometry* **2014**, *29* (9), 1630-1639.
111. Hadioui, M.; Peyrot, C.; Wilkinson, K. J., Improvements to single particle ICPMS by the online coupling of ion exchange resins. *Analytical Chemistry* **2014**, *86* (10), 4668-4674.

112. Fréchet-Viens, L.; Hadioui, M.; Wilkinson, K. J., Quantification of ZnO nanoparticles and other Zn containing colloids in natural waters using a high sensitivity single particle ICP-MS. *Talanta* **2019**, *200*, 156-162.
113. Tan, S. H.; Horlick, G., Matrix-effect observations in inductively coupled plasma mass spectrometry. *Journal of Analytical Atomic Spectrometry* **1987**, *2* (8), 745-763.
114. Hendriks, L.; Ramkorun-Schmidt, B.; Gundlach-Graham, A.; Koch, J.; Grass, R. N.; Jakubowski, N.; Günther, D., Single-particle ICP-MS with online microdroplet calibration: toward matrix independent nanoparticle sizing. *Journal of Analytical Atomic Spectrometry* **2019**, *34* (4), 716-728.
115. Mehrabi, K.; Günther, D.; Gundlach-Graham, A., Single-particle ICP-TOFMS with online microdroplet calibration for the simultaneous quantification of diverse nanoparticles in complex matrices. *Environmental Science: Nano* **2019**, *6* (11), 3349-3358.
116. Pin, C.; Lacombe, S.; Telouk, P.; Imbert, J.-L., Isotope dilution inductively coupled plasma mass spectrometry: a straightforward method for rapid and accurate determination of uranium and thorium in silicate rocks. *Analytica Chimica Acta* **1992**, *256* (1), 153-161.
117. Vanhaecke, F.; Vanhoe, H.; Dams, R.; Vandecasteele, C., The use of internal standards in ICP-MS. *Talanta* **1992**, *39* (7), 737-742.
118. Lee, S.; Bi, X.; Reed, R. B.; Ranville, J. F.; Herckes, P.; Westerhoff, P., Nanoparticle size detection limits by single particle ICP-MS for 40 elements. *Environmental Science & Technology* **2014**, *48* (17), 10291-10300.
119. Donovan, A. R.; Adams, C. D.; Ma, Y.; Stephan, C.; Eichholz, T.; Shi, H., Single particle ICP-MS characterization of titanium dioxide, silver, and gold nanoparticles during drinking water treatment. *Chemosphere* **2016**, *144*, 148-153.
120. Reed, R.; Martin, D.; Bednar, A.; Montañó, M.; Westerhoff, P.; Ranville, J., Multi-day diurnal measurements of Ti-containing nanoparticle and organic sunscreen chemical release during recreational use of a natural surface water. *Environmental Science: Nano* **2017**, *4* (1), 69-77.
121. Londono, N.; Donovan, A. R.; Shi, H.; Geisler, M.; Liang, Y., Impact of TiO₂ and ZnO nanoparticles on an aquatic microbial community: effect at environmentally relevant concentrations. *Nanotoxicology* **2017**, *11* (9-10), 1140-1156.
122. Donovan, A. R.; Adams, C. D.; Ma, Y.; Stephan, C.; Eichholz, T.; Shi, H., Fate of nanoparticles during alum and ferric coagulation monitored using single particle ICP-MS. *Chemosphere* **2018**, *195*, 531-541.
123. Gondikas, A.; von der Kammer, F.; Kaegi, R.; Borovinskaya, O.; Neubauer, E.; Navratilova, J.; Praetorius, A.; Cornelis, G.; Hofmann, T., Where is the nano? Analytical approaches for the detection and quantification of TiO₂ engineered nanoparticles in surface waters. *Environmental Science: Nano* **2018**, *5* (2), 313-326.
124. Peters, R. J.; van Bommel, G.; Milani, N. B.; den Hertog, G. C.; Undas, A. K.; van der Lee, M.; Bouwmeester, H., Detection of nanoparticles in Dutch surface waters. *Science of the Total Environment* **2018**, *621*, 210-218.
125. Venkatesan, A. K.; Reed, R. B.; Lee, S.; Bi, X.; Hanigan, D.; Yang, Y.; Ranville, J. F.; Herckes, P.; Westerhoff, P., Detection and sizing of Ti-containing particles in recreational waters using single particle ICP-MS. *Bulletin of Environmental Contamination and Toxicology* **2018**, *100* (1), 120-126.
126. Loosli, F.; Wang, J.; Rothenberg, S.; Bizimis, M.; Winkler, C.; Borovinskaya, O.; Flamigni, L.; Baalousha, M., Sewage spills are a major source of titanium dioxide engineered (nano)-particle release into the environment. *Environmental Science: Nano* **2019**, *6* (3), 763-777.
127. Phalyvong, K.; Sivry, Y.; Pauwels, H.; Gélabert, A.; Tharaud, M.; Wille, G.; Bourrat, X.; Benedetti, M. F., Occurrence and Origins of Cerium Dioxide and Titanium

Dioxide Nanoparticles in the Loire River (France) by Single Particle ICP-MS and FEG-SEM Imaging. *Frontiers in Environmental Science* **2020**, *8*, 141.

128. Rand, L. N.; Bi, Y.; Poustie, A.; Bednar, A. J.; Hanigan, D. J.; Westerhoff, P.; Ranville, J. F., Quantifying temporal and geographic variation in sunscreen and mineralogic titanium-containing nanoparticles in three recreational rivers. *Science of The Total Environment* **2020**, *743*, 140845.

129. Phalyvong, K.; Sivry, Y.; Pauwels, H.; Gélabert, A.; Tharaud, M.; Wille, G.; Bourrat, X.; Ranville, J. F.; Benedetti, M. F., Assessing CeO₂ and TiO₂ Nanoparticle Concentrations in the Seine River and Its Tributaries Near Paris. *Frontiers in Environmental Science* **2021**, *8*, 549896.

130. Nabi, M. M.; Wang, J.; Meyer, M.; Croteau, M.-N.; Ismail, N.; Baalousha, M., Concentrations and size distribution of TiO₂ and Ag engineered particles in five wastewater treatment plants in the United States. *Science of The Total Environment* **2021**, *753*, 142017.

131. Mehrabi, K.; Kaegi, R.; Günther, D.; Gundlach-Graham, A., Emerging investigator series: automated single-nanoparticle quantification and classification: a holistic study of particles into and out of wastewater treatment plants in Switzerland. *Environmental Science: Nano* **2021**, (Advance Article).

132. Donovan, A. R.; Adams, C. D.; Ma, Y.; Stephan, C.; Eichholz, T.; Shi, H., Detection of zinc oxide and cerium dioxide nanoparticles during drinking water treatment by rapid single particle ICP-MS methods. *Analytical and Bioanalytical Chemistry* **2016**, *408* (19), 5137-5145.

133. Jreije, I.; Azimzada, A.; Hadioui, M.; Wilkinson, K. J., Measurement of CeO₂ Nanoparticles in Natural Waters Using a High Sensitivity, Single Particle ICP-MS. *Molecules* **2020**, *25* (23), 5516.

134. Morel, E.; Jreije, I.; Tetreault, V.; Hauser, C.; Zerges, W.; Wilkinson, K. J., Biological impacts of Ce nanoparticles with different surface coatings as revealed by RNA-Seq in *Chlamydomonas reinhardtii*. *NanoImpact* **2020**, *19*, 100228.

135. Hadioui, M.; Leclerc, S.; Wilkinson, K. J., Multimethod quantification of Ag⁺ release from nanosilver. *Talanta* **2013**, *105*, 15-19.

136. Furtado, L. M.; Hoque, M. E.; Mitrano, D. M.; Ranville, J. F.; Cheever, B.; Frost, P. C.; Xenopoulos, M. A.; Hintelmann, H.; Metcalfe, C. D., The persistence and transformation of silver nanoparticles in littoral lake mesocosms monitored using various analytical techniques. *Environmental Chemistry* **2014**, *11* (4), 419-430.

137. Mitrano, D.; Ranville, J. F.; Bednar, A.; Kazor, K.; Hering, A. S.; Higgins, C. P., Tracking dissolution of silver nanoparticles at environmentally relevant concentrations in laboratory, natural, and processed waters using single particle ICP-MS (spICP-MS). *Environmental Science: Nano* **2014**, *1* (3), 248-259.

138. Telgmann, L.; Metcalfe, C.; Hintelmann, H., Rapid size characterization of silver nanoparticles by single particle ICP-MS and isotope dilution. *Journal of Analytical Atomic Spectrometry* **2014**, *29* (7), 1265-1272.

139. Jiménez-Lamana, J.; Slaveykova, V. I., Silver nanoparticle behaviour in lake water depends on their surface coating. *Science of the Total Environment* **2016**, *573*, 946-953.

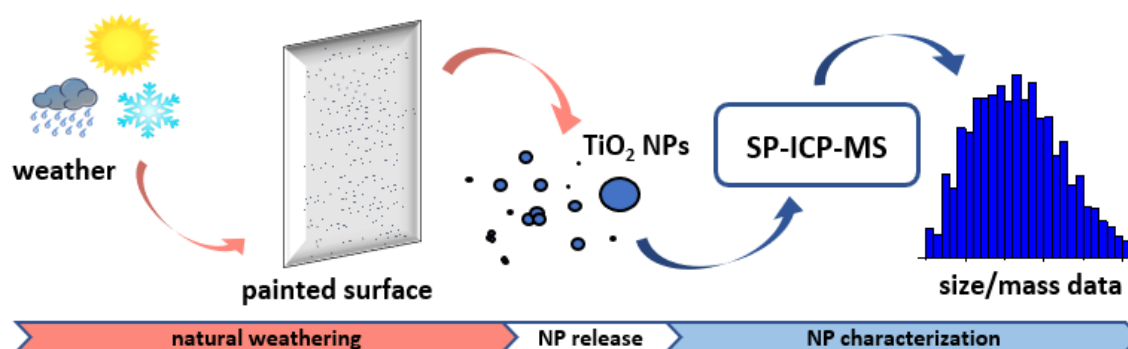
140. Telgmann, L.; Nguyen, M. T. K.; Shen, L.; Yargeau, V.; Hintelmann, H.; Metcalfe, C. D., Single particle ICP-MS as a tool for determining the stability of silver nanoparticles in aquatic matrixes under various environmental conditions, including treatment by ozonation. *Analytical and Bioanalytical Chemistry* **2016**, *408* (19), 5169-5177.

141. Martin, J. D.; Telgmann, L.; Metcalfe, C. D., A method for preparing silver nanoparticle suspensions in bulk for ecotoxicity testing and ecological risk assessment. *Bulletin of Environmental Contamination and Toxicology* **2017**, *98* (5), 589-594.

142. Tuoriniemi, J.; Jürgens, M. D.; Hassellöv, M.; Cornelis, G., Size dependence of silver nanoparticle removal in a wastewater treatment plant mesocosm measured by FAST single particle ICP-MS. *Environmental Science: Nano* **2017**, *4* (5), 1189-1197.
143. Martin, J. D.; Frost, P. C.; Hintelmann, H.; Newman, K.; Paterson, M. J.; Hayhurst, L.; Rennie, M. D.; Xenopoulos, M. A.; Yargeau, V.; Metcalfe, C. D., Accumulation of silver in yellow perch (*Perca flavescens*) and northern pike (*Esox lucius*) From a lake dosed with nanosilver. *Environmental Science & Technology* **2018**, *52* (19), 11114-11122.
144. Luo, L.; Yang, Y.; Li, H.; Ding, R.; Wang, Q.; Yang, Z., Size characterization of silver nanoparticles after separation from silver ions in environmental water using magnetic reduced graphene oxide. *Science of The Total Environment* **2018**, *612*, 1215-1222.
145. Loosli, F.; Wang, J.; Sikder, M.; Afshinnia, K.; Baalousha, M., Analysis of engineered nanomaterials (Ag, CeO₂ and Fe₂O₃) in spiked surface waters at environmentally relevant particle concentrations. *Science of The Total Environment* **2020**, *715*, 136927.
146. Lu, D.; Liu, Q.; Zhang, T.; Cai, Y.; Yin, Y.; Jiang, G., Stable silver isotope fractionation in the natural transformation process of silver nanoparticles. *Nature Nanotechnology* **2016**, *11* (8), 682-686.
147. Yang, X.; Liu, X.; Zhang, A.; Lu, D.; Li, G.; Zhang, Q.; Liu, Q.; Jiang, G., Distinguishing the sources of silica nanoparticles by dual isotopic fingerprinting and machine learning. *Nature Communications* **2019**, *10* (1), 1620.
148. Wigginton, N. S.; Haus, K. L.; Hochella Jr, M. F., Aquatic environmental nanoparticles. *Journal of Environmental Monitoring* **2007**, *9* (12), 1306-1316.
149. Wagner, S.; Gondikas, A.; Neubauer, E.; Hofmann, T.; von der Kammer, F., Spot the difference: engineered and natural nanoparticles in the environment—release, behavior, and fate. *Angewandte Chemie International Edition* **2014**, *53* (46), 12398-12419.
150. del Real, A. E. P.; Castillo-Michel, H.; Kaegi, R.; Larue, C.; de Nolf, W.; Reyes-Herrera, J.; Tucoulou, R.; Findling, N.; Salas-Colera, E.; Sarret, G., Searching for relevant criteria to distinguish natural vs. anthropogenic TiO₂ nanoparticles in soils. *Environmental Science: Nano* **2018**, *5* (12), 2853-2863.
151. Kaegi, R.; Ulrich, A.; Sinnet, B.; Vonbank, R.; Wichser, A.; Zuleeg, S.; Simmler, H.; Brunner, S.; Vonmont, H.; Burkhardt, M., Synthetic TiO₂ nanoparticle emission from exterior facades into the aquatic environment. *Environmental Pollution* **2008**, *156* (2), 233-239.
152. Gogos, A.; Wielinski, J.; Voegelin, A.; von der Kammer, F.; Kaegi, R., Quantification of anthropogenic and geogenic Ce in sewage sludge based on Ce oxidation state and rare earth element patterns. *Water research X* **2020**, *9*, 100059.
153. Nabi, M. M.; Wang, J.; Baalousha, M., Episodic surges in titanium dioxide engineered particle concentrations in surface waters following rainfall events. *Chemosphere* **2021**, *263*, 128261.
154. Wang, J.; Nabi, M. M.; Mohanty, S. K.; Afrooz, A. N.; Cantando, E.; Aich, N.; Baalousha, M., Detection and quantification of engineered particles in urban runoff. *Chemosphere* **2020**, *248*, 126070.
155. Olabarrieta, J.; Zorita, S.; Peña, I.; Rioja, N.; Monzón, O.; Benguria, P.; Scifo, L., Aging of photocatalytic coatings under a water flow: long run performance and TiO₂ nanoparticles release. *Applied Catalysis B: Environmental* **2012**, *123*, 182-192.
156. Zuin, S.; Gaiani, M.; Ferrari, A.; Golanski, L., Leaching of nanoparticles from experimental water-borne paints under laboratory test conditions. *Journal of Nanoparticle Research* **2014**, *16* (1), 2185.
157. Zhang, X.; Wang, M.; Guo, S.; Zhang, Z.; Li, H., Effects of weathering and rainfall conditions on the release of SiO₂, Ag, and TiO₂ engineered nanoparticles from paints. *Journal of Nanoparticle Research* **2017**, *19* (10), 338.

Chapter 2 Release of TiO₂ nanoparticles from painted surfaces in cold climates: characterization using a high sensitivity single-particle ICP-MS

Connecting text: Paints and coatings represent one of the major applications of TiO₂ nanoparticles (NPs). While it has been previously shown that NPs are released from painted surfaces, there is still a lack of experimental data on their release rates under natural conditions and on the size distributions of the NPs following release. Here, the outdoor experiments along with indoor control studies were designed to quantify/characterize the paint-leached TiO₂ NPs and identify the main weathering factors that contribute to enhanced NP release. To this end, an analytical methodology using a highly sensitive single particle inductively coupled plasma mass spectrometer (SP-ICP-MS) was developed that improved the size detection limit of the technique down to < 20 nm for TiO₂ NPs. The results indicated that the release and subsequent fate of NPs are strongly dependent on meteorological conditions, *e.g.* temperature, precipitation, and freeze-thaw.



Published as: Azimzada, A., Farner, J. M., Hadioui, M., Liu-Kang, C., Jreije, I., Tufenkji, N., & Wilkinson, K. J., Release of TiO₂ nanoparticles from painted surfaces in cold climates: characterization using a high sensitivity single-particle ICP-MS. *Environmental Science: Nano* 2020, 7(1), 139-148.

2.1 Introduction

Recent advances in nanotechnology have led to greater numbers of nano-enabled products and increased production volumes of engineered nanomaterials (ENMs).¹ With the growing production and applications of ENMs, their release into the environment is inevitable, necessitating research into their environmental fate.²⁻⁴ TiO₂ nanoparticles (NPs) are the most widely produced ENM on a mass basis.⁵⁻⁷ Among other applications, they are extensively used in paints and coatings, where they can provide UV protection and self-cleaning properties.⁸⁻¹⁰

While the use of TiO₂ NPs in paints is on the rise and their release from aged painted surfaces is imminent, their reliable risk assessment remains a challenge in environmental systems.^{1, 9, 10} This is largely due to limited existing knowledge on their mass and number concentrations, measurements of their surface-release rates and information on their particle size distributions and persistence in the environment.^{5, 11, 12} Among the limited analytical data available, lab-controlled tests conducted in simple media have clearly shown significant NP leaching of painted surfaces, with some of the released NPs still embedded in the organic paint matrix.^{13, 14} Olabarrieta *et al.*¹⁵ and Al-Kattan *et al.*¹⁶ demonstrated that TiO₂ NPs were released from coatings weathered by flowing water, while Zhang *et al.*¹⁷ and Zuin *et al.*¹⁸ showed that static immersion in water could induce NP release.

Outdoor studies^{13, 19-21}, while more difficult to control, are more appropriate for evaluating real-world NP release scenarios. For example, Kaegi *et al.*^{19,13} followed the release of Ti and Ag from a painted exterior façade over 1 year and concluded that much of the released metal was in nanoparticulate form, with the estimated primary particle sizes for TiO₂ between 20 and 300 nm and Ag below 15 nm. To the best of our knowledge, outdoor studies investigating NP release in cold climates – where snow, freezing and freeze-thaw conditions are relevant – are not yet available.

Most of the above studies estimated release based on an increase in total metal concentrations in the waters that were in contact with the painted surface and confirmed the presence of NPs using microscopic data. In such cases, it is difficult to quantify to what extent NPs or dissolved metals were released. An additional difficulty in outdoor studies is the significant presence of the target elements in the incoming precipitation^{22, 23}. Overall, NP analysis in complex waters is a challenging task,²⁴⁻²⁶ requiring accurate NP release determinations that can identify, size and quantify the NPs on a particle-by-particle basis. To that end, single-particle ICP-MS (SP-ICP-MS) is well suited to provide information on NP size

distributions and number concentrations in natural waters.^{27, 28} It is based on the ultrafast measurement and analysis of the transient ICP-MS signal. NPs typically generate high intensity signals (spikes, ca. 300-500 μ s) that can be discriminated from a continuous (generally low-intensity) background, representative of the dissolved metals (and small NPs).²⁹ While the technique is extremely sensitive for several metallic NPs (*e.g.* Ag, Au, Ce), the analysis of TiO₂ is more challenging, due primarily to high levels of background interferences.^{24, 25, 29} For this reason, most of the reported size detection limits (SDL) for TiO₂ NPs are above 50 nm,³⁰⁻³² restricting characterization of the smaller NPs, which are thought to be of higher risk to both the environment and human health.³³

Given this context, the goal of the study was to quantify the release of TiO₂ NPs from nano-enhanced surfaces under natural weathering conditions. The study was designed to: (i) characterize release of TiO₂ NPs by measuring NP concentrations and size distributions with time and (ii) explore the role of temperature fluctuations (*i.e.* freeze, thaw) and wet/dry conditions on NP release. Experiments were designed to provide insight into the release and persistence of these important NPs in the environment.

2.2 Materials and Methods

Preparation of exposure panels. Untreated oak slats (0.64 cm thick x 6.4 cm wide) were cut to 8.4 cm long panels, which were primed and painted with a white paint advertised for its Nanoguard Technology (Behr Premium Plus Ultra Exterior Satin Enamel Ultra Pure White paint). A uniform coating was obtained by applying 15 mL/side to each panel and removing excess paint with an applicator (Bird Film Applicator, Inc, Washington, USA) in order to get a wet film thickness of 4 mm. Both sides of the panel were coated twice, and the paint was allowed to dry for at least two days before the addition of the next layer. The final dry paint loading on each panel was 400 ± 40 g m⁻² (or 4.4 g/panel).

Outdoor weathering setup. For outdoor weathering experiments, replicate samples of the painted panels were placed vertically in pre-weighed, wide-mouth polypropylene containers (500 mL, Fisher Scientific). Containers were randomly ordered within plastic bins and placed outdoors (**Fig. S1**) on a 4th floor roof (M. H. Wong building, McGill University, Montreal, Canada), where they were left uncovered. The base of the bin was lined with sand bags to prevent tipping. Samples were left undisturbed during the weathering period except when snowfall buried the containers. In those cases, excess snow was carefully scraped off the top of the containers to prevent overflow when the snow melted. Winter weathering experiments

were conducted for 10 weeks beginning in mid-February (2018), while 7 weeks of summer experiments were initiated in early June (2018). At each experimental timepoint, four control samples (container containing no painted panel) and four samples (container containing painted panels) were sacrificed.

Indoor (controlled) weathering setup. For controlled weathering experiments, panels were placed in pre-weighed polypropylene containers (4 sample replicates), which were either filled with 380 mL of Milli-Q water (wet) or not (dry). Samples were then aged under room temperature (RT), freezing (FR), or freeze-thaw (FT) conditions. For FR and FT conditions, samples were placed in a -10 °C freezer. FT conditions consisted of repeated 48 h cycles in which samples were first allowed to freeze overnight (for 24 h), then removed from the freezer and placed in a closed box on the benchtop, where they were allowed to thaw (for 24 h). The experiment was conducted for a total of 42 d (21 FT cycles). At the end of the 42-d exposure, dry FR samples were soaked for 1 d in Milli-Q water, while wet FR samples were allowed to thaw (1 d). For the wet samples (both RT & FT), in addition to the 42 d timepoint, small samples (16-18 mL) were removed at intermediate timepoints during the exposure. The sampled volume was replaced with fresh Milli-Q water in order to maintain a constant exposure surface.

Sample preparation for SP-ICP-MS. For each timepoint, the outdoor and control containers to be tested were capped and all snow or ice was allowed to melt. The contents of the containers were then gently mixed, and the panels were carefully removed. Water was weighed, mixed, and then placed in a sonicator bath for 30 minutes (Branson Ultrasonic Cleaner, 5510R-DTH Model, 135 W, 42 kHz \pm 6%). Following sonication, 8-10 mL of sample was filtered through a 0.45 μ m, 33 mm diameter PVDF syringe filter that had been pre-rinsed with 12 mL Milli-Q water and 6 mL of sample. Filtration was performed to avoid blockage of the microflow nebulizers, without removing significant quantities of NPs.

SP-ICP-MS analysis and data acquisition. All NP measurements were performed on a sector field ICP-MS (AttoM ES, Nu Instruments, UK), at low resolution (300), using single ion acquisition in fast-scan mode. Liquid samples were introduced through a micro-flow concentric glass nebulizer (free aspiration rate of 200 μ L min⁻¹ for 1 L min⁻¹ Ar) into a quartz cyclonic spray chamber cooled at 4 °C. The enhanced sensitivity^{27, 34} of the sector-field instrument (with respect to a quadrupole-based instrument) allowed us to analyse ⁴⁹Ti, which has a lower natural abundance, but also fewer interferences. An optimized dwell time of 50 μ s was used³⁵, with an

acquisition time of 50 s, which resulted in ca. 10^6 datapoints per replicate. Sensitivity calibrations for ^{49}Ti were based on ionic standards (High Purity Standards). Transport efficiency (TE) measurements were performed using a suspension of ultra-uniform 30 nm Au NPs (NanoComposix, AUXU30-1M), which were prepared daily at 50 ng L^{-1} . TE measurements were validated with a second standard reference material (60 nm Au NPs, NIST8013). TE values ranged within $0.10\text{-}0.12 \mu\text{L s}^{-1}$ (3.4-3.8 %). Standard additions were performed on ionic Ti standards ($1, 5$ and $10 \mu\text{g L}^{-1}$) and spikes of engineered TiO_2 NPs (P25 Aeroxide, Evonik, Germany; nominal size 25 nm) in the rain or snow melt water in order to assess possible matrix effects. Size calculations were performed using an assumed TiO_2 density of 4.23 g cm^{-3} (*i.e.* rutile). Filtered samples were diluted 10-50x in order to ensure that the number of particle events was significant (> 500 events), while minimizing the possibility for co-incident events (less than 10,000 events, or 1 % of the total datapoints).

SP-ICP-MS data processing. SP-ICP-MS data was processed using NuQuant software version 2.2 (Nu Instruments, UK),²⁷ based on the methodology laid out by Hadioui *et al.*³⁵ and Shaw *et al.*³⁴ In summary, data processing involved the identification of NP peaks, calculation of the local backgrounds and integration of the peaks. An average of the local peak backgrounds was used to calculate dissolved metal content. Values of the full-width at half-maximum (FWHM) were used to flag peak events that could potentially be co-incident NP peaks or background artifacts (*i.e.* very slender or very wide peaks with low intensity). Flagged events were visually inspected, and if necessary, the samples were diluted further.

Total metal analysis. Following the filtration of samples for SP-ICP-MS, aliquots of the filtered samples were added to polypropylene tubes containing 67-70 % HNO_3 (ultratrace grade, BDH Aristar Ultra) in order to achieve a final acid content of 20% v/v. Tubes were left for 16 h at $85 \text{ }^\circ\text{C}$ using a DigiPREP digestion system (SCP Science) and then diluted with Milli-Q water to obtain a final HNO_3 content of 4% v/v, which was used for quantitative ICP-MS analysis. Given the well documented difficulties in digesting TiO_2 ³⁶, these measurements should be operationally defined as acid-extractable Ti.

2.3 Results and Discussion

Optimization of SP-ICP-MS for TiO_2 NPs. In comparison to other prevalent NPs such as Ag, CeO_2 and Au, detection and characterization of TiO_2 NPs using SP-ICP-MS is significantly more challenging.³⁰ This is primarily due to isobaric/polyatomic interferences that increase the background signal for ^{48}Ti , which is of greatest natural abundance.³⁷ To overcome these challenges, the study used recently published³⁵, optimized SP-ICP-MS strategies (for further

details, refer to SI). Consequently, the combination of high sensitivity, low background and improved NP peak resolution/recognition led to SDLs that were as low as 20 nm for TiO₂ NPs in the snow and rain waters, which were the matrix of interest. Indeed, the particle size distribution (PSD) of TiO₂ NPs (**Fig. 2-1A**) and the raw signal intensities corresponding to the smallest detected NP (**Fig. 2-1B**) are presented for NPs detected in a snow melt sample.

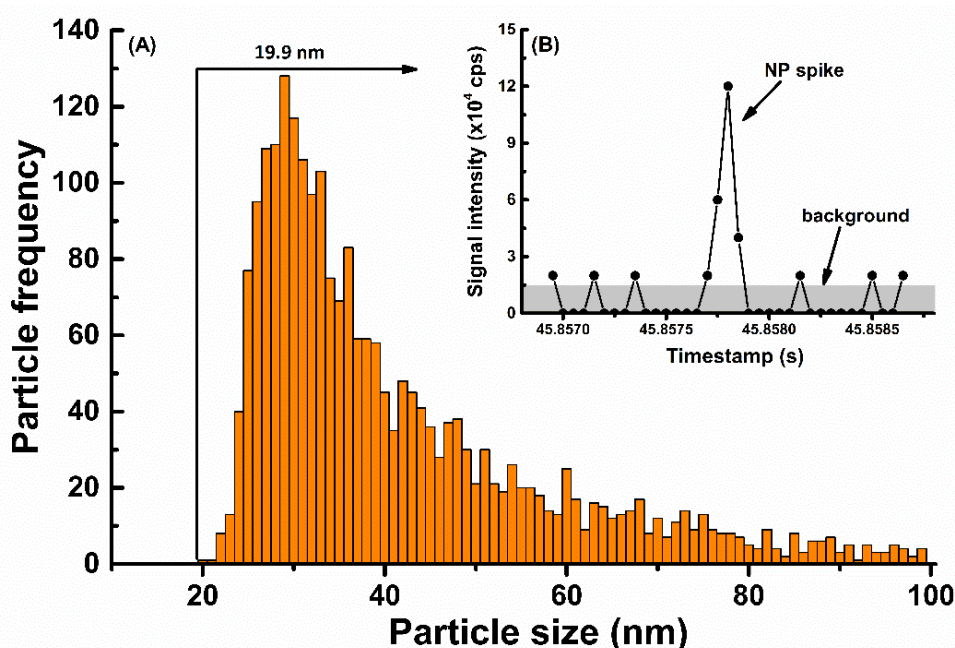


Figure 2-1. (A) Particle size distribution of Ti-containing NPs found in snow melt water, as measured with high-sensitivity magnetic-sector ICP-MS using a dwell time of 50 μ s. (B) Raw signal intensity (cps) near the particle size detection limit. Particle diameters were calculated on the assumption that the particles were TiO₂.

Verification of an absence of matrix effect is difficult with TiO₂ NPs, given the difficulty to obtain monodisperse TiO₂ standards. Therefore, several strategies were undertaken to verify and reduce matrix effects during the measurements of TiO₂ NPs: (i) tests on the matrix effect were performed using ionic Ti; (ii) TiO₂ NPs were measured following their spike into a natural rainwater matrix, which had a pre-existing NP background; (iii) SP-ICP-MS measurements were performed in media that were diluted at least 10x. Indeed, nearly identical recoveries (*i.e.* 102 %) were obtained for a spike of ionic Ti measured in Milli-Q water or rainwater (**Table 2-S1**), suggesting that the matrix effect for ⁴⁹Ti was minimal. When spiking TiO₂ NPs (nominal size of 25 nm) into the rainwater, a recovery of 92% was attained, following correction for particle numbers in the unspiked rainwater (**Fig. 2-S2**). In that case, the slightly

lower recoveries may have been caused by TiO₂ losses following their agglomeration in the rainwater matrix.

Detection of Ti NPs in natural precipitation. Very early in the weathering study, it became clear that significant NP concentrations were being detected in the precipitation, prior to it coming in contact with the painted surfaces. Owing their presence to a variety of natural, urban or industrial sources, nano- and micron-sized particles are ubiquitous in the atmosphere, and they are especially important in urban and industrial areas subjected to pollution.^{22, 23, 38, 39} Therefore, it was essential to accurately determine Ti NP concentrations in the natural precipitation in order to correct for their presence during the paint-release studies. Given that we have no *a priori* information on the full chemical composition of the Ti-containing NPs, sizes have been calculated based upon the assumption that they are primarily TiO₂. It is thus important to acknowledge that, for particles that are more likely to have multi-element compositions, such as natural nanominerals,^{22, 38, 40} actual particle sizes would be underestimated. On the other hand, for some particles, such as Magneli phase Ti (Ti_xO_{2x-1}), which are produced incidentally during coal combustion²², sizes would be overestimated. Indeed, in this study, numerous metals, including Ti, Ce, Fe, La, Nd, U and Ag were found in particulate forms by SP-ICP-MS time-scan (**Fig. 2-S3**), with the results strongly indicating the presence of atmospheric NPs containing Ti (**Fig. 2-2A**). Micron-sized particles were also present in the precipitation; when comparing ICP-MS measurements on acidified samples measured before and after filtration, >90% of the particulate Ti was generally removed by a 0.45 μm membrane (based on total Ti mass balances). SP-ICP-MS measurements performed on the filtered samples showed that the remaining NPs had diameters with a mode around 30 nm and a size distribution extending from the SDL (20 nm) to beyond 100 nm (**Fig. 2-2B**). Snow and rain samples were analysed for both total Ti by ICP-MS and Ti NPs by SP-ICP-MS, with the results showing that significant numbers of Ti-containing NPs were found in the snow and rain samples. A subsequent experiment where Milli-Q water was left outdoors for 2 d under dry summer conditions also showed significant particle numbers (**Fig. 2-S4**), suggesting that dry deposition was an important source of the Ti NPs. This observation was also observed for a Milli-Q water sample exposed to indoor air (**Fig. 2-S5**). The ubiquitous presence of Ti NPs in the air demonstrates the importance of multiple control experiments in order to avoid false positives in the paint release experiments.

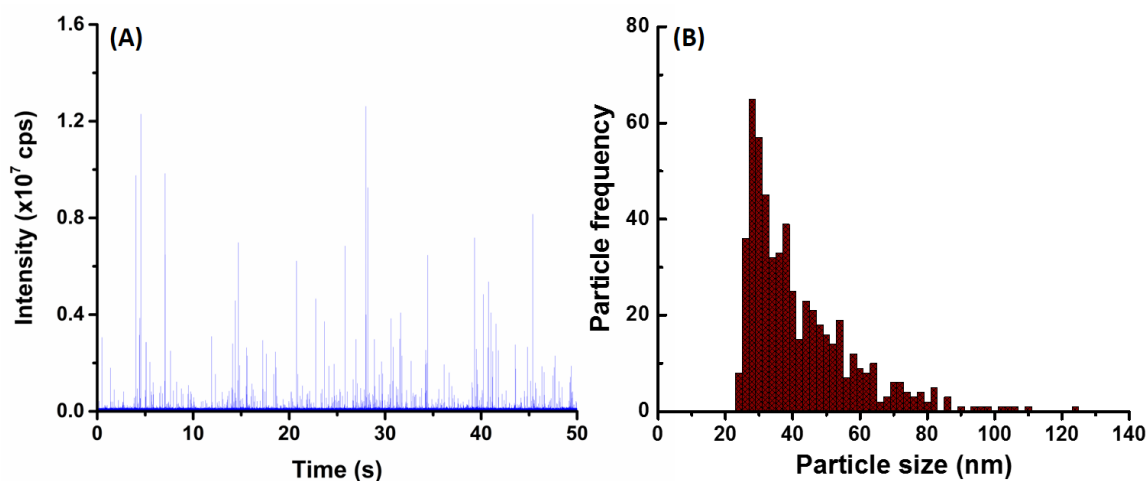


Figure 2-2. (A) Time-resolved SP-ICP-MS signal and the corresponding (B) particle size distribution obtained for Ti-containing NPs in snow melt (10x diluted). The snow was collected during 2 weeks in February 2018, and the measurements were performed by high-sensitivity magnetic-sector ICP-MS. Particle diameters were calculated on the assumption that particles were TiO₂.

TiO₂ NPs in paint. The water-based acrylic paint was tested for TiO₂ NPs using SP-ICP-MS after dilution ($2 \times 10^7 \times$ (w/w)) in Milli-Q water. The PSD for TiO₂ extended from 20 nm (SDL) to beyond 200 nm, with most of the detected NPs around 150 ± 10 nm (mode) with a mean NP diameter of 131 ± 1 nm (Fig. 2-S6A). There were approx. $(6.8 \pm 0.1) \times 10^{15}$ NPs/kg-paint (*i.e.* below 250 nm) in the liquid paint, which corresponded to about 5.0 % by weight. This measured NP fraction is in agreement with other reports for paints,^{5, 8, 16, 41} where experimental or predicted TiO₂ fractions are reported to be around 1-15% by weight.

TiO₂ NP release due to weathering. Experimental containers with or without a painted panel were placed outdoors. In the control samples (*i.e.* without panels), NP numbers were significant and generally increased with time, in both the winter and summer sampling periods. The actual measured concentrations ranged from 8.1×10^5 NP/mL after two weeks to 1.2×10^7 NP/mL after 7 weeks in the winter and hovered around $2 - 4 \times 10^6$ NP/mL for 7 weeks during the summer. The observed increase in NP numbers is primarily attributed to cumulative NP deposition (directly via rain/snow or indirectly via dry deposition, see Fig. 2-S4), although part of the variation can be attributed to differences in the sample volumes at the time of collection (due to the timing of evaporation/precipitation events). When the data were normalized by exposure surface area of the painted panels, both total Ti and Ti NP (Fig. 2-3A, 2-3B, orange

bars) consistently increased with time at an approximate rate of $9.2 \mu\text{g-Ti m}^{-2} \text{ week}^{-1}$ (this corresponds to a rate of $30.9 \mu\text{g-Ti m}^{-2} \text{ week}^{-1}$ when normalized by footprint area).

In spite of this relatively large and increasing background signal, greater NP numbers (and masses) were observed in the containers containing painted surfaces (**Fig. 2-3A, 2-3B**). Raw SP-ICP-MS data comparing the precipitation (snow meltwater) (**Fig. 2-4A**) to snow meltwater that was in contact (2 weeks) with the painted panel (**Fig. 2-4B**) showed significantly more spikes, which was attributed to the release of particles from the paint. PSDs were strikingly similar (**Fig. 2-4C, 2-4D**), with most of the NPs uniformly observed for sizes below 60 nm.

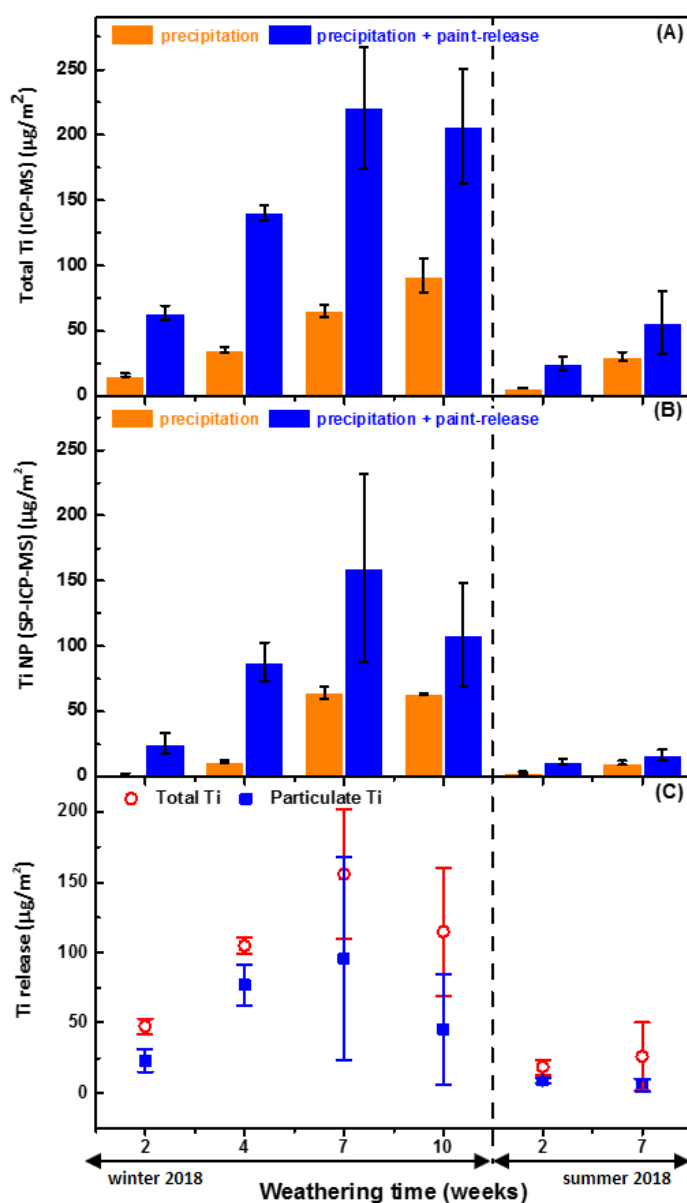


Figure 2-3. Quantification of Ti in the natural precipitation as well as the precipitation following its contact with painted panels: **(A)** total Ti measured by ICP-MS, **(B)** Ti NP measured by SP ICP-MS, and **(C)** the net release of total and nanoparticulate Ti during the winter and summer seasons. The quantities are expressed in terms of Ti metal content and are normalized by the exposure area of the painted panels. Error bars indicate standard deviations, where n=4.

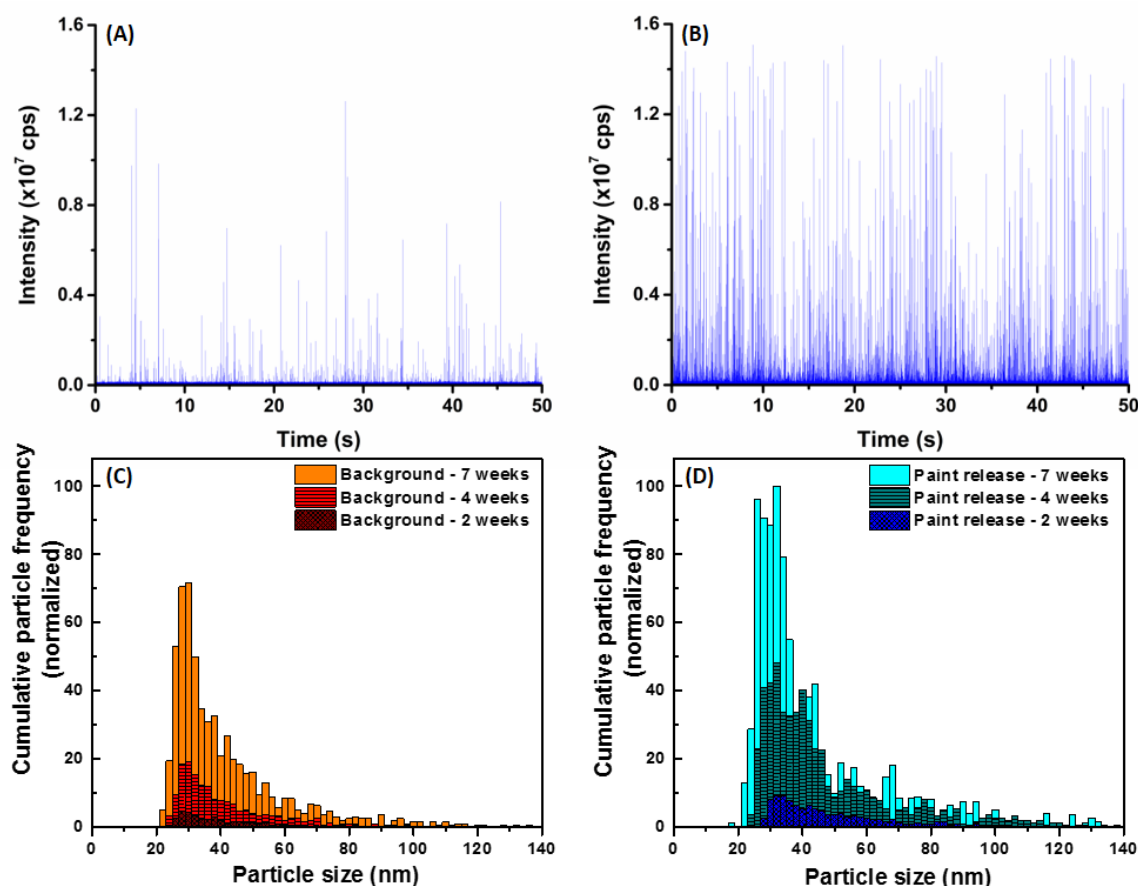


Figure 2-4. Time-resolved SP-ICP-MS signal (*i.e.* raw data) for Ti-containing NPs in **(A)** snow meltwater and **(B)** snow after 2 weeks of contact with a painted panel. Particle size distributions were obtained for **(C)** Ti-containing NPs in the natural precipitation background and **(D)** for NP released from the painted surfaces, over several weeks during the winter season. Note that paint-released NP frequencies are already corrected for background NPs occurring in the precipitation. Particle diameters were calculated on the assumption that particles were TiO₂.

Significant release of Ti (ANOVA, $p < 0.05$) was observed (**Fig. 2-3C**), with a large proportion (55% on average) of it being attributed to the Ti NPs. In the winter, NP release appeared to peak at $168 \pm 121 \mu\text{g m}^{-2}$, corresponding to $(3.4 \pm 2.5) \times 10^{11} \text{ NP m}^{-2}$ after 7 weeks and may have decreased after 10 weeks of exposure (**Fig. 2-3C, Table 2-1**), although the data are admittedly disparate due to the dynamic nature of this long-term exposure. Since

sampling was conducted in a sacrificial manner in order to take into account the cumulative nature of the exposure medium, error bars increased with time, especially for the longer exposures. Certainly, NP concentrations will change as the NPs undergo physicochemical transformations (*e.g.* agglomeration, dissolution)^{42, 43}, as the precipitation undergoes modifications (*e.g.* evaporation, wind removal of snow, pH changes, new precipitation renewal), or as sorptive losses occur¹¹.

Table 2-1. Quantification of the release of particulate TiO₂ NPs (<450 nm) from painted panel surfaces, following their natural weathering for several weeks in Winter 2018 and Summer 2018. Quantities are reported in terms of TiO₂ NP mass and number released per painted surface area or mass of dry paint load on the panel. The measurements were performed by high-resolution SP-ICP-MS.

Paint release of TiO ₂ NPs (<450 nm fraction)					
Season	Weathering time weeks	NP mass per surface area $\mu\text{g m}^{-2}$	NP mass per g-dry-paint $\text{ng g}^{-1}\text{-dry-paint}$	NP number per surface area NPs m^{-2}	NP number per g-dry-paint $\text{NPs g}^{-1}\text{-dry-paint}$
Winter	2	38 ± 14	119 ± 48	$(6.6 \pm 1.8) \times 10^{10}$	$(2.0 \pm 0.7) \times 10^8$
	4	128 ± 25	314 ± 40	$(2.3 \pm 0.6) \times 10^{11}$	$(5.4 \pm 1.4) \times 10^8$
	7	168 ± 121	370 ± 163	$(3.4 \pm 2.5) \times 10^{11}$	$(8.1 \pm 3.1) \times 10^8$
	10	75 ± 66	166 ± 153	$(1.2 \pm 1.7) \times 10^{11}$	$(2.3 \pm 3.9) \times 10^8$
Summer	2	15 ± 4	26 ± 7	$(3.2 \pm 0.6) \times 10^{10}$	$(5.3 \pm 0.9) \times 10^7$

There appeared to be greater NP release in the winter as compared to the summer. While NP release during the first 2 weeks of summer weathering could be easily distinguished from background levels in the precipitation, this distinction became statistically insignificant (ANOVA, $p > 0.05$) after 7 weeks due to lower release-to-background ratios. Lower release in the summer did not appear to be correlated to the quantity of precipitation since rain events during the summer averaged 3.0 mm day⁻¹ over the 7 weeks of exposure, whereas 2.5 mm day⁻¹ (water equivalent) of snow and rain was recorded during the 10 weeks of cold weather. Whereas summer precipitation was mostly limited to a few abundant rainfall events, the winter precipitation was more uniformly distributed (Fig. 2-S7).

In summary, the data clearly show that weathering of the painted panels increased NP concentrations in the precipitation. The outdoor data also suggest that weathering was likely more important in the winter than in the summer and that the sizes of the released NP were generally smaller than those in the original paint. These two points are examined in more detail in the following sections.

How did weathering conditions affect TiO₂ NP release? For the experiments conducted in the summer, less release was observed when compared to measurements performed in the

winter (*i.e.* **Fig. 2-3C**). The weather data (**Fig. 2-S7**) suggested that the summer samples underwent frequent wet-dry cycles with shorter liquid-surface interaction times, whereas the winter samples were nearly constantly exposed to snow or ice in addition to undergoing freeze-thaw cycles. Several controlled laboratory experiments were therefore designed to isolate the roles of seasonal variability, including the role of temperature, the role of moisture and the role of FT (freeze-thaw) cycles on the release of NPs from a painted surface. For a 42-day (6 week) exposure, cold conditions, wet conditions and FT conditions all contributed to increased NP release (**Fig. 2-5**). Among the different weathering conditions, exposure to water and FT cycles stood out as being important factors to boost NP release. For example, 27x more NPs were released from samples that underwent 21 FT cycles as compared to samples that were simply frozen (**Fig. 2-5**). On the other hand, wet RT samples released 12x more NPs than dry. Surprisingly, water did not appear to have an effect on the samples that were kept in the freezer in the absence of FT (**Fig. 2-5**). The data suggest that NP release is enhanced under wet conditions with high liquid-surface interaction times and increased further if the surface undergoes FT cycles. These results agree well with those for the natural weathering, consistent with the hypothesis that wet conditions along with FT cycles could indeed explain the increased NP release that was observed during the winter season.

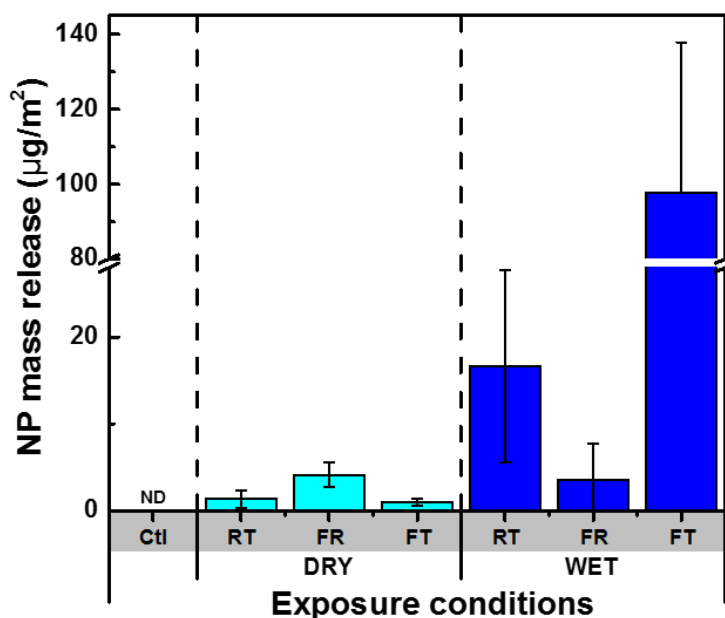


Figure 2-5. NP mass release under different exposure conditions, quantified by SP-ICP-MS and normalized by the exposure area of painted panels. Ctl refers to a control condition, where no panel was used. The exposure conditions consisted of dry and wet conditions, with RT, FR and FT denoting the sub-conditions of room temperature, only-freezing, and freeze-thaw,

respectively. The exposure duration was 42 days or 21 cycles (in the case of FT). ND denotes “not detected” (ANOVA, $p > 0.05$). Error bars indicate standard deviations, where $n = 4$.

In addition, time-resolved monitoring of the NP release was performed for the wet RT or FT (**Fig. 2-6**). During the first 18 days of weathering, no significant difference in the release quantities were observed; however, during the following 4 weeks of weathering (14 FT cycles), the mass of NPs released under FT conditions greatly surpassed those under RT conditions (**Fig. 2-6A**). Furthermore, while NP mass (and numbers) appeared to increase in the later stages of the FT experiments, they stabilized or decreased for the samples held at room temperature (**Fig. 2-6A**). As above, we hypothesize that NP loss is primarily driven by agglomeration⁴³ leading to sedimentation⁴⁴ of the NPs, as well as sorptive processes¹¹. This is consistent with the observation that the proportion of NP > 100 nm consistently increased during the 4 weeks of weathering, prior to declining slightly around 6 weeks (**Fig. 2-7**).

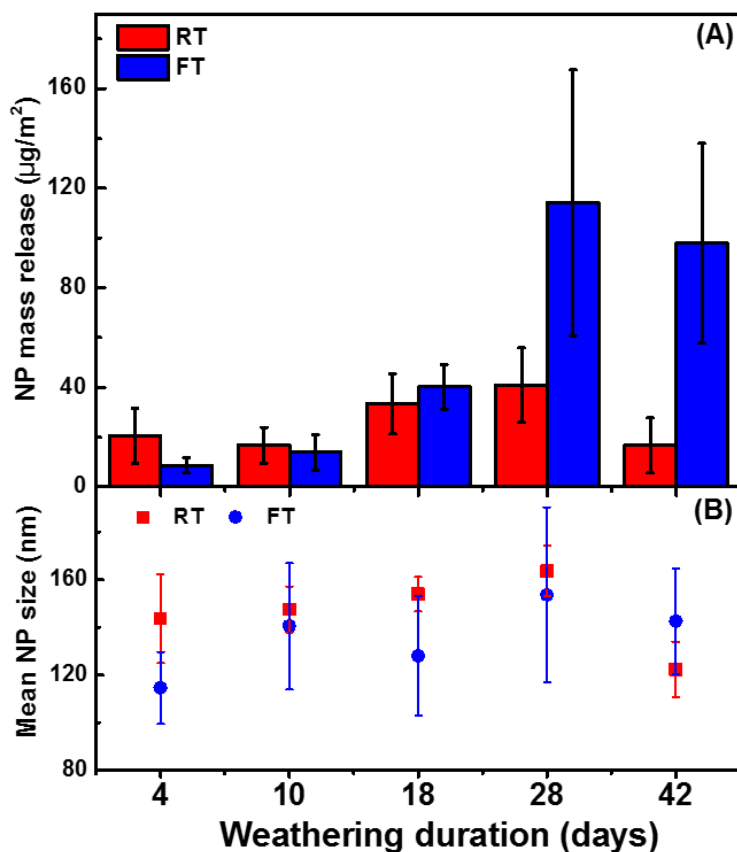


Figure 2-6. (A) NP mass release normalized by the exposure area of painted panels, for samples that were exposed to Milli-Q water (no NP background) under (wet) conditions of room temperature (RT) and freeze-thaw (FT) and (B) the corresponding mean NP sizes. The weathering duration of 4, 10, 18, 28 and 42 d correspond to 2, 5, 9, 14, and 21 FT cycles, respectively. Error bars indicate standard deviations, where $n = 4$.

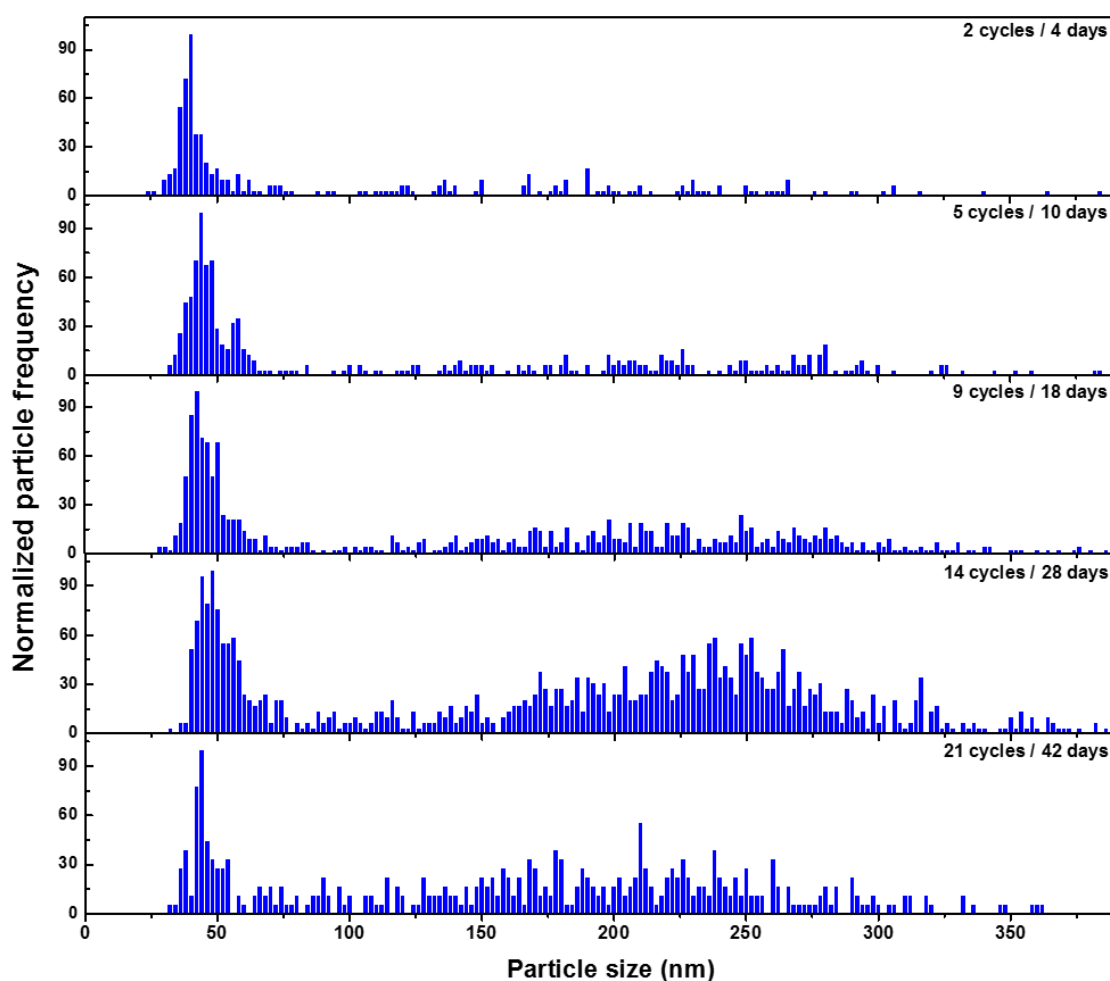


Figure 2-7. Particle size distributions for TiO₂ NPs following their release from painted surfaces that were exposed to several weeks of FT cycles in Milli-Q water (no NP background). Each cycle consisted of 1 day of freezing and 1 day of thawing. Particle diameters were calculated on the assumption that particles were TiO₂.

Are the sizes of weathered TiO₂ NPs similar to those that were originally in the paint?

The particle size distributions of the weathered NPs (**Fig. 2-4D**) appeared to be smaller than sizes that were obtained in the original paint sample (**Fig. 2-S6A**). Two experiments were conducted to validate this observation: (i) first, a painted board was soaked in Milli-Q water in a closed container for 4 d at room temperature (20 °C), in order to more easily detect NP release by reducing the background signal; (ii) second, under the assumption that the NPs were originally agglomerated in the paint, the paint was diluted ($2 \times 10^7 \times$), sonicated (30 min) and then stabilized through the addition of 5 mg L⁻¹ of a fulvic acid.⁴⁵

In Milli-Q water, a significant number of NPs were leached into solution and these NPs had a size distribution (**Fig. 2-S8**) that was very similar to what was observed under natural

conditions, *i.e.* most of the NPs were smaller than 60 nm with a wide size distribution extending beyond 200 nm. Significantly more NPs were detected at the lower end of the size distribution ($(8.4 \pm 0.1) \times 10^{15}$ NPs kg⁻¹-paint or 5.5 ± 0.1 % by weight) as compared to the diluted (unsonicated) paint sample ($(6.8 \pm 0.1) \times 10^{15}$ NPs kg⁻¹-paint or 5.0 ± 0.1 % by weight). This observation suggests that the NPs in the paint were at least partially dispersed by the sonication and stabilization (**Fig. 2-S6B**), resulting in the detection of more primary particles in the smaller size ranges.

Environmental considerations and implications. The natural and lab weathering data present firm evidence that TiO₂ NPs were leached out of painted surfaces, with the strongest release observed under wet and cold conditions – particularly, under conditions where freeze-thaw occurred. Although release escalated during the winter, the absolute quantity of release, even at its peak, was rather small, corresponding to <0.001 % of total TiO₂ NP load on the boards. While the weathering was fairly harsh, the study was conducted for 10 weeks only, and thus, given several years of life expectancy for painted façades (before renewal), increasingly more release could be expected, during long-term weathering and degradation of the surfaces. The results showed that environmental factors (*e.g.* temperature, moisture) will affect the quantity of NPs released in addition to influencing their fate through processes such as agglomeration, sedimentation and sorption.^{31, 46-49} These processes will certainly have an impact on the mobility and bio-accessibility of these released NPs and will thus alter their environmental risk.

Acknowledgements. This research was supported by the Natural Sciences and Engineering Research Council of Canada (NSERC), the Fonds du Recherche du Québec- Nature et Technologies (FRQNT), Environment and Climate Change Canada, and McGill Engineering Doctoral Award (MEDA). We thank Prof. S. Ghoshal (McGill University) for helpful discussions. The authors declare that they have no conflicts of interest.

2.4 References

1. Vance, M. E.; Kuiken, T.; Vejerano, E. P.; McGinnis, S. P.; Hochella Jr, M. F.; Rejeski, D.; Hull, M. S., Nanotechnology in the real world: Redeveloping the nanomaterial consumer products inventory. *Beilstein Journal of Nanotechnology* **2015**, *6* (1), 1769-1780.
2. Gottschalk, F.; Nowack, B., The release of engineered nanomaterials to the environment. *Journal of Environmental Monitoring* **2011**, *13* (5), 1145-1155.
3. Nowack, B.; Ranville, J. F.; Diamond, S.; Gallego-Urrea, J. A.; Metcalfe, C.; Rose, J.; Horne, N.; Koelmans, A. A.; Klaine, S. J., Potential scenarios for nanomaterial release and subsequent alteration in the environment. *Environmental Toxicology and Chemistry* **2012**, *31* (1), 50-59.

4. Giese, B.; Klaessig, F.; Park, B.; Kaegi, R.; Steinfeldt, M.; Wigger, H.; von Gleich, A.; Gottschalk, F., Risks, release and concentrations of engineered nanomaterial in the environment. *Scientific Reports* **2018**, *8* (1), 1565.
5. Sun, T. Y.; Gottschalk, F.; Hungerbühler, K.; Nowack, B., Comprehensive probabilistic modelling of environmental emissions of engineered nanomaterials. *Environmental Pollution* **2014**, *185*, 69-76.
6. Loosli, F.; Wang, J.; Rothenberg, S.; Bizimis, M.; Winkler, C.; Borovinskaya, O.; Flamigni, L.; Baalousha, M., Sewage spills are a major source of titanium dioxide engineered (nano)-particle release into the environment. *Environmental Science: Nano* **2019**, *6* (3), 763-777.
7. Weir, A.; Westerhoff, P.; Fabricius, L.; Hristovski, K.; Von Goetz, N., Titanium dioxide nanoparticles in food and personal care products. *Environmental Science & Technology* **2012**, *46* (4), 2242-2250.
8. Hincapié, I.; Caballero-Guzman, A.; Hiltbrunner, D.; Nowack, B., Use of engineered nanomaterials in the construction industry with specific emphasis on paints and their flows in construction and demolition waste in Switzerland. *Waste Management* **2015**, *43*, 398-406.
9. Hischer, R.; Nowack, B.; Gottschalk, F.; Hincapie, I.; Steinfeldt, M.; Som, C., Life cycle assessment of façade coating systems containing manufactured nanomaterials. *Journal of Nanoparticle Research* **2015**, *17* (2), 68.
10. Van Broekhuizen, P.; van Broekhuizen, F.; Cornelissen, R.; Reijnders, L., Use of nanomaterials in the European construction industry and some occupational health aspects thereof. *Journal of Nanoparticle Research* **2011**, *13* (2), 447-462.
11. Azimzada, A.; Tufenkji, N.; Wilkinson, K. J., Transformations of silver nanoparticles in wastewater effluents: links to Ag bioavailability. *Environmental Science: Nano* **2017**, *4* (6), 1339-1349.
12. Coll, C.; Notter, D.; Gottschalk, F.; Sun, T.; Som, C.; Nowack, B., Probabilistic environmental risk assessment of five nanomaterials (nano-TiO₂, nano-Ag, nano-ZnO, CNT, and fullerenes). *Nanotoxicology* **2016**, *10* (4), 436-444.
13. Kaegi, R.; Sinnet, B.; Zuleeg, S.; Hagendorfer, H.; Mueller, E.; Vonbank, R.; Boller, M.; Burkhardt, M., Release of silver nanoparticles from outdoor facades. *Environmental Pollution* **2010**, *158* (9), 2900-2905.
14. Al-Kattan, A.; Wichser, A.; Zuin, S.; Arroyo, Y.; Golanski, L.; Ulrich, A.; Nowack, B., Behavior of TiO₂ released from nano-TiO₂-containing paint and comparison to pristine nano-TiO₂. *Environmental Science & Technology* **2014**, *48* (12), 6710-6718.
15. Olabarrieta, J.; Zorita, S.; Peña, I.; Rioja, N.; Monzón, O.; Benguria, P.; Scifo, L., Aging of photocatalytic coatings under a water flow: long run performance and TiO₂ nanoparticles release. *Applied Catalysis B: Environmental* **2012**, *123*, 182-192.
16. Al-Kattan, A.; Wichser, A.; Vonbank, R.; Brunner, S.; Ulrich, A.; Zuin, S.; Nowack, B., Release of TiO₂ from paints containing pigment-TiO₂ or nano-TiO₂ by weathering. *Environmental Science: Processes & Impacts* **2013**, *15* (12), 2186-2193.
17. Zhang, X.; Wang, M.; Guo, S.; Zhang, Z.; Li, H., Effects of weathering and rainfall conditions on the release of SiO₂, Ag, and TiO₂ engineered nanoparticles from paints. *Journal of Nanoparticle Research* **2017**, *19* (10), 338.
18. Zuin, S.; Gaiani, M.; Ferrari, A.; Golanski, L., Leaching of nanoparticles from experimental water-borne paints under laboratory test conditions. *Journal of Nanoparticle Research* **2014**, *16* (1), 2185.
19. Kaegi, R.; Ulrich, A.; Sinnet, B.; Vonbank, R.; Wichser, A.; Zuleeg, S.; Simmler, H.; Brunner, S.; Vonmont, H.; Burkhardt, M., Synthetic TiO₂ nanoparticle emission from exterior facades into the aquatic environment. *Environmental Pollution* **2008**, *156* (2), 233-239.

20. Lankone, R. S.; Challis, K. E.; Bi, Y.; Hanigan, D.; Reed, R. B.; Zaikova, T.; Hutchison, J. E.; Westerhoff, P.; Ranville, J.; Fairbrother, H., Methodology for quantifying engineered nanomaterial release from diverse product matrices under outdoor weathering conditions and implications for life cycle assessment. *Environmental Science: Nano* **2017**, *4* (9), 1784-1797.
21. Künniger, T.; Gerecke, A. C.; Ulrich, A.; Huch, A.; Vonbank, R.; Heeb, M.; Wichser, A.; Haag, R.; Kunz, P.; Faller, M., Release and environmental impact of silver nanoparticles and conventional organic biocides from coated wooden façades. *Environmental Pollution* **2014**, *184*, 464-471.
22. Hochella, M. F.; Mogk, D. W.; Ranville, J.; Allen, I. C.; Luther, G. W.; Marr, L. C.; McGrail, B. P.; Murayama, M.; Qafoku, N. P.; Rosso, K. M., Natural, incidental, and engineered nanomaterials and their impacts on the Earth system. *Science* **2019**, *363* (6434), eaau8299.
23. Rahim, M. F.; Pal, D.; Ariya, P. A., Physicochemical studies of aerosols at Montreal Trudeau Airport: The importance of airborne nanoparticles containing metal contaminants. *Environmental Pollution* **2019**, *246*, 734-744.
24. Gondikas, A.; von der Kammer, F.; Kaegi, R.; Borovinskaya, O.; Neubauer, E.; Navratilova, J.; Praetorius, A.; Cornelis, G.; Hofmann, T., Where is the nano? Analytical approaches for the detection and quantification of TiO₂ engineered nanoparticles in surface waters. *Environmental Science: Nano* **2018**, *5* (2), 313-326.
25. Tharaud, M.; Gondikas, A. P.; Benedetti, M. F.; von der Kammer, F.; Hofmann, T.; Cornelis, G., TiO₂ nanomaterial detection in calcium rich matrices by spICPMS. A matter of resolution and treatment. *Journal of Analytical Atomic Spectrometry* **2017**, *32* (7), 1400-1411.
26. Fréchette-Viens, L.; Hadioui, M.; Wilkinson, K. J., Practical limitations of single particle ICP-MS in the determination of nanoparticle size distributions and dissolution: case of rare earth oxides. *Talanta* **2017**, *163*, 121-126.
27. Fréchette-Viens, L.; Hadioui, M.; Wilkinson, K. J., Quantification of ZnO nanoparticles and other Zn containing colloids in natural waters using a high sensitivity single particle ICP-MS. *Talanta* **2019**, *200*, 156-162.
28. Hadioui, M.; Peyrot, C.; Wilkinson, K. J., Improvements to Single Particle ICPMS by the Online Coupling of Ion Exchange Resins. *Anal Chem* **2014**, *86* (10), 4668-4674.
29. Meermann, B.; Nischwitz, V., ICP-MS for the analysis at the nanoscale—a tutorial review. *Journal of Analytical Atomic Spectrometry* **2018**, *33* (9), 1432-1468.
30. Lee, S.; Bi, X.; Reed, R. B.; Ranville, J. F.; Herckes, P.; Westerhoff, P., Nanoparticle size detection limits by single particle ICP-MS for 40 elements. *Environmental Science & Technology* **2014**, *48* (17), 10291-10300.
31. Gondikas, A. P.; Kammer, F. v. d.; Reed, R. B.; Wagner, S.; Ranville, J. F.; Hofmann, T., Release of TiO₂ nanoparticles from sunscreens into surface waters: a one-year survey at the old Danube recreational Lake. *Environmental Science & Technology* **2014**, *48* (10), 5415-5422.
32. Peters, R. J.; van Bommel, G.; Milani, N. B.; den Hertog, G. C.; Undas, A. K.; van der Lee, M.; Bouwmeester, H., Detection of nanoparticles in Dutch surface waters. *Science of the Total Environment* **2018**, *621*, 210-218.
33. Auffan, M.; Rose, J.; Bottero, J.-Y.; Lowry, G. V.; Jolivet, J.-P.; Wiesner, M. R., Towards a definition of inorganic nanoparticles from an environmental, health and safety perspective. *Nature Nanotechnology* **2009**, *4* (10), 634.
34. Shaw, P.; Donard, A., Nano-particle analysis using dwell times between 10 μs and 70 μs with an upper counting limit of greater than 3 × 10⁷ cps and a gold nanoparticle detection limit of less than 10 nm diameter. *Journal of Analytical Atomic Spectrometry* **2016**, *31* (6), 1234-1242.

35. Hadioui, M.; Knapp, G. v.; Azimzada, A.; Jreije, I.; Frechette-Viens, L.; Wilkinson, K. J., Lowering the size detection limits of Ag and TiO₂ nanoparticles by Single Particle ICP-MS. *2019*, *91* (20), 13275-13284.
36. De la Calle, I.; Menta, M.; Seby, F., Current trends and challenges in sample preparation for metallic nanoparticles analysis in daily products and environmental samples: A review. *Spectrochimica Acta Part B: Atomic Spectroscopy* **2016**, *125*, 66-96.
37. May, T. W.; Wiedmeyer, R. H., A table of polyatomic interferences in ICP-MS. *Atomic Spectroscopy* **1998**, *19*, 150-155.
38. Hochella, M. F.; Lower, S. K.; Maurice, P. A.; Penn, R. L.; Sahai, N.; Sparks, D. L.; Twining, B. S., Nanominerals, mineral nanoparticles, and earth systems. *Science* **2008**, *319* (5870), 1631-1635.
39. Wagner, S.; Gondikas, A.; Neubauer, E.; Hofmann, T.; von der Kammer, F., Spot the difference: engineered and natural nanoparticles in the environment—release, behavior, and fate. *Angewandte Chemie International Edition* **2014**, *53* (46), 12398-12419.
40. Plathe, K. L.; Von Der Kammer, F.; Hassellöv, M.; Moore, J. N.; Murayama, M.; Hofmann, T.; Hochella Jr, M. F., The role of nanominerals and mineral nanoparticles in the transport of toxic trace metals: Field-flow fractionation and analytical TEM analyses after nanoparticle isolation and density separation. *Geochimica et Cosmochimica Acta* **2013**, *102*, 213-225.
41. Hischier, R.; Nowack, B.; Gottschalk, F.; Hincapie, I.; Steinfeldt, M.; Som, C. J. J. o. n. r., Life cycle assessment of façade coating systems containing manufactured nanomaterials. **2015**, *17* (2), 68.
42. Domingos, R.; Gelabert, A.; Carreira, S.; Cordeiro, A.; Sivry, Y.; Benedetti, M. In *Metals in the aquatic environment-Interactions and implications for the speciation and bioavailability*, ABSTRACTS OF PAPERS OF THE AMERICAN CHEMICAL SOCIETY, AMER CHEMICAL SOC 1155 16TH ST, NW, WASHINGTON, DC 20036 USA: 2016.
43. Ottofuelling, S.; Von Der Kammer, F.; Hofmann, T., Commercial titanium dioxide nanoparticles in both natural and synthetic water: comprehensive multidimensional testing and prediction of aggregation behavior. *Environmental Science & Technology* **2011**, *45* (23), 10045-10052.
44. Botta, C.; Labille, J.; Auffan, M.; Borschneck, D.; Miche, H.; Cabié, M.; Masion, A.; Rose, J.; Bottero, J.-Y., TiO₂-based nanoparticles released in water from commercialized sunscreens in a life-cycle perspective: Structures and quantities. *Environmental Pollution* **2011**, *159* (6), 1543-1550.
45. Domingos, R. F.; Tufenkji, N.; Wilkinson, K. J., Aggregation of titanium dioxide nanoparticles: role of a fulvic acid. *Environmental Science & Technology* **2009**, *43* (5), 1282-1286.
46. Zhou, D.; Ji, Z.; Jiang, X.; Dunphy, D. R.; Brinker, J.; Keller, A. A., Influence of material properties on TiO₂ nanoparticle agglomeration. *PLoS One* **2013**, *8* (11), e81239.
47. Reed, R.; Martin, D.; Bednar, A.; Montañó, M.; Westerhoff, P.; Ranville, J., Multi-day diurnal measurements of Ti-containing nanoparticle and organic sunscreen chemical release during recreational use of a natural surface water. *Environmental Science: Nano* **2017**, *4* (1), 69-77.
48. Farner, J. M.; Cheong, R. S.; Mahé, E.; Anand, H.; Tufenkji, N., Comparing TiO₂ nanoparticle formulations: stability and photoreactivity are key factors in acute toxicity to *Daphnia magna*. *Environmental Science: Nano* **2019**, *6*, 2532-2543.
49. Christian, P.; Von der Kammer, F.; Baalousha, M.; Hofmann, T., Nanoparticles: structure, properties, preparation and behaviour in environmental media. *Ecotoxicology* **2008**, *17* (5), 326-343.

2.5 Supplementary Information

Optimization of SP-ICP-MS for TiO₂ NPs. Since the lowest size that can be detected (*i.e.* SDL) is inversely related to the ratio of signal (S) to background (B) ($SDL=f(B/S)^{1/3}$), SDL will increase with increasing complexity of the matrix and is particularly high in the environmental media, where ⁴⁸Ca, S, N and O (*i.e.* S-N, S-O polyatomic interferences) concentrations are important.^{1, 2} Indeed, SDL of 50-100 nm are generally reported for TiO₂ NPs.³⁻⁶ Therefore, several strategies were employed to improve the ratio of signal-to-noise (background) and thereby lower the SDL⁷: (i) a high sensitivity magnetic-sector ICP-MS was used rather than a quadrupole ICP-MS; (ii) interferences were minimized by analyzing an isotope, Ti-49, that had relatively few interferences in natural matrices, and (iii) very small dwell times (50 μs) were employed, which helped further reduce the background and yield well-defined NP peaks. In addition, discrimination of NP from the background signal used a powerful peak recognition algorithm that took into account the local background variations and facilitated identification of peak artifacts. Raw data showing peaks near the SDL were visually monitored to ensure that each peak consisted of at least 4 integration points (*i.e.* minimum peak width of 200 μs). Further details on the technique and data processing can be found in our previous work⁷.



Figure 2-S1. A photo of the outdoor weathering setup on the 4th floor roof of Wong building (McGill University, Montreal, QC). The photo was taken on the start day of winter weathering experiments, February 13, 2018.

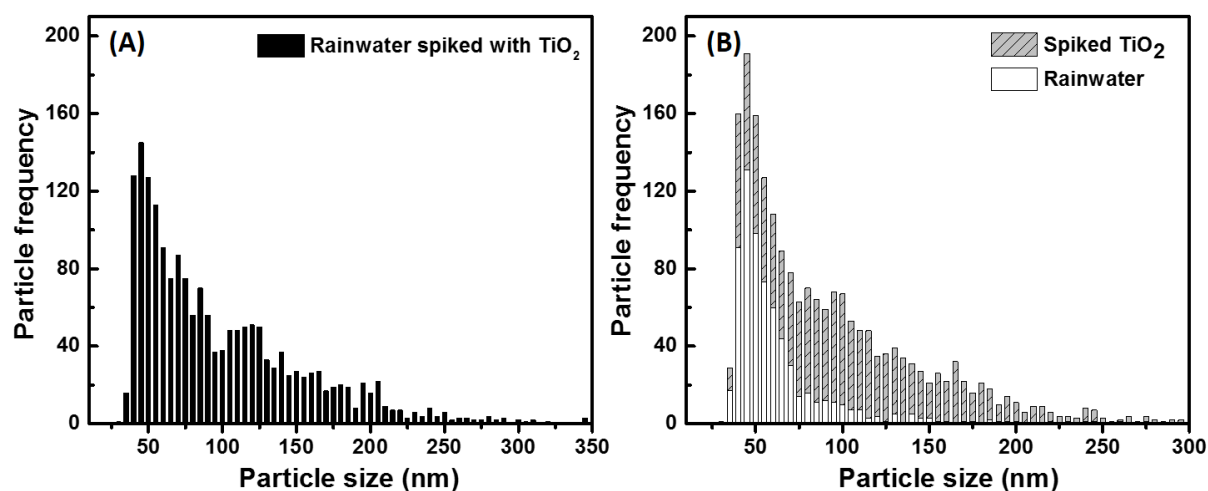


Figure 2-S2. (A) Particle size distribution of TiO₂ NPs (148,100 NP/mL) after spiking engineered TiO₂ NPs (nominal size of 25 nm) into the rainwater medium, (B) Cumulative particle size distributions of TiO₂ in the rainwater (54,640 NP/mL) and for the TiO₂ NPs suspended in Milli-Q water (106,500 NP/mL) before mixing. Measurements were performed on a magnetic-sector ICP-MS. Particle diameter were calculated on the assumption that particles were solely TiO₂.

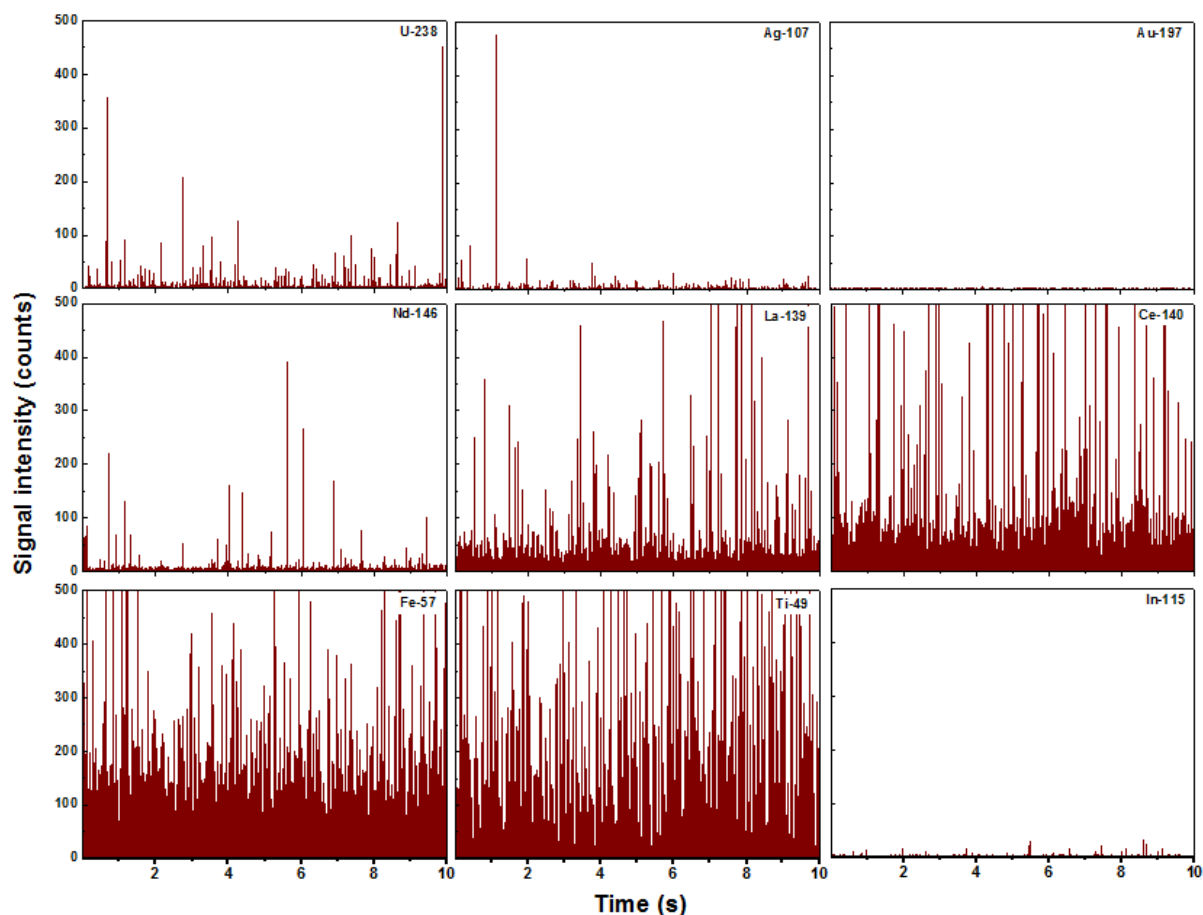


Figure 2-S3. Time-resolved SP-ICP-MS signals (*i.e.* raw data) obtained for ^{238}U , ^{107}Ag , ^{197}Au , ^{146}Nd , ^{139}La , ^{140}Ce , ^{57}Fe , ^{49}Ti and ^{115}In in a filtered ($0.45\ \mu\text{m}$) rainwater sample (collected in Montreal, QC). Data were acquired for a total of 10 s using a dwell time of $50\ \mu\text{s}$ on a magnetic-sector ICP-MS. Signal spikes indicate the presence of metallic particles.

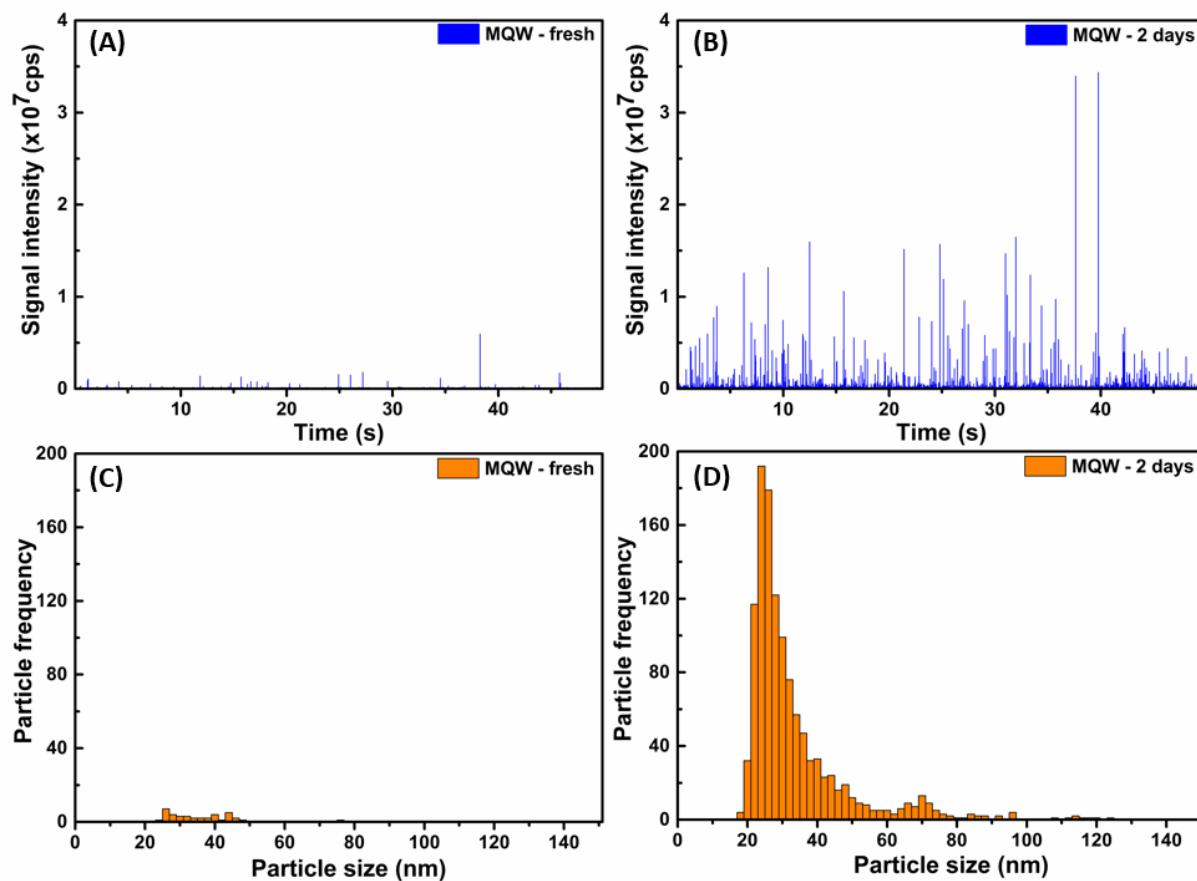


Figure 2-S4. Time-resolved SP-ICP-MS signal obtained following the analysis of (A) fresh Milli-Q water and (B) Milli-Q water exposed to outdoor air for 2 days, as well as (C, D) their corresponding particle size distributions. Particle diameters were calculated on the assumption that particles were TiO₂.

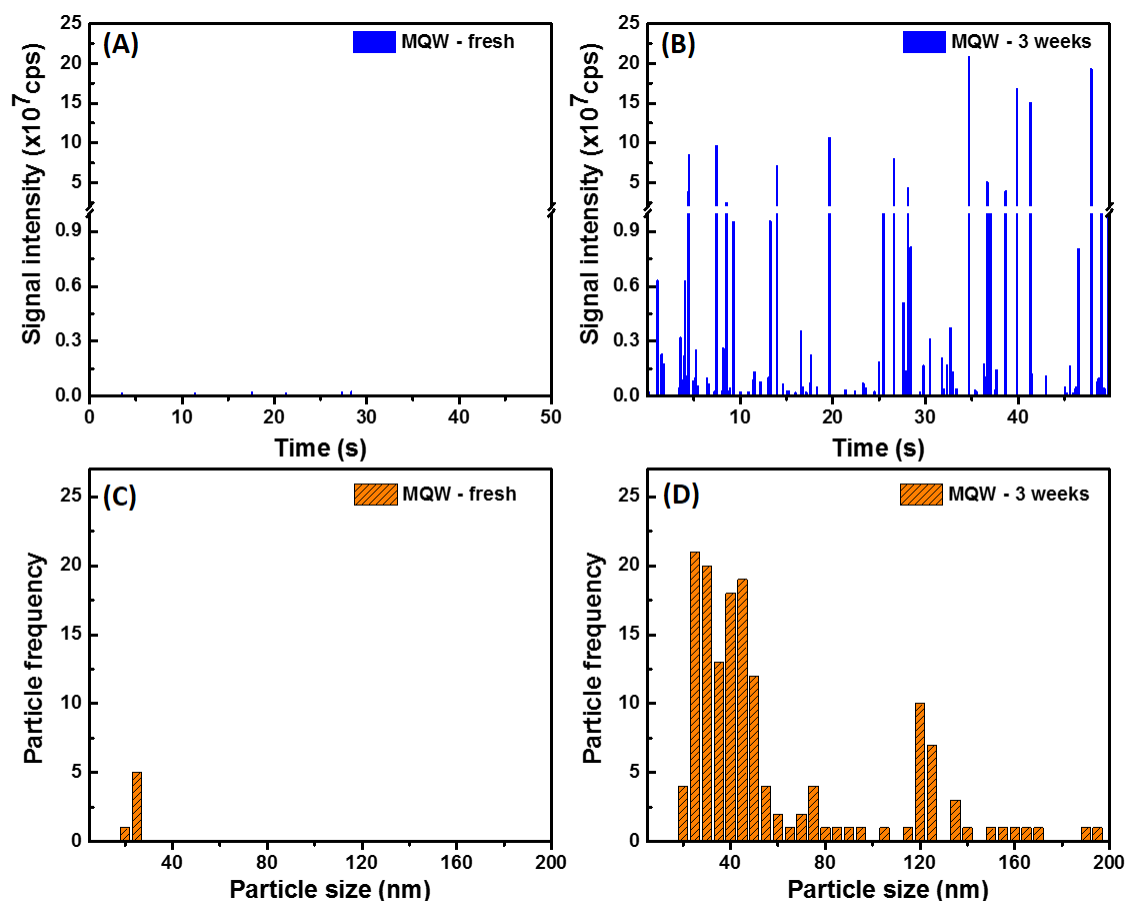


Figure 2-S5. Time-resolved SP-ICP-MS signal obtained following the analysis of (A) fresh Milli-Q water and (B) Milli-Q water exposed to indoor air for 3 weeks, as well as (C, D) their corresponding particle size distributions. As opposed to the outdoor air, 3 weeks was required in order to get a non-negligible signal. Particle diameters were calculated on the assumption that particles were solely TiO_2 .

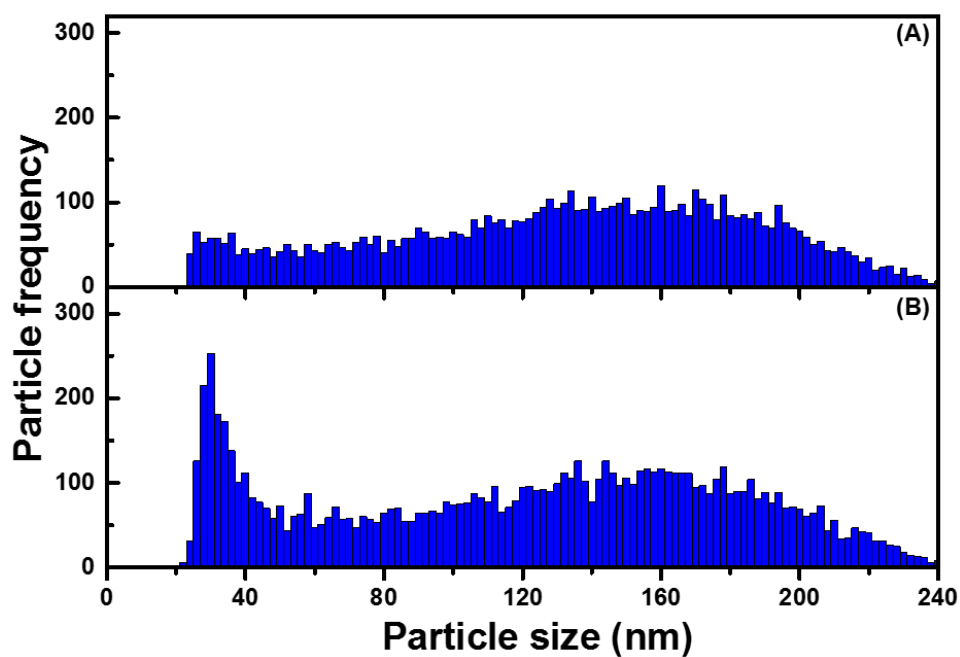


Figure 2-S6. Particle size distributions obtained for TiO₂ NPs in a liquid paint sample diluted 2×10^7 x w/w with (A) Milli-Q water and (B) 5 mg L⁻¹ of fulvic acid (Suwannee River standard fulvic acid, SRFA II) following 30 min of ultrasonication. Particle diameters were calculated on the assumption that particles were solely TiO₂.

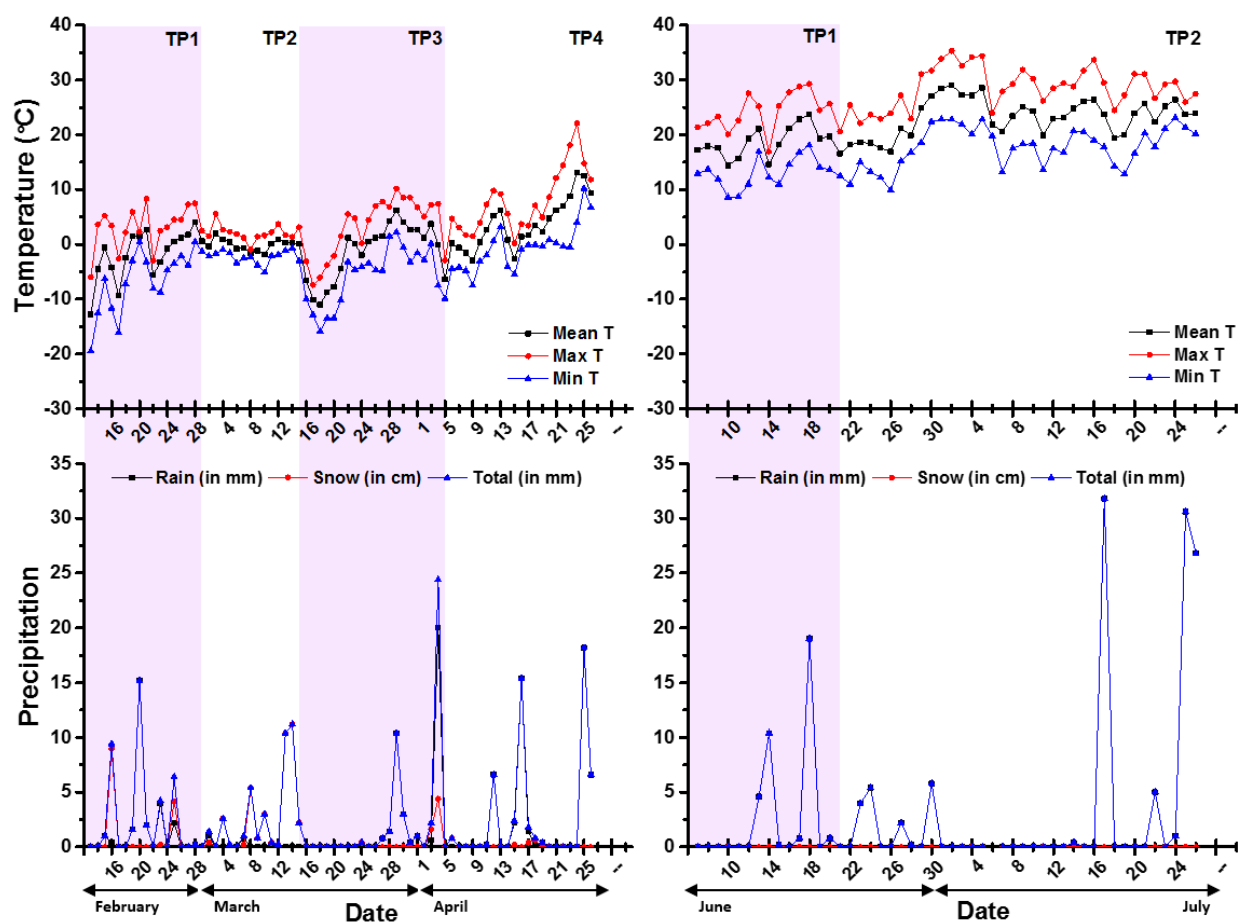


Figure 2-S7. Daily temperatures (maxima, minima and mean T) as well as precipitation (rain, snow, total precipitation) in the winter and summer of 2018, as collected from Montreal International Airport weather station (45°28'14.000" N, 73°44'27.000" W) and retrieved from the Environment and Climate Change Canada database. Timepoints (TP) refer to the cumulative period in which the respective sample was taken.

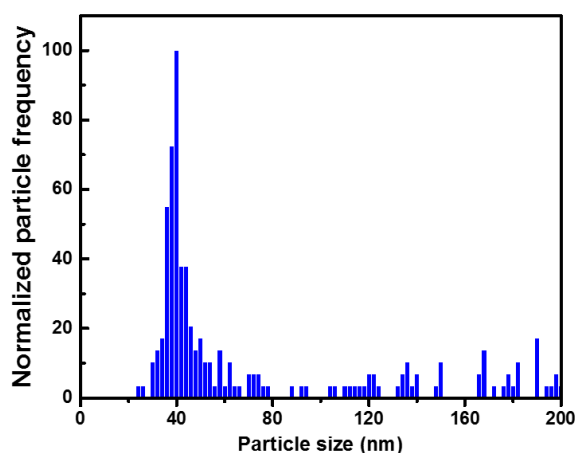


Figure 2-S8. Particle size distribution of TiO₂ NPs released following a 4-day soaking of a painted panel in Milli-Q water (no NP background).

Table 2-S1. Recoveries (%) of ionic Ti (based on Ti-49 isotope) as well as those of TiO₂ NPs spiked in a rainwater matrix. Given sizes are nominal particle diameters, as provided by the manufacturer.

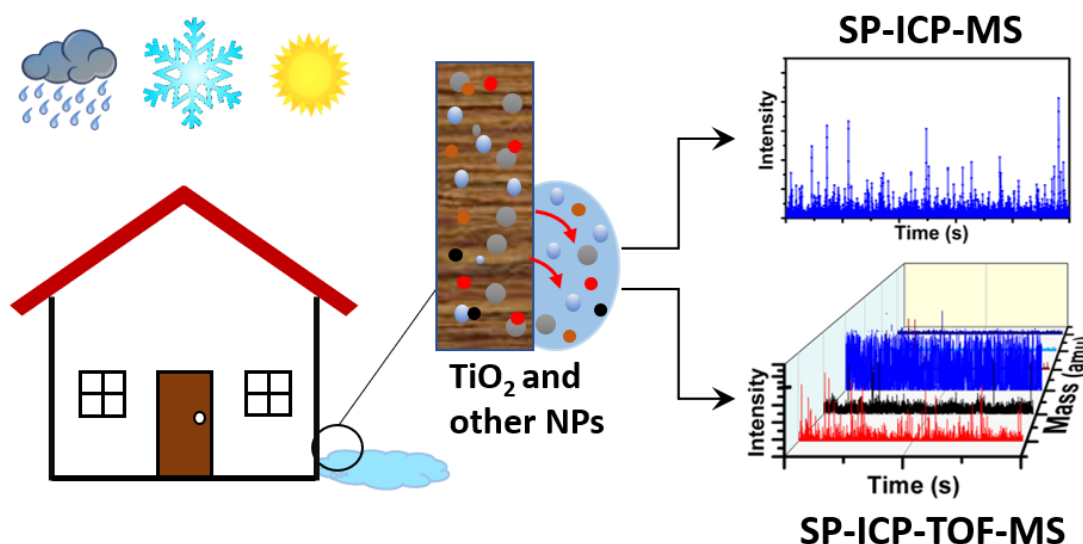
	Ionic recovery (%)		
Ti - 1 ppb	103.0	±	1.6
Ti - 5 ppb	102.6	±	0.8
Ti - 10 ppb	101.6	±	1.0
	NP recovery (%)		
TiO ₂ NPs (25 nm)	92.2	±	2.0

References

1. May, T. W.; Wiedmeyer, R. H., A table of polyatomic interferences in ICP-MS. *Atomic Spectroscopy* **1998**, *19*, 150-155.
2. Tharaud, M.; Gondikas, A. P.; Benedetti, M. F.; von der Kammer, F.; Hofmann, T.; Cornelis, G., TiO₂ nanomaterial detection in calcium rich matrices by spICPMS. A matter of resolution and treatment. *Journal of Analytical Atomic Spectrometry* **2017**, *32* (7), 1400-1411.
3. Gondikas, A. P.; Kammer, F. v. d.; Reed, R. B.; Wagner, S.; Ranville, J. F.; Hofmann, T., Release of TiO₂ nanoparticles from sunscreens into surface waters: a one-year survey at the old Danube recreational Lake. *Environmental Science & Technology* **2014**, *48* (10), 5415-5422.
4. Kaegi, R.; Englert, A.; Gondikas, A.; Sinnet, B.; von der Kammer, F.; Burkhardt, M., Release of TiO₂-(Nano) particles from construction and demolition landfills. *NanoImpact* **2017**, *8*, 73-79.
5. Peters, R. J.; van Bommel, G.; Milani, N. B.; den Hertog, G. C.; Undas, A. K.; van der Lee, M.; Bouwmeester, H., Detection of nanoparticles in Dutch surface waters. *Science of the Total Environment* **2018**, *621*, 210-218.
6. Lee, S.; Bi, X.; Reed, R. B.; Ranville, J. F.; Herckes, P.; Westerhoff, P., Nanoparticle size detection limits by single particle ICP-MS for 40 elements. *Environmental Science & Technology* **2014**, *48* (17), 10291-10300.
7. Hadioui, M.; Knapp, G. v.; Azimzada, A.; Jreije, I.; Frechette-Viens, L.; Wilkinson, K. J., Lowering the size detection limits of Ag and TiO₂ nanoparticles by Single Particle ICP-MS. *Analytical Chemistry* **2019**, *91* (20), 13275-13284.

Chapter 3 Single- and multi-element quantification and characterization of TiO₂ nanoparticles released from outdoor stains and paints

Connecting text: While the previous chapter demonstrated the role of different weathering factors in coating-release of NPs, this chapter comprehensively examines NP release patterns under natural weathering – with respect to (i) seasonal weather, (ii) surface exposure scenario (immersion or dripping), and (iii) coating matrix (paint or stain). Additionally, (prototype) time-of-flight ICP-MS measurements provide multiplexed information on the multi-element compositions of individual NPs in the liquid coating matrices, coating leachates, and natural precipitation. The generated data are of high significance from the perspective of the environmental risk analysis.



Published as: Azimzada, A.; Farner, J. M.; Jreije, I.; Hadioui, M.; Liu-Kang, C.; Tufenkji, N.; Shaw, P.; Wilkinson, K. J., Single-and multi-element quantification and characterization of TiO₂ nanoparticles released from outdoor stains and paints. *Frontiers in Environmental Science* 2020, 8, 91

3.1 Introduction

A rapid increase in the adoption of nanotechnologies across numerous industries has been a major driver in the production and use of engineered nanomaterials (ENMs).^{1, 2} Paints and stains represent two important applications of ENMs, for which TiO₂ nanoparticles (NPs) are extensively used for improved UV protection and self-cleaning properties.^{3, 4} The increasing development of nano-enabled coatings will invariably lead to increased environmental release of TiO₂ NPs, prompting questions about their fate and bioavailability.⁵⁻

11

Although some environmental and health hazards have been associated with TiO₂ NPs¹²⁻¹⁵, the extent of their release from different outdoor coatings has not been well investigated, especially under variable climatic conditions. The near absence of measured environmental concentrations of TiO₂ (or any other) NPs greatly complicates their risk assessment. Indeed, most laboratory and *in situ* studies on NP release from coatings have been limited to a qualitative or semi-quantitative demonstration of release (*e.g.* with microscopy) or quantitative measurements based on the total metal content^{3, 4, 16-23} – rather than a specific determination of the NP forms. Using a sensitive, magnetic-sector ICP-MS, we were recently²⁴ able to quantify mass and number release rates of TiO₂ NPs from painted surfaces during natural weathering cycles. While that study provided valuable information on real-life NP release quantities and particle size distributions, the data was mainly relevant for surfaces that were likely to retain the incoming snow or rainwater. It showed that the wet surface interaction time (*i.e.* contact time between the precipitation and the surface) was a critical environmental variable affecting NP release. Nonetheless, the study did not look at other outdoor surfaces, notably façades, or other nano-enhanced surfaces, such as stains. Furthermore, a major difficulty was the ability to distinguish Ti-rich natural colloids from TiO₂ NPs.^{25, 26}

Both exposure conditions and the nature of the coating will influence NP leaching and their interactions with other chemical constituent(s). For example, paint-released NPs have been shown to be embedded in their original paint matrix,^{27, 28} which may result in them acting as a vector for the release and transport of other potentially toxic chemicals. Furthermore, while metal-based, manufactured NPs are often assumed to be composed of single elements or metal oxides,²⁹ only limited datasets are available with respect to their actual chemical identities, including metallic impurities, surface coatings, etc. While quantitative measurements of NP exposure concentrations are necessary for risk determinations, characterization of the released NP and their associations with other elements is necessary in order to define chemical hazard.

ICP-MS based techniques are well-suited for NP quantification as they are extremely sensitive, high-throughput and analyte-specific techniques that can quantify metal-based NPs and determine their size distributions on a single particle basis.³⁰⁻³³ By analyzing the transient ICP-MS signal, NPs are identified as high-intensity spikes against a continuous background signal that is attributed to dissolved metals and background interferences.^{34, 35} While single-particle ICP-MS (SP-ICP-MS) provides targeted single-element analysis of the NPs, SP-ICP-time-of-flight-MS (SP-ICP-TOF-MS) is able to simultaneously identify and quantify a full spectrum of elements in single particles.³⁶⁻³⁸ Nonetheless, due to the nature of the technology and the multiplicity of analytes in a single particle, SP-ICP-TOF-MS generally has higher size detection limits than SP-ICP-MS.^{30, 39} For example, for Ti-containing NPs in surface waters, minimum detectable sizes of <20 nm have been determined using a high-resolution SP-ICP-MS,^{24, 40} whereas size detection limits are typically above 60 nm when using SP-ICP-TOF-MS.^{32, 39}

Given the above knowledge gaps, this study was designed to analyze TiO₂ NP release from two nano-enhanced surfaces under different weathering scenarios. Technical challenges were addressed by using recent improvements⁴⁰ in sensitivity and data treatment for both SP-ICP-MS and SP-ICP-TOF-MS. The specific objectives were: (i) to quantify and characterize TiO₂ NP release from a paint and a stain under natural weathering scenarios, and (ii) to distinguish TiO₂ NPs from the high quantity of colloidal Ti particles found in natural precipitation.

3.2 Materials and Methods

Weathering panels. Untreated oak slats were cut to obtain panels that were 0.64 cm thick, 6.4 cm wide and 8.4 cm long. They were subsequently painted (Behr Premium Plus Ultra Exterior Satin Enamel Ultra-Pure White paint) or stained (SICO exterior semi-transparent wood stain) with products that were advertised for their Nanoguard Technology and/or nano-sized pigments. The paint was uniformly distributed by applying 15 mL per side of each panel using a film applicator (Bird Film Applicator, Inc, Washington, USA)²⁴ with removal of the excess paint. Due to its lower viscosity, 5 mL of stain was applied per side using a paintbrush. Panel surfaces were coated twice on each side and at least two days was allowed for drying between each coat. The final dry paint or stain loadings were similar among panels for each coating type: 400 ± 40 g-paint m⁻² (or 4.4 g-paint per panel) and 36 ± 3 g-stain m⁻² (or 0.4 g-stain per panel).

Natural weathering setups. The outdoor weathering setup consisted of two experimental designs – namely, vertical and slanted designs – that simulated two environmentally relevant weathering scenarios. The vertical design was designed to be more representative of a scenario where a surface is weathered by stationary water or snow accumulation (*e.g.* puddle or snow on a deck), whereas the slanted design was designed to represent the weathering of outdoor façades where precipitation does not accumulate on the surface. In the *vertical design*, painted/stained panels were vertically positioned in pre-weighed, wide-mouth polypropylene containers (500 mL, Fisher Scientific) (**Fig. 3-1A**). Every 2-3 weeks, panels were removed from the containers, and then placed outside in a new (empty) container. In the *slanted design*, two polypropylene containers were fixed on top of each other and separated by a polypropylene mesh (**Fig. 3-1B**). The mesh supported the panel, which was fixed in a slanted position in the top section. Rain came into contact with the panel and then flowed into the bottom container (the leachate collector), whereas snow had a tendency to sometimes collect on the surface of the panel. For each timepoint, the bottom container was removed, capped and replaced by another pre-labeled, pre-weighed and pre-cleaned container.

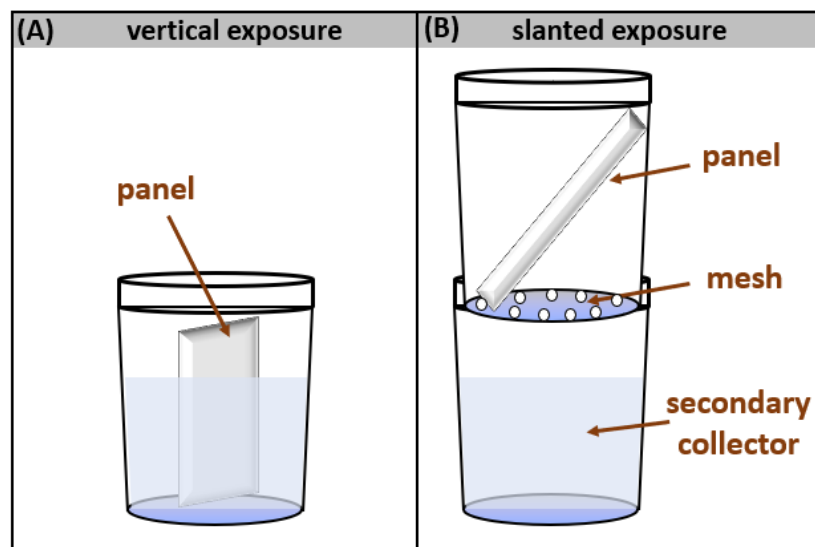


Figure 3-1. Experimental setups for two weathering scenarios: (A) vertical exposure – consisting of a painted/stained panel vertically positioned in a polypropylene container, (B) slanted exposure – made up of two containers stacked on top of each other and separated by a polypropylene mesh, where the top container contains a painted/stained panel fixed in a slanted position. The vertical exposure is more representative of a surface in more sustained contact with precipitation whereas the slanted exposure is designed to be more representative of the weathering of an outdoor façade. Panels did not extend out of the containers, but rather they were custom cut to fit in the containers, while leaving an overhead space equivalent to 15% of the container height.

Due to the ubiquitous presence of nano- and micron-sized particles in the precipitation,^{24, 41, 42} one critical challenge in the experiments was to quantitatively distinguish NPs that were leached out of painted surfaces from background NPs in the natural precipitation.²⁶ Control experiments were thus critical to accurately determining NP release, with sufficient replication at each timepoint (n=4). The use of untreated wooden panels was ruled out based on the preliminary observations that they rapidly disintegrated when subjected to natural weathering. Thus, for both designs, controls consisted of empty containers that were placed alongside exposure samples in order to collect the incoming precipitation.²⁴ Containers were randomly placed in plastic bins, which protected them from tipping over by minimizing the impact of side winds. Bins were then placed outdoors on a 7th floor roof (Pavillon Roger-Gaudry, University of Montreal, Montreal, Canada). Samples were left undisturbed, unless they were buried by snow, in which case, excess snow was carefully scraped off the top of the containers.²⁴ Fall weathering experiments started at the beginning of October 2018 and lasted for 11 weeks, while winter weathering experiments extended from late January (2019) until early April for a duration of 12 weeks. All exposure and control samples included 4 replicates. For the last two timepoints of the fall weathering series, the slanted samples tipped over and thus, the results for those timepoints are not available.

Indoor weathering. To characterize surface-leached NPs using SP-ICP-TOF-MS, painted and stained (each with 4 replicates) panels were placed vertically into pre-weighed polypropylene containers, which were filled with 380 mL of Milli-Q water (*i.e.* panels fully immersed). Surfaces were then subjected to accelerated aging under freeze-thaw conditions, which involved successive cycles of 24 h freezing and 24 h thawing over 3 weeks.²⁴ Following the freeze-thaw cycles, leachates were collected and prepared for SP-ICP-TOF-MS analysis.

Sample preparation for SP-ICP-MS/SP-ICP-TOF-MS. At each timepoint, samples (exposure and controls) were brought inside the lab, left to melt and then gently mixed. The samples were then weighed and placed in a sonicator bath for 30 minutes (Branson Ultrasonic Cleaner, 5510R-DTH Model, 135 W, 42 kHz \pm 6%). Eight (8) to 10 mL of the samples were filtered (0.45 μ m cut-off) through a 33 mm diameter PVDF (Polyvinylidene fluoride) syringe filter (Sigma-Aldrich) that had been pre-rinsed with 12 mL Milli-Q water and 6 mL of sample.²⁴ The filtration step is designed to protect the nebulizers by avoiding build-up and blockage, while being large enough to minimize exclusion of the NPs. While pre-rinsing the

filter with sample minimizes adsorptive losses, the 0.45 μm cutoff is nonetheless operationally defined- particle losses would lead to an underestimation of particle numbers.

SP-ICP-MS analysis and data acquisition. SP-ICP-MS measurements were performed on a magnetic sector ICP-MS (AttoM ES, Nu Instruments, UK), at low resolution (300), using single ion acquisition in fast-scan mode.⁴³ To further enhance the sensitivity, the ICP-MS used a desolvator (Aridus II, Teledyne Cetac Technologies), which utilized a PFA (perfluoroalkoxy) micro-flow nebulizer (self-aspiration rate of 200 $\mu\text{L min}^{-1}$ at 1 L min^{-1} of Ar).^{40, 44} Optimized membrane sweep gas (argon) flow rates typically ranged between 3-7 L min^{-1} , while the nebulizer gas (argon) flow was between 0.7-1.0 L min^{-1} . In accordance with previously optimized strategies⁴⁰ to lower the size detection limits (SDL), ⁴⁹Ti was chosen for analysis. With an acquisition time of 50 s per sample and an optimized dwell time of 50 μs ,⁴⁰ *ca.* 10^6 datapoints were obtained per replicate. Sensitivity calibrations for ⁴⁹Ti were based on ionic standards (High Purity Standards) and transport efficiency (TE) measurements were performed using a suspension of ultra-uniform 30 nm Au NPs (NanoComposix, AUXU30-1M) that were previously validated using a second standard reference material (60 nm Au NPs, NIST8013).⁴⁰ Standards for TE measurements were prepared daily at 50 ng L^{-1} . TE values ranged between 13-15%, corresponding to an actual sample injection into the plasma of 0.45-0.55 $\mu\text{L s}^{-1}$. Filtered samples were diluted up to 10x to ensure that the incidences of concurrent peaks were minimized (less than 10,000 events or 1% of total datapoints), while ensuring a statistically significant number of NPs (>500 events). Matrix effects were not observed.²⁴

SP-ICP-TOF-MS analysis and data acquisition. SP-ICP-TOF-MS measurements were performed on a time-of-flight ICP-MS (Nu Vitesse, Nu Instruments, UK), using a segmented reaction cell with *ca.* 4-6 $\text{cm}^3 \text{min}^{-1}$ of He and *ca.* 4 $\text{cm}^3 \text{min}^{-1}$ of H_2 gas introduced to eliminate argon and nitrogen-based interferences. This method improved the sensitivity of the technique by allowing the higher abundance isotopes of elements like Si, K, Ca, Cr, Fe and Se to be monitored without interference. A near full range of time-of-flight mass spectra (23-238 amu) were acquired every 25.5 μs , and 3 acquisitions were combined before electronics noise was subtracted and isotope signals were integrated over their defined mass positions to produce individually stored measurements for Na to U, every 76 μs . Data were acquired for a total sampling time of about 30 s, for the most concentrated samples, to a maximum of 2 min for dilute samples. Mass spectra were acquired continuously, in an uninterrupted manner and without loss of data. Sensitivity was further improved by using an Aridus II desolvator as above, with similar parameters as the magnetic sector instrument. TE was determined using

the particle size method⁴⁵ by measuring the instrument sensitivity (counts s⁻¹ ng L⁻¹) for ionic gold standards and mass sensitivity (counts ng⁻¹) for a highly monodisperse Au NP standard (known size and density). This led to TE values ranging between 10-15%. An ultra-uniform NP standard of 30 nm (NanoComposix, AUXU30-1M) was used to calculate TE, while 60 nm Au NP (NanoComposix) and 40 nm Ag (NanoComposix) standards were used for validation of the TE values. A multi-element standard (SPEX CertiPrep) containing all metals was used for ionic sensitivity determinations.

SP-ICP-MS/SP-ICP-TOF-MS data processing. SP-ICP-MS data were analyzed using NuQuant software version 2.2 (Nu Instruments, UK), based on the methodology described in Hadioui *et al.*⁴⁰ and Shaw *et al.*⁴³. In summary, the data analysis algorithm used data smoothing to reduce baseline fluctuations; created rolling search windows where it searched for NP peaks based on maximum intensities; and calculated local backgrounds for each peak based on data preceding the pre-inflection points. For each detected NP, the local background was subtracted from the integrated raw data, while the average of local peak backgrounds was used to calculate dissolved metal contents.

For SP-ICP-TOF-MS data, a modified version of NuQuant software (NuQuant Vitesse prototype, Nu Instruments, UK) was used, where the algorithm searched for a target isotope, here ⁴⁸Ti, using similar smoothing and peak detection parameters as in the single-particle analysis. The start and end timestamps for each detected particle event were determined and used to identify counts for all isotopes. The full width half maximum (FWHM) values, along with the standard deviation of the background (for each isotope) were used to estimate the noise threshold, above which particle events were reported. This threshold, typically consisting of 5-7 multiples of the standard deviation of the background, was applied to filter out background artifacts while optimizing the detection of real NP peaks. Elements of interest (especially those with low intensities) were visually checked to ensure that background artifacts were avoided (*i.e.* very slender or very wide peaks with low intensity).

NP masses (and sizes if density and shape can be assumed) were calculated using calibrated multi-element sensitivities and transport efficiency measurements obtained for the monodisperse Au NPs.⁴⁵ Size calculations for TiO₂ were performed by assuming a spherical particle with a density of 4.23 g cm⁻³, corresponding to rutile.²⁴

Ti analysis by quantitative ICP-MS. Given the very low Ti concentrations in the precipitation samples (*i.e.* ng L⁻¹ levels) and dilutions required to reduce acid concentrations prior to ICP-

MS analysis, the use of digestion protocols^{29, 46} to obtain total Ti was unfortunately not viable here. Ti measurements were nonetheless performed on leachate samples, following filtration over a 0.45- μm PVDF filter and addition of 67-70% HNO_3 (ultratrace grade, BDH Aristar Ultra) in polypropylene tubes to obtain a final acid content of 20% v/v. Samples were left for 16 h at 85 °C in a DigiPREP digestion system (SCP Science)²⁴ and then diluted 5-10x with Milli-Q water to obtain a final HNO_3 content of 2-4% v/v for the ICP-MS analysis. The measured Ti nominally included dissolved Ti as well as any of the sub-0.45- μm particles. Although the addition of concentrated HNO_3 is not sufficient for the complete digestion of the TiO_2 ⁴⁷, measurements were performed to provide some additional validation of the single-particle techniques for which particle concentrations are determined from the number of transient peaks, using a non-acidified sample (i.e. greater potential for adsorptive losses). Digested Ti thus represents an operationally defined fraction²⁴ that may not capture all of the colloidal Ti in the sample.

3.3 Results and Discussion

Technical considerations in the SP-ICP-MS and SP-ICP-TOF-MS measurements. Fewer than 3 spikes per min were generally observed for a Milli-Q water blank⁴⁴. By assuming that the detection of 10 NPs during a 50 s acquisition would be required in order to have sufficient confidence that particles were being detected⁴⁸, one can estimate a detection threshold of ca. 360 NP mL^{-1} with a minimum detectable (TiO_2 equivalent) particle size of ~ 15 nm (**Fig. 3-S1A**). The size detection limit compare favorably with those that have generally been determined by SP-ICP-MS (~ 60 nm^{46, 49}). The SP-TOF-ICP-MS had higher, matrix-sensitive size detection limits, ranging from 30 nm (in Milli-Q water) to 46 nm (in the rain) (i.e. assuming spherical TiO_2 particles, **Fig. 3-S2**). In that case, minimum detectable particle numbers were kept < 1000 mL^{-1} by increasing the acquisition time to 120 s. For both techniques, raw data corresponding to NPs that are close to instrumental size detection limits have been provided in **Figs. 3-S1B and 3-S2B, D, and F** for the different matrices. In all cases, NP concentrations in the samples were consistently above 10,000 mL^{-1} , well above the detection limits. While these detection limits are among the lowest in the literature for TiO_2 , it is important to note that ‘nanoparticle’ number measurements presented below are necessarily for particles that are larger than the lower size detection limits (e.g. 15 nm by magnetic sector SP-ICP-MS; 34 nm by SP-TOF-ICP-MS) but smaller than the filtration cut-off (i.e. 0.45 μm).

Characterization of TiO₂ NPs in the paint and stain. Immediately prior to analysis by SP-ICP-MS, liquid acrylic paint was diluted 2x10⁷x in Milli-Q water, while stain was diluted 2x10⁵x. TiO₂ NPs in the paint were fairly polydisperse with a particle size distribution extending from about 20 nm (just above the size detection limit) to beyond 200 nm (**Fig. 3-S3A**), with a concentration of $(6.8 \pm 0.1) \times 10^{15}$ NPs kg-paint⁻¹. TiO₂ NPs in the stain were smaller with a majority (>95 %) of the particles between 20 and 100 nm (**Fig. 3-S3B**) and a concentration of $(2.9 \pm 0.4) \times 10^{13}$ NPs kg-stain⁻¹. Number-based average particle sizes corresponded to 131 ± 53 nm in the liquid paint and 42 ± 24 nm in the stain, where standard deviations reflected polydispersities, rather than errors determined on repeated measurements (typically ~3 nm). Particle concentrations corresponded to about 5% w/w in the paint and 0.001 % w/w NP in the stain.

Release of NPs from painted and stained surfaces. In spite of precautions that included the use of four replicates for samples and controls; their randomization in the protective bins and the lowering of detection limits of the SP-ICP-MS technique; there were still cases where NPs in the leachates were quantitatively indistinguishable from those in the precipitation (t-test, p>0.05). This result was more frequently observed for the slanted exposures (**Fig. 3-2**) and was primarily due to relatively high background concentrations with respect to the low quantities of released NPs. In agreement with Azimzada *et al.*²⁴, while no or low release appeared to occur during specific weathering conditions, such as a lack of precipitation (**Fig. 3-S4**), background concentrations were also highly episodic. Given that the errors were cumulative, detection of NP release was only significant for cases where release was high, and background was low (**Fig. 3-2**). This implies that the measured release quantities are minimum values only, since low release quantities can easily be masked by pre-existing high background concentrations of the Ti containing NPs.

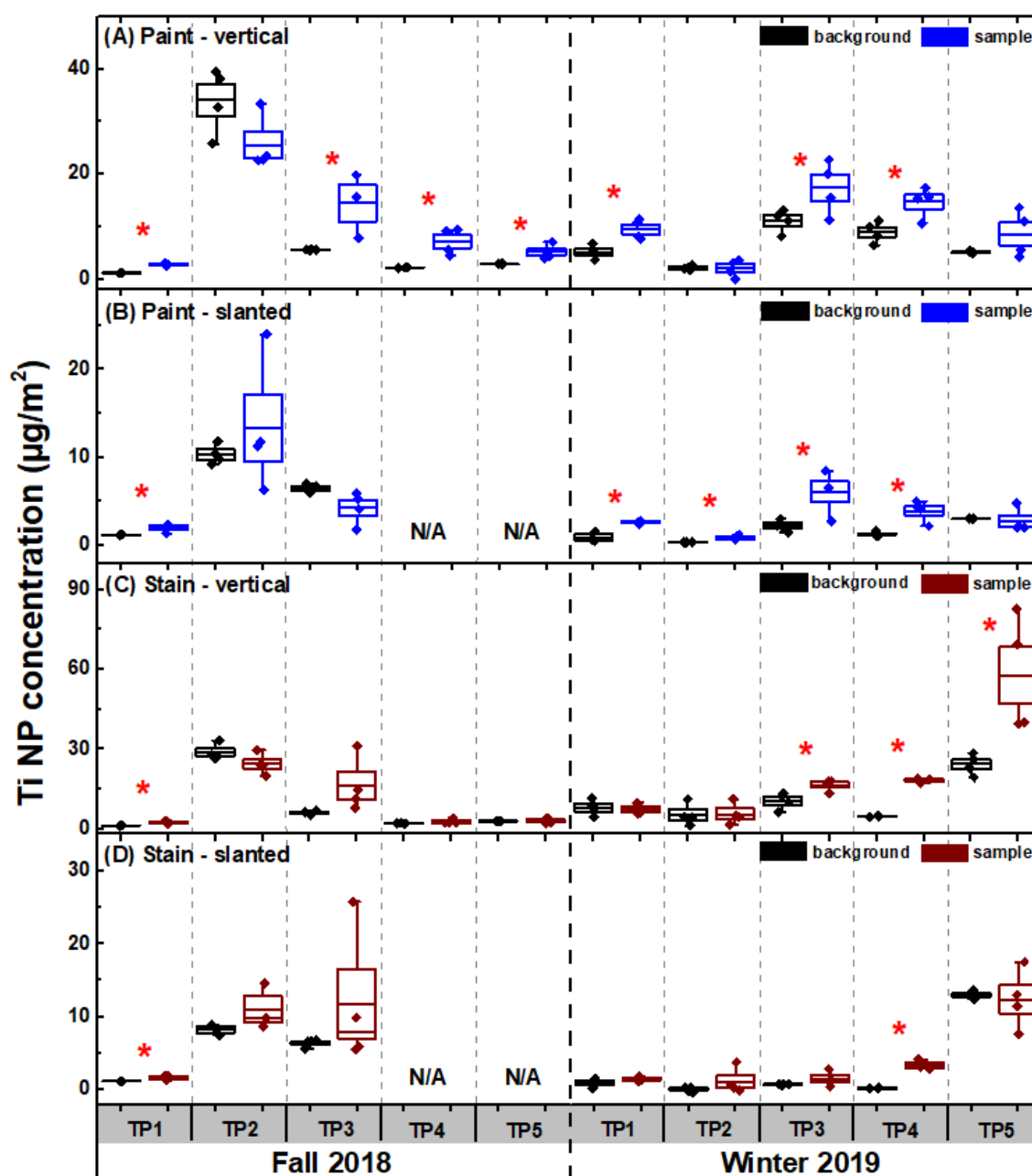


Figure 3-2. Quantification of Ti-containing NPs in the precipitation (*i.e.* background) and in the precipitation following its contact with (A-B) painted and (C-D) stained panels (*i.e.* sample). Sample weathering experiments were conducted using two exposure designs (Fig. 1), (A, C) vertical and (B, D) slanted, for painted and stained panels. A red star indicates a significant difference ($N=4$, student t-test, $p < 0.05$) between the NP content in the background and the NP content in the sample. NP concentrations were normalized by the surface area of the painted/stained panels subjected to weathering. Containers were renewed at each timepoint (TP). Measurements were performed using a magnetic sector ICP-MS in single particle mode. Measured NP content includes particles between the instrumental size detection limit of ~ 15 nm and the filtration cut-off ($0.45 \mu\text{m}$). Error bars indicate standard deviations ($n=4$). N/A denotes two samples that were lost.

In addition to characterizing the NPs by SP-ICP-MS, Ti in the 0.45- μm filtrate was measured using quantitative ICP-MS, following acidification and heating of the samples. The concentration of NPs determined by integration of the SP-ICP-MS peaks corresponded to about 10-30 % of the values determined based on the digested filtrates of the paint and stain leachates. While the remaining fraction of Ti could be dissolved forms or Ti NPs below the instrumental detection limits, it is also important to acknowledge that a fraction of the missing mass balance could be attributed to sorptive losses in the sample introduction system^{31, 40, 50} and losses due to incomplete ionization^{30, 40, 51} (recall that SP-ICP-MS is necessarily performed on non-acidified samples).

The size distributions of the NPs released from the painted (**Fig. 3-S5B**) and stained (**Fig. 3-S5C**) surfaces were similar to NPs found in the natural precipitation (**Fig. 3-S5A**). For example, paint-released NPs were mostly <60 nm, with a size range from 15-120 nm in agreement with our previous results²⁴. Generally, they had smaller sizes than those originally found in the liquid paint (**Fig. 3-S3A**), indicating that there was some agglomeration in the original paint mixture. In contrast, NPs released from the stained surfaces ranged from 15-100 nm with a size distribution (**Fig. 3-S5C**) that was similar to the original particles in the stain (**Fig. 3-S3B**).

Role of exposure mode (vertical or slanted), season (fall or winter) and coating type (paint or stain). Generally speaking, less TiO₂ NP release was observed for the slanted exposures where precipitation was not allowed to remain in contact with the panels (**Fig. 3-3 and 3-4**). Furthermore, NP release from the vertical painted surfaces was still several times less than that observed in Azimzada *et al.*²⁴ and others^{17, 19, 20, 23}, where much longer weathering times or accelerated weathering conditions were used in a similar experimental design. The results show that NPs are more likely to be leached from surfaces that have a prolonged exposure to precipitation.

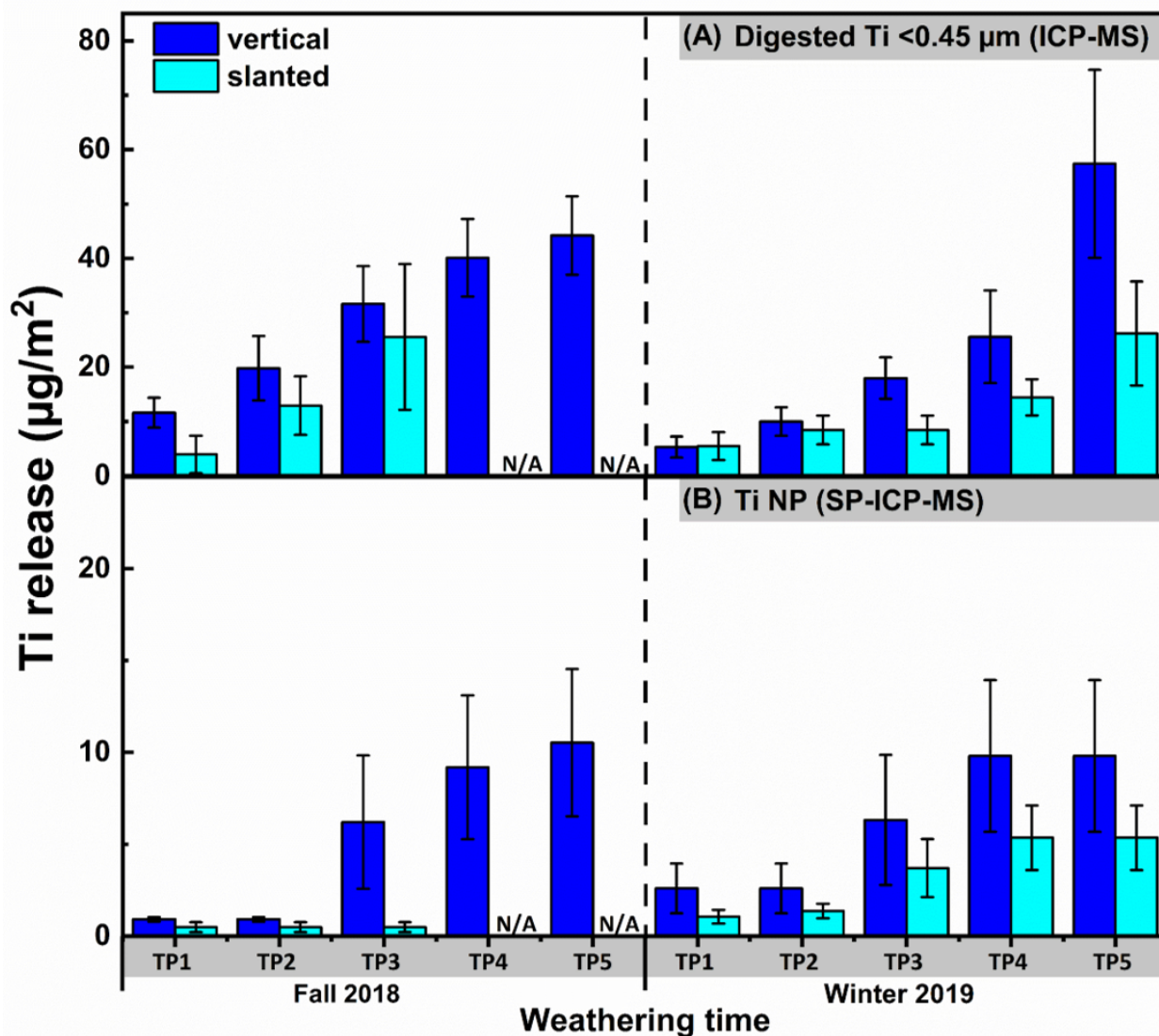


Figure 3-3. Cumulative concentrations of sub-0.45-µm Ti determined by (A) ICP-MS on acidified samples and (B) SP-ICP-MS, obtained by integration of the NP peaks. Ti was measured following its release from the **painted** surfaces in vertical and slanted exposure modes (N=4 for each condition). Release was normalized by the surface area of the painted panels that were subject to weathering and corrected for the pre-existing natural background in the precipitation. Measurements were performed using a magnetic sector ICP-MS. N/A denotes two samples that were lost. Error bars indicate standard deviations, where n=4.

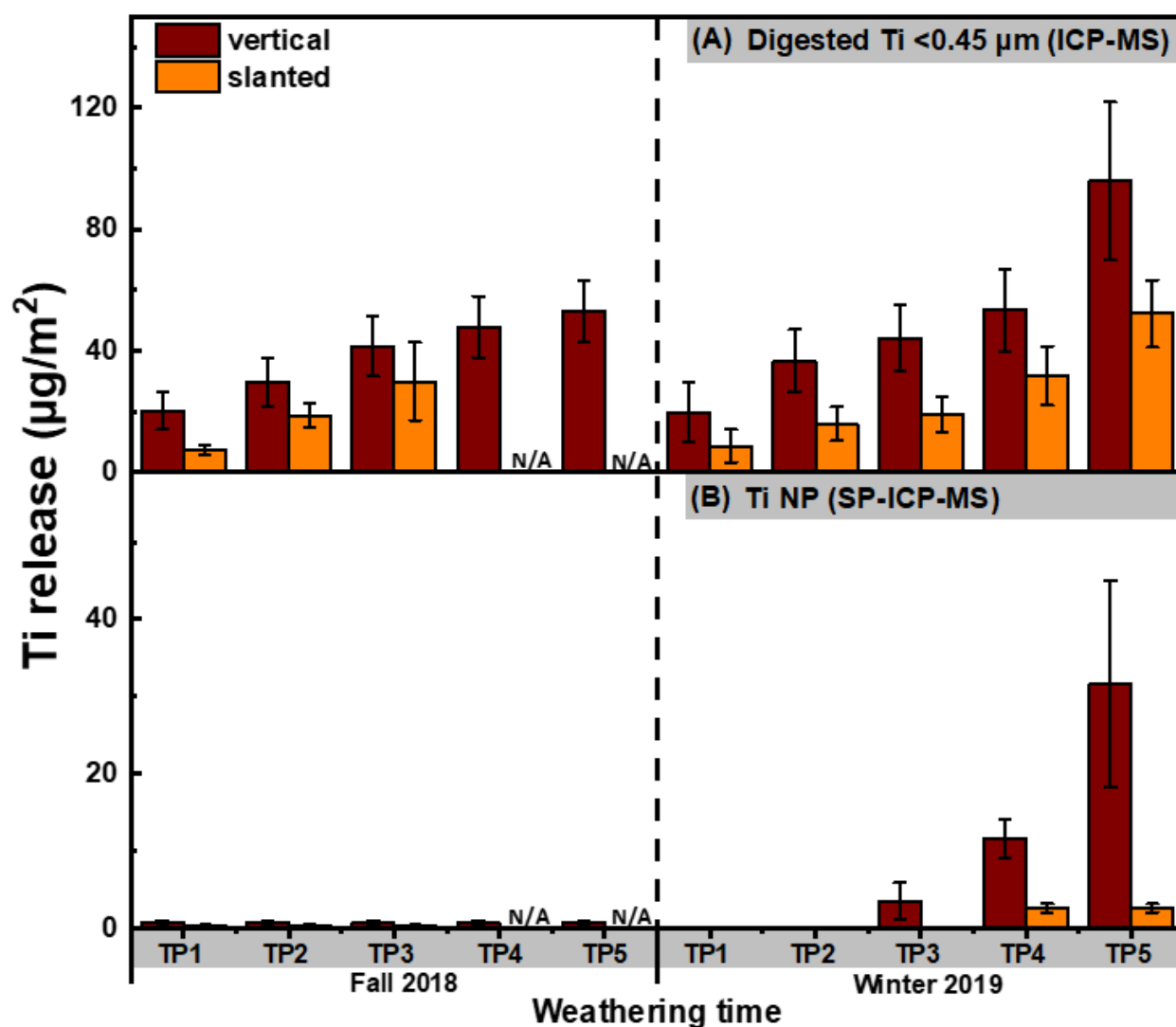


Figure 3-4. Cumulative concentrations of sub-0.45- μm Ti determined by (A) ICP-MS on acidified samples and (B) SP-ICP-MS, obtained by integration of the NP peaks. Ti was measured following its release from the **stained** surfaces in vertical and slanted exposure modes ($N=4$ for each condition). Release was normalized by the surface area of the painted panels that were subject to weathering and corrected for the pre-existing natural background in the precipitation. Measurements were performed using a magnetic sector ICP-MS. N/A denotes two samples that were lost. Error bars indicate standard deviations, where $n=4$.

While comparable NP release was observed for the painted surfaces that were weathered in fall or winter; for the stain, NP release was clearly greater in the winter (t-test, $p<0.05$) (Fig. 3-3B, 4B). It is also notable that most NP release did not occur in the initial stages of the exposure ($<3 \mu\text{g-Ti m}^{-2}$ over the first 4-5 weeks, corresponding to timepoints 1 and 2), but rather during the final 6-7 weeks (*i.e.* last 3 timepoints) of the weathering period. This observation could be attributed to two possible explanations: (i) an initial weathering period

rendered the samples more vulnerable to NP release in the subsequent weeks, or (ii) the samples were exposed to conditions that were more conducive to NP release during the final weeks of the fall and winter exposure period.²⁴ Indeed, weather data (**Fig. 3-S4**) reveals that more numerous incidents of precipitation, slushy snow and freeze-thaw conditions (about 20 rainy/snowy days with temperatures fluctuating between +10 °C and -10 °C) were observed near the end of fall and winter seasons. Irrespective of the NP release trend, Ti NPs in the leachate consistently increased over time in both the fall and winter (**Fig. 3-3A, 4A**).

NP release from painted surfaces was fairly small, eventually surpassing 10 $\mu\text{g-Ti m}^{-2}$ by the end of the 11-week fall weathering experiment and remaining slightly below 10 $\mu\text{g-Ti m}^{-2}$ during the winter exposure (**Fig. 3-3B**). Release from stained surfaces was very low ($<1 \mu\text{g-Ti m}^{-2}$) and neither increased throughout fall, nor during the first 4 weeks of the winter exposure (**Fig. 3-4B**). During the spring snowmelt period, however, the quantities of NPs released from the stain greatly surpassed those released from paint, eventually exceeding 30 $\mu\text{g-Ti m}^{-2}$. While the absolute quantities (mass normalized by surface area) released from painted and stained surfaces were generally on the same order of magnitude, when given as a proportion of the total Ti NPs in the coatings, Ti release from the stained surfaces (max release about 6%) was several orders of magnitude greater than that released from painted surfaces (max release about $5 \times 10^{-5} \%$). This result might be related to the size distribution in the original coating, as smaller particles are thought to be more easily released from the matrix due to weathering/crack formation, etc.,⁵² which could also help explain the similarity of the release histograms observed in Fig S5. Overall, it is clear that NP leaching is strongly influenced by the chemistry of the coating and that some nano-enhanced surfaces (*e.g.* stained surfaces) are much more vulnerable to NP release than others.

Distinguishing the engineered NPs from background NPs in the precipitation using SP-ICP-TOF-MS. SP-ICP-TOF-MS measurements on the NPs in the diluted paint and stain showed that in addition to Ti-containing NPs, several other particle types were observed including those containing Fe, Al, Zr, Ce and Si. In both paints and stains, Ce (*i.e.* CeO_2)^{22, 53, 54} and Si (*i.e.* SiO_2)⁵⁵⁻⁵⁷ are known to impart thermal/mechanical resistance and weathering durability (*e.g.* against UV) to the coatings, while Al, Fe and Zr NPs could be purposefully added to improve coating properties⁵⁴ or could simply be present as impurities from the manufacturing process. Clear differences were observed when comparing the nature of the particles in the paint (**Fig. 3-S6**) to those in the stain (**Fig. 3-S7**). Peak co-incidences indicated that the Ti-containing NPs in the liquid paint (**Fig. 3-5A, 5B**) were often associated with Al

(<20% of TiO₂ NPs) and rarely with Zr (<1% of TiO₂ NPs) (**Fig. 3-6A**). Nonetheless, over 70% of the particles had Ti/Al or Ti/Zr mass ratios above 10, when calculated on a particle-by-particle basis (**Fig. 3-7A, 7B**). Three alternative explanations are proposed to explain these high ratios in the paint: (i) traces of Al or Zr, whether in dissolved or small NP forms, were bound to Ti-containing NPs or their agglomerates; (ii) these metals (or their oxides) were used as coatings on Ti-containing NPs²⁹; or (iii) there were impurities in the Ti-containing NPs. In contrast to measurements on the liquid paint, no Al and almost no Zr were detected in the Ti-containing NPs in the paint leachate (**Fig. 3-6B**), even though high amounts of dissolved Al were observed as compared to the controls (**Fig. 3-S8**). The absence of Al in the Ti NPs found in the leachate suggests that during the weathering of the painted surface, TiO₂ NPs were separated from an Al-containing matrix (hypothesis i), resulting in increased dissolved Al concentrations. The low detection of Zr in the leachate could simply be explained by its low concentration (relative to instrument detection limits).

In the liquid stain, Ti-containing NPs were often associated with Fe (~7%) and Si (~8%) and less often with Al (~3 %, **Fig. 3-5C, 5D**). This result is not direct evidence that Fe, Si, or Al co-occurred with the Ti of a given NP, since Ti-containing NPs could have simply been associated with particles such as aluminosilicates within heteroagglomerates. Indeed, given that the Ti fraction was often below 0.2 (**Fig. 3-6C**), it is possible that small TiO₂ NPs (often <50 nm, **Fig. 3-S3B**) were associated with larger Fe and Si based particles in the liquid stain (**Fig. 3-7C, 7D**). This hypothesis of heteroagglomeration was reinforced by the relatively high particle numbers that were found for the Fe and Si NPs, *i.e.* 1 Ti NP was detected per 25 Fe NPs /10 Si NPs. Given that the vast majority of Ti NPs in the leachate (>95 % of NPs) were not associated with any other metals (including Fe or Si) (**Fig. 3-6D**), the results are another indication that the nature of the Ti NPs within the painted or stained surfaces is different from that found in the leachate, following the weathering process. The observation that Ti NPs in the leachate are primarily ‘pure’ particles is important from the perspective of risk analysis.

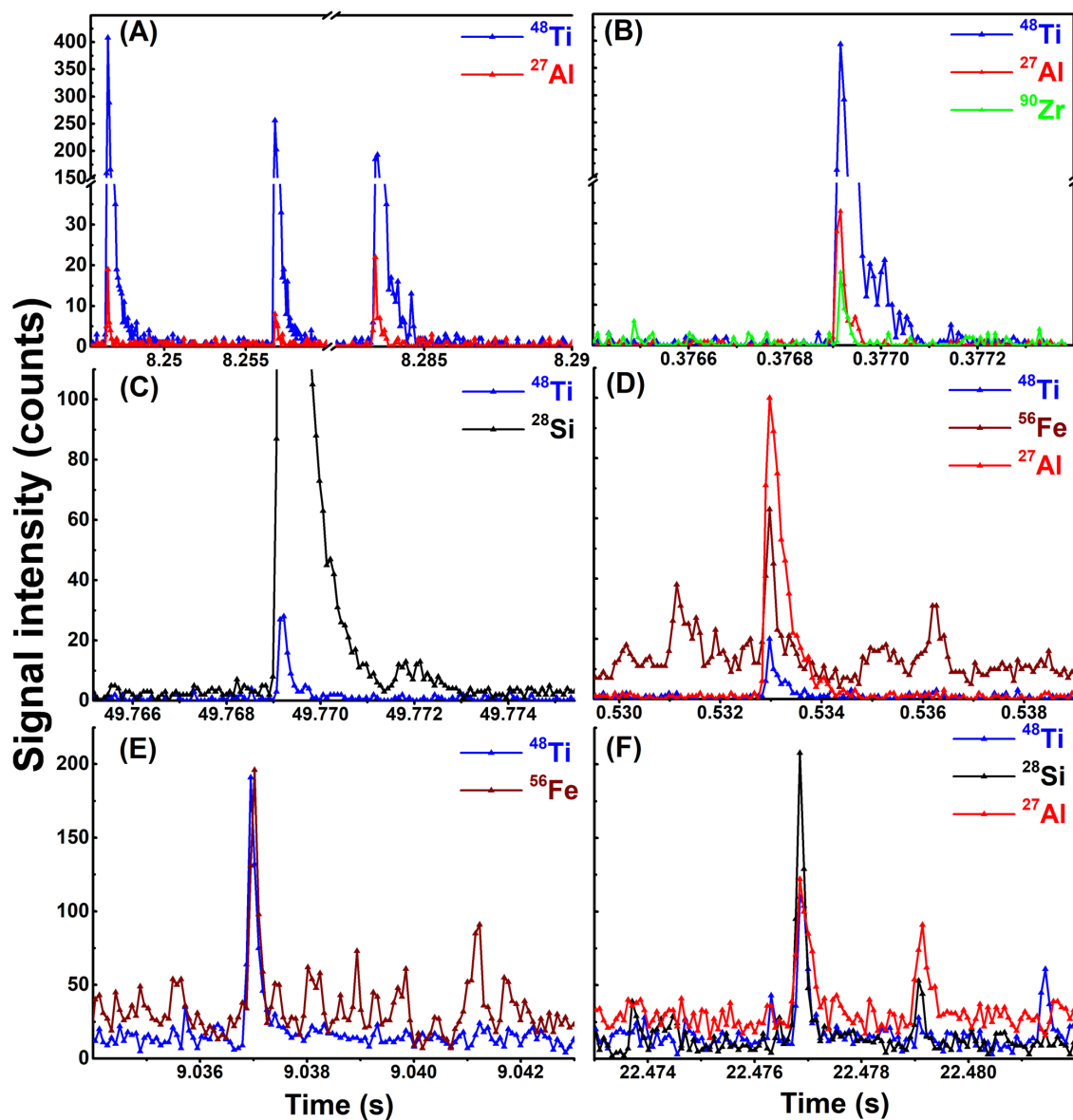


Figure 3-5. Examples of SP-ICP-TOF-MS raw peak data corresponding to Ti-containing NPs detected in the different matrices. Association of Ti with (A) Al or with (B) Al and Zr in the liquid paint. Association of Ti with (C) Si or with (D) Fe and Al in the liquid stain. Association of Ti with (E) Fe and (F) Si and Al in Montreal rain.

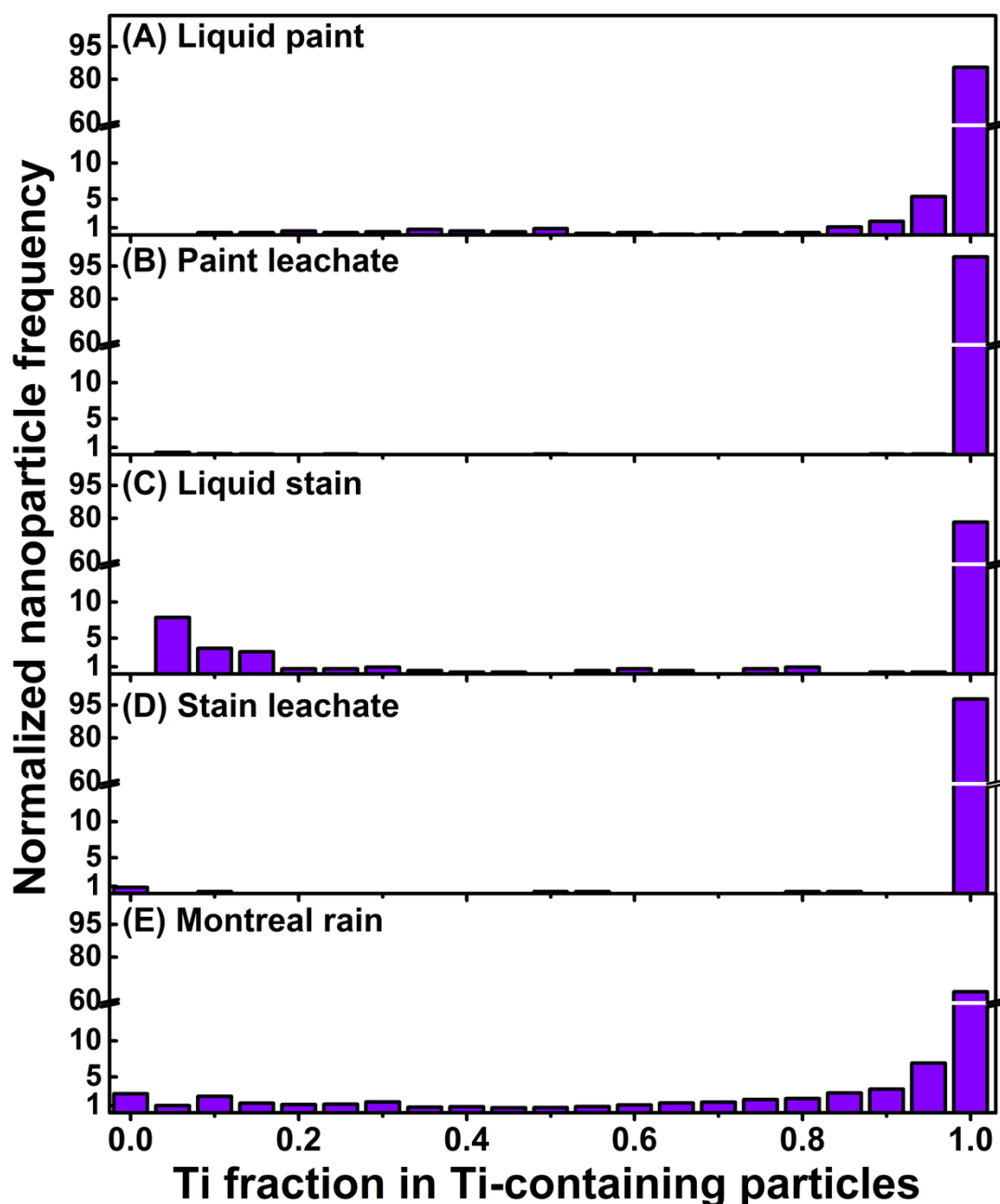


Figure 3-6. Elemental fractions of Ti in Ti-containing NPs for (A) liquid paint (diluted in Milli-Q water), (B) paint leachate, (C) liquid stain (diluted in Milli-Q water), (D) stain leachate, and (E) Montreal rainwater. Measurements were performed using a SP-ICP-TOF-MS. Under the described conditions, a Ti fraction of 1 implies that the NP is primarily composed of Ti (or TiO_2 , *i.e.* single metal), whereas fractions <1 indicate the presence of additional metals within the NP or agglomerate. Paint and stain leachates were collected during accelerated weathering experiments of the coated panels in Milli-Q water.

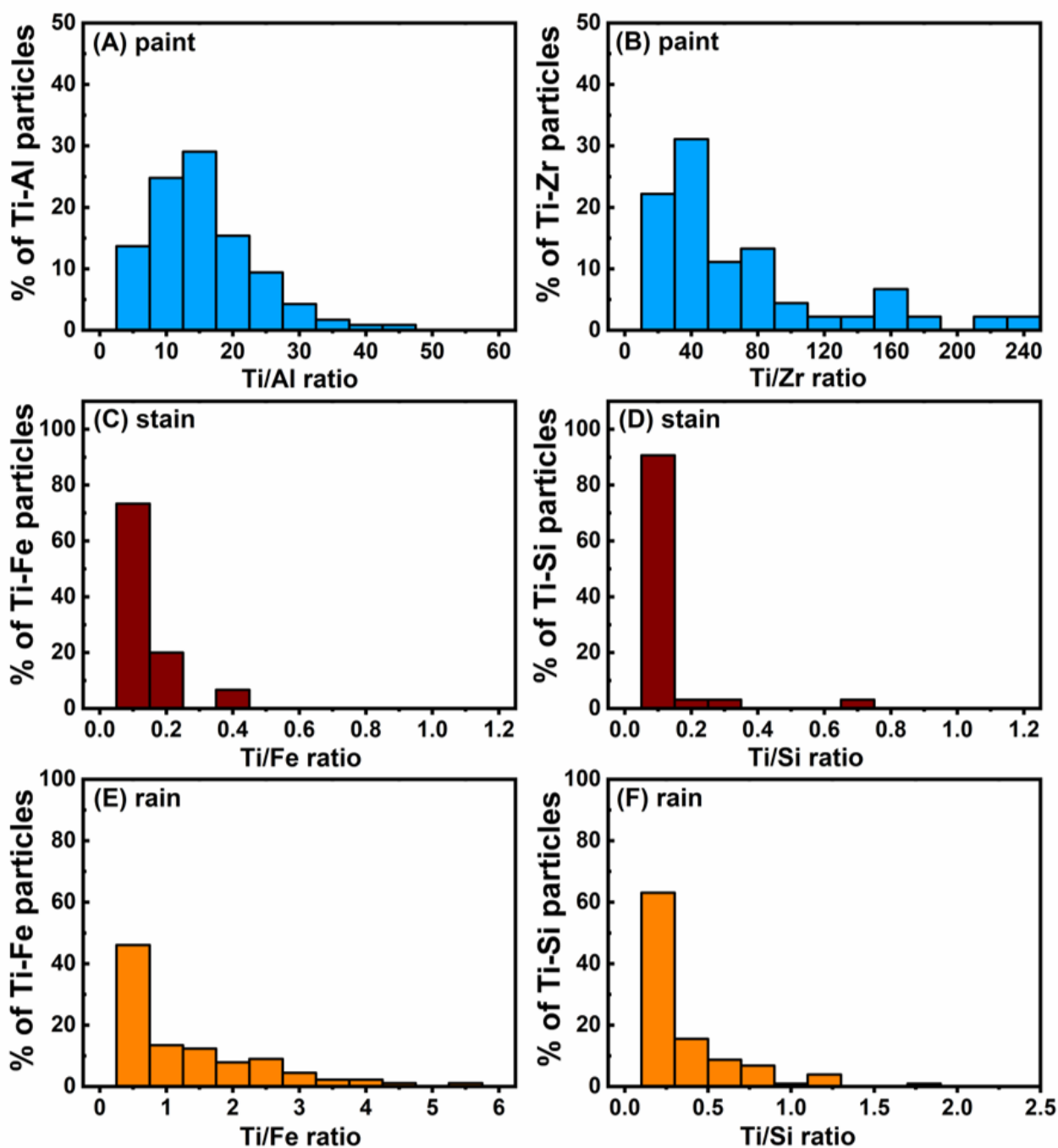


Figure 3-7. Elemental mass ratios measured on individual particles for major associations of the Ti in (A-B) liquid paint, (C-D) liquid stain and (E-F) Montreal rain samples. Measurements were performed using a SP-ICP-TOF-MS.

SP-ICP-MS measurements showed a significant presence of Ti-containing NPs in the rain and snow, which are thought to result from both anthropogenic activities and natural processes.^{41, 42} Generally, engineered NPs are assumed to contain a single element with trace impurities (if any),³⁶ whereas NPs of natural origin are believed to more often contain multiple

elements. Using elemental purity as an indicator for the origin of the NPs, up to 50% of the Ti-containing NPs in Montreal rain/snowmelt could be classified as engineered NPs (with >99 % purity), while the rest had multi-element identities (**Fig. 3-6E**). In the multi-element particles, Ti typically co-occurred with Fe and less often with Al and Si (**Fig. 3-5E, 5F, 7E, 7F**), further supporting the hypothesis that they were naturally occurring particulates.^{58, 59} Nonetheless, the ratio of single element particles should be used carefully when distinguishing NP source since it will vary geographically and temporally, as a function of urban, industrial or natural setting of the location and/or episodic events. While multi-element Ti particles predominate in nature, it is possible for TiO₂ nanoparticles to occur naturally. The environmental release of anthropogenic TiO₂, including those from the paints and stains, will nevertheless increase the overall proportion of Ti in the Ti-containing particles (Fig. 6), providing an indication of particle source.

Environmental implications. TiO₂ NPs were leached out of both painted and stained surfaces under natural weathering conditions. For the products tested here, absolute release quantities were comparable (*i.e.* within one order of magnitude), although this was mainly because there were initially far more NPs in the paint and far greater release by the stain. NP release dynamics were largely driven by the nature of contact with the precipitation. For instance, for scenarios where the panels were in extended contact with sitting water or snow (*e.g.* on a deck), stronger NP release was observed as compared to the weathering of surfaces where precipitation was not allowed to accumulate (*e.g.* outdoor facades). While the weathering experiments were performed under realistic environmental scenarios, losses of the NPs due to agglomeration^{24, 60} and a potential underestimation of the measured NP concentrations^{31, 40} imply that the actual release rates could be higher in environmental systems. On the other hand, the recovered (measured) NP concentrations are likely to represent the most mobile and bioavailable fraction that is likely to be of highest environmental relevance.

It is of note that the individual NP appeared to be associated with multiple elements in the pure stain and paint, whereas after weathering of the dried compounds from the surfaces, particles were more elementally pure, suggesting dissociation from a complex matrix. The results also indicated that the particles in the leachates were smaller than NPs detected in the rain, which often had multi-element identities, and thus, larger sizes than those estimated using analysis with a single isotope (*i.e.* SP-ICP-MS). This implies that, in addition to NPs, other compounds, including potentially toxic ones, are being released during the degradation of these nano-enhanced surfaces. Finally, while anthropogenic NPs already appear to have a significant

presence in precipitation, NP release from consumer products, such as paints and stain, will only contribute further to their presence in the environment.

Acknowledgements. This research was supported by the Natural Sciences and Engineering Research Council of Canada (NSERC), Environment and Climate Change Canada, a McGill Engineering Doctoral Award (MEDA), Pollution in Urban Environments (PURE) and an EcotoQ Excellence Scholarship. PS is an employee of Nu Instruments, UK. The other authors declare that they have no conflict of interest. We thank Prof. Ghoshal (McGill University) for providing access to a film applicator.

Author Contributions. KW, JF, NT and AA conceived the study and designed the experimental plan. AA, JF, IJ and CK prepared the weathering setups, collected the samples and prepared them for single particle and total metal analysis. AA and MH conducted SP-ICP-MS analysis. AA and PS conducted SP-ICP-TOF-MS analysis. AA, MH and PS performed the SP-ICP(-TOF)-MS data treatment. AA organized all data and performed statistics. AA and KW wrote the manuscript, with complementary input from other authors.

3.4 References

1. Vance, M. E.; Kuiken, T.; Vejerano, E. P.; McGinnis, S. P.; Hochella Jr, M. F.; Rejeski, D.; Hull, M. S., Nanotechnology in the real world: Redeveloping the nanomaterial consumer products inventory. *Beilstein Journal of Nanotechnology* **2015**, *6* (1), 1769-1780.
2. Robichaud, C. O.; Uyar, A. E.; Darby, M. R.; Zucker, L. G.; Wiesner, M. R., Estimates of upper bounds and trends in nano-TiO₂ production as a basis for exposure assessment. *Environmental Science & Technology* **2009**, *43* (12), 4227-4233.
3. Hincapié, I.; Caballero-Guzman, A.; Hiltbrunner, D.; Nowack, B., Use of engineered nanomaterials in the construction industry with specific emphasis on paints and their flows in construction and demolition waste in Switzerland. *Waste Management* **2015**, *43*, 398-406.
4. Hischier, R.; Nowack, B.; Gottschalk, F.; Hincapie, I.; Steinfeldt, M.; Som, C. J. J. o. n. r., Life cycle assessment of façade coating systems containing manufactured nanomaterials. **2015**, *17* (2), 68.
5. Coll, C.; Notter, D.; Gottschalk, F.; Sun, T.; Som, C.; Nowack, B., Probabilistic environmental risk assessment of five nanomaterials (nano-TiO₂, nano-Ag, nano-ZnO, CNT, and fullerenes). *Nanotoxicology* **2016**, *10* (4), 436-444.
6. Hischier, R.; Nowack, B.; Gottschalk, F.; Hincapie, I.; Steinfeldt, M.; Som, C., Life cycle assessment of façade coating systems containing manufactured nanomaterials. *Journal of Nanoparticle Research* **2015**, *17* (2), 68.
7. Nowack, B.; Ranville, J. F.; Diamond, S.; Gallego-Urrea, J. A.; Metcalfe, C.; Rose, J.; Horne, N.; Koelmans, A. A.; Klaine, S. J., Potential scenarios for nanomaterial release and subsequent alteration in the environment. *Environmental Toxicology and Chemistry* **2012**, *31* (1), 50-59.
8. Sun, T. Y.; Gottschalk, F.; Hungerbühler, K.; Nowack, B., Comprehensive probabilistic modelling of environmental emissions of engineered nanomaterials. *Environmental Pollution* **2014**, *185*, 69-76.

9. Van Broekhuizen, P.; van Broekhuizen, F.; Cornelissen, R.; Reijnders, L., Use of nanomaterials in the European construction industry and some occupational health aspects thereof. *Journal of Nanoparticle Research* **2011**, *13* (2), 447-462.
10. Mitrano, D. M.; Motellier, S.; Clavaguera, S.; Nowack, B., Review of nanomaterial aging and transformations through the life cycle of nano-enhanced products. *Environment international* **2015**, *77*, 132-147.
11. Auffan, M.; Rose, J.; Wiesner, M. R.; Bottero, J.-Y., Chemical stability of metallic nanoparticles: a parameter controlling their potential cellular toxicity in vitro. *Environmental Pollution* **2009**, *157* (4), 1127-1133.
12. Liu, S.; Zeng, P.; Li, X.; Thuyet, D. Q.; Fan, W., Effect of chronic toxicity of the crystalline forms of TiO₂ nanoparticles on the physiological parameters of *Daphnia magna* with a focus on index correlation analysis. *Ecotoxicology and Environmental Safety* **2019**, *181*, 292-300.
13. Simonin, M.; Martins, J. M.; Le Roux, X.; Uzu, G.; Calas, A.; Richaume, A., Toxicity of TiO₂ nanoparticles on soil nitrification at environmentally relevant concentrations: Lack of classical dose–response relationships. *Nanotoxicology* **2017**, *11* (2), 247-255.
14. Zhu, X.; Zhou, J.; Cai, Z., TiO₂ nanoparticles in the marine environment: impact on the toxicity of tributyltin to abalone (*Haliotis diversicolor supertexta*) embryos. *Environmental Science Technology* **2011**, *45* (8), 3753-3758.
15. Farner, J. M.; Cheong, R. S.; Mahé, E.; Anand, H.; Tufenkji, N., Comparing TiO₂ nanoparticle formulations: stability and photoreactivity are key factors in acute toxicity to *Daphnia magna*. *Environmental Science: Nano* **2019**, *6*, 2532-2543.
16. Al-Kattan, A.; Wichser, A.; Vonbank, R.; Brunner, S.; Ulrich, A.; Zuin, S.; Nowack, B., Release of TiO₂ from paints containing pigment-TiO₂ or nano-TiO₂ by weathering. *Environmental Science: Processes & Impacts* **2013**, *15* (12), 2186-2193.
17. Olabarrieta, J.; Zorita, S.; Peña, I.; Rioja, N.; Monzón, O.; Benguria, P.; Scifo, L., Aging of photocatalytic coatings under a water flow: long run performance and TiO₂ nanoparticles release. *Applied Catalysis B: Environmental* **2012**, *123*, 182-192.
18. Kaegi, R.; Englert, A.; Gondikas, A.; Sinnet, B.; von der Kammer, F.; Burkhardt, M., Release of TiO₂–(Nano) particles from construction and demolition landfills. *NanoImpact* **2017**, *8*, 73-79.
19. Zhang, X.; Wang, M.; Guo, S.; Zhang, Z.; Li, H., Effects of weathering and rainfall conditions on the release of SiO₂, Ag, and TiO₂ engineered nanoparticles from paints. *Journal of Nanoparticle Research* **2017**, *19* (10), 338.
20. Zuin, S.; Gaiani, M.; Ferrari, A.; Golanski, L., Leaching of nanoparticles from experimental water-borne paints under laboratory test conditions. *Journal of Nanoparticle Research* **2014**, *16* (1), 2185.
21. Clar, J. G.; Platten III, W. E.; Baumann, E.; Remsen, A.; Harmon, S. M.; Rodgers, K.; Thomas, T. A.; Matheson, J.; Luxton, T. P., Release and transformation of ZnO nanoparticles used in outdoor surface coatings for UV protection. *Science of the Total Environment* **2019**, *670*, 78-86.
22. Clar, J. G.; Platten III, W. E.; Baumann Jr, E. J.; Remsen, A.; Harmon, S. M.; Bennett-Stamper, C. L.; Thomas, T. A.; Luxton, T. P., Dermal transfer and environmental release of CeO₂ nanoparticles used as UV inhibitors on outdoor surfaces: Implications for human and environmental health. *Science of the Total Environment* **2018**, *613*, 714-723.
23. Kaegi, R.; Ulrich, A.; Sinnet, B.; Vonbank, R.; Wichser, A.; Zuleeg, S.; Simmler, H.; Brunner, S.; Vonmont, H.; Burkhardt, M., Synthetic TiO₂ nanoparticle emission from exterior facades into the aquatic environment. *Environmental Pollution* **2008**, *156* (2), 233-239.

24. Azimzada, A.; Farner, J. M.; Hadioui, M.; Liu-Kang, C.; Jreije, I.; Tufenkji, N.; Wilkinson, K. J., Release of TiO₂ nanoparticles from painted surfaces in cold climates: characterization using a high sensitivity single-particle ICP-MS. *Environmental Science: Nano* **2020**, *7* (1), 139-148.
25. del Real, A. E. P.; Castillo-Michel, H.; Kaegi, R.; Larue, C.; de Nolf, W.; Reyes-Herrera, J.; Tucoulou, R.; Findling, N.; Salas-Colera, E.; Sarret, G., Searching for relevant criteria to distinguish natural vs. anthropogenic TiO₂ nanoparticles in soils. *Environmental Science: Nano* **2018**, *5* (12), 2853-2863.
26. Wagner, S.; Gondikas, A.; Neubauer, E.; Hofmann, T.; von der Kammer, F., Spot the difference: engineered and natural nanoparticles in the environment—release, behavior, and fate. *Angewandte Chemie International Edition* **2014**, *53* (46), 12398-12419.
27. Al-Kattan, A.; Wichser, A.; Zuin, S.; Arroyo, Y.; Golanski, L.; Ulrich, A.; Nowack, B., Behavior of TiO₂ released from nano-TiO₂-containing paint and comparison to pristine nano-TiO₂. *Environmental Science & Technology* **2014**, *48* (12), 6710-6718.
28. Kaegi, R.; Sinnet, B.; Zuleeg, S.; Hagendorfer, H.; Mueller, E.; Vonbank, R.; Bollner, M.; Burkhardt, M., Release of silver nanoparticles from outdoor facades. *Environmental Pollution* **2010**, *158* (9), 2900-2905.
29. Loosli, F.; Wang, J.; Rothenberg, S.; Bizimis, M.; Winkler, C.; Borovinskaya, O.; Flamigni, L.; Baalousha, M., Sewage spills are a major source of titanium dioxide engineered (nano)-particle release into the environment. *Environmental Science: Nano* **2019**, *6* (3), 763-777.
30. Meermann, B.; Nischwitz, V., ICP-MS for the analysis at the nanoscale—a tutorial review. *Journal of Analytical Atomic Spectrometry* **2018**, *33* (9), 1432-1468.
31. Azimzada, A.; Tufenkji, N.; Wilkinson, K. J., Transformations of silver nanoparticles in wastewater effluents: links to Ag bioavailability. *Environmental Science: Nano* **2017**, *4* (6), 1339-1349.
32. Gondikas, A.; von der Kammer, F.; Kaegi, R.; Borovinskaya, O.; Neubauer, E.; Navratilova, J.; Praetorius, A.; Cornelis, G.; Hofmann, T., Where is the nano? Analytical approaches for the detection and quantification of TiO₂ engineered nanoparticles in surface waters. *Environmental Science: Nano* **2018**, *5* (2), 313-326.
33. Montañño, M. D.; Olesik, J. W.; Barber, A. G.; Challis, K.; Ranville, J. F., Single Particle ICP-MS: Advances toward routine analysis of nanomaterials. *Analytical and Bioanalytical chemistry* **2016**, *408* (19), 5053-5074.
34. Degueldre, C.; Favarger, P.-Y.; Wold, S., Gold colloid analysis by inductively coupled plasma-mass spectrometry in a single particle mode. *Analytica Chimica Acta* **2006**, *555* (2), 263-268.
35. Tharaud, M.; Gondikas, A. P.; Benedetti, M. F.; von der Kammer, F.; Hofmann, T.; Cornelis, G., TiO₂ nanomaterial detection in calcium rich matrices by spICPMS. A matter of resolution and treatment. *Journal of Analytical Atomic Spectrometry* **2017**, *32* (7), 1400-1411.
36. Praetorius, A.; Gundlach-Graham, A.; Goldberg, E.; Fabienke, W.; Navratilova, J.; Gondikas, A.; Kaegi, R.; Günther, D.; Hofmann, T.; von der Kammer, F., Single-particle multi-element fingerprinting (spMEF) using inductively-coupled plasma time-of-flight mass spectrometry (ICP-TOFMS) to identify engineered nanoparticles against the elevated natural background in soils. *Environmental Science: Nano* **2017**, *4* (2), 307-314.
37. Hendriks, L.; Gundlach-Graham, A.; Günther, D., Analysis of inorganic nanoparticles by single-particle inductively coupled plasma time-of-flight mass spectrometry. *CHIMIA International Journal for Chemistry* **2018**, *72* (4), 221-226.
38. Hendriks, L.; Gundlach-Graham, A.; Hattendorf, B.; Günther, D., Characterization of a new ICP-TOFMS instrument with continuous and discrete introduction of solutions. *Journal of Analytical Atomic Spectrometry* **2017**, *32* (3), 548-561.

39. Mozhayeva, D.; Engelhard, C., A critical review of single particle inductively coupled plasma mass spectrometry—A step towards an ideal method for nanomaterial characterization. *Journal of Analytical Atomic Spectrometry* **2020**, *35*, 1740-1783.
40. Hadioui, M.; Knapp, G. v.; Azimzada, A.; Jreije, I.; Fréchette-Viens, L.; Wilkinson, K. J., Lowering the size detection limits of Ag and TiO₂ nanoparticles by Single Particle ICP-MS. *Analytical Chemistry* **2019**, *91* (20), 13275-13284.
41. Rahim, M. F.; Pal, D.; Ariya, P. A., Physicochemical studies of aerosols at Montreal Trudeau Airport: The importance of airborne nanoparticles containing metal contaminants. *Environmental Pollution* **2019**, *246*, 734-744.
42. Hochella, M. F.; Mogk, D. W.; Ranville, J.; Allen, I. C.; Luther, G. W.; Marr, L. C.; McGrail, B. P.; Murayama, M.; Qafoku, N. P.; Rosso, K. M., Natural, incidental, and engineered nanomaterials and their impacts on the Earth system. *Science* **2019**, *363* (6434), eaau8299.
43. Shaw, P.; Donard, A., Nano-particle analysis using dwell times between 10 μs and 70 μs with an upper counting limit of greater than 3×10^7 cps and a gold nanoparticle detection limit of less than 10 nm diameter. *Journal of Analytical Atomic Spectrometry* **2016**, *31* (6), 1234-1242.
44. Fréchette-Viens, L.; Hadioui, M.; Wilkinson, K. J., Quantification of ZnO nanoparticles and other Zn containing colloids in natural waters using a high sensitivity single particle ICP-MS. *Talanta* **2019**, *200*, 156-162.
45. Pace, H. E.; Rogers, N. J.; Jarolimek, C.; Coleman, V. A.; Higgins, C. P.; Ranville, J. F., Determining transport efficiency for the purpose of counting and sizing nanoparticles via single particle inductively coupled plasma mass spectrometry. *Analytical Chemistry* **2011**, *83* (24), 9361-9369.
46. Gondikas, A. P.; Kammer, F. v. d.; Reed, R. B.; Wagner, S.; Ranville, J. F.; Hofmann, T., Release of TiO₂ nanoparticles from sunscreens into surface waters: a one-year survey at the old Danube recreational Lake. *Environmental Science & Technology* **2014**, *48* (10), 5415-5422.
47. De la Calle, I.; Menta, M.; Seby, F., Current trends and challenges in sample preparation for metallic nanoparticles analysis in daily products and environmental samples: A review. *Spectrochimica Acta Part B: Atomic Spectroscopy* **2016**, *125*, 66-96.
48. Laborda, F.; Gimenez-Ingalature, A. C.; Bolea, E.; Castillo, J. R., Single particle inductively coupled plasma mass spectrometry as screening tool for detection of particles. *Spectrochimica Acta Part B: Atomic Spectroscopy* **2019**, *159*, 105654.
49. Lee, S.; Bi, X.; Reed, R. B.; Ranville, J. F.; Herckes, P.; Westerhoff, P., Nanoparticle size detection limits by single particle ICP-MS for 40 elements. *Environmental Science & Technology* **2014**, *48* (17), 10291-10300.
50. Fréchette-Viens, L.; Hadioui, M.; Wilkinson, K. J., Practical limitations of single particle ICP-MS in the determination of nanoparticle size distributions and dissolution: case of rare earth oxides. *Talanta* **2017**, *163*, 121-126.
51. Goodall, P.; Foulkes, M. E.; Ebdon, L., Slurry nebulization inductively coupled plasma spectrometry—the fundamental parameters discussed. *Spectrochimica Acta Part B: Atomic Spectroscopy* **1993**, *48* (13), 1563-1577.
52. Bossa, N.; Chaurand, P.; Levard, C.; Borschneck, D.; Miche, H.; Vicente, J.; Geantet, C.; Aguerre-Chariol, O.; Michel, F. M.; Rose, J., Environmental exposure to TiO₂ nanomaterials incorporated in building material. *Environmental Pollution* **2017**, *220*, 1160-1170.
53. Scifo, L.; Chaurand, P.; Bossa, N.; Avellan, A.; Auffan, M.; Masion, A.; Angeletti, B.; Kieffer, I.; Labille, J.; Bottero, J.-Y., Non-linear release dynamics for a CeO₂ nanomaterial

embedded in a protective wood stain, due to matrix photo-degradation. *Environmental Pollution* **2018**, *241*, 182-193.

54. Piccinno, F.; Gottschalk, F.; Seeger, S.; Nowack, B. J. J. o. N. R., Industrial production quantities and uses of ten engineered nanomaterials in Europe and the world. **2012**, *14* (9), 1109.

55. Zhou, S.; Wu, L.; Sun, J.; Shen, W., The change of the properties of acrylic-based polyurethane via addition of nano-silica. *Progress in Organic Coatings* **2002**, *45* (1), 33-42.

56. Mizutani, T.; Arai, K.; Miyamoto, M.; Kimura, Y., Application of silica-containing nano-composite emulsion to wall paint: A new environmentally safe paint of high performance. *Progress in Organic Coatings* **2006**, *55* (3), 276-283.

57. Al-Kattan, A.; Wichser, A.; Vonbank, R.; Brunner, S.; Ulrich, A.; Zuin, S.; Arroyo, Y.; Golanski, L.; Nowack, B., Characterization of materials released into water from paint containing nano-SiO₂. *Chemosphere* **2015**, *119*, 1314-1321.

58. Plathe, K. L.; Von Der Kammer, F.; Hassellöv, M.; Moore, J. N.; Murayama, M.; Hofmann, T.; Hochella Jr, M. F., The role of nanominerals and mineral nanoparticles in the transport of toxic trace metals: Field-flow fractionation and analytical TEM analyses after nanoparticle isolation and density separation. *Geochimica et Cosmochimica Acta* **2013**, *102*, 213-225.

59. Hochella, M. F.; Lower, S. K.; Maurice, P. A.; Penn, R. L.; Sahai, N.; Sparks, D. L.; Twining, B. S., Nanominerals, mineral nanoparticles, and earth systems. *Science* **2008**, *319* (5870), 1631-1635.

60. Farner, J. M.; De Tommaso, J.; Mantel, H.; Cheong, R. S.; Tufenkji, N., Effect of freeze/thaw on aggregation and transport of nano-TiO₂ in saturated porous media. *Environmental Science: Nano* **2020**, *7* (6), 1781-1793.

3.5 Supplementary Information

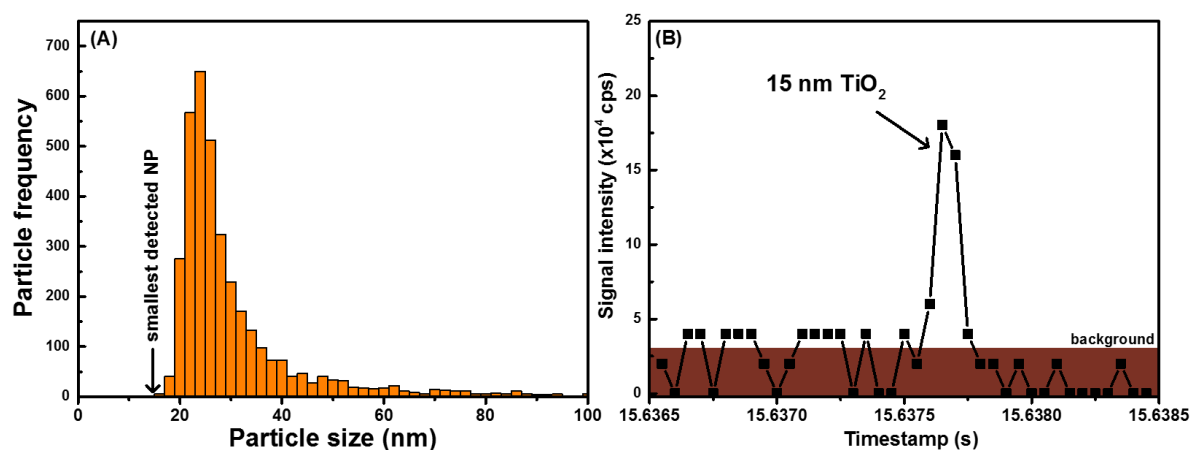


Figure 3-S1. (A) Particle size distribution of Ti-containing NPs in a melted snow as measured by a magnetic-sector SP-ICP-MS coupled to a desolvator and using a dwell time of 50 μ s. While the measurable size detection limits were below 15 nm, the NP detection thresholds were conservatively set so that 15 nm was the smallest detected NP across all samples. (B) an example of the raw ICP-MS signal data for the smallest detected NP with a size of 15 nm. Particle diameters were calculated on the assumption that particles were solely spherical TiO_2 .

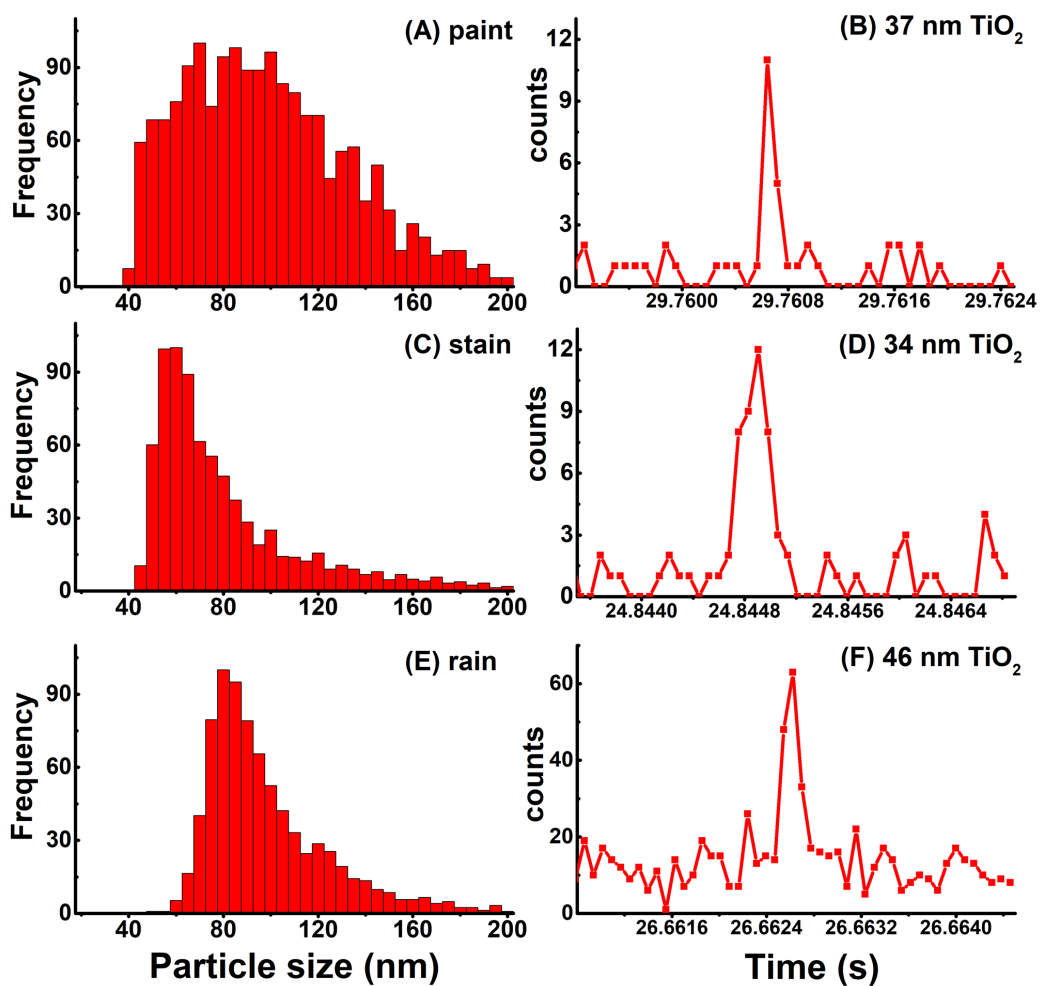


Figure 3-S2. Particle size distributions measured using SP-ICP-TOF-MS for Ti-containing NPs in (A) diluted paint, (C) diluted stain and (E) rainwater, as well as the raw peak data for NPs that were near the instrumental size detection limits. Sizes have been calculated by assuming that Ti-NPs were made up of solely spherical TiO₂.

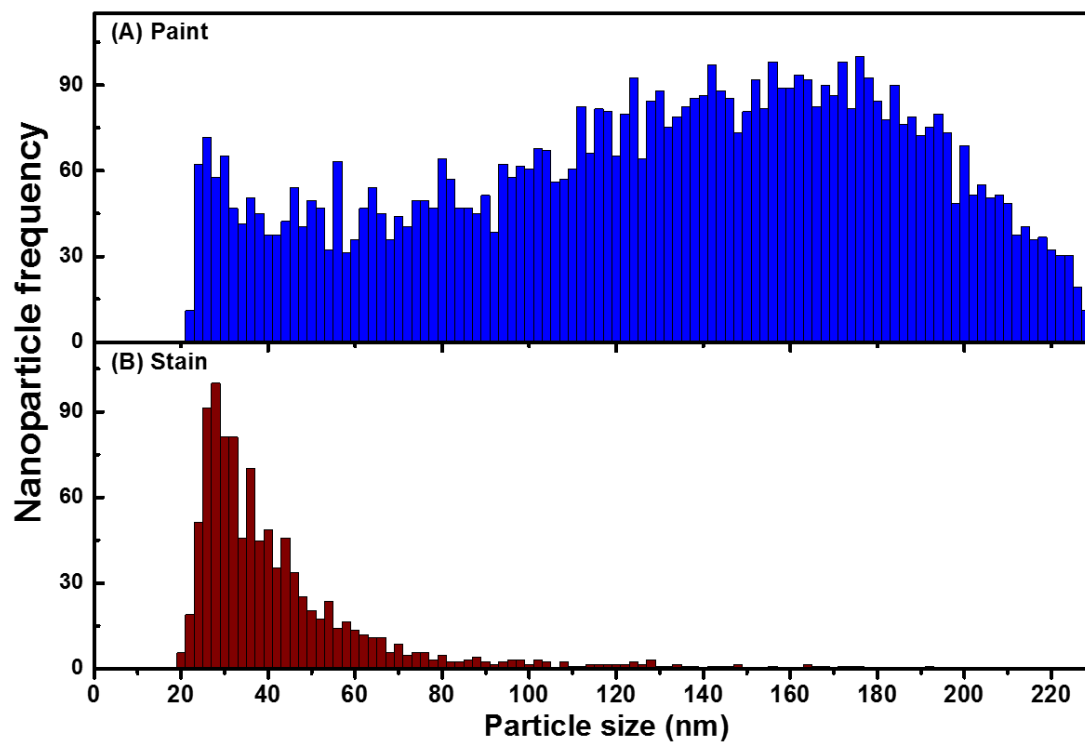


Figure 3-S3. Particle size distribution of TiO₂ NPs in (A) liquid paint and (B) liquid stain, as measured by a high-resolution SP-ICP-MS. The samples were analyzed immediately following a $2 \times 10^7 \times$ dilution of the liquid paint and $2 \times 10^5 \times$ times dilution of the stain in Milli-Q water. Particle diameters were calculated on the assumption that particles were solely spherical TiO₂.

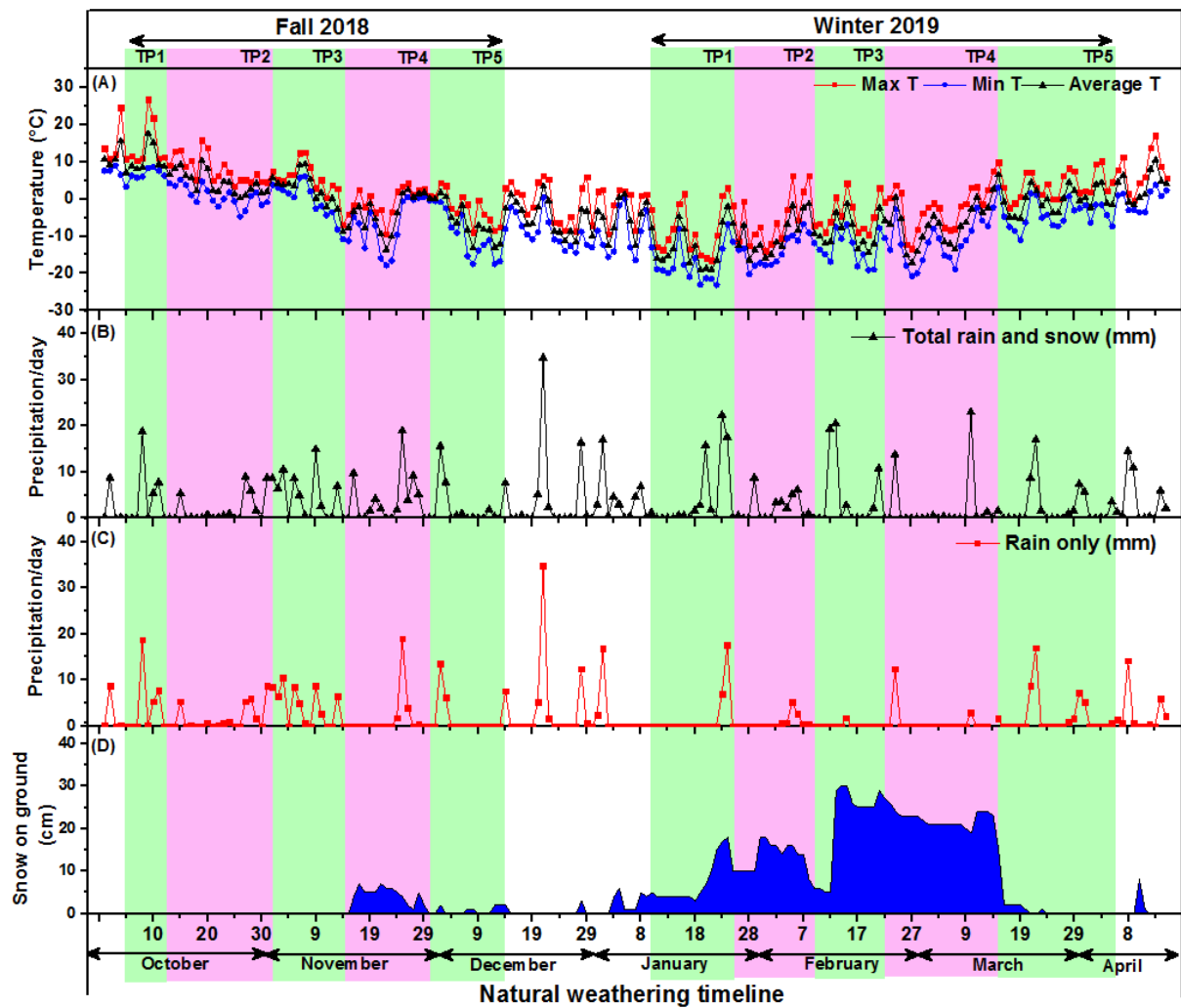


Figure 3-S4. (A) Daily temperatures (maxima, minima and mean T), (B) total precipitation (total liquid equivalent of rain and snow), (C) rain precipitation and (D) snow on ground data for the fall of 2018 and winter of 2019, as collected from the Montreal International Airport weather station (45°28'14.000" N, 73°44'27.000" W) and retrieved from the Environment and Climate Change Canada database. Timepoints (TP) indicate when the respective fall or winter samplings were conducted.

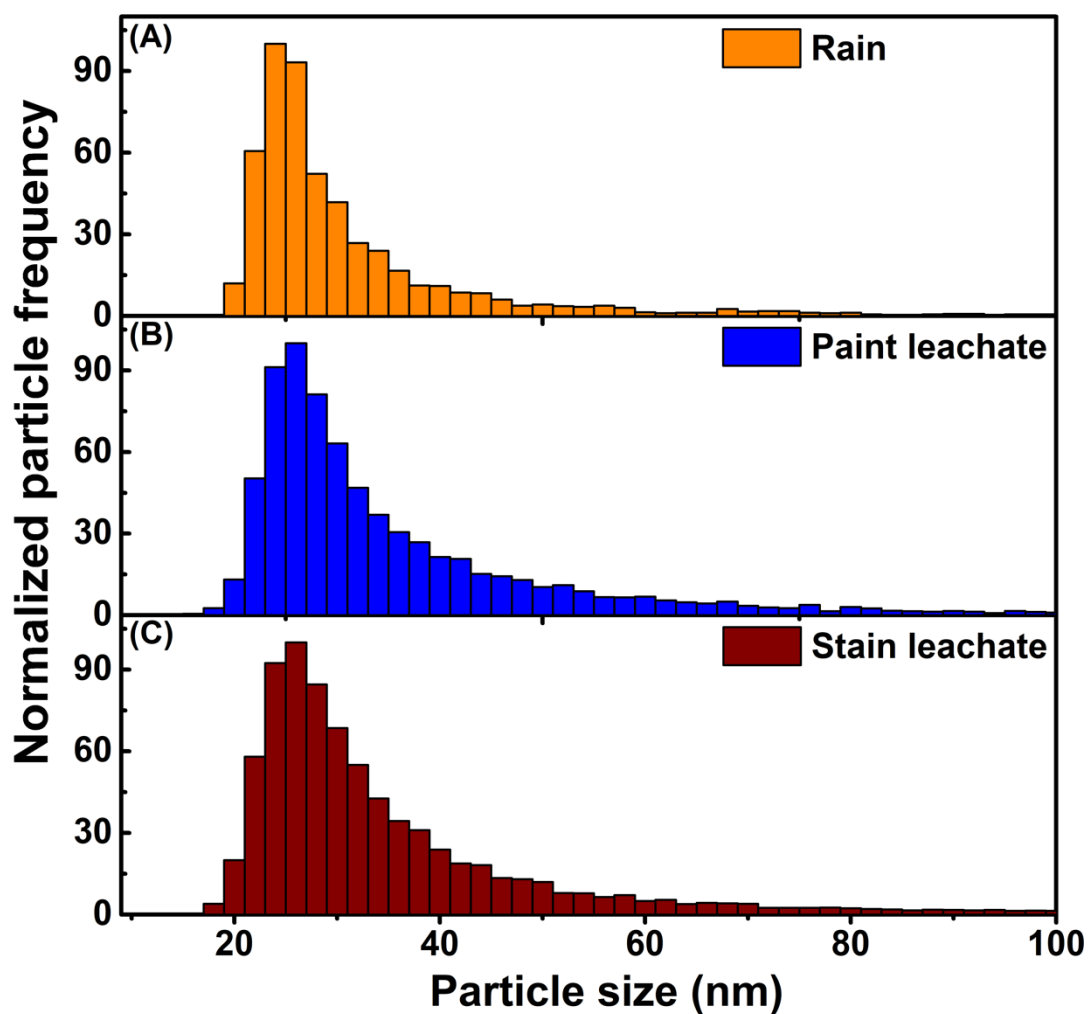


Figure 3-S5. Examples of particle size distributions of Ti-containing NPs (A) in a rainwater as well as in the leachates of (B) paint and (C) stain. NP frequencies in the leachate samples were calculated following the subtraction of the background NPs (*i.e.* pre-existing NPs in the rainwater). Samples were measured by a magnetic-sector SP-ICP-MS, and the particle diameters were calculated by assuming that Ti-containing NPs were solely spherical TiO_2 .

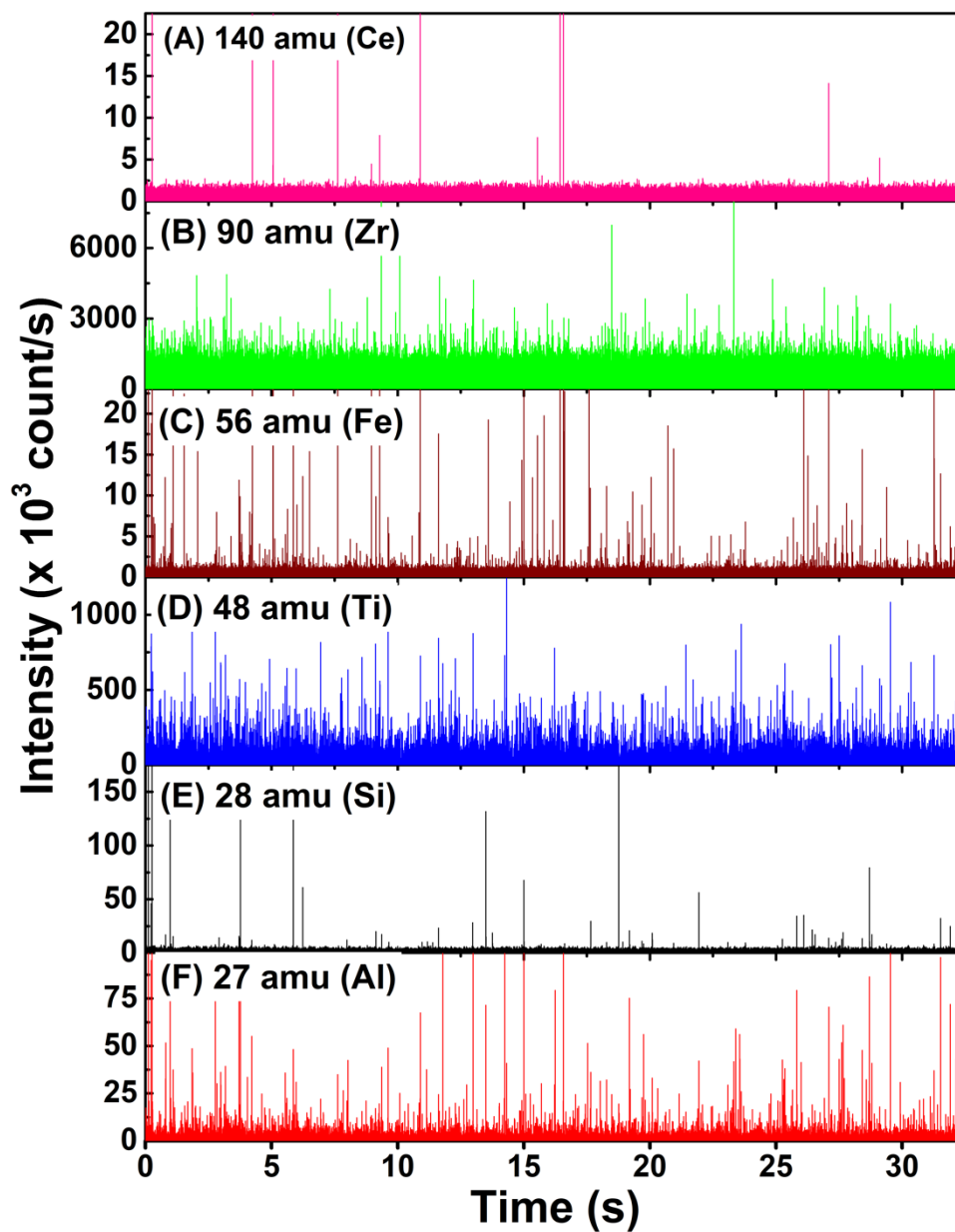


Figure 3-S6. Time-resolved ICP-TOF-MS signal simultaneously measured for (A) Ce, (B) Zr, (C) Fe, (D) Ti, (E) Si and (F) Al in liquid paint that was diluted 2×10^7 x with Milli-Q water.

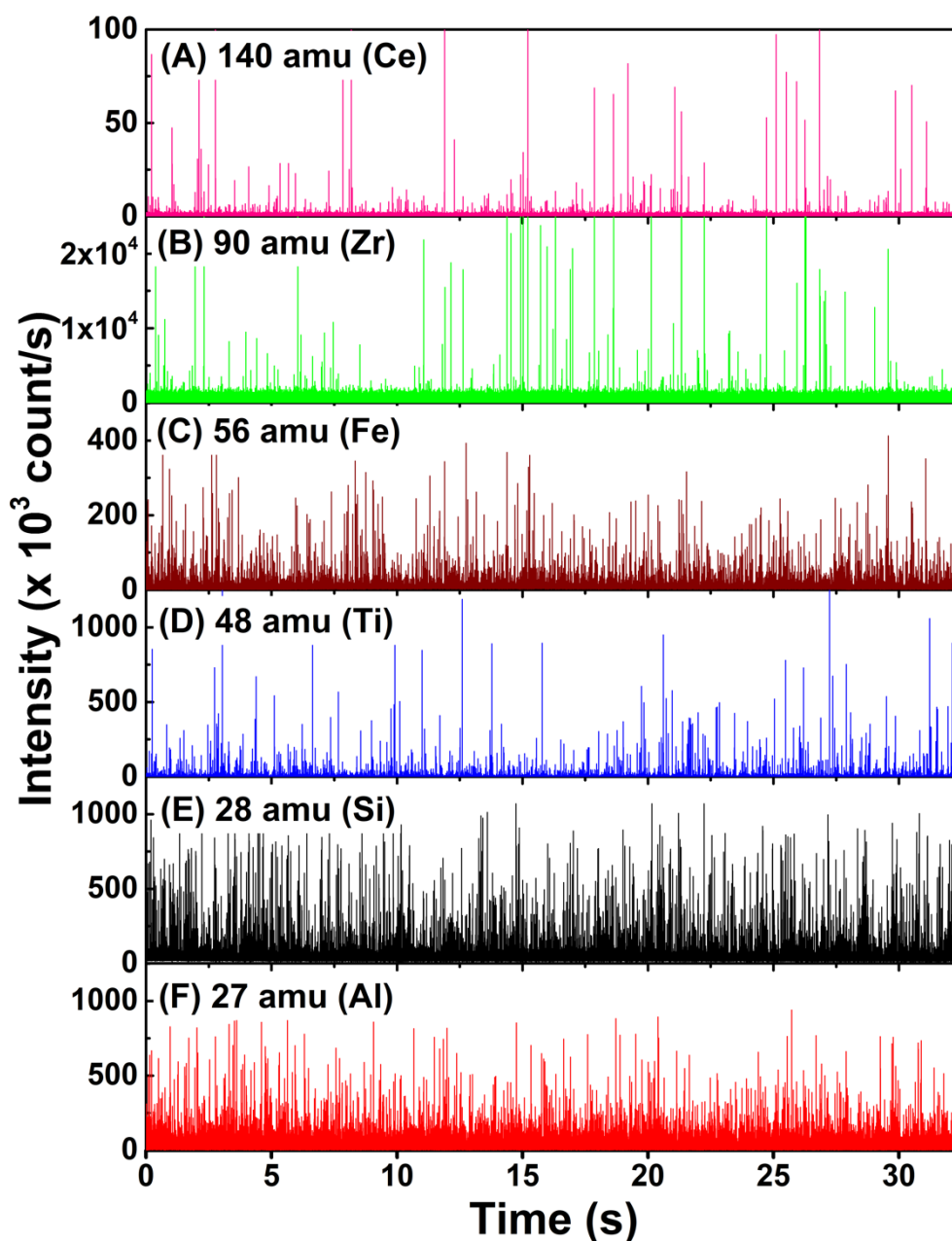


Figure 3-S7. Time-resolved ICP-TOF-MS signal simultaneously measured for (A) Ce, (B) Zr, (C) Fe, (D) Ti, (E) Si and (F) Al in the liquid stain that was diluted with Milli-Q water. While Ce, Zr, Ti, Si and Al were measured in 2×10^4 x diluted samples, Fe was measured in 2×10^5 x diluted samples due to its relatively higher concentration.

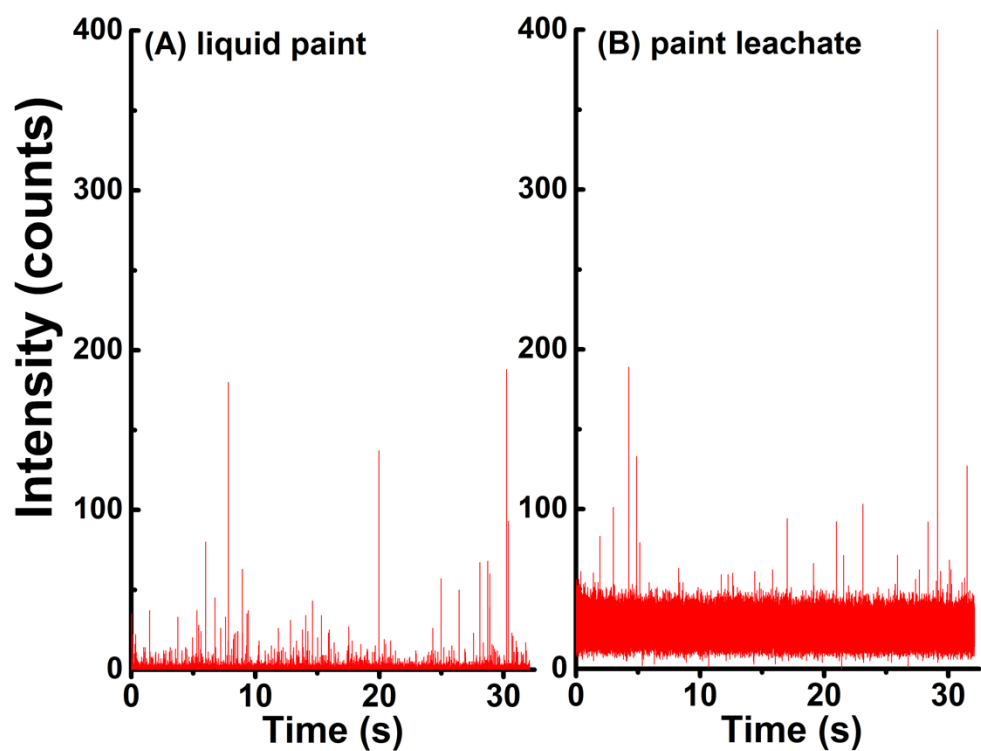
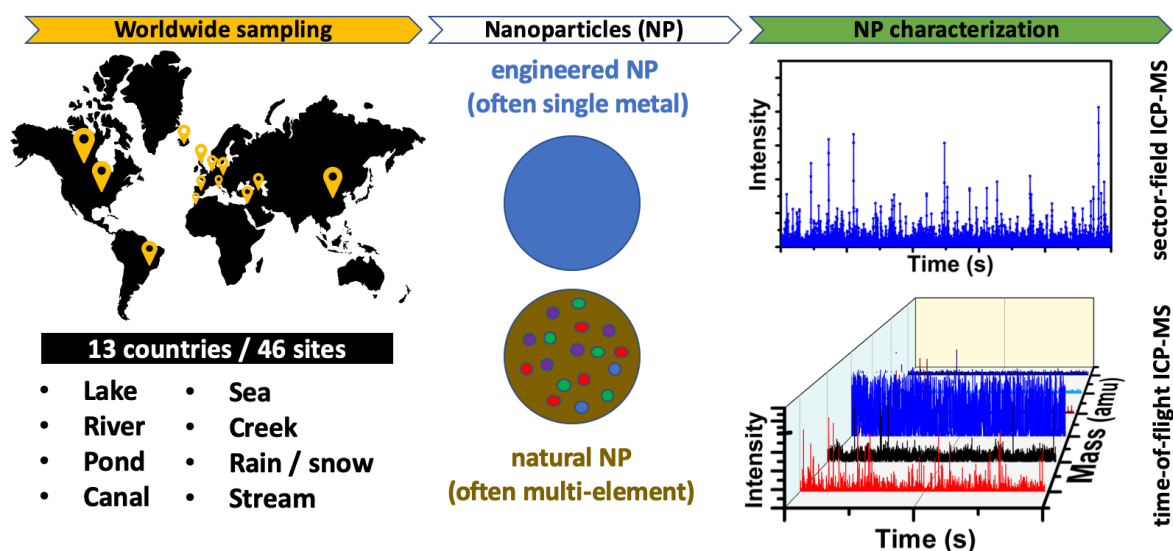


Figure 3-S8. Time-resolved ICP-TOF-MS signal measured for ^{27}Al in diluted liquid paint ($2 \times 10^7 \times$) and in the leachate following the weathering of a painted surface in Milli-Q water.

Chapter 4 Quantification and characterization of Ti-, Ce- and Ag-nanoparticles in global surface waters and precipitation

Connecting text: Nanoparticle (NP) emissions to the environment are increasing as a result of anthropogenic activities, prompting concerns for the ecosystem and human health. In order to evaluate the risk of NPs, it is necessary to know not only their product-release rates (*e.g.* paint-release, textile-release), but also their existing concentrations in various environmental compartments; however, these data have remained largely elusive due to the analytical difficulties of measuring NPs in complex natural matrices. Here, we measure NP concentrations and sizes for Ti-, Ce- and Ag-containing NPs in numerous global surface waters and precipitation samples, and we provide insight into their compositions and origins (natural or anthropogenic). The results link NP occurrences and distributions to particle type, origin, and sampling location. This work lays the foundation for broader experimental NP surveys, which will be critical for reliable NP risk assessments and the regulation of nano-enabled products.



Published as: Azimzada, A., Jreije, I., Hadioui, M., Shaw, P., Farnier, J. M., & Wilkinson, K. J., Quantification and characterization of Ti-, Ce- and Ag-nanoparticles in global surface waters and precipitation. *Environmental Science & Technology* **2021**, 55, 14, 9836-9844.

4.1 Introduction

Nanoparticles (NPs) are small (with three dimensions below 100 nm) particles that are found in many modern products and technologies and which are hypothesized to be in all environmental compartments.^{1,2} Although *natural* forms of NPs are ubiquitous,^{3,4} their impact on ecosystems and human health has really only been questioned in recent decades, coinciding with the increased production and disposal of *engineered* NPs.^{1,5,6} Engineered NPs have been developed due to their generally enhanced chemical reactivities with respect to bulk materials of similar composition, which implies enhanced biological reactivity and potentially increased risk.⁷

To date, the vast majority of data on NP concentrations in the environment have been extrapolated from global production volumes⁸ and (often assumed) product-release rates⁹, generated through modelling¹⁰ and based on contaminant transport patterns^{11,12}. Authors of these studies have systematically noted a very large uncertainty due to the poor quality of input data, the use of a large number of simplifying assumptions and the limited inclusion of environmental fate processes (*e.g.* agglomeration, heteroaggregation, dissolution, phase transformations). Although recently developed time-sensitive and size-specific probabilistic models^{13,14} represent a significant improvement, they may still overlook (i) the complexity of NP transformation or transport patterns; (ii) the time-dependence of input parameters; (iii) the role of geo-specific factors, *e.g.* scale, terrain, weathering; and (iv) the occurrences of episodic or localized events. Reliable risk assessments for the NPs will thus require experimental measurements¹⁵⁻¹⁹ of the exposure concentrations, including spatially and temporally resolved data on their composition, size, and origin, across regions.²⁰ The near absence of NP measurements is due, in large part, to the analytical challenges of analyzing NPs in complex natural matrices, where NPs co-exist with various environmental colloids, particulates and dissolved molecules and ions, including natural organic matter.^{21,22}

Single-particle inductively coupled plasma mass spectrometry (SP-ICP-MS) is a promising state-of-the-art technique, providing data on NP mass and number concentrations and size distributions.²³ Indeed, recent developments with sector-field SP-ICP-MS have enabled the detection and characterization of NPs with sizes down to a few nm (*i.e.* 3-4 nm for Ag- and CeO₂-NPs; 12 nm for TiO₂-NPs).^{18,24,25} The size detection limits (SDL) are critical since they provide the lower end of the range of quantified NPs; NPs below the SDL are mistakenly classified as dissolved. Another important aspect of nanoanalytics is the source discrimination of NPs, with the ultimate goal of quantifying anthropogenic NP contributions.

Given that anthropogenic NPs are often pure, while natural NPs tend to exhibit chemical heterogeneities,²⁶⁻²⁸ differences in particle compositions (*i.e.* purity, elemental associations) have previously been used for source attribution of NPs. Fortunately, recent advances in single-particle time-of-flight ICP-MS (SP-ICP-TOF-MS) have allowed whole elemental mass spectra at sub-millisecond data acquisition rates, on a particle-by-particle basis.²⁹ These advances have paved the way for experimental determinations of NPs in complex natural settings, providing information on their mass/number concentrations, sizes, compositions and origins.

Here, we provide the first large-scale measurements of NPs for a wide range of surface waters and precipitation samples that were collected from around the world. NP measurements were performed using a high sensitivity sector-field ICP-MS and a prototype, high-speed ICP-TOF-MS. They were focused on three NPs (Ag, TiO₂, CeO₂) that have suspected high anthropogenic contributions³⁰. The objectives were (i) to provide experimentally measured NP concentrations and sizes; (ii) to explore NP composition and its link to NP size; and (iii) provide insight into the origin (natural or anthropogenic) of the NPs. The data will be useful for modelling studies and risk assessments and provide a baseline with respect to future determinations of environmental NPs.

4.2 Materials and Methods

Global sampling campaign. Surface water and precipitation samples were collected at 46 sampling sites across 13 countries, including time-resolved measurements in Montreal (Quebec, Canada). The logistical challenges of conducting a large-scale sampling campaign were overcome with the help of 21 collaborators. In order to harmonize the sampling process, experimental material kits, as well as detailed sampling protocols were sent to each of the destinations in advance of the sampling date. Each kit contained, at a minimum, 50 mL polypropylene centrifuge tubes (Fisher Scientific) (10 used to collect triplicate rainwater samples), 15 mL polypropylene centrifuge tubes (Fisher Scientific) (>3 per sample), 20-30 mL syringes with no rubber gaskets (Henke-Sass Wolf, Germany) (>3 per sample), 0.45- μ m 33 mm PVDF (polyvinylidene fluoride) syringe filters (Sigma-Aldrich) (>3 per sample), ParafilmTM M wrapping films (Fisher Scientific) and a few pairs of non-powdered nitrile gloves (Kimberley-Clark).

Surface water samples were collected from the top 5-10 cm and immediately filtered on-site using the PVDF filters, which were pre-rinsed²⁹ with ~6 mL of the sample (corresponds to >50x filter void volume) in order to minimize sorptive losses. Higher volumes were avoided

to minimize the risk of concentration polarization artefacts on the filter membrane. Sample filtrate was then added to triplicate 15 mL tubes, to the brim. The filtration step was designed to assist with the preservation of the samples during transport by removing most microbes and large particles. Based upon measured sizes and particle numbers, the NP appeared to be stable for at least 12 days (**Fig. 4-S1**).

Precipitation (rain) samples were collected by leaving out 6-8 of the 50 mL centrifuge tubes (>0.5 m above the ground) during rainfall events. In order to avoid/minimize sample evaporation and dry deposition of atmospheric (nano)particles, the duration of rain collection was limited to a single precipitation event and to <2 hours. The collected rain fractions were then combined into triplicate 15 mL tubes (filled to the brim). All tubes were labeled, and sampling geo coordinates were recorded. The tubes were then sealed with parafilm, placed into a padded envelope, and express delivered to the Montreal laboratory (typically, 1-2 days for Canada; 3-4 days for Europe, USA and Brazil; 7-12 days for China). Once received, samples were refrigerated at 4 °C until analysis.

Sample preparation for analysis. Precipitation samples, on the day of their arrival in the lab, were ultrasonicated for 30 minutes (Branson Ultrasonic Cleaner, 5510R-DTH Model, 135 W, 42 kHz \pm 6%) and then filtered using 0.45 μ m poresize PVDF filters that had been pre-rinsed with 6 mL of sample. On the day of analysis, all filtered samples (surface or precipitation) were treated with 10 min of ultrasonication, and then, if necessary, were diluted 5-50x for measurements by ICP-MS.

SP-ICP-MS measurements. SP-ICP-MS data were acquired on a double-focusing sector-field ICP-MS (AttoM ES, Nu Instruments, United Kingdom), at low resolution (300) and using single ion acquisition, in fast scan mode.²⁴ While Ce-NP analysis could be optimally performed using a wet aerosol¹⁸, for Ti- and Ag-NP analysis, the sensitivity was further enhanced by coupling the ICP-MS to a desolvator (Aridus II, Teledyne Cetac Technologies) that used a PFA (perfluoroalkoxy) micro-flow nebulizer (self-aspiration rate of 200 μ L min⁻¹ for 1 L min⁻¹ of Ar)²⁹. The flow rates of the nebulizer gas (argon) and membrane sweep gas (argon) typically ranged between 0.7-1.0 L min⁻¹ and 3-7 L min⁻¹, respectively. As per previously optimized strategies^{18, 24}, ⁴⁹Ti, ¹⁴⁰Ce and ¹⁰⁷Ag were measured during the analysis. Notably, the choice of ⁴⁹Ti was predicated on the fact that, despite its low abundance, it has fewer interferences, and its analysis was enabled by the high-sensitivity system. Data acquisition spanned 50 s with an optimized dwell time of 50 μ s, resulting in ca. 10⁶ datapoints per replicate. This yielded SDLs of \sim 15 nm for TiO₂, and \sim 4 nm for CeO₂ and Ag NPs^{18, 24, 29}. Sensitivity calibrations were determined based on ionic standards of Ti, Ce and Ag (High Purity Standards). Transport

efficiencies (TE) were determined by the particle frequency method³¹ using ultra-uniform 30 nm Au NPs (NanoComposix, AUXU30-1M) with a known particle number concentration. TE measurements were validated with a second standard reference material (60 nm Au NPs, NIST 8013). TE values typically ranged between 0.11-0.15 $\mu\text{L s}^{-1}$ or 3.5-4.5 % for Ce analysis (*i.e.* wet mode) and 0.45-0.55 $\mu\text{L s}^{-1}$ or 13-15% for Ti and Ag analysis (*i.e.* dry mode). Wherever necessary, filtered samples were diluted (1-50x) to minimize the incidences of concurrent peaks ($< 10,000$ events or 1% of total datapoints), while ensuring a statistically significant number of NPs. Detection thresholds of ~ 360 NP mL^{-1} Ti-NPs, 1500 NP mL^{-1} Ce-NPs and 900 NP mL^{-1} Ag-NPs could be established by requiring that the peak numbers collected over a 50 s acquisition exceeded those in the blanks by at least a factor of 3.³²

SP-ICP-TOF-MS measurements. SP-ICP-TOF-MS data were acquired on a prototype high-speed time-of-flight ICP-MS (Nu Vitesse, Nu Instruments, United Kingdom) that enabled the characterization of multi-element particles on a particle-by-particle basis.²⁹ The instrument was equipped with a segmented reaction cell, into which ca. 4-6 $\text{cm}^3 \text{min}^{-1}$ of He and ca. 4 $\text{cm}^3 \text{min}^{-1}$ of H_2 gas were introduced to eliminate argon and nitrogen-based interferences (*e.g.* for elements such as K, Ca, Cr, Fe and Si). To further increase the sensitivity, the instrument was coupled to an Aridus II desolvator (Teledyne Cetac Technologies), with similar nebulizer gas (argon) and sweep gas (argon) conditions as were used for the sector-field instrument. Signal acquisitions were performed every 25.5 μs for a near full range of time of flight mass spectra (23-238 amu), continuously and with no loss of data. Following the accumulation of 3 consecutive acquisitions, electronic noise was subtracted, and signals were integrated and individually stored for each isotope (*i.e.* from Na to U every 76 μs). Total sampling time ranged between 0.5-10 min and was adjusted according to particle numbers in the samples (*i.e.* to achieve statistically significant particle counts). Sensitivity calibrations were built following the analysis of custom-prepared multi-element standards (CLMS-1, CLMS-2, CLMS-3 and CLMS-4, SPEX CertiPrep). TEs were determined using the particle size method³¹ and were based on ionic Au sensitivities and an ultra-uniform NP standard of 30 nm (NanoComposix, AUXU30-1M). For NPs considered to be composed of a single metal, SDLs on the ICP-TOF-MS corresponded to ~ 30 nm (TiO_2) and ~ 16 nm (CeO_2 and Ag).

Data processing for SP-ICP-MS/SP-ICP-TOF-MS. SP-ICP-MS data was processed using Nu Quant software version 2.2 (Nu Instruments, United Kingdom), as previously described in Hadioui *et al.* (2019)²⁴ and Shaw and Donard (2016)³³. Briefly, the data processing algorithm used data smoothing to reduce background fluctuations for time-resolved raw data. A rolling search window was created at time zero, where the algorithm searched for a peak maximum

and set its pre- and post-inflection points. Once found, the window was shifted in order to detect more peaks – a process that spanned the whole data acquisition period. For each detected peak, the local background was calculated based on the stored inflection point data. It was then subtracted from the integrated raw data for the peak (further details in the SI). The average of local backgrounds (*i.e.* global background) was used to calculate dissolved metal content or interferences. NP masses and sizes were calculated based on ionic sensitivities and TE measurements, while assuming spherical shapes and particle densities of 4.23, 7.13 and 10.49 g cm⁻³ for TiO₂, CeO₂ and Ag NPs, respectively.

SP-ICP-TOF-MS data was processed using a modified version of NuQuant software (NuQuant Vitesse prototype, Nu Instruments, United Kingdom).²⁹ The software algorithm used similar smoothing and peak detection parameters, as for the single-isotope analysis, however, it searched for multiple target isotopes (*e.g.* ⁴⁸Ti, ²⁷Al, ⁵⁶Fe for Ti-, Al- and Fe-containing NPs) simultaneously, determining start and end timestamps for each particle event. Based on the timestamps, counts for all isotopes were then identified. Given the full width half maximum (FWHM) values and the baseline standard deviations, a noise threshold was applied to filter out background artifacts, often arising from high-background metals (*e.g.* Na, Ca, Zn). While FWHM values were used to screen potential peak artifacts, the rapid monitoring of NPs was also conducted by sorting the detected NP peaks by isotope type and intensities in order to focus on peaks of potential concern, *i.e.* very slender or very wide peaks with low intensity). NP masses were calculated based on multi-element calibrations and TE measurements.

4.3 Results and Discussion

NP occurrence and concentrations across the globe. Concentrations of Ti-, Ce-, and Ag-containing NPs are presented for both surface waters and precipitation (**Fig. 4-1**) for a wide geographical range of samples (further details in **Tables 4-S1, S2, S3** and **S4**). Samples from 46 sites across 13 countries were analyzed, representing an array of natural and artificial water bodies, including lakes, rivers, ponds, canals, coastal marine water and natural precipitation, and encompassing a wide range of water types (*i.e.* salinities, natural organic matter content, hydrodynamic regimes). La-containing NPs were also reported (**Fig. 4-S2**) to provide additional insight into particle origins. Based upon global production volumes^{1, 2, 8}, we would expect La-containing NPs to be predominantly from natural sources, Ce- and Ti-NPs to be from both natural and anthropogenic sources and Ag-NPs to be predominantly from anthropogenic sources.

It is notable that NP concentrations varied substantially with respect to both sampling location and NP type. For example, while Ti- and Ce-NP concentrations in surface and precipitation waters typically ranged between $10^4 - 10^6$ NP mL⁻¹, Ag-NPs were often below detection limits of 900 NP mL⁻¹ and were only seldomly measured in the higher concentration range of $10^4 - 10^5$ NP mL⁻¹. Among the sampling sites examined, Ti-NPs were at the lowest concentrations in the Canadian far north (Yukon territories), whereas snow samples from the Sólheimajökull glacier (Iceland) contained the greatest number of particles (**Fig. 4-1**). While low NP concentrations were intuitively expected for samples relatively less impacted by urban/industrial activities (*e.g.* Yukon), in the absence of particle influx due to long-range transport,^{5, 11} the observed high NP concentrations of Iceland demonstrated the region-specific nature of NP emissions. Indeed, the geographical position of the Sólheimajökull glacier between two volcanoes (Eyjafjallajökull and Katla) renders it vulnerable to volcanically generated particulate pollution, which is known to contain Fe and Ti.^{34, 35}

Ce-NPs generally followed a similar distribution pattern to that of the Ti-NPs, except in the case of the marine samples. While this may have been caused by significant particle agglomeration and sedimentation (potentially due to charge screening),³⁶ it is nonetheless puzzling that Ti-NPs were not subjected to a similar fate. It is possible that this observation is related to particle-specific properties of the NPs. For example, TiO₂ NPs have been shown previously to partition into the top (more hydrophobic) layers of surface waters rather than remain uniformly distributed in the water column³⁷. When compared to La-NPs (**Fig. 4-S2**), which often hovered around 10^6 NP mL⁻¹, Ti- and Ce-NP concentrations exhibited substantially more variability across sampling locations, likely caused by larger and more variable anthropogenic contributions of these two NPs. Furthermore, Ag-NPs showed concentration trends that were vastly different from both Ti- and Ce-NPs. Given that Ag is much less abundant on Earth as compared to Ti or Ce, one could hypothesize that its concentration is more influenced by anthropogenic processes – such as incineration/burning, metal smelting or mining activities.^{38, 39} The observation that Ag-NP concentrations were often below detection limits (900 NP mL⁻¹) but with maxima in the range of $\sim 10^4$ NP mL⁻¹ is indeed consistent with their input via anthropogenic sources¹⁹ – probably as a result of localized pollution or episodic events – and their low thermodynamic stabilities⁴⁰.

NPs are thought to be scavenged by rainwaters, so concentrations in rain will also depend greatly on the frequency and duration of precipitation events, preceding the sampling. While it is difficult to speculate on the sources of the Ag NPs in the precipitation, the high

concentrations observed in the Hohhot (CHN) rain sample are nonetheless consistent with China currently being the largest producer of silver in the Asia Pacific.

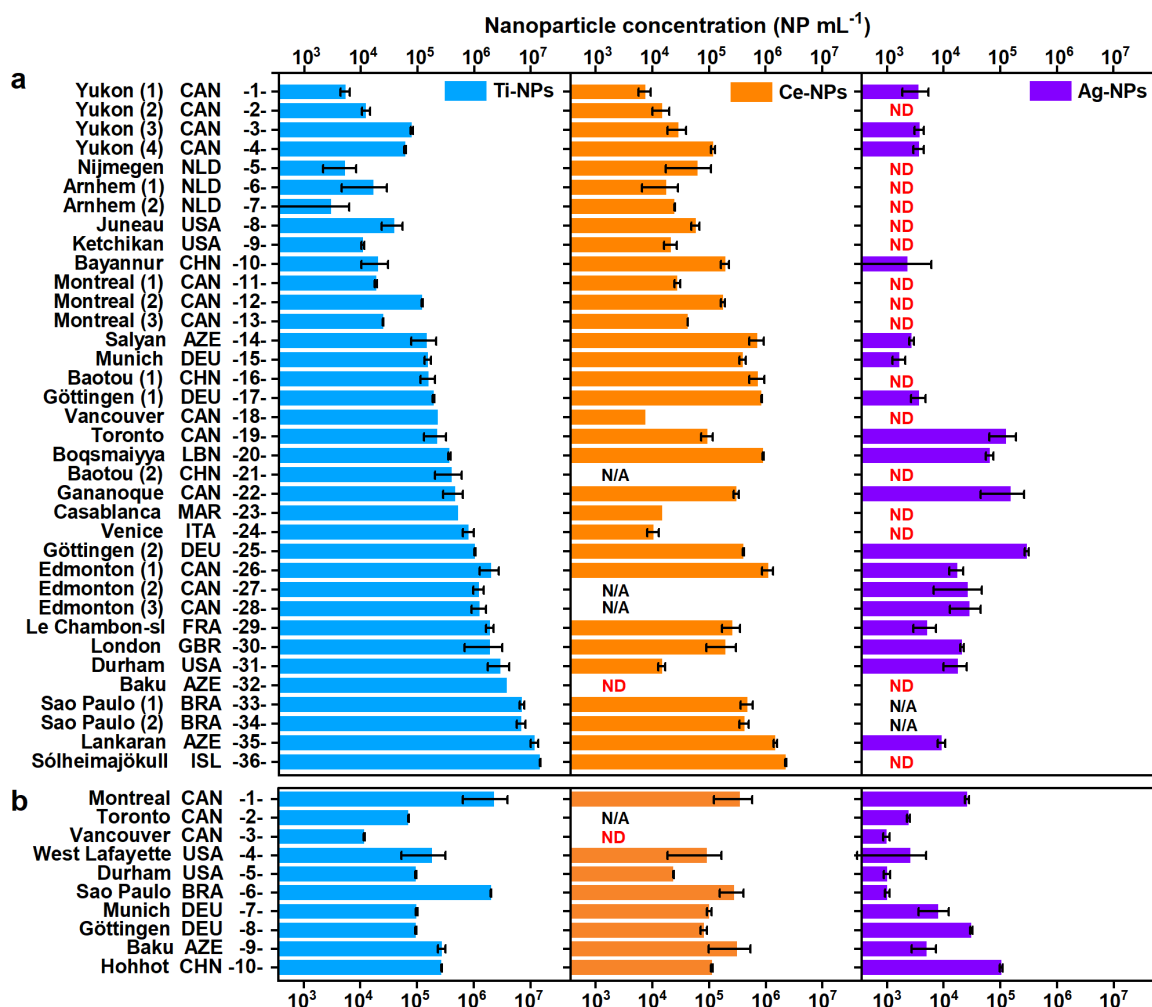


Figure 4-1. Nanoparticle concentrations in global surface waters and precipitation. Particle number concentrations for Ti-, Ce- and Ag-containing NPs (denoted by blue, orange and violet bars, respectively) collected at 46 sampling sites across 13 countries and measured in surface waters (a) and precipitation (b). Sampling sites are indicated by city/province names and ISO country codes. Measurements were performed using a sector-field ICP-MS. ND stands for “not detected” and refers to concentrations below the detection limits of the technique (ca. 1500 NP mL⁻¹ for Ce and ca. 900 NP mL⁻¹ for Ag). N/A refers to samples that were not analyzed. Error bars represent the standard deviations of triplicate samples.

The measurements presented here represent punctual determinations of NP concentrations and size distributions that are continually subjected to environmental factors, including precipitation, temperature, freeze-thaw, wind and episodic NP emission or transport events. Indeed, measurements of Ti- and Ce-containing NPs measured in Montreal surface waters over 5 weeks (Fig. 4-S3) showed that NP concentrations fluctuated by ~2-5x and appeared to be affected by the frequency/duration of precipitation events. For example, higher

concentrations of Ti- and Ce-NPs were observed immediately after significant rain events and were potentially related to increased urban run-off⁴¹.

NP composition and origins. Select international locations were used to explore the source of the Ti- NPs using SP-ICP-TOF-MS. Particle purity was used as an indicator of particle origin^{3, 27}, under the assumption that anthropogenic NPs often occur as pure particles, whereas naturally occurring NPs often contain multiple elements. While the purity assumption is not a rigorous criterion for determining NP source, it can provide insight into particle origin when coupled with data on individual elemental associations and region-specific pollution scenarios. Multi-element analyses of the Ti-NPs in precipitation (**Fig. 4-2a**) showed that the NPs exhibited a range of complex associations with other metals. For example, for 80% of the Ti-NPs detected in Sao Paulo and Montreal rainwaters, only Ti could be detected (*i.e.* >99.9 % Ti), whereas this fraction dropped to about 50% for rainwater samples collected in Munich or Durham and to <30% for samples collected from Vancouver and Sólheimajökull. Associations with specific elemental tracers, such as Al, Si and Fe (*i.e.* aluminosilicates)^{16, 42, 43} were particularly enlightening. For example, in the precipitation from Sao Paulo and Montreal, Ti-containing NPs were found more frequently than Al-, Si- and Fe-containing NPs (**Fig. 4-3a,b**). Furthermore, Al, Si or Fe could only be detected in a small fraction (<10%) of the Ti-containing NPs (**Fig. 4-3c,d**), reinforcing the contention that there may have been a substantial anthropogenic input of Ti-NPs.⁴⁴ In contrast, for the Vancouver rainwater, Ti-NPs were overwhelmingly less present than the Si- and Fe-containing NPs (**Fig. 4-3a,b**), with a majority of the Ti-containing NPs (>90%), also containing Si, Fe and Al (**Fig. 4-3c,d**). For the sample from the Sólheimajökull glacier, Ti-NPs were predominantly enriched with Fe (70% of cases), occasionally with Al (15%) and very rarely with Si (1%) – an observation that is consistent with this environment being a major sink/carrier for natural Fe-containing nanominerals.^{4, 45}

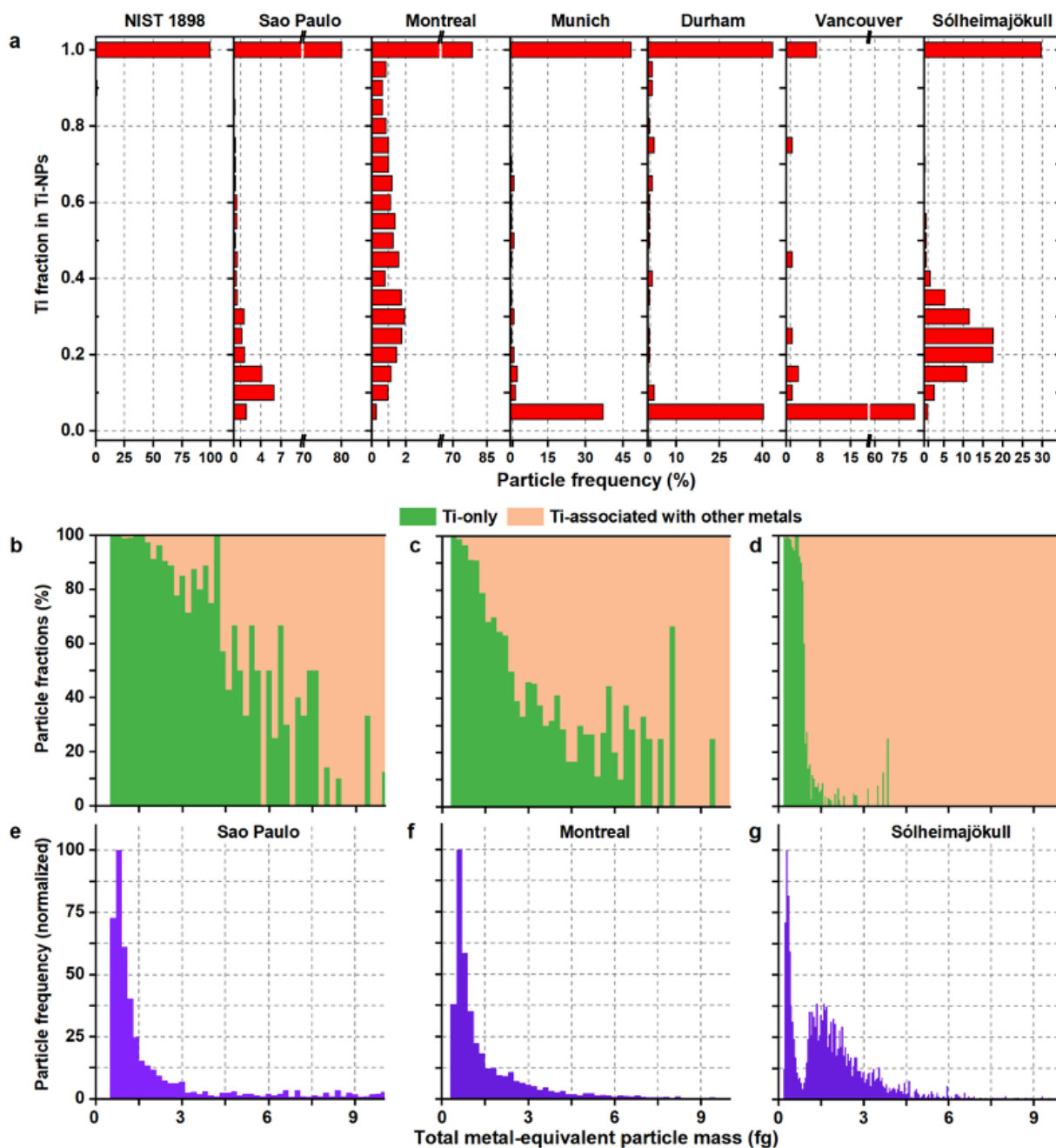


Figure 4-2. Particle compositions and their link to particle masses (or sizes). a, Ti fractions in Ti-containing particles as determined in TiO₂ nanoparticle standard (NIST 1898) and in natural precipitation samples collected at six locations: Sao Paulo (BRA), Montreal (CAN), Munich (DEU), Durham (USA), Vancouver (CAN) and Sólheimajökull (ISL). b-g, In selected samples of Sao Paulo, Montreal and Sólheimajökull, each Ti-particle is identified as containing ‘only Ti’ or ‘Ti with additional metals/metalloids’ and the corresponding number fraction (%) (b-d) of these particle categories as a function of total metallic particle mass (*i.e.* distributions, e-f) are reported. All calculations are based on data that was collected using single-particle ICP-TOF-MS.

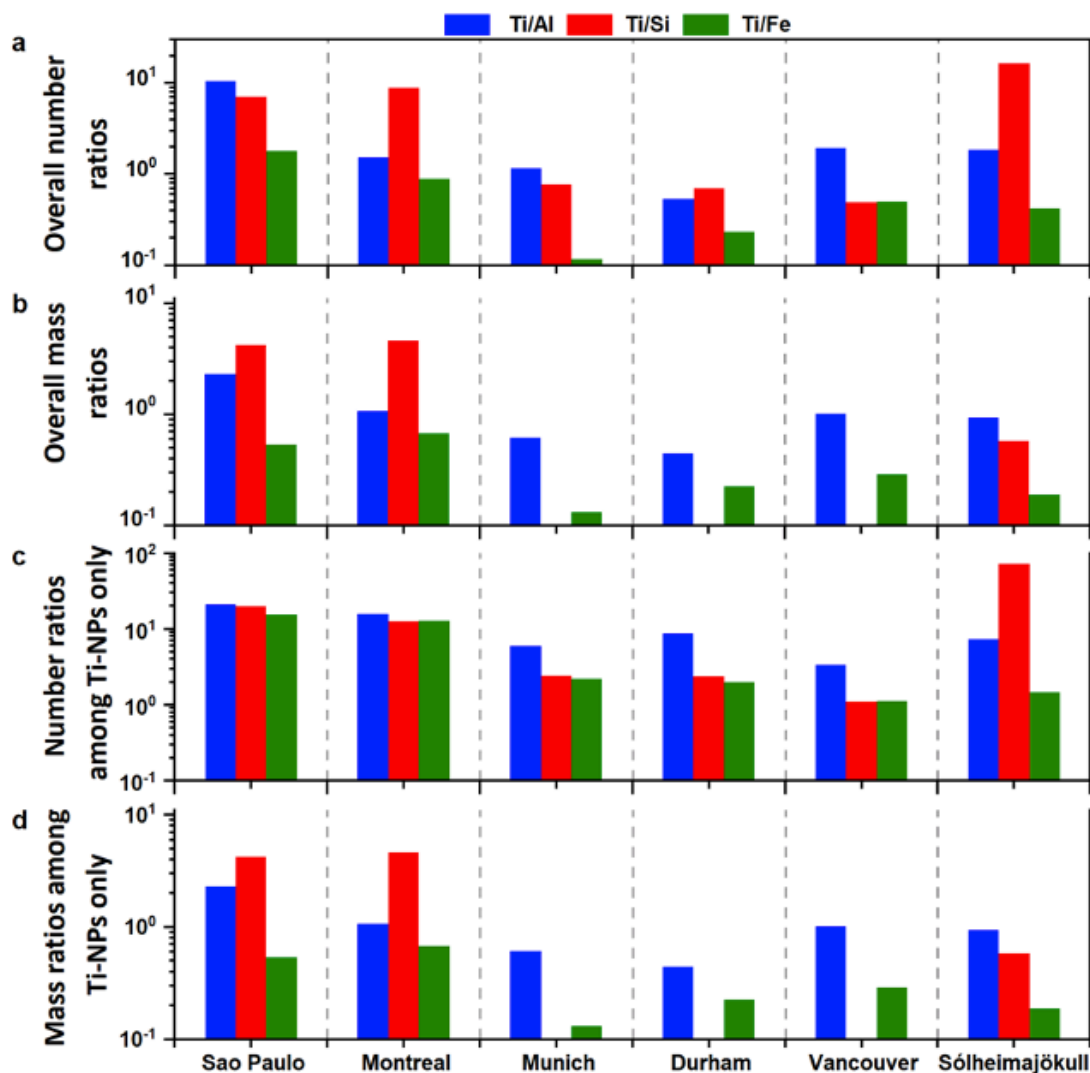


Figure 4-3. Metallic associations of nanoparticles on a single particle level. **a**, Ratios of the number of Ti-containing NPs to the number of Al-, Si- or Fe-containing NPs. **b**, Ratios of Ti mass to mass of Al, Si or Fe in the NP. **c**, Ratios of the number of Ti-containing NPs to the number of those both Ti-Al, Ti-Si or Ti-Fe. **d**, Ratios of the total mass of Ti in Ti-containing NPs to that of the Al, Si or Fe. Blue, red, and green bars denote Ti/Al, Ti/Si and Ti/Fe (mass or number) ratios, respectively. When these ratios are below 0.1 (*i.e.* low cut-off on y-axis), bars were not visible, meaning that the second metal (Al, Si or Fe) was much more present as compared to Ti. Calculations are performed for natural precipitation samples from Sao Paulo (BRA), Montreal (CAN), Munich (DEU), Durham (USA), Vancouver (CAN) and Sólheimajökull (ISL). Measurements were performed using single particle ICP-TOF-MS.

NP sizes and origins. Equivalent diameters were calculated based upon the assumption that NPs were spherical and contained only TiO₂, CeO₂ or Ag. In that case, there was significant overlap in the size distributions of the respective NPs in the different surface waters, with modes for the diameters often occurring at ~30-60 nm for the Ti-NPs and below 20 nm for the

Ce-NPs and Ag-NPs (note the detection limits of ~15 nm for TiO₂, ~4 nm for CeO₂ and Ag; example distributions are provided in **Fig. 4-4a**; mean sizes in **Fig. 4-4b,c**). Nonetheless, particle sizes appeared to be affected by the sample nature. For example, mean diameters of Ti- and Ce-NPs detected in the rivers and rains were generally larger than those found in artificial water bodies, such as ponds and canals, or saline waters (**Fig. 4-4b,c**). This tendency may have been dictated by a combination of physiochemical (*e.g.* ionic strength, natural organic matter, redox conditions) and hydrodynamic (*i.e.* turbulence in water) factors and the way different NP types respond to them. Another notable source of variability is that the location of some of the water bodies might have favored the influx of certain types of NPs. For example, the observation of smaller NP sizes in artificial water bodies (*e.g.* ponds, canals) is consistent with the fact that these waters are mainly found in urban environments, which render them more susceptible to pollution with anthropogenic NPs (which generally tend to be smaller).

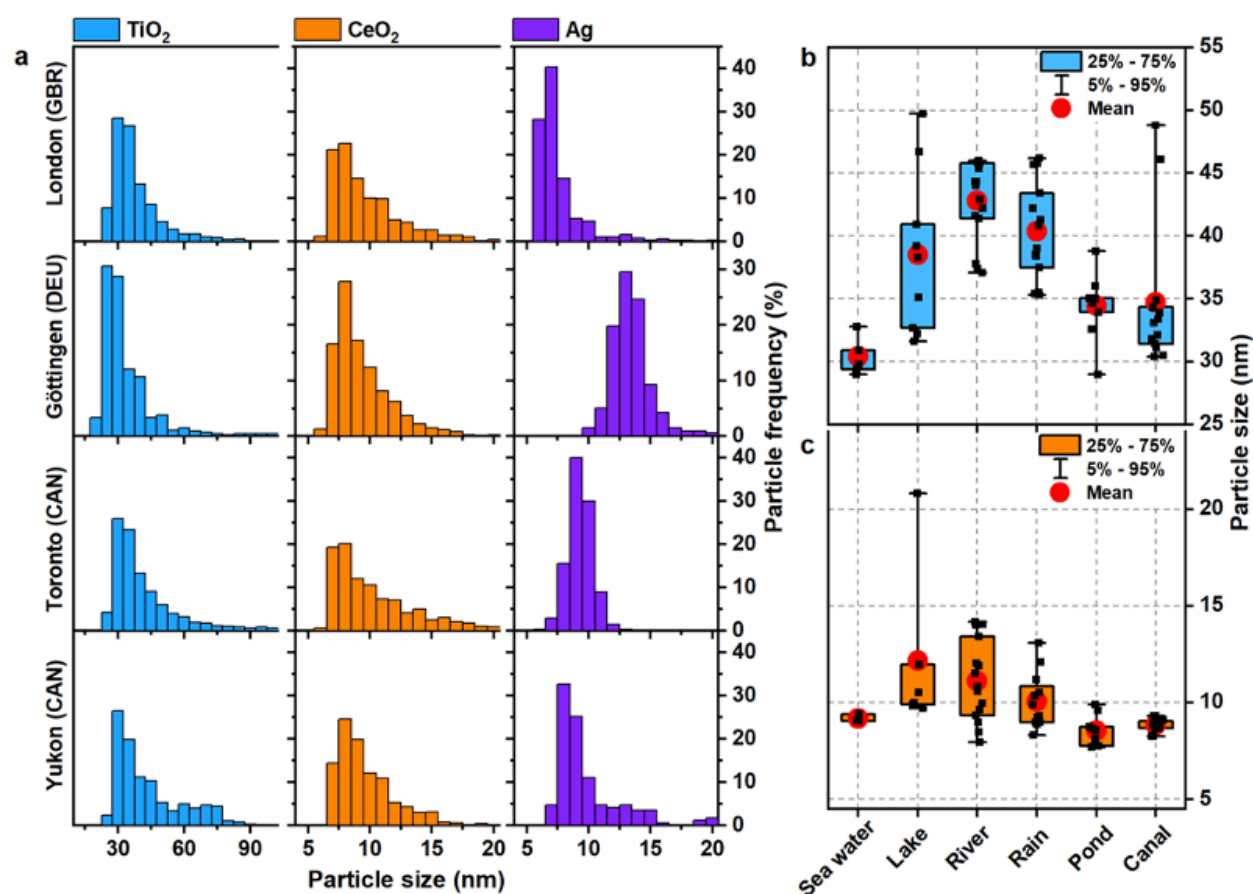


Figure 4-4. Nanoparticle size distributions and mean sizes by water type. a. Particle size distributions as determined for Ti-, Ce- and Ag-containing NPs in London (The Long Water Lake), Göttingen (Leine River), Toronto (Lake Ontario) and Yukon (Kluane Lake) surface waters. Measured (mean) sizes for Ti- (**b**) and Ce-containing (**c**) NPs detected in 46 samples.

Samples were categorized by water type. Limits of the boxes and whiskers represent 25%-75% and 5%-95% percentiles, respectively. Red solid circles represent the mean sizes, observed within each water category. NP measurements were performed using a sector-field ICP-MS. For all determinations, particle sizes were calculated by assuming that Ti-, Ce- and Ag-containing NPs occurred solely in the forms of spherical TiO₂, CeO₂ and Ag, respectively.

While the above estimates are relevant for pure NP populations, sizes for multi-element NPs are more complicated to calculate (**Fig. 4-S4**) due to an uncertainty on the particle densities and the unquantified contribution of several elements in the NPs (*e.g.* oxygen, halogens). For size estimates determined by taking into account the multi-elemental nature of particles, it was possible to observe two distinct peaks in the particle size distribution (*e.g.* **Fig. 4-S4** for the Icelandic sample). When the NPs were profiled as a function of their purity, only Ti (<1 fg per NP) was detected in the peak of the smaller NPs, whereas the peak corresponding to larger NPs systematically contained multiple elements (**Fig. 4-2d,g**). Similar observations were made for samples from Sao Paulo (**Fig. 4-2b,e**) and Montreal (**Fig. 4-2c,f**), where the smallest NPs were generally of much higher purity as compared to the larger NPs. Although it might be possible to attribute the absence of small multi-element NPs to instrumental detection limits (**Fig. S5**), it was nonetheless extremely rare to find pure Ti-NPs (oxides) among the larger particles. Such results show, as has often been assumed in the literature, that the anthropogenically generated NPs tend to be smaller and purer particles.

Global environmental implications. These results represent the first large-scale experimental determinations of NPs in surface waters and precipitation, encompassing three major NPs that are known to be emitted as a result of human activities. Data clearly show that NPs, whether anthropogenic or natural, have reached far corners of the world, albeit at concentrations that are dependent on the nature of the NPs, the geographical sampling location and the sampling time. Ti- and Ce-NP concentrations, which were impacted by both natural and anthropogenic inputs, showed the greatest variability across regions, ranging between 10⁴-10⁷ NP mL⁻¹. In contrast, the sporadic nature of the Ag NPs, and their generally lower concentrations (up to 10⁵ NP mL⁻¹), showed that while anthropogenic (episodic) inputs of Ag NPs are occurring, they are likely still relatively infrequent or low concentration events. For all NPs, particle concentrations and sizes were influenced by the water type, the nature of the sampling location and short- or long-range particle transport. Regardless of their nature, NP concentrations were often below 10⁶ NP mL⁻¹ (*i.e.* <1 ng L⁻¹ for Ag-NPs; <100 ng L⁻¹ for Ce-NPs; <10 µg L⁻¹ for

Ti-NPs), which are levels that presently do not appear to pose a high risk to ecotoxicological⁴⁶⁻⁴⁸ or human health⁴⁹.

In spite of the challenges of quantitatively distinguishing NPs with respect to their origins, the determinations of particle purity and size presented here indicated that smaller and purer NPs of possibly anthropogenic origin may indeed already dominate certain environments, such as large urban centers. It is worth noting that anthropogenic NPs are not only limited to the engineered NPs (*i.e.* manufactured), as they may also include NPs that are incidentally generated as a result of anthropogenic processes.⁵ For example, magneli phase titania ($\text{Ti}_x\text{O}_{2x-1}$), while rarely present in geological settings, was recently shown⁵⁰ to be emitted from industrial coal burning, since Ti-minerals are an essential part of coal (*i.e.* >0.1 wt%). Consequently, while we do not have control over the spread of natural NPs, the increased industrialization and use of nanomaterials is likely to lead to the increased release and distribution of the smaller (and likely more biologically available) anthropogenic NPs at concentrations that exceed those of natural NPs. This will increasingly contribute to added ecotoxicological stress.

While the analytical measurements were state-of-the-art, it is nonetheless extremely important to point out that the data were only a snapshot of a single sampling day at a given location. It is thus highly speculative to compare multiple sites or make inferences on the sources of the NPs, without complementary data on the spatial or temporal variations at a given site. Indeed, spatiotemporal distributions of NPs are likely impacted by geo-meteorological factors (*e.g.* geochemistry, terrain, precipitation, air currents), as well as numerous transformational processes that are occurring and which are influenced by the physicochemistry of the media, including pH, ligand concentrations and redox potential. This can lead to highly variable distributions of NPs, even on limited spatial scales. Indeed, the concentration of Ag NPs collected from Kiese Lake (pond) in Göttingen (DEU), which was formerly a quarry pit, contained almost two orders of magnitude more Ag NPs, as compared to a sample from the Leine River (**Fig. 4-1**), even though sampling spots were within 2 km of each other. This observation suggests that in the absence of analytical data, it will be very difficult for large scale models to account for important short-range or on-site contributions of the NPs.

This work lays the foundation for more thorough experimental measurements of NPs, which can be used as both input data and to validate models being developed to assess the risk

of NP. Future technical improvements to the sensitivity of analysis techniques, particularly for the multi-element analysis of single nanoparticles – aided by isotopic fingerprinting using machine learning^{51, 52} – will pave the way for the full quantitative profiling of the NPs by origin. This will in turn enable a more quantitative evaluation of the impact of burgeoning nanotechnology industries on local, regional, and global scales.

Acknowledgements

This work was supported by the Natural Sciences and Engineering Research Council of Canada (NSERC), the NSERC PURE CREATE network, the *Fonds de Recherche du Quebec - Nature and Technologies*, a McGill Engineering Doctoral award (MEDA) and an EcotoQ Excellence Scholarship to AA. We thank Prof. Hayes (University of Montreal) for his contributions to data interpretation and C. Liu-Kang for her assistance with sample preparation. We are extremely grateful to our global sampling collaborators; namely, A. Alishbayli, N. Azimli, J. Bachelder, M. Bernhard, S. Chaba, N. Farner, R. Farner, J. Galhardi, Y. Gu, P. Hayes, D. Israfilov, C. Liu-Kang, K.S. Luko, E. Mahammadov, G. Nafeh, L.M.S. Oliveira, Z. Ruiqing, E.T. Sulato, A. Turner, R. Yusifov and Y. Zhu.

Author Contributions

AA, JF and KW conceived of the idea and designed the study, while KW supervised the work. AA coordinated the sampling campaign. AA, IJ and KW performed some of the sampling. AA, IJ and MH performed the SP-ICP-MS measurements and the relevant data treatment. AA and PS performed the SP-ICP-TOF-MS measurements and the relevant data treatment. AA organized the data and created the figures. All authors contributed to the interpretation of the data. AA and KW wrote the manuscript, with complementary input from the other authors. All authors contributed to the article and approved it.

Competing interests

PS is an employee of Nu Instruments (United Kingdom). The other authors declare no competing interests.

4.4 References

1. Keller, A. A.; McFerran, S.; Lazareva, A.; Suh, S., Global life cycle releases of engineered nanomaterials. *Journal of Nanoparticle Research* **2013**, *15* (6), 1692.

2. Vance, M. E.; Kuiken, T.; Vejerano, E. P.; McGinnis, S. P.; Hochella Jr, M. F.; Rejeski, D.; Hull, M. S., Nanotechnology in the real world: Redeveloping the nanomaterial consumer products inventory. *Beilstein Journal of Nanotechnology* **2015**, *6* (1), 1769-1780.
3. Hochella, M. F.; Lower, S. K.; Maurice, P. A.; Penn, R. L.; Sahai, N.; Sparks, D. L.; Twining, B. S., Nanominerals, mineral nanoparticles, and earth systems. *Science* **2008**, *319* (5870), 1631-1635.
4. Maddenc, A. S., Naturally Occurring Inorganic Nanoparticles: General Assessment and a Global Budget for One of Earth's Last Unexplored Major Geochemical Components. In *Nature's Nanostructures*, 2012; pp 1-42.
5. Hochella, M. F.; Mogk, D. W.; Ranville, J.; Allen, I. C.; Luther, G. W.; Marr, L. C.; McGrail, B. P.; Murayama, M.; Qafoku, N. P.; Rosso, K. M., Natural, incidental, and engineered nanomaterials and their impacts on the Earth system. *Science* **2019**, *363* (6434), eaau8299.
6. Nowack, B.; Ranville, J. F.; Diamond, S.; Gallego-Urrea, J. A.; Metcalfe, C.; Rose, J.; Horne, N.; Koelmans, A. A.; Klaine, S. J., Potential scenarios for nanomaterial release and subsequent alteration in the environment. *Environmental Toxicology and Chemistry* **2012**, *31* (1), 50-59.
7. Auffan, M.; Rose, J.; Bottero, J.-Y.; Lowry, G. V.; Jolivet, J.-P.; Wiesner, M. R., Towards a definition of inorganic nanoparticles from an environmental, health and safety perspective. *Nature Nanotechnology* **2009**, *4* (10), 634.
8. Kuenen, J.; Pomar-Portillo, V.; Vilchez, A.; Visschedijk, A.; van der Gon, H. D.; Vázquez-Campos, S.; Nowack, B.; Adam, V., Inventory of country-specific emissions of engineered nanomaterials throughout the life cycle. *Environmental Science: Nano* **2020**, *7*, 3824-3839.
9. Sun, T. Y.; Mitrano, D. M.; Bornhöft, N. A.; Scheringer, M.; Hungerbühler, K.; Nowack, B., Envisioning nano release dynamics in a changing world: using dynamic probabilistic modeling to assess future environmental emissions of engineered nanomaterials. *Environmental Science & Technology* **2017**, *51* (5), 2854-2863.
10. Song, R.; Qin, Y.; Suh, S.; Keller, A. A., Dynamic model for the stocks and release flows of engineered nanomaterials. *Environmental Science & Technology* **2017**, *51* (21), 12424-12433.
11. Prospero, J. M., Long-range transport of mineral dust in the global atmosphere: Impact of African dust on the environment of the southeastern United States. *Proceedings of the National Academy of Sciences* **1999**, *96* (7), 3396-3403.
12. Praetorius, A.; Tufenkji, N.; Goss, K.-U.; Scheringer, M.; von der Kammer, F.; Elimelech, M., The road to nowhere: equilibrium partition coefficients for nanoparticles. *Environmental Science: Nano* **2014**, *1* (4), 317-323.
13. Zheng, Y.; Nowack, B., Size-Specific, Dynamic, Probabilistic Material Flow Analysis of Titanium Dioxide Releases into the Environment. *Environmental Science & Technology* **2021**, *55* (4), 2392-2402.
14. Nowack, B.; Baalousha, M.; Bornhöft, N.; Chaudhry, Q.; Cornelis, G.; Cotterill, J.; Gondikas, A.; Hassellöv, M.; Lead, J.; Mitrano, D. M., Progress towards the validation of modeled environmental concentrations of engineered nanomaterials by analytical measurements. *Environmental Science: Nano* **2015**, *2* (5), 421-428.
15. Gondikas, A. P.; Kammer, F. v. d.; Reed, R. B.; Wagner, S.; Ranville, J. F.; Hofmann, T., Release of TiO₂ nanoparticles from sunscreens into surface waters: a one-year survey at the old Danube recreational Lake. *Environmental Science & Technology* **2014**, *48* (10), 5415-5422.
16. Loosli, F.; Wang, J.; Rothenberg, S.; Bizimis, M.; Winkler, C.; Borovinskaya, O.; Flamigni, L.; Baalousha, M., Sewage spills are a major source of titanium dioxide engineered

- (nano)-particle release into the environment. *Environmental Science: Nano* **2019**, *6* (3), 763-777.
17. Peters, R. J.; van Bommel, G.; Milani, N. B.; den Hertog, G. C.; Undas, A. K.; van der Lee, M.; Bouwmeester, H., Detection of nanoparticles in Dutch surface waters. *Science of the Total Environment* **2018**, *621*, 210-218.
 18. Jreije, I.; Azimzada, A.; Hadioui, M.; Wilkinson, K. J., Measurement of CeO₂ Nanoparticles in Natural Waters Using a High Sensitivity, Single Particle ICP-MS. *Molecules* **2020**, *25* (23), 5516.
 19. Wang, J.-L.; Alasonati, E.; Tharaud, M.; Gelabert, A.; Fisicaro, P.; Benedetti, M. F., Flow and fate of silver nanoparticles in small French catchments under different land-uses: The first one-year study. *Water Research* **2020**, *176*, 115722.
 20. Svendsen, C.; Walker, L. A.; Matzke, M.; Lahive, E.; Harrison, S.; Crossley, A.; Park, B.; Lofts, S.; Lynch, I.; Vázquez-Campos, S., Key principles and operational practices for improved nanotechnology environmental exposure assessment. *Nature Nanotechnology* **2020**, *15* (9), 731-742.
 21. Corsi, I.; Bergami, E.; Grassi, G., Behavior and bio-interactions of anthropogenic particles in marine environment for a more realistic ecological risk assessment. *Frontiers in Environmental Science* **2020**, *8*, 60.
 22. Cornelis, G.; Hund-Rinke, K.; Kuhlbusch, T.; Van den Brink, N.; Nickel, C., Fate and bioavailability of engineered nanoparticles in soils: a review. *Critical Reviews in Environmental Science and Technology* **2014**, *44* (24), 2720-2764.
 23. Mozhayeva, D.; Engelhard, C., A critical review of single particle inductively coupled plasma mass spectrometry—A step towards an ideal method for nanomaterial characterization. *Journal of Analytical Atomic Spectrometry* **2020**, *35*, 1740-1783.
 24. Hadioui, M.; Knapp, G. v.; Azimzada, A.; Jreije, I.; Frechette-Viens, L.; Wilkinson, K. J. J. A. c., Lowering the size detection limits of Ag and TiO₂ nanoparticles by Single Particle ICP-MS. **2019**, *91* (20), 13275-13284.
 25. Azimzada, A.; Farner, J. M.; Hadioui, M.; Liu-Kang, C.; Jreije, I.; Tufenkji, N.; Wilkinson, K. J., Release of TiO₂ nanoparticles from painted surfaces in cold climates: characterization using a high sensitivity single-particle ICP-MS. *Environmental Science: Nano* **2020**, *7* (1), 139-148.
 26. Wigginton, N. S.; Haus, K. L.; Hochella Jr, M. F., Aquatic environmental nanoparticles. *Journal of Environmental Monitoring* **2007**, *9* (12), 1306-1316.
 27. del Real, A. E. P.; Castillo-Michel, H.; Kaegi, R.; Larue, C.; de Nolf, W.; Reyes-Herrera, J.; Tucoulou, R.; Findling, N.; Salas-Colera, E.; Sarret, G., Searching for relevant criteria to distinguish natural vs. anthropogenic TiO₂ nanoparticles in soils. *Environmental Science: Nano* **2018**, *5* (12), 2853-2863.
 28. Von der Kammer, F.; Ferguson, P. L.; Holden, P. A.; Masion, A.; Rogers, K. R.; Klaine, S. J.; Koelmans, A. A.; Horne, N.; Unrine, J. M., Analysis of engineered nanomaterials in complex matrices (environment and biota): general considerations and conceptual case studies. *Environmental Toxicology and Chemistry* **2012**, *31* (1), 32-49.
 29. Azimzada, A.; Farner, J. M.; Jreije, I.; Hadioui, M.; Liu-Kang, C.; Tufenkji, N.; Shaw, P.; Wilkinson, K. J., Single-and multi-element quantification and characterization of TiO₂ nanoparticles released from outdoor stains and paints. *Frontiers in Environmental Science* **2020**, *8*, 91.
 30. Janković, N. Z.; Plata, D. L., Engineered nanomaterials in the context of global element cycles. *Environmental Science: Nano* **2019**, *6* (9), 2697-2711.
 31. Pace, H. E.; Rogers, N. J.; Jarolimek, C.; Coleman, V. A.; Higgins, C. P.; Ranville, J. F., Determining transport efficiency for the purpose of counting and sizing nanoparticles via

- single particle inductively coupled plasma mass spectrometry. *Analytical Chemistry* **2011**, *83* (24), 9361-9369.
32. Laborda, F.; Gimenez-Ingalaturre, A. C.; Bolea, E.; Castillo, J. R., Single particle inductively coupled plasma mass spectrometry as screening tool for detection of particles. *Spectrochimica Acta Part B: Atomic Spectroscopy* **2019**, *159*, 105654.
33. Shaw, P.; Donard, A., Nano-particle analysis using dwell times between 10 μ s and 70 μ s with an upper counting limit of greater than 3×10^7 cps and a gold nanoparticle detection limit of less than 10 nm diameter. *Journal of Analytical Atomic Spectrometry* **2016**, *31* (6), 1234-1242.
34. Groot Zwaafink, C. D.; Arnalds, Ó.; Dagsson-Waldhauserova, P.; Eckhardt, S.; Prospero, J. M.; Stohl, A., Temporal and spatial variability of Icelandic dust emissions and atmospheric transport. *Atmospheric Chemistry and Physics* **2017**, *17* (17), 10865-10878.
35. Urupina, D.; Lasne, J.; Romanias, M.; Thiery, V.; Dagsson-Waldhauserova, P.; Thevenet, F., Uptake and surface chemistry of SO₂ on natural volcanic dusts. *Atmospheric Environment* **2019**, *217*, 116942.
36. Gondikas, A.; Gallego-Urrea, J.; Halbach, M.; Derrien, N.; Hassellöv, M., Nanomaterial fate in seawater: A rapid sink or intermittent stabilization? *Frontiers in Environmental Science* **2020**, *8*, 151.
37. Labille, J.; Slomberg, D.; Catalano, R.; Robert, S.; Apers-Tremelo, M.-L.; Boudenne, J.-L.; Manasfi, T.; Radakovitch, O., Assessing UV filter inputs into beach waters during recreational activity: A field study of three French Mediterranean beaches from consumer survey to water analysis. *Science of the Total Environment* **2020**, *706*, 136010.
38. Hao, Z.; Li, F.; Liu, R.; Zhou, X.; Mu, Y.; Sharma, V. K.; Liu, J.; Jiang, G., Reduction of Ionic Silver by Sulfur Dioxide as a Source of Silver Nanoparticles in the Environment. *Environmental Science & Technology* **2021**, *55* (8), 5569-5578.
39. Wiklund, J. A.; Kirk, J. L.; Muir, D. C.; Gleason, A.; Carrier, J.; Yang, F., Atmospheric trace metal deposition to remote Northwest Ontario, Canada: Anthropogenic fluxes and inventories from 1860 to 2010. *Science of The Total Environment* **2020**, *749*, 142276.
40. Levard, C.; Hotze, E. M.; Lowry, G. V.; Brown Jr, G. E., Environmental transformations of silver nanoparticles: impact on stability and toxicity. *Environmental Science & Technology* **2012**, *46* (13), 6900-6914.
41. Wang, J.; Nabi, M. M.; Mohanty, S. K.; Afrooz, A. N.; Cantando, E.; Aich, N.; Baalousha, M., Detection and quantification of engineered particles in urban runoff. *Chemosphere* **2020**, *248*, 126070.
42. Slomberg, D. L.; Auffan, M.; Guéniche, N.; Angeletti, B.; Campos, A.; Borschneck, D.; Aguerre-Chariol, O.; Rose, J., Anthropogenic release and distribution of titanium dioxide particles in a river downstream of a nanomaterial manufacturer industrial site. *Frontiers in Environmental Science* **2020**, *8* (76).
43. Gondikas, A.; von der Kammer, F.; Kaegi, R.; Borovinskaya, O.; Neubauer, E.; Navratilova, J.; Praetorius, A.; Cornelis, G.; Hofmann, T., Where is the nano? Analytical approaches for the detection and quantification of TiO₂ engineered nanoparticles in surface waters. *Environmental Science: Nano* **2018**, *5* (2), 313-326.
44. Rahim, M. F.; Pal, D.; Ariya, P. A., Physicochemical studies of aerosols at Montreal Trudeau Airport: The importance of airborne nanoparticles containing metal contaminants. *Environmental Pollution* **2019**, *246*, 734-744.
45. Frisia, S.; Weyrich, L. S.; Hellstrom, J.; Borsato, A.; Golledge, N. R.; Anesio, A. M.; Bajo, P.; Drysdale, R. N.; Augustinus, P. C.; Rivard, C., The influence of Antarctic subglacial volcanism on the global iron cycle during the Last Glacial Maximum. *Nature Communications* **2017**, *8* (1), 1-9.

46. Heinlaan, M.; Ivask, A.; Blinova, I.; Dubourguier, H.-C.; Kahru, A., Toxicity of nanosized and bulk ZnO, CuO and TiO₂ to bacteria *Vibrio fischeri* and crustaceans *Daphnia magna* and *Thamnocephalus platyurus*. *Chemosphere* **2008**, *71* (7), 1308-1316.
47. Aruoja, V.; Pokhrel, S.; Sihtmäe, M.; Mortimer, M.; Mädler, L.; Kahru, A., Toxicity of 12 metal-based nanoparticles to algae, bacteria and protozoa. *Environmental Science: Nano* **2015**, *2* (6), 630-644.
48. Wigger, H.; Kägi, R.; Wiesner, M.; Nowack, B., Exposure and Possible Risks of Engineered Nanomaterials in the Environment—Current Knowledge and Directions for the Future. *Reviews of Geophysics* **2020**, *58* (4), e2020RG000710.
49. Westerhoff, P.; Atkinson, A.; Fortner, J.; Wong, M. S.; Zimmerman, J.; Gardea-Torresdey, J.; Ranville, J.; Herckes, P., Low risk posed by engineered and incidental nanoparticles in drinking water. *Nature Nanotechnology* **2018**, *13* (8), 661.
50. Yang, Y.; Chen, B.; Hower, J.; Schindler, M.; Winkler, C.; Brandt, J.; Di Giulio, R.; Ge, J.; Liu, M.; Fu, Y., Discovery and ramifications of incidental Magnéli phase generation and release from industrial coal-burning. *Nature Communications* **2017**, *8* (1), 1-11.
51. Praetorius, A.; Gundlach-Graham, A.; Goldberg, E.; Fabienke, W.; Navratilova, J.; Gondikas, A.; Kaegi, R.; Günther, D.; Hofmann, T.; von der Kammer, F., Single-particle multi-element fingerprinting (spMEF) using inductively-coupled plasma time-of-flight mass spectrometry (ICP-TOFMS) to identify engineered nanoparticles against the elevated natural background in soils. *Environmental Science: Nano* **2017**, *4* (2), 307-314.
52. Yang, X.; Liu, X.; Zhang, A.; Lu, D.; Li, G.; Zhang, Q.; Liu, Q.; Jiang, G., Distinguishing the sources of silica nanoparticles by dual isotopic fingerprinting and machine learning. *Nature Communications* **2019**, *10* (1), 1620.

4.5 Supplementary Information

Additional information on NP data processing

Data processing was performed using NuQuant version 2.2 (or NuQuant Vitesse prototype for simultaneous multi-element analysis). This method is extensively discussed in Hadioui *et al.*¹, but can briefly be summarized as:

- Data smoothing
- Creating a peak search window that rolls over the span of the whole acquisition period
- Searching for a maximum (within a window) and establishing pre-max and post-max inflection points, where PEAK data points = in between pre-max and post-max inflection points
- Establishing local background (mean and SD) based on the remaining points in the window
- Calculating Net PEAK area (*i.e.* subtraction of equivalent background from PEAK raw data)
- Setting NP qualification criteria: $I_{\text{thld}} = [\text{local background average}] + n \times [\text{local background standard deviation}]$, where n was often set to 3 (in this case)
- PEAKs that meet the above criterion are now qualified as a “NP peak”
- Data can be viewed with respect to isotope type, intensity (counts) or full-width half-maximum (FWHM) values, which allows for flexible screening of possible artifacts

Supplementary Figures

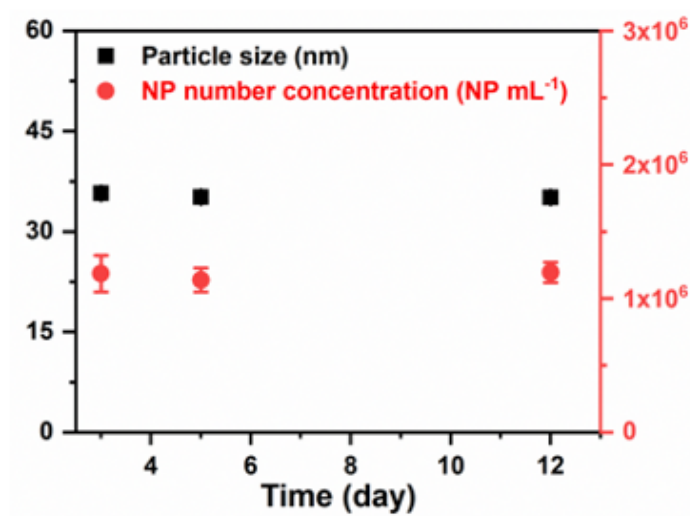


Figure 4-S1. Particle stability. Time-resolved particle number concentrations and sizes as measured for TiO₂ NPs in a melted snow sample collected in Montreal, Quebec. Measurements were performed using a sector-field ICP-MS in a single particle mode, 3, 5 and 12 days following the filtration of the sample.

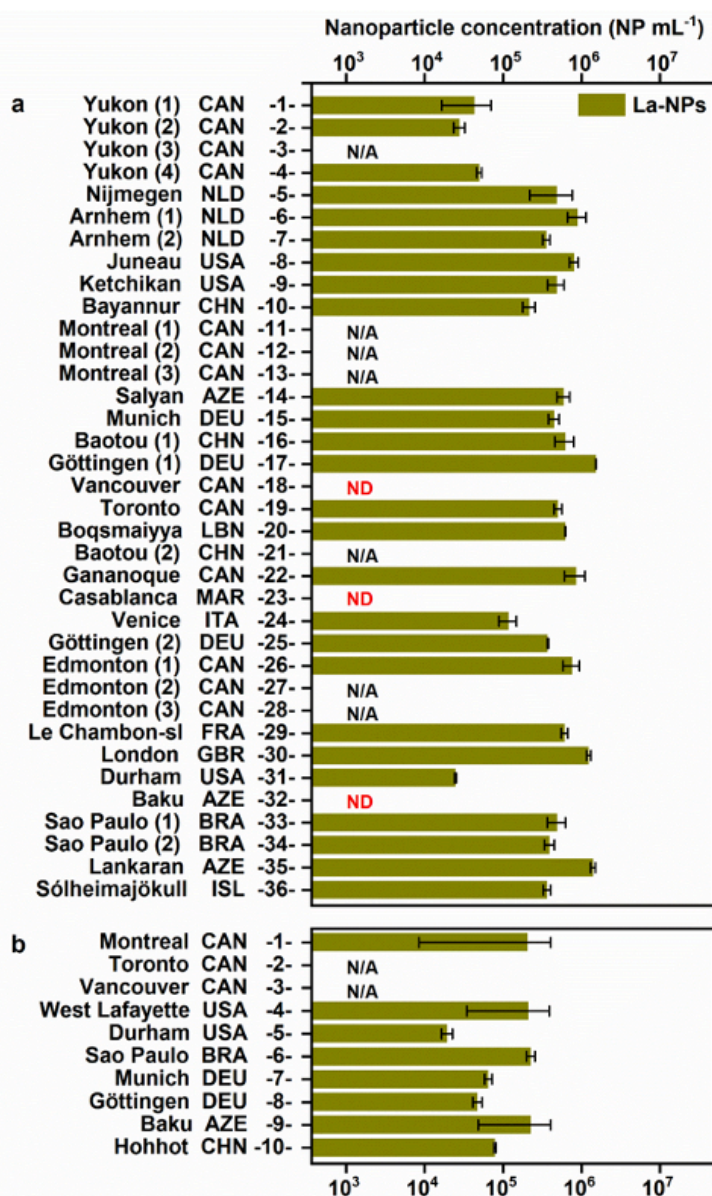


Figure 4-S2. Concentrations of La nanoparticles in global precipitation and surface waters. a,b, Particle number concentrations for La-containing NPs as measured in surface waters (**a**) and precipitation (**b**) collected at 46 sampling sites across 13 countries. Sampling sites are indicated by city/province names and ISO country codes. Measurements were performed using a sector-field ICP-MS. ND stands for “not detected” and refers to concentrations below the detection limits of the technique. N/A refers to samples that were not analyzed. Error bars indicate standard deviations of triplicate samples.

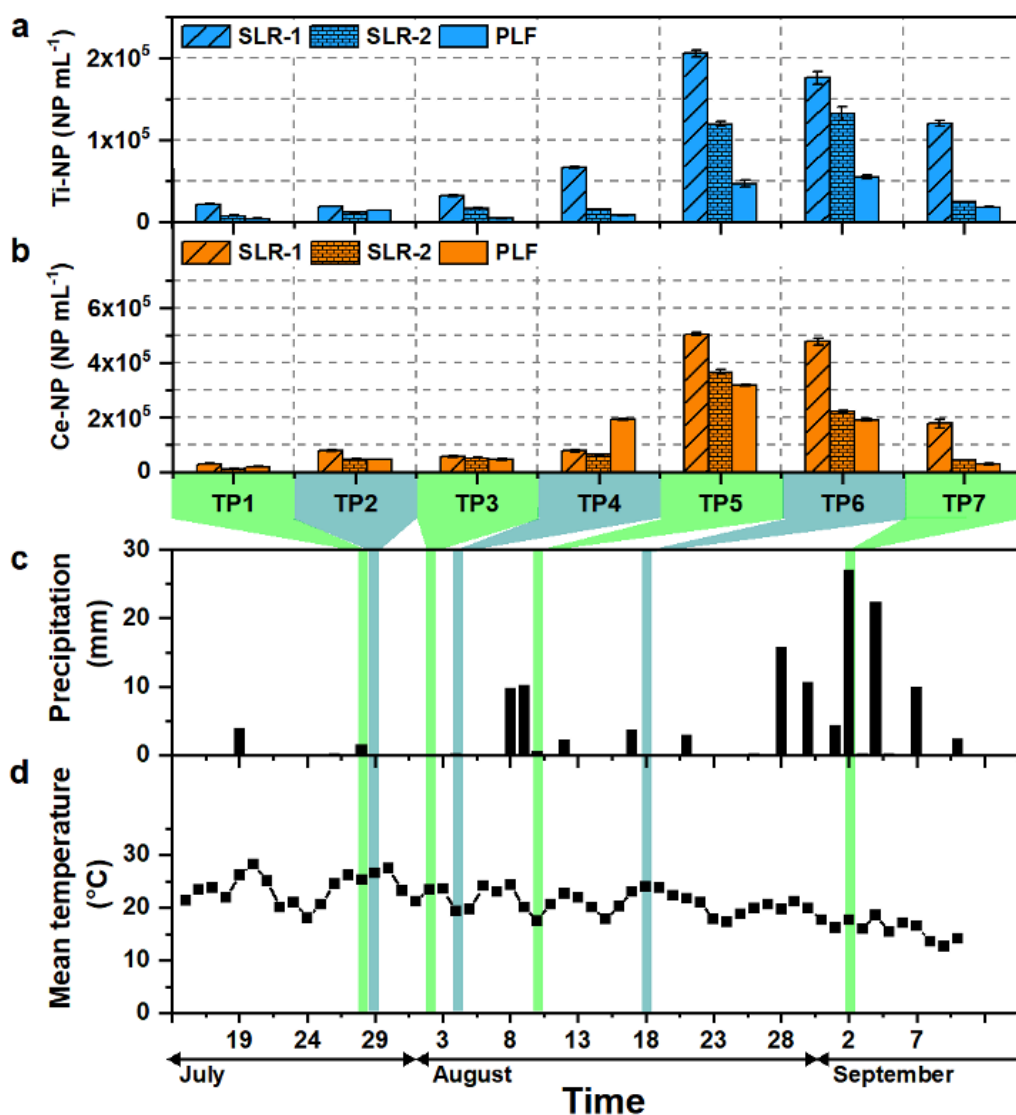


Figure 4-S3. Time-resolved measurements of nanoparticles in surface waters. **a,b**, Particle number concentrations measured for Ti- (**a**) and Ce-containing (**b**) NPs in surface water samples collected from two sampling points at Saint Lawrence River (SLR) and a recreational pond in Parc La Fontaine (PLF) in Montreal (Quebec, Canada). Each timepoint (TP) refer to the date when the samplings were performed. **c,d**, Natural precipitation (**c**) and temperature (**d**) data are collected from the Montreal International Airport weather station (45°28'14.000" N, 73°44'27.000" W) and retrieved from the Environment and Climate Change Canada database. Measurements were performed using a sector-field ICP-MS. Error bars indicate standard deviations, where n=3.

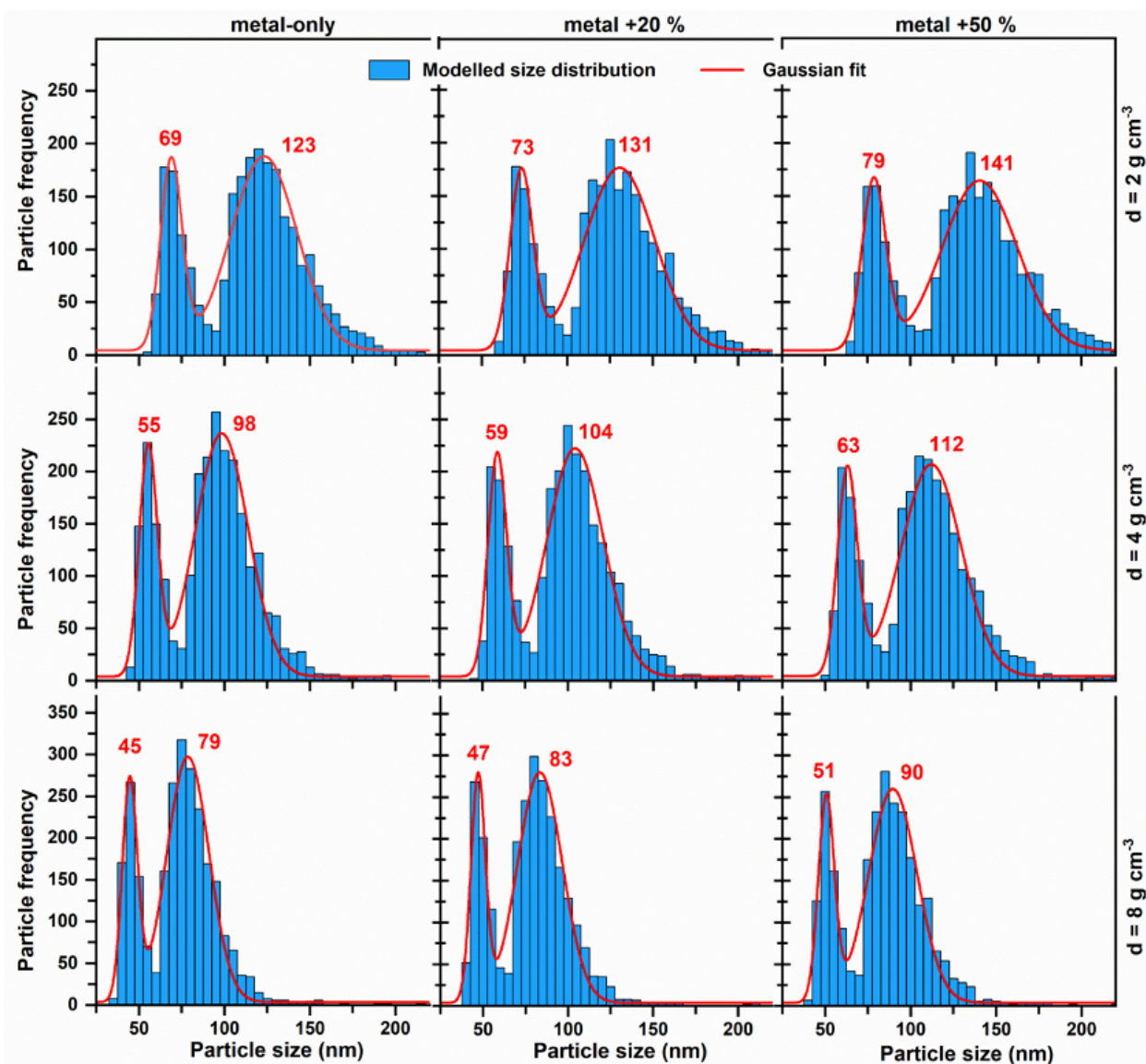


Figure 4-S4. Modelled size distributions taking into account multi-element nature of particles. Modelled size distributions of NPs detected in snow from the Sólheimajökull glacier (ISL), assuming a range of particle densities ($2\text{-}8 \text{ g cm}^{-3}$). Given that the experimental determinations were limited to metals and metalloids only (*i.e.* excluded oxygen, halogens, etc.), particle sizes were predicted based upon the total masses of (almost) all metals/metalloids (*i.e.* 23-238 amu) detected in single particles (*i.e.* metal only). Total masses were assigned additional mass uncertainties of 20% (column 2) or 50% (column 3), due to the presence of the undetected elements. Data is fitted with Gaussian fit (red line), and the sizes corresponding to the peak maxima of the bimodal distributions are indicated. Measurements were performed with a single-particle time-of-flight ICP-MS.

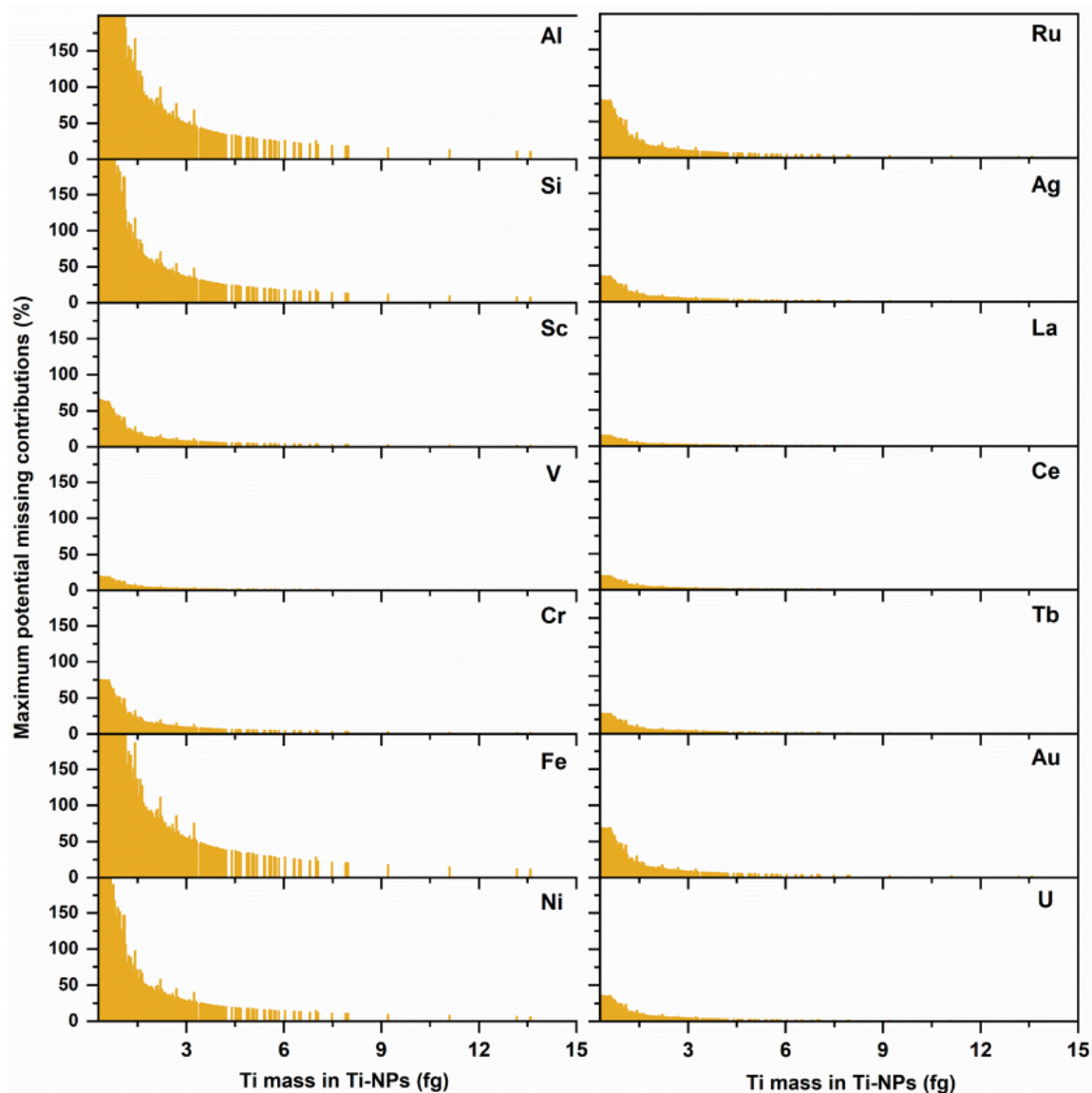


Figure 4-S5. Detection limits of the multi-element analysis. Upper limits of the potential missing contributions of 14 metals in Ti-containing NPs, for cases in which Ti was detected as the only metallic component. % values are calculated based on the mass detection limit of each metal in relationship to the Ti content detected in individual Ti-containing NPs. Measurements were performed with single-particle time-of-flight ICP-MS, using 1953 NPs detected in a Montreal rainwater. In general, the probability of labelling a NP as pure TiO_2 when it is not, increases for the very small particles and when detecting small quantities of the secondary elements with the poorest detection limits (Al, Si, Fe, Ni).

Table 4-S1. Sampling information for global surface water samples

	Region/territory	Country		Water body	Sampling date	Geo coordinates	
					Year 2019	Longitude	Latitude
1	Yukon (1)	CAN	Canada	Christmas Bay (Kluane Lake)	May 29	-138.368602	61.0626
2	Yukon (2)	CAN	Canada	KLRS (Kluane Lake)	May 31	-138.416049	61.027543
3	Yukon (3)	CAN	Canada	- (lake)	Jun 6	-138.372576	61.080076
4	Yukon (4)	CAN	Canada	- (lake)	Jun 6	-138.371875	61.069704
5	Nijmegen	NLD	Netherlands	Waal River	Jul 25	5.858128	51.853724
6	Arnhem (1)	NLD	Netherlands	Nederrijn River	Jul 26	5.907252	51.975722
7	Arnhem (2)	NLD	Netherlands	Grote Vijver Lake	Jul 26	5.896827	51.995696
8	Juneau	USA	United States	Gold Creek	May 10	-134.419994	58.298831
9	Ketchikan	USA	United States	Ketchikan Creek	May 13	-131.642421	55.341255
10	Bayannur	CHN	China	Ulansu Lake	Sep 8	108.836444	40.885944
11	Montreal (1)	CAN	Canada	Parc La Fontaine (pond)	Sep 2	-73.5679645	45.5232449
12	Montreal (2)	CAN	Canada	St Lawrence River (1)	Sep 2	-73.5485275	45.5090203
13	Montreal (3)	CAN	Canada	St Lawrence River (2)	Sep 2	-73.5467532	45.5081442
14	Salyan	AZE	Azerbaijan	Kür (Mtkvari) River	Jun 3	48.963551	39.630592
15	Munich	DEU	Germany	Isar River	Apr 30	11.581167	48.128583
16	Baotou (1)	CHN	China	Yellow River	Sep 10	109.987822	40.5128
17	Göttingen (1)	DEU	Germany	Leine River	May 1	9.919656	51.542811
18	Vancouver	CAN	Canada	Strait of Georgia (Pacific Ocean)	Mar 18	-123.261953	49.262093
19	Toronto	CAN	Canada	Lake Ontario	Mar 2	-79.380009	43.639518
20	Boqsmayya	LBN	Lebanon	El-Jaouz River	May 1	35.727279	34.271688
21	Baotou (2)	CHN	China	Yellow River (2)	Sep 10	109.804561	40.500669
22	Gananoque	CAN	Canada	St Lawrence River (3)	Feb 9	-76.158768	44.325066
23	Casablanca	MAR	Morocco	Atlantic Ocean	Mar 9	-7.640465	33.604793
24	Venice	ITA	Italy	Rio del Gozzi Canal	Aug 6	12.337964	45.44212
25	Göttingen (2)	DEU	Germany	Kiessee Lake	May 1	9.921195	51.51951
26	Edmonton (1)	CAN	Canada	Saskatchewan River (1)	May 14	-113.520076	53.5302
27	Edmonton (2)	CAN	Canada	Saskatchewan River (2)	May 14	-113.525406	53.532853
28	Edmonton (3)	CAN	Canada	Saskatchewan River (3)	May 14	-113.514956	53.531665
29	Le Chambon-si	FRA	France	Lignon du Velay River	Aug 8	4.315863	45.052825
30	London	GBR	United Kingdom	The Long Water Lake	Mar 3	-0.173268	51.506563
31	Durham	USA	United States	- (stream)	Mar 25	-78.9526	35.9611
32	Baku	AZE	Azerbaijan	Caspian Sea	Jun 14	49.800351	40.304766
33	Sao Paulo (1)	BRA	Brazil	Rio Passo River (1)	Aug 19	-47.716875	-22.419259
34	Sao Paulo (2)	BRA	Brazil	Rio Passo River (2)	Aug 19	-47.720028	-22.414361
35	Lankaran	AZE	Azerbaijan	Xanbulan Lake	June 8	48.771991	38.66092
36	Sólheimajökull	ISL	Iceland	Sólheimajökull Glacier	Feb 15	-20.634801	64.066452

Table 4-S2. Sampling information for global natural precipitation samples

	City/town	Country		Water type	Sampling date	Geo coordinates	
					Year 2019	Longitude	Latitude
1	Montreal	CAN	Canada	rain	Apr 26	-73.616052	45.502324
2	Toronto	CAN	Canada	rain	Mar 11	-123.241472	49.264229
3	Vancouver	CAN	Canada	rain	Sep 3	-79.394651	43.657773
4	West Lafayette	USA	United States	rain	Apr 12	-86.955001	40.438851
5	Durham	USA	United States	rain	Mar 3	-78.9527	35.9613
6	Sao Paulo	BRA	Brazil	rain	Aug 4	-47.552083	-22.398778
7	Munich	DEU	Germany	rain	Apr 29	11.580363	48.13405
8	Göttingen	DEU	Germany	rain	Apr 30	9.923772	51.531163
9	Baku	AZE	Azerbaijan	rain	Jun 8	49.84392	40.37331
10	Hohhot	CHN	China	rain	Aug 3	111.68502	40.75769

Table 4-S3. Nanoparticle measurements on surface water samples. Measurements were performed by a high-sensitivity sector-field single-particle ICP-MS. NP mass concentrations were calculated by assuming that all Ti-, Ce- and Ag-containing NPs occurred in the forms of TiO₂, CeO₂ and Ag, respectively. ND stands for “not detected” and refers to concentrations that were below the detection limits of the technique. N/A refers to samples that were not analyzed.

	Region/territory	NP number concentrations (NP mL ⁻¹)			NP mass concentration (ng L ⁻¹)		
		Ti-NPs	Ce-NPs	Ag-NPs	TiO ₂	CeO ₂	Ag
1	Yukon (1)	(5.4±1.0)×10 ³	(7.5±1.8)×10 ³	(3.6±1.8)×10 ³	2.1 ± 0.7	0.13 ± 0.06	0.025 ± 0.010
2	Yukon (2)	(1.2±0.2)×10 ⁴	(1.5±0.5)×10 ⁴	ND	1.9 ± 0.2	0.27 ± 0.15	ND
3	Yukon (3)	(7.9±0.4)×10 ⁴	(2.9±1.0)×10 ⁴	(3.7±0.7)×10 ³	8.8 ± 1.0	0.52 ± 0.17	0.016 ± 0.006
4	Yukon (4)	(6.0±0.2)×10 ⁴	(1.2±0.1)×10 ⁵	(3.7±0.8)×10 ³	7.8 ± 1.7	2.03 ± 0.16	0.010 ± 0.002
5	Nijmegen	(5.2±3.1)×10 ³	(6.3±4.5)×10 ⁴	ND	1.5 ± 0.7	0.57 ± 0.39	ND
6	Arnhem (1)	(1.7±1.2)×10 ⁴	(1.8±1.1)×10 ⁴	ND	5.8 ± 5.6	0.14 ± 0.10	ND
7	Arnhem (2)	(3.0±3.3)×10 ³	(2.5±0.0)×10 ⁴	ND	0.6 ± 0.7	0.25 ± 0.12	ND
8	Juneau	(3.9±1.5)×10 ⁴	(5.9±1.0)×10 ⁴	ND	8.4 ± 4.6	0.15 ± 0.02	ND
9	Ketchikan	(1.1±0.0)×10 ⁴	(2.2±0.6)×10 ⁴	ND	1.1 ± 0.0	0.07 ± 0.02	ND
10	Bayannur	(2.0±1.0)×10 ⁴	(1.9±0.3)×10 ⁵	(2.3±3.7)×10 ³	6.4 ± 4.8	1.66 ± 0.26	0.024 ± 0.038
11	Montreal (1)	(1.9±0.1)×10 ⁴	(2.8±0.3)×10 ⁴	ND	5.4 ± 0.6	0.12 ± 0.01	ND
12	Montreal (2)	(1.2±0.0)×10 ⁵	(1.8±0.1)×10 ⁵	ND	49.2 ± 0.8	1.04 ± 0.26	ND
13	Montreal (3)	(2.5±0.0)×10 ⁴	(4.2±0.0)×10 ⁴	ND	13.3 ± 1.1	0.49 ± 0.35	ND
14	Salyan	(1.5±0.7)×10 ⁵	(7.1±2.0)×10 ⁵	(2.7±0.2)×10 ³	33.8 ± 12.8	4.67 ± 1.06	0.028 ± 0.005
15	Munich	(1.5±0.2)×10 ⁵	(4.0±0.5)×10 ⁵	(1.7±0.4)×10 ³	75.1 ± 11.5	2.74 ± 0.49	0.025 ± 0.007
16	Baotou (1)	(1.6±0.4)×10 ⁵	(7.3±2.1)×10 ⁵	ND	32.7 ± 5.0	10.07 ± 3.55	ND
17	Göttingen (1)	(1.9±0.1)×10 ⁵	(8.5±0.1)×10 ⁵	(3.7±1.0)×10 ³	101.5 ± 20.6	3.44 ± 0.17	0.105 ± 0.028
18	Vancouver*	(2.3±0)×10 ⁵	(7.5±0)×10 ³	ND	15.5	0.04	ND
19	Toronto	(2.2±0.9)×10 ⁵	(9.4±2.1)×10 ⁴	(1.3±0.6)×10 ⁵	31.6 ± 9.5	0.51 ± 0.09	0.501 ± 0.253
20	Boqsmayyya	(3.6±0.2)×10 ⁵	(9.1±0.2)×10 ⁵	(6.5±1.0)×10 ⁴	98.1 ± 8.5	8.44 ± 0.46	0.150 ± 0.038
21	Baotou (2)	(4.0±2.0)×10 ⁵	N/A	ND	114.4 ± 60.3	N/A	ND
22	Gananoque	(4.6±1.8)×10 ⁵	(3.1±0.3)×10 ⁵	(1.5±1.1)×10 ⁵	92.0 ± 26.0	1.97 ± 0.28	0.367 ± 0.275
23	Casablanca*	(5.2±0)×10 ⁵	(1.5±0)×10 ⁴	ND	48.9	0.06	ND
24	Venice	(8.0±1.8)×10 ⁵	(1.1±0.3)×10 ⁴	ND	143.4 ± 113.5	0.14 ± 0.10	ND
25	Göttingen (2)	(1.0±0.0)×10 ⁶	(4.1±0.1)×10 ⁵	(2.9±0.2)×10 ⁵	190.3 ± 10.0	2.83 ± 0.08	1.290 ± 0.105
26	Edmonton (1)	(2.0±0.7)×10 ⁶	(1.1±0.3)×10 ⁶	(1.7±0.5)×10 ⁴	954.1 ± 439.5	20.39 ± 4.46	0.188 ± 0.016
27	Edmonton (2)	(1.2±0.3)×10 ⁶	N/A	(2.7±2.0)×10 ⁴	494.1 ± 86.1	N/A	0.148 ± 0.060
28	Edmonton (3)	(1.3±0.4)×10 ⁶	N/A	(2.9±1.6)×10 ⁴	527.5 ± 125.7	N/A	0.678 ± 0.401
29	Le Chambon-sl	(1.9±0.3)×10 ⁶	(2.6±0.9)×10 ⁵	(5.1±2.2)×10 ³	332.0 ± 56.9	4.75 ± 1.66	0.021 ± 0.008
30	London	(1.9±1.2)×10 ⁶	(1.9±1.0)×10 ⁵	(2.1±0.2)×10 ⁴	134.9 ± 45.9	1.3 ± 0.65	0.066 ± 0.003
31	Durham	(2.9±1.2)×10 ⁶	(1.5±0.2)×10 ⁴	(1.8±0.8)×10 ⁴	524.0 ± 255.1	0.18 ± 0.09	0.170 ± 0.150
32	Baku*	(3.8±0)×10 ⁶	ND	ND	347.1 ± 0	ND	ND
33	Sao Paulo (1)	(7.0±0.6)×10 ⁶	(4.7±1.1)×10 ⁵	N/A	2324.2 ± 131.6	7.86 ± 1.98	N/A
34	Sao Paulo (2)	(6.8±1.2)×10 ⁶	(4.3±0.8)×10 ⁵	N/A	2262.2 ± 422.5	7.53 ± 1.60	N/A
35	Lankaran	(1.2±0.2)×10 ⁷	(1.5±0.1)×10 ⁶	(9.3±1.4)×10 ³	2961.0 ± 318.0	78.10 ± 4.0	0.092 ± 0.039
36	Sólheimajökull	(1.5±0.0)×10 ⁷	(2.3±0.0)×10 ⁶	ND	3140.7 ± 68.0	19.45 ± 1.50	ND

Table 4-S4. Nanoparticle measurements on natural precipitation samples. Measurements were performed by a high-sensitivity sector-field single-particle ICP-MS. NP mass concentrations were calculated by assuming that all Ti-, Ce- and Ag-containing NPs occurred in the forms of TiO₂, CeO₂ and Ag, respectively. N/A refers to samples that were not analyzed.

	City/town	NP number concentrations (NP mL ⁻¹)			NP mass concentration (ng L ⁻¹)		
		Ti-NPs	Ce-NPs	Ag-NPs	TiO ₂	CeO ₂	Ag
1	Montreal	(2.3±1.6)×10 ⁶	(3.5±2.3)×10 ⁵	(2.6±0.2)×10 ⁴	89.7 ± 3.3	2.3 ± 1.5	0.040 ± 0.010
2	Toronto	(7.0±0.1)×10 ⁴	N/A	(2.4±0.1)×10 ³	1.7 ± 0.1	N/A	0.026 ± 0.010
3	Vancouver	(1.2±0.0)×10 ⁴	ND	(9.9±1.3)×10 ²	26.1 ± 2.8	ND	0.026 ± 0.010
4	West Lafayette	(1.9±1.3)×10 ⁵	(9.3±7.5)×10 ⁴	(2.6±2.3)×10 ³	42.8 ± 29.4	0.5 ± 0.4	0.014 ± 0.008
5	Durham	(9.4±0.2)×10 ⁴	(2.4±0.0)×10 ⁴	(1.0±0.1)×10 ³	24.0 ± 0.3	0.1 ± 0.0	0.006 ± 0.001
6	Sao Paulo	(2.0±0.0)×10 ⁶	(2.8±1.2)×10 ⁵	(1.0±0.1)×10 ³	846.8 ± 8.4	3.8 ± 1.6	0.005 ± 0.001
7	Munich	(9.8±0.3)×10 ⁴	(1.0±0.1)×10 ⁵	(8.0±4.4)×10 ³	31.0 ± 3.0	1.0 ± 0.2	0.044 ± 0.005
8	Göttingen	(9.5±0.2)×10 ⁴	(8.1±1.0)×10 ⁴	(3.1±0.1)×10 ⁴	40.6 ± 2.2	0.4 ± 0.1	0.094 ± 0.010
9	Baku	(2.7±0.4)×10 ⁵	(3.1±2.2)×10 ⁵	(5.0±2.2)×10 ³	86.8 ± 24.9	2.5 ± 1.2	0.035 ± 0.018
10	Hohhot	(2.7±0.0)×10 ⁵	(1.1±0.0)×10 ⁵	(1.0±0.1)×10 ⁵	119.0 ± 4.2	2.3 ± 0.4	0.281 ± 0.017

References

1. Hadioui, M.; Knapp, G. v.; Azimzada, A.; Jreije, I.; Frechette-Viens, L.; Wilkinson, K. J., Lowering the size detection limits of Ag and TiO₂ nanoparticles by Single Particle ICP-MS. *Analytical Chemistry* **2019**, *91* (20), 13275-13284.

Chapter 5 Conclusions and Future Outlook

5.1 Conclusions and environmental implications

Growing industrialization and proliferation of nanotechnologies are increasing NP emissions into the environment, raising concerns for the ecosystem and human health. Reliable risk assessments of the NPs require experimental data on their exposure concentrations (*i.e.* mass and number), as well as their size distributions and particle compositions. To date, such data are nearly absent, owing in large part, to the analytical challenges of detecting and characterizing NPs in complex natural media. Using state-of-the-art ICP-MS systems, this work first developed methodologies to enable the analysis of the smallest NPs, *i.e.* as small as 4 nm for CeO₂ and Ag NPs, and <15 nm for TiO₂ NPs. These smaller NP fractions are thought to be of greater environmental risk (*i.e.* smaller NPs exhibit higher biological reactivities). Furthermore, multi-element single-particle measurements provided unique insight into particle compositions on a particle-by-particle basis – information that can be indicative of particle origins/sources. The experiments were designed to provide us with multiplexed data in two important environmental contexts: (i) release of TiO₂ NPs from a widely-used nano-enabled product, *i.e.* surface coatings, and (ii) occurrences and distributions of Ti-, Ce- and Ag-NPs of anthropogenic or natural origin in global natural waters.

Paints and coatings represent an important application of engineered NPs, and hence, an important potential source of their emission into the environment. This work extensively examined TiO₂ NP release patterns from surface coatings under natural weathering scenarios, by performing measurements of particle mass/number concentrations and sizes (distributions) as well as single particle compositions. The data clearly showed the strong impact of weathering on NP release trends, with release quantities varying significantly as a function of seasonal weather, exposure (contact) times, and the initial coating matrix. Notably, release was enhanced under wet and freeze-thaw conditions, with frequent rainfall events and slushy snow conditions favouring NP leaching. While the exact mechanism of release was not elucidated, it is likely that temperature cycles, phase changes, and water-surface interactions induced the formation of micro-cracks and degradation of the polymer matrix of the coating, thereby facilitating NP leaching. If such observations can be extrapolated across different regions, it is anticipated that outdoor façade coatings in cold and wet climates may indeed emit more NPs as compared to those in moderate dry climates. Nonetheless, colder weather does not necessarily correlate with higher emissions, as only limited NP release was observed for continuously freezing temperatures (*i.e.* less dynamic interaction). Release data were not

collected under very warm conditions (*i.e.* >30 °C); however, in such a scenario, UV weathering is expected to strongly affect the NP release behaviour.

The results indicated that while the painted surfaces emitted <0.001 % of their total TiO₂ NP load over several weeks of weathering, the corresponding release from the stained surfaces was – a few orders of magnitude higher – up to 6%. The absolute release quantities from paints and stains were still similar, given that the stain contained a much lower initial TiO₂ NP content. Moreover, release was shown to be exacerbated when the surfaces were immersed under water or covered with snow (*e.g.* stained deck), as opposed to surface runoff only (*e.g.* painted façade). The data altogether indicated the important role of coating type (chemistry) and the exposure scenario in NP leaching. Given the wide range of coating formulations, exposure scenarios and weathering conditions, NP release rates under different conditions may indeed vary by orders of magnitude. Although the release quantities, even under the harshest scenarios, did not surpass 200 µg-Ti m⁻²-coating, it is important to note that the weathering experiments were performed for a limited period only. Hence, not only the absolute release quantities, but also the rates of release (*i.e.* µg m⁻² month⁻¹) may increase with the ageing and degradation of the coatings over time.

Coating released particles were predominantly small (<60 nm) and pure (*i.e.* TiO₂), and thus were likely to exhibit higher biological reactivity, which translates to greater environmental risk. Nonetheless, a fraction of the released NPs was observed to agglomerate and sediment, effectively moving out of the nano-size range. These processes, while expected, are hard to predict for dynamic natural media, given that they are controlled by temporally and spatially varying environmental factors (*e.g.* organic matter, ionic strength). It is thus clear that while release is a primary determinant in environmental risk, subsequent NP behaviour, leading to NP losses or re-suspension, can be equally critical. This case also demonstrates the need for particle-by-particle probing of the NPs with respect to their origins, which can help identify the proportion of NPs that are of anthropogenic origin, at a given time. An important part of this work thus consisted of experiments that were targeted to determining NP mass/number concentrations, sizes, and compositions, which along with information on the local characteristics of the sampling sites, could provide a insight into particle origins.

State-of-the-art analytical methodologies were applied for the analysis of a wide range of surface water and precipitation samples, *i.e.* 46 sites from 13 countries. The results indicated that NP concentrations were dependent on the nature of the NPs, sampling site characteristics,

sampling time, and meteorological conditions. Notably, while Ti- and Ce-NPs (often within 10^4 - 10^7 NP mL⁻¹) were likely influenced by both anthropogenic and natural NP input, the local and infrequent occurrences of Ag-NPs, with generally low concentrations (up to 10^5 NP mL⁻¹), was consistent with them being primarily human-derived. The detection of NPs at significant quantities in the precipitation samples was particularly interesting, demonstrating the ubiquity of NPs in the air. The observation of high-purity NPs (*i.e.* single-metal oxides) at higher frequencies in urban areas was indicative of the susceptibility of these environments to be exposed to high levels of anthropogenic pollution. In this respect, it is important to note that NP concentrations and sizes were shown to be affected by the type of water. For example, Ti- and Ce-NPs found in natural surface waters, such as lakes and rivers, tended to be larger than those found in artificial water bodies (*e.g.* canals, ponds) or saline waters. This demonstrates that the fate and bioaccessibility of NPs are significantly influenced by their transformation and persistence in the environment – an aspect that is poorly considered (if at all) by environmental fate models.

Despite providing a snapshot view only, the presented data demonstrates that small NPs of high purity and/or of presumably anthropogenic nature (*e.g.* Ag NPs) may be found even in the remotest landscapes, such as Northwest Canada (Yukon) and Iceland glaciers – albeit still at low concentrations. Given growing industrialization and uses of nanotechnologies, both urban environments and pristine landscapes are expected to receive increasingly higher loading of NPs over the next decades. In addition to temporal variations, NP concentrations may vary by orders of magnitude, even on limited spatial scales (*e.g.* 1-2 km), as revealed in this work. These variabilities can be caused by a number of factors, notably including the proximity to and the distribution of NP emission sources, and NP thermodynamic stabilities. All these points highlight that models – without the input of spatially and temporally resolved analytical data – are likely to fail to reliably predict exposure to NPs.

Using state-of-the-art methods, this work generated multiplexed analytical data that was used to understand the potential emission of NPs from an important nano-enabled product, *i.e.* surface coatings, providing detailed insight into their physicochemical states and transformations. The work also explored the occurrences and distributions of three major NPs in global natural waters, providing experimental data on their concentrations, sizes and compositions, as well as examining the questions regarding their emission sources, transport potential, and transformations. The generated data can be used on two fronts: (i) correct parametrization of models with respect to the release characteristics of NPs from surface

coatings; (ii) validation of models for NP risk assessment. This body of research lays a foundation for broader analysis of NP release patterns from different nano-enabled products and of NP distributions in various environmental compartments.

5.2 Future research directions and recommendations

The following research priorities are proposed in order to reliably assess anthropogenic NP emissions on local, global, and regional scales:

- Further improvements to the sensitivity of (simultaneous) multi-element analysis techniques (*e.g.* SP-ICP-TOF-MS) so that the smallest NPs with ultratrace impurities can be characterized
- Development of data analysis algorithms, relying on machine learning, that will be able to count NPs, quantify their multi-element compositions, and profile/cluster them with respect to their origins/sources (*i.e.* anthropogenic or natural; manufacturer source) on a particle-by-particle basis. The source discrimination criteria may be predicated on one or a combination of the following (output) variables, and be pre-defined or developed by training a machine learning model with large datasets, using particles with known properties:
 - Particle purity
 - Elemental associations on a single particle basis
 - Isotopic composition variations on a single particle basis (*e.g.* $^{48}\text{Ti}/^{49}\text{Ti}$)
- The above analytical strategies can be applied in different environment contexts, to generate temporally and spatially resolved data that will be useful for parametrization and validation of mass flow and environmental fate models. This may include data on:
 - Release characteristics from different nano-enabled products (*e.g.* coatings, concrete, cosmetic products) or technical sources (*e.g.* manufacturing plant) under variable weathering conditions;
 - Transformations and persistence of NPs following their emissions in natural media;
 - Determination of transfer factors from technical compartments (*e.g.* wastewater treatment plant) to the environment and from one environmental compartment to another;
 - Spatial and temporal distributions, concentrations and physicochemical states of NPs in different environmental compartments (*e.g.* soil, water, air).